INFRARED SPECTROSCOPY OF CATION-WATER COMPLEXES

by

BISWAJIT BANDYOPADHYAY

(Under the Direction of Michael A. Duncan)

ABSTRACT

Cation-water complexes are produced in a pulsed supersonic expansion source. Metal containing ions are produced by laser vaporization and the electric discharge technique is used for protonated complexes. Mass-selected ions are investigated with infrared laser photodissociation spectroscopy and the method of rare gas predissociation. The infrared spectra of singly charged metal cation-water complexes show red shifts in the O-H stretching frequencies compared to corresponding stretches of the isolated water molecule. The red shift is caused by polarization of water induced by the metal cation. The symmetric stretch gains more intensity than that of the asymmetric stretch in the metal cation-water systems. These effects are more prominent for the doubly charged ions. Partially resolved rotational structures for the $Sc^+(H_2O)Ar$ and $Cr^+(H_2O)$ complexes show that the H-O-H bond angle is larger than it is in the free water molecule. Multiple argons on $Mn^+(H_2O)$ and multiple waters on $Zn^+(H_2O)$ produce various low energy isomers. $Zn^+(H_2O)Ar$ shows the largest red shift in the O-H stretching frequencies, whereas for $Cr^+(H_2O)Ar$ this shift is smaller in magnitude. For doubly charged metal-water complexes, the O-H stretches are observed roughly at the same positions. Fragmentation and the spectral pattern shows that the coordination of M^{2+}(M = Sc, V, Cr) is filled with six ligands.

Mixed protonated complexes of water and nitrogen have $H_3O^+(N_2)_n$ structures with a partial proton sharing interaction. The proton affinity of benzene is higher than that of water, but in the $[H(C_6H_6)(H_2O)]^+$ complex the proton resides closer to water as an effect of a favorable solvation energy. The shared proton stretch for this complex shows a larger red shift than the O-H stretches of H_3O^+. The larger $[H(C_6H_6)_m(H_2O)_n]^+$ sizes have structures of protonated water clusters solvated by benzene. The shared proton stretch shows a larger blue shift in $[H(C_6H_6)(H_2O)_2]^+$ compared to the corresponding stretch of $H_5O_2^+$-Ar due to a greater polarization effect of benzene. The preferential site of protonation is always on water in the systems with multiple benzenes. The strength of the π-hydrogen bonds decreases as the system is progressively solvated by benzene. The coordination of $H_5O_2^+$ is completed with four benzenes.

INDEX WORDS: Spectroscopy, Infrared photodissociation, Metal ion solvation, Ion chemistry, Protonated complexes, Shared proton interactions, Density functional theory

INFRARED SPECTROSCOPY OF CATION-WATER COMPLEXES

by

BISWAJIT BANDYOPADHYAY

M.Sc., Indian Institute of Technology-Bombay, 2006

A Dissertation Submitted to the Graduate Faculty of The University of Georgia in Partial Fulfillment of the Requirements for the Degree

DOCTOR OF PHILOSOPHY

ATHENS, GEORGIA

2012

INFRARED SPECTROSCOPY OF CATION-WATER COMPLEXES

by

BISWAJIT BANDYOPADHYAY

Major Professor: Michael A. Duncan

Committee: Gary E. Douberly
Nigel G. Adams

Electronic Version Approved:

Maureen Grasso
Dean of the Graduate School
The University of Georgia
May 2012

DEDICATION

I dedicate this dissertation to my parents – Rita and Ranjit Banerjee for their love and support throughout my life.

I would also like to dedicate this work to my educators, without them I could not have come this far.

ACKNOWLEDGEMENTS

At the very outset I would like to acknowledge the support and guidance of Professor Mike Duncan, without whom this work would not have seen the light of day. He is a great scientist who has changed my outlook towards research. It has been a privilege to work with and learn from him.

At the Duncanlab, I was fortunate to work with some amazing people. I am indebted to Prosser Carnegie who taught me the nuts and bolts of the experiments. Being a representative of the Wofford football team, he introduced me to the American Football and explained how it's different from Rugby. I would also like to give special thanks to Dr. Gary Douberly, a former post-doctoral fellow in our lab, for the hours spent in useful discussions about spectroscopy. No word of thanks is enough for Tim, my principal partner in crime in the lab, with whom I "tag teamed" during long scans and had lots of fun at the Ohio State molecular spectroscopy symposium every year. I would also like to express my sincere gratitude to all other lab-mates for making every part of this journey a memorable one.

The beautiful city of Athens, the "home away from home", and its people which we fondly refer to as our "Athenian family" has given me all the warmth and strength during these years. Every day had its own small special moments which I will cherish for the rest of my life. I thank all of my fellow Athenian friends from the bottom of my heart for their support and encouragements.

I would also like to acknowledge the contribution of my Alma-mater: Kanyapur High School as well as the years spent at the Ramkrishna Mission Vidyamndira, Belur and the Indian

Institute of Technology (IIT), Bombay. Vidyamandira helped me to build my character and introduced me to some wonderful friends, without whom my life would have been different and incomplete. IIT gave me a flavor of the modern day research and was a stepping stone for higher studies in the United States.

Last but not the least, I acknowledge the support of the US Department of Energy for funding for the last five years.

TABLE OF CONTENTS

Page

CHAPTER 1

INTRODUCTION

Water is the most common solvent and many chemical processes take place in aqueous solutions. The cation solvation process involves a subtle interplay between electrostatic and covalent forces between ions and water. Therefore, there has been a quest to understand solvation processes at the molecular level. Among many solutes, metal ions are ubiquitous throughout chemistry and biology.[1-5] Gas phase metal ion-water complexes are convenient model systems with which to study solvation processes at the fundamental level.[6] Apart from solvation, the other important property of water is that it auto-ionizes in aqueous solutions to form hydronium ion (H_3O^+). This dynamic species is susceptible to rapid proton transfer in aqueous solution between two limiting structures. The first is the "Eigen" cation in which H_3O^+ is solvated by three additional water molecules and each water molecule accepts a hydrogen bond from the cation. The second is the "Zundel" cation, i.e. $H_5O_2^+$ where the proton is equally shared between two water molecules. The structures of the solvated proton are hard to characterize from condensed phase studies, and so these structures have been studied in the gas phase in recent years.[7-15] More recently, the proton sharing interaction of hydrated water with other molecules has been an active area of research.[13c, 15c,f,g, 17] Infrared spectroscopy in the gas phase is such a powerful tool that it makes it possible to study the structures of these proton bound dimers.[15-22] In the first part of this dissertation (Chapters 3 and 4), we present the infrared

spectroscopic studies of metal ion-water complexes, which investigate the interaction of water with metal ions to understand the early stage solvation process. The second part (Chapters 5 and 6) describes the proton sharing interactions of water with two other molecules (nitrogen and benzene) via infrared laser photodissociation spectroscopy.

Metal ions in their various oxidation states govern many chemical processes in aqueous solutions.[1-3] A number of biological systems, such as enzymes, have metal ions in their active sites.[4-5] A cluster of four manganese ions plays a crucial role in the water splitting reaction during photosynthesis.[5a] In various chemical environments, the electrostatic interaction of metal ions influences the outcome of significant chemistry. For example, the selective transport of metal ions through cell membranes is believed to be determined by specific electrostatic interactions.[5b] It is therefore important to understand these interactions at the fundamental level. Gas phase metal ion-water complexes are tractable model systems which can probe the structures and bonding, which in turn helps to understand the solvation process.[6] Therefore, these complexes have been studied using mass spectrometry for many years.[24-30] These mass spectrometric studies investigated the reactivity and thermodynamic properties of cation-water complexes. Both collision induced dissociation and equilibrium measurements have been employed to measure the cation-solvent binding energies.[24-26, 28-30]

The structural information of metal ion-water complexes has been obtained from spectroscopic measurements on these systems.[31-42] Electronic spectroscopy has been successful to study monohydrated complexes of metal ions.[31-36] Duncan et al. and others have reported the electronic spectroscopy of mass-selected cation-water complexes of group II metals (Mg^+, Ca^+, Sr^+, etc.). [32, 33] The single valence electrons of these cations showed strong low energy electronic transitions. Unfortunately, the larger clusters with more than one water produced broad and

structureless spectra due to the effects of predissociation and excited state insertion reactions. ZEKE photoelectron spectroscopy has been employed for certain metals with low ionization potentials (alkalis, aluminum) to obtain ground state vibrations of metal cation-water complexes.[37-38] Infrared spectroscopy has been more productive for direct structural elucidation of cation-water complexes.[40-42] However, the ion densities produced in the supersonic expansion are too low to perform traditional absorption measurements. Therefore, photodissociation spectroscopy has been employed to study cation-water species. However, the binding energies of M^+-(H_2O) are much greater (typically 25-40 kcal/mol, 8700-14000 cm^{-1})[24-28] than the photon energy in the O-H stretch region (3000-4000 cm^{-1}). Therefore, photodissociation is not possible with a single photon. In order to achieve photofragmentation, the method of rare gas "tagging" is used.[40-42] The binding energies of M^+-Ar or M^+-Ne are much lower and so the tag atoms (Ar or Ne) can be eliminated upon vibrational excitations. However, external water molecules in larger M^+-$(H_2O)_n$ clusters have lower binding energies and can be eliminated with photoexcitation.[30, 41d] Lisy and coworkers have employed infrared photodissociation spectroscopy and the method of rare gas tagging to study alkali cation-water complexes.[40] Nishi et al. have studied some of the main group and transition metal ion-water systems using infrared photodissociation.[42] Duncan group has employed infrared photodissociation spectroscopy to investigate a number of main group and transition metal ion-water complexes produced by the laser vaporization technique.[41] Numerous theoretical studies with the new and improved computational tools complemented these experiments.[43-57]

Spectroscopic studies on metal-water complexes have been limited mainly to singly charged species because multiply charged ions are harder to produce in the gas phase.[58-65] The difficulty arises because multiply charged ion-molecule complexes are intrinsically unstable with

respect to charge transfer. The second ionization energy of the metal atom is often greater than the first ionization energy of water (12.6 eV).[66] Therefore, charge transfer from the doubly charged metal to the water molecule can occur producing two singly charged ions which repel each other. Metal ions in higher charge states also have this critical problem. However, asymptotically unstable complexes may be stabilized by the strong Coulombic attraction which dominates at short bonding distances. Under some conditions, the ions can be trapped in the potential energy surface relative to the curve crossing between the $M^{2+} + H_2O$ and $M^{+} + H_2O^{+}$ potentials.[60, 62-64] One of the widely applied methods used to produce multiply charged ions in the gas phase is electrospray ionization, where $M^{n+}(H_2O)_m$ ions in solution are taken directly into the gas phase to avoid charge transfer.[58,61] Other sources have been demonstrated by several research groups.[59,63,64] The laser vaporization technique also has proven to be useful to produce doubly charged metal ion complexes under certain conditions, including asymptotically unstable systems.[63,64] The advantage of the laser vaporization source over electrospray ionization is that the M^{2+}-(H_2O) complexes can be produced directly in the gas phase without any desolvation process. This makes it possible to study the interaction of a metal ion with a single water molecule.

With any of these sources, though, ion densities of multiply charged complexes are much lower than those available for singly charged species, and therefore spectroscopic measurements on these systems are more challenging. Metz and coworkers have employed an electrospray source for studies of electronic photodissociation spectroscopy of doubly charged transition metal ion complexes.[35b-e] Williams and coworkers have reported infrared spectroscopy on doubly and triply charged complexes of several different metals with multiple water molecules, also produced by electrospray.[61,67] Stace and coworkers have measured electronic spectra for dication

complexes using their oven-beam production method.[59] Our research group has employed infrared photodissociation spectroscopy to study doubly charged metal ion-water complexes produced in a laser vaporization source.[68]

Protonation and proton transfer processes play a significant role in numerous chemical and biological processes,[69-74] including acid-base reactions,[69,70] electrochemical processes,[70,71] photosynthesis,[72] and atmospheric chemistry.[73,74] Therefore, proton transfer processes have been studied extensively for many years exploring the detailed mechanism of the unusual rate of proton transfer in solutions.[75-78] The structures and various properties of protonated water clusters have been investigated by several experimental and theoretical studies.[7-22, 79-111] More recently, understanding the behavior of protons at the interface of water and hydrophobic media has been an active area of research.[112-117] These studies show that the surface charge density plays a crucial role in stabilizing ions at hydrophobic interfaces.[115-117] Infrared spectroscopy in the gas phase has been successful to study the structures of protonated systems.[7-22] Many of these studies have explored the protonated water and its proton sharing interaction with other molecules.[13c, 15c,f,g,17] In recent years, these studies have been extended to mixed complexes in which the molecular components have different proton affinities, polarizabilities and dipole moments, etc.[15g,17]

Protonated water clusters have been studied extensively using mass spectrometry for many years.[79-91] The various isomeric structures of protonated water clusters have been investigated by a number of theoretical methods.[92-111] The infrared spectroscopic studies of protonated water clusters started with the high resolution measurements of the hydronium cation performed by Oka, Saykally and Nesbitt.[7-9] Schwarz and coworkers have reported the infrared studies of protonated water clusters.[10] Small mass-selected protonated water clusters $H^+(H_2O)_n$

(n=2-8) were studied by Lee and coworkers using cluster ion beams and infrared photodissociation spectroscopy in the O-H stretching region.[11] The low frequency shared proton stretch and bends of protonated water dimer were studied by Asmis et al. using the free electron laser "FELIX".[12a] The same study was repeated at "CLIO"[13a] and both the laboratories confirmed that the protonated water dimer has the symmetric "Zundel" structure rather than that of hydronium solvated by a water molecule. Our research group, in collaboration with Johnson and coworkers, used an IR optical parametric oscillator laser system to study protonated water complexes.[14] Recently, Johnson and coworkers studied hydronium and protonated water dimer with isotopic substitution.[15d,e] Several theoretical studies investigated protonated water dimer using reduced dimensional and full dimensional anharmonic calculations.[102] Our research group recently reported infrared photodissociation studies on small protonated water clusters $H^+(H_2O)_n$ (n=3-5), which investigated the role of tagging with argon and the effect of deuteration.[23]

π-electron clouds in aromatic rings are highly polarizable and therefore these systems are known to play key roles in intermolecular interactions such as π-hydrogen bonding and π- π stacking.[118,119] Many spectroscopic studies involving π-electrons have been carried out to elucidate the nature of intermolecular interactions.[120-124] For example, neutral benzene-$(water)_n$ clusters, where the water moiety forms a sub-cluster of $(water)_n$ sticking on the benzene ring, have been studied as a prototype of π-hydrogen bonding.[121-124] However, on photoionization or protonation the charge distribution of an aromatic ring may drastically change. Our research group has studied the protonated benzene complex employing infrared spectroscopy and the method of rare gas tagging.[125] Mikami and coworkers have studied benzene cation-$(water)_n$ systems, $[(C_6H_6)(H_2O)_n]^+$ for n = 1-6, using infrared spectroscopy and they have investigated the structural changes upon photoionization and resulting proton transfer reactions.[126] Chang and

coworkers have employed infrared spectroscopy along with theoretical calculations to study protonated benzene-(water)$_2$, $[H(C_6H_6)(H_2O)_2]^+$.[127]

In the present work, we use two different techniques to produce cation-water complexes. Metal containing systems are produced by laser vaporization, while the protonated species are produced using the electric discharge technique. Mass-selected complexes are investigated with laser photodissociation spectroscopy. In Chapter 3, the spectroscopy of singly charged metal cation-water complexes is discussed. The spectra of mono argon tagged metal (Sc^+, Cr^+, Mn^+, and Zn^+)–water complexes show variations in the O-H stretch region depending on the electronic structure of the metal or the location of argon in the respective complexes. For $Mn^+(H_2O)Ar_n$, where n=1-4, different binding sites of argon atoms produce various low energy isomers. Similarly, the spectra of $Zn^+(H_2O)_nAr$ show evidence of different isomers. The spectroscopy of doubly charged metal (Sc^{2+}, V^{2+}, Cr^{2+}, and Mn^{2+})-water complexes is discussed in Chapter 4. A comparison of singly and doubly charged metal ion-water species is also included in that chapter. Chapters 5 and 6 discuss the proton sharing interactions of water with nitrogen and benzene. The proton affinity of water (691.0 kJ/mol) is much greater than that of nitrogen (493.8 kJ/mol).[66] The spectra of mixed protonated complexes of water and nitrogen show $H_3O^+(N_2)_n$ structures with a partial proton sharing interaction (more hydronium character). Although the proton affinity of benzene (751.4 kJ/mol)[66] is greater than that of water, water gets protonated due to the favorable solvation energy. The shared proton interaction is much stronger in benzene-water complexes than that of the nitrogen-water system. The higher cluster sizes with multiple waters or multiple benzenes are found to have protonated water clusters solvated by benzene.

CHAPTER 2

EXPERIMENTAL

Cation-water complexes are produced in a pulsed supersonic expansion source using two different techniques. Metal containing complexes are produced by laser vaporization of a translating and rotating metal rod using the second (532 nm) or third (355 nm) harmonic of a Nd:YAG laser (Continuum Surelite or Spectra Physics INDI). Protonated complexes are produced employing the needle electric discharge technique. In this technique, two sewing needles are mounted in a Teflon block on the faceplate of a pulsed valve (General Valve, series 9). Needle tips are separated by approximately 2-5 mm and are centered on the beam axis 5 mm downstream from the valve orifice. A high voltage pulser (DEI Model PVX-4140) is used to generate ~1-50 μs wide ~1000-3000 V pulse. The high voltage pulse is applied to one needle keeping the other needle grounded to produce the electric discharge.

The pulsed nozzle source and details of molecular beam apparatus have been described previously.[6, 128-133] Figure 2.1 shows a schematic of our apparatus. Laser vaporization or electric discharge is carried out in the cluster formation chamber (known as the "source" chamber). This chamber operates at ~10^{-4} torr. The buffer gas (generally Ar, He, He-Ne mixture, H_2, N_2) is pulsed through a series 9 valve perpendicular to laser vaporization. Both laser vaporization and electric discharges produce a plasma containing neutrals, cations and anions. These species encounter many collisions with the supersonically cooled expansion gas, which leads to efficient formation of "cold" ion-molecule and ion-rare gas complexes.

The molecular beam is collimated with a 3 mm diameter skimmer (Beam Dynamics) and sent into the second differentially pumped chamber (known as the "mass-spec" chamber) equipped with a specially designed reflectron time-of-flight (RTOF) mass spectrometer. The "mass-spec" chamber is kept under a vacuum of 10^{-7} torr. In the first leg of the RTOF, the cations are pulse extracted by a series of acceleration plates. A field in the reflectron assembly brings the ions to zero velocity before reaccelerating them into the second drift tube. At the end of the second tube the ions are detected using an electron multiplier tube (EMT) detector (Hamamatsu R595). The signal from the detector is amplified by a pre-amplifier (Stanford SR 445A) and then fed into a digital oscilloscope (LeCroy WaveRunner LT342). The digital oscilloscope is interfaced to a personal computer via an IEE 488 digital card. The signal of the ions appears as voltage spikes as a function of flight time through both legs of the mass spectrometer.

In the first leg of the flight tube, prior to the reflectron assembly, a pair of pulsed deflection plates is used to select a specific ion of interest based on its flight time. The deflection plates are kept at constant positive voltage (+600-800 V) which deflects ions from the beam axis. These plates are pulsed to ground for a variable period of time based on the mass/charge ratio of specific ion of interest. This allows only the selected ion to pass through this "mass-gate" and all the other ions are deflected into the wall of the flight tube. The mass selected ions are intersected with the tunable output of an infrared Optical Parametric Oscillator/ Optical Parametric Amplifier (IR-OPO/OPA) laser system (LaserVision). The ion optics and pulse timing are adjusted to achieve maximum overlap between the ion packet and the incident laser beam. Photodissociation of mass selected ion occurs on resonant absorption, provided that at

least one of the bonds is weaker than the infrared photon energy. The intensity of the fragment ion is monitored as a function of the infrared photon energy in order to obtain a spectrum.

Figure 2.2 shows a schematic of the OPO/OPA system. This system is pumped using 500 mJ/pulse of 1064 nm light from a Nd:YAG (Spectra Physics Pro 230) operating at 10 Hz. The pump beam is split into two beams using a 70:30 beam splitter. The low energy beam is passed through a KDP doubling crystal to generate 532 nm light. The 532 nm (~18800 cm^{-1}) light is sent through the OPO stage (consists of a KTP crystal) where the 532 nm beam is split into two beams (signal and idler) by optical parametric conversion. The frequency of the pump beam (ν_{pump}) has to be equal to the frequencies of signal and idler beams ($\nu_{signal} + \nu_{idler}$) due to energy conversion, i.e. ν_{pump}(18800 cm^{-1}) = $\nu_{signal} + \nu_{idler}$. The signal beam is tunable from 710-880 nm (14085 – 11364 cm^{-1}) and the idler beam is tunable from 134 -212 nm (4715 – 7436 cm^{-1}) by angle tuning of the KTP crystal. In this configuration of the OPO/OPA system the signal beam is not used and the idler beam is sent to the OPA stage (consisting of four KTA crystals which also can be angle tuned). The higher energy residual beam at 1064 nm (9400 cm^{-1}) from the YAG laser is directly sent to the OPA stage where difference frequency mixing with the idler beam generates tunable light from 2000-4700 cm^{-1}(mid-IR). The idler and mid-IR beams are orthogonally polarized and separated using a polarizer. The lower frequency light is obtained using an $AgGaSe_2$ (silver gallium selenide) crystal where the difference frequency mixing of the idler and the mid-IR beams produces tunable light from 600-2200 cm^{-1}. This IR-OPO/OPA system has a linewidth of 1-2 cm^{-1} in the 600-4700 cm^{-1} region. This table top laser covers almost the whole infrared region which allows studying the spectra of a variety of molecular and ionic systems.

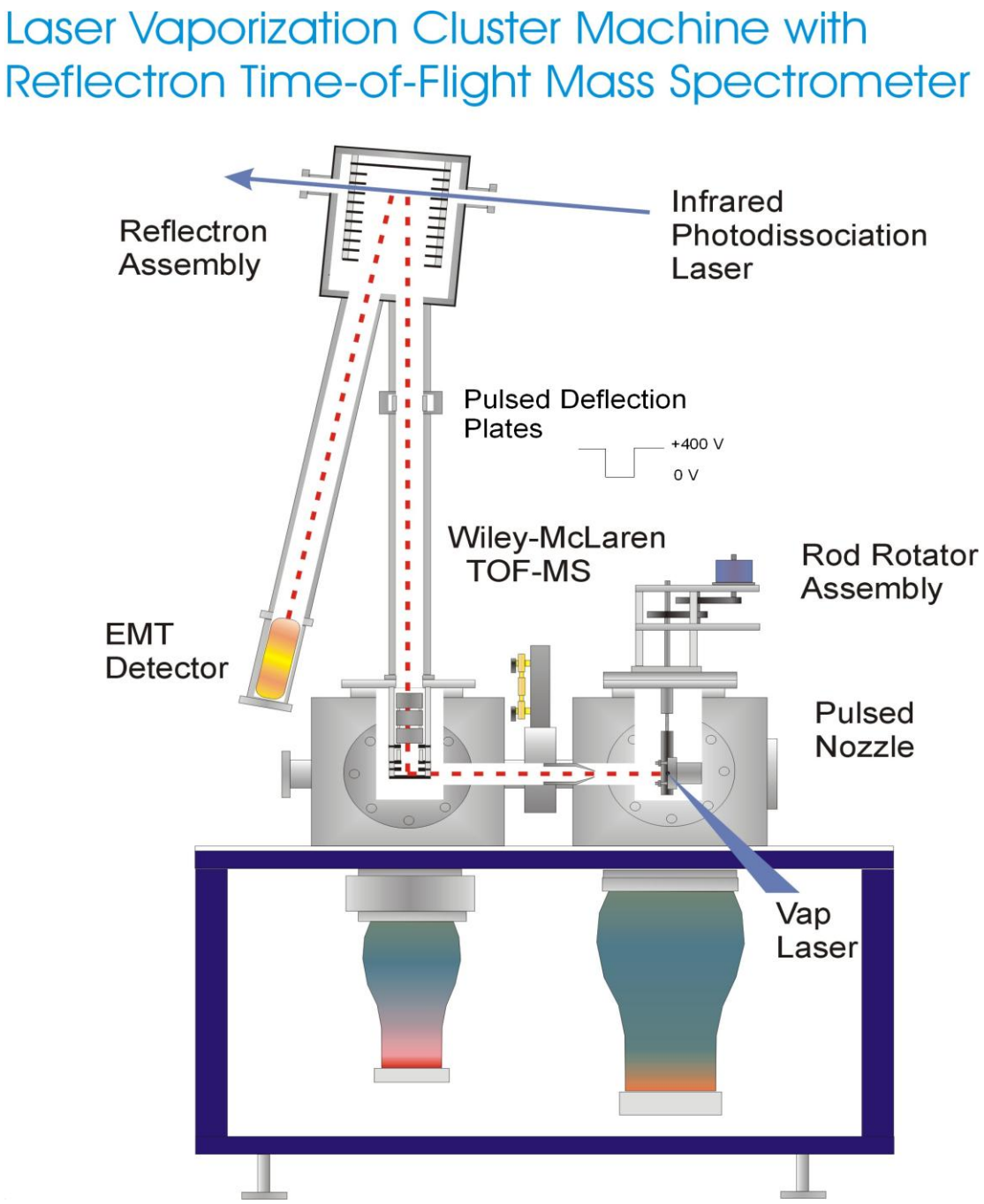

Figure 2.1: Schematic of the laser vaporization molecular beam machine coupled to a reflectron time-of-flight mass spectrometer.

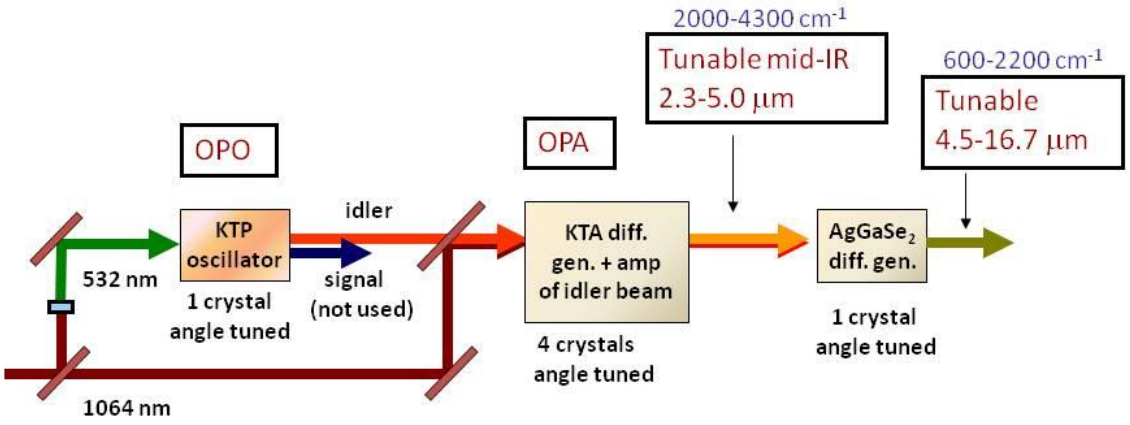

Figure 2.2: Schematic of the LaserVision infrared optical parametric oscillator/optical parametric amplifier (IR-OPO/OPA) laser system.

CHAPTER 3

SINGLY CHARGED TRANSITION METAL CATION-WATER COMPLEXES

3.1 Introduction

Much of chemistry in aqueous solutions involves metal cation solvation by water. [1-3] A number of biological systems, such as enzymes have metal ions in their active sites.[4-5] A fundamental understanding of solvation requires a molecular level investigation of metal ion-water interactions. Measurements in solution are averaged over numerous configurations, making it difficult to characterize specific solvation structures or coordination numbers.[134-137] On the other hand, gas phase metal ion-water complexes provide convenient models to understand the cation solvation process at the molecular level.[6] Therefore, metal cation-water complexes have been studied using mass spectrometry for many years.[24-30] Thermodynamic properties, such as cation-solvent bond energies have been measured using collision induced dissociation and equilibrium techniques.[24-26,28-30] Spectroscopic studies have investigated the structures of metal cation-water complexes.[31-42] Numerous theoretical studies complimented these experiments with new and improved computational tools.[43-52]

Electronic spectroscopy has been widely applied to study monohydrated complexes of metal ions.[31-36] However, the larger $M^+(H_2O)_n$ clusters produced broad and featureless spectra due to the effects of predissociation and excited state reactions. Infrared spectroscopy has been more productive for direct structural elucidation of metal cation-water complexes.[40-42] Lisy and coworkers have employed infrared photodissociation spectroscopy and the method of rare gas

"tagging" to study alkali cation-water complexes.[40] Nishi and coworkers have studied some of the main group and transition metal ion-water systems using infrared photodissociation.[42] Our research group has used infrared photodissociation spectroscopy to investigate a number of main group and transition metal ion-water complexes produced by laser vaporization.[41] In this present work, we extended these studies on singly charged monohydrated complexes of Sc^+, Cr^+, Mn^+ and Zn^+ employing the method of rare gas tagging. We also describe the spectroscopy of the $Mn^+(H_2O)Ar_n$ complexes (where n=1-4) showing the effect of argon solvation. A similar study with $Zn^+(H_2O)_nAr$ (where n=1-4) is also presented describing the effects of multiple water solvation.

3.2 Experimental

Singly charged metal cation-water complexes are produced in a pulsed-nozzle laser vaporization source which has been described in detail in Chapter 2. In the supersonic expansion, argon is used as buffer gas and a few drops of water are added into the gas flow to produce mixed complexes. The metal rod is vaporized by the third harmonic (355 nm) of a Nd:YAG laser. Mass-selected ions are investigated with infrared photodissociation spectroscopy in the O-H stretching region using an infrared optical parametric oscillator/amplifier laser system (OPO/OPA; LaserVision, Inc.) pumped by a Nd:YAG laser (Continuum 8010). Laser excitation occurs in the turning region of the reflectron field, where ion optics and pulse timing are adjusted to obtain optimized spatial and temporal overlap between the laser and the ion beam. Resonant single photon absorption leads to elimination of argon from the $M^+(H_2O)Ar_n$ species. The fragment ion intensity is recorded as a function of the infrared laser frequency using a digital oscilloscope connected to a computer.

Density functional theory (DFT) is employed to investigate the structures and vibrational spectra of the $M^+(H_2O)Ar_n$ complexes for comparison to the experiment. These computations use the B3LYP functional in the Gaussian 03W package and the 6-311+G (d, p) basis set.[138] The computed vibrational frequencies are scaled by a factor of 0.9575, which is the recommended value for the B3LYP/6-311+G (d, p) method.[139]

3.3 Results and Discussion

The binding energies of $M^+(H_2O)$ complexes, where M= Sc, Cr, Mn and Zn are 34.1, 31.7, 29.1 and 33.2 kcal/mol (~10000-15000 cm^{-1}) respectively.[14] Therefore, photodissociation is not possible with a single photon in the O-H stretch region (3000-4000 cm^{-1}). Multiphoton excitation is not feasible with the available laser pulse energies (5-10 mJ/pulse, unfocused). In order to obtain photofragmentation, we must use the method of rare gas tagging since M^+-Ar bonds are much weaker than M^+-H_2O bonds. Infrared excitation of the O-H stretches leads to elimination of loosely bound argon atom from the $M^+(H_2O)Ar$ complex .

Figure 3.1 shows the infrared spectrum measured for the $Sc^+(H_2O)Ar$ complex in the mass channel corresponding to the elimination of argon. There are several peaks observed for this complex in the 3500-3800 cm^{-1} region, where the symmetric and asymmetric O-H stretches (3657 and 3756 cm^{-1} for isolated water molecule)[66] are expected. The spectrum of $Sc^+(H_2O)Ar$ has four main peaks at 3580, 3641, 3668 and 3695 cm^{-1} and couple of weaker features at 3613, 3720 and 3746 cm^{-1}. The pattern of these peaks is similar to those observed for alkali metal cation-water complexes.[40] The computed structure of $Sc^+(H_2O)Ar$ is shown in the inset of Figure 3.1. This complex has C_{2v} symmetry and argon binds to the Sc^+ ion on the C_2 axis opposite to water. In this C_{2v} configuration, all the heavy atoms (Sc^+, O and Ar) are on the C_2

axis and only the light hydrogen atoms are off the axis. Therefore, the *A* rotational constant corresponds approximately to the rotational constant of the isolated water molecule, where the O-H groups rotate along the symmetry axis and only the light hydrogen masses contributes to the moment of inertia. The peaks in the spectrum of $Sc^+(H_2O)Ar$ arise from the symmetric and asymmetric O-H vibrational bands and their partially resolved rotational structure. The broader band centered at 3580 cm^{-1} is assigned to the symmetric O-H stretch of water in this complex. This is a parallel type vibration band with unresolved rotational structure along its contour. The asymmetric O-H stretch is a perpendicular type vibration and therefore K-type rotational sub bands are expected to be resolved as an effect of the large *A* rotational constant. The peaks at 3641, 3668 and 3695 cm^{-1}, and the weaker features either side of these, are assigned to the K-type sub bands of the perpendicular type asymmetric stretch.

To confirm this assignment, we have simulated the rotational structure of these vibrational bands using a program *Asyrotwin*, as shown in the lower trace of Figure 3.1. The simulation includes the nuclear spin statistical weights for the ortho-para (odd:even =3:1) values of K. The assignments of K-type rotational sub bands (K', K'') are also shown in the simulated spectrum. The bands in the observed spectrum are best described by a rotational temperature of 50K. The ground and excited state rotational constants obtained from observed and simulated spectra are shown in the inset. Band origins of the symmetric and asymmetric stretches (3580 and 3656 cm^{-1}) are also determined from the simulated spectrum.

The O-H stretching frequencies for the $Sc^+(H_2O)Ar$ complex are 77 and 101 cm^{-1} red shifted compared to the symmetric and asymmetric stretches of the free water molecule (3657 and 3756 cm^{-1} respectively). [66] The red shift is caused by polarization of the lone pair of electrons on the oxygen induced by the metal cation. The non-bonding molecular orbital of the

water accommodating the lone pair has some partial bonding character along the O-H bonds. Polarization of the electron density from this orbital remove electron density from the O-H bonds resulting in weaker and longer bonds which accounts for the red shifts in O-H stretching frequencies.

Figure 3.2 shows the spectrum of the $Sc^+(H_2O)Ar_2$ complex. The symmetric and asymmetric O-H stretches are observed at 3546 and 3637 cm^{-1}, which are further shifted to the red from the band origins of the corresponding stretches of $Sc^+(H_2O)Ar$ (3580 and 3656 cm^{-1} respectively). DFT predicts that the lowest energy isomer has the second argon atom attached to the O-H bond of water, as shown in the inset. The other isomer corresponding to $Ar_2Sc^+OH_2$ (both argons on metal) has 5.3 kcal/mol higher energy than that of $ArSc^+OH_2Ar$. As a result of the argon interaction with the O-H bond, the argon-bound O-H stretches shift to lower frequencies and the partially resolved rotational structure is lost. The predicted frequencies for $ArSc^+OH_2Ar$ are 3560 and 3652 cm^{-1}, which agree well with the observed spectrum. The predicted frequencies for $Ar_2Sc^+OH_2$ are 3607 and 3679 cm^{-1}, which are much higher than the observed frequencies.

Another interesting aspect of these spectra is the intensities of the symmetric and asymmetric O-H stretch vibrations. For the $Sc^+(H_2O)Ar$ complex, the asymmetric stretch appears as multiplet band structure and the integrated intensities of these bands are roughly 2-3 times more intense than that of the symmetric stretch. The intensity ratio of these stretches for $Sc^+(H_2O)Ar_2$ is roughly 1:1. For both the $Sc^+(H_2O)Ar_{1,2}$ complexes, the intensity ratio is significantly different from that of the isolated water, where the symmetric stretch is ~18 times less intense than the asymmetric stretch.[66] The intensity of an infrared vibration depends on the dipole moment derivative. The symmetric stretch in a metal cation-water system is a parallel

type vibration which modulates the charge density more effectively than the perpendicular type asymmetric stretch. This greater modulation of charge density in the symmetric stretch leads to a higher change in dynamical dipole moment than that of the asymmetric stretch. Therefore, in a cation-water system the symmetric stretch gains more intensity than the asymmetric stretch.

Figure 3.3 shows the spectrum of $Cr^+(H_2O)Ar$. The pattern of bands in the O-H stretch region is similar to that observed for $Sc^+(H_2O)Ar$. The band at 3616 cm^{-1} is assigned to the parallel type symmetric O-H stretch vibration with unresolved rotational structure along its contour. The 3676, 3729 and 3782 cm^{-1} peaks, and the weaker features either side of these peaks represent the K-type sub bands of the perpendicular type asymmetric O-H stretch. A rotational temperature of 130K reproduces the main features of the observed spectrum. The ground state and excited state rotational constants obtained from the observed and simulated spectra are shown in the inset. The rotational constants are roughly the same for both the $Cr^+(H_2O)Ar$ (A"=13.1, A'=13.0) and $Sc^+(H_2O)Ar$ (A" =13.7, A'=13.4) complexes. The band origins for the symmetric and asymmetric O-H stretches are determined to be 3620 and 3690 cm^{-1} respectively. These are 37 and 67 cm^{-1} shifted to the red from the free water stretches. The amount of red shift is much less for $Cr^+(H_2O)Ar$ than that of $Sc^+(H_2O)Ar$ (77 and 101 cm^{-1}). Sc^+ has one electron in the d-orbital, whereas Cr^+ has four electrons in the valence shell. Apparently, a lower number of d-electrons on metal ion enhance the polarization of the electrons of oxygen. As a result, $Sc^+(H_2O)Ar$ shows more red shift in O-H stretches than that of $Cr^+(H_2O)Ar$.

The *A* rotational constant is used to calculate the H-O-H bond angle of the $Cr^+(H_2O)Ar$ complex. The value of this constant is determined by the distance of the hydrogen atoms from the C_2 axis, which is related to both the O-H bond lengths and the H-O-H bond angle. Therefore, one rotational constant is not sufficient to determine both these geometric parameters

simultaneously. We assume that the O-H bond distances of water do not change significantly upon binding to the metal ion. Assuming the fixed O-H bond distances and using the *A* value we can calculate the H-O-H bond angle. Using this procedure we calculated the H-O-H bond angle to be 111.1^{o}. This angle is greater than the corresponding H-O-H angle of the isolated water molecule (104.7^{o}).[66] Although the calculated value for $Cr^{+}(H_2O)Ar$ is not expected to be exact due to some approximation associated with this procedure, it makes sense that the metal cation removes electron density from the lone pair of oxygen which leads to a greater H-O-H bond angle.

The lower trace of Figure 3.4 shows the infrared spectrum measured for the $Mn^{+}(H_2O)Ar$ complex in the O-H stretch region. The spectrum has two peaks at 3584 and 3660 cm^{-1} corresponding to the symmetric and asymmetric O-H stretches with roughly a 1:1.3 intensity ratio. These bands are 73 and 96 cm^{-1} shifted to the red from the corresponding stretches of the isolated water molecule. This magnitude of red shift is close to that observed for $Sc^{+}(H_2O)Ar$ (77 and 100 cm^{-1} respectively). The intensity pattern is also consistent with the general feature observed for these two vibrations. We notice that the partially resolved rotational structure is absent in the spectrum. The DFT computed structure shows that the argon atom binds to the side of Mn^{+} with a ~90^{o} O-Mn^{+}-Ar bond angle. Since argon binds to Mn^{+} off the C_2 axis the rotational constant for $Mn^{+}(H_2O)Ar$ is much smaller and the asymmetric stretch loses the multiplet band structure. The valence shell electronic configuration of the isolated ground state Mn^{+} ion is ($3d^5 4s^1$) is similar to that of Mg^{+} ($2p^6 3s^1$). As discussed previously for the $Mg^{+}(H_2O)Ar$ system, the valence shell s^1 electron is back polarized by the water, inducing a negative lobe around Mg^{+} along the C_2 axis opposite to water.[27d] Therefore, the argon atom

tends not to bind along the C_2 axis. In the $Mn^+(H_2O)Ar$ complex, a similar situation is observed where argon binds to the side of Mn^+.

The upper three traces of Figure 3.4 show the spectra of the $Mn^+(H_2O)Ar_{2-4}$ complexes. DFT predicts various low energy isomers depending on the binding sites of the argon atoms. Table 3.1 lists the relative energies of these isomers and corresponding predicted vibrational frequencies. The four peaks (3549, 3584, 3643 and 3662 cm^{-1}) in the spectrum of $Mn^+(H_2O)Ar_2$ arise from O-H stretches of two different isomers corresponding to the $Ar_2Mn^+OH_2$ (two argons on metal) and $ArMn^+OH_2Ar$ (one argon on metal, one argon on O-H) structures. The predicted frequencies (3518/3586 cm^{-1}, 3535/3636 cm^{-1}) for these structures agree well with the observed frequencies. The spectrum of $Mn^+(H_2O)Ar_3$ also has four peaks (3554, 3586, 3644 and 3665 cm^{-1}) corresponding to two different isomers. However, the set of peaks corresponding to the stretches for $Ar_2Mn^+OH_2Ar$ (two argon on metal, one on O-H) at 3554 and 3644 cm^{-1} is more intense than that observed for $Ar_3Mn^+(H_2O)$ at 3586 and 3665 cm^{-1}. Apparently, the relative abundance of the isomer in which argon binds to the O-H bond increases as the system is solvated by more argon. The spectrum of $Mn^+(H_2O)Ar_4$ has three intense peaks at 3557, 3614, 3648 cm^{-1} and two weaker peaks at 3545 and 3665 cm^{-1}. The set of peaks at 3557/3668 cm^{-1} is assigned to the O-H stretches of $Ar_3Mn^+OH_2Ar$ and the set of peaks at 3545/3665 cm^{-1} corresponds to the O-H stretches of $Ar_4Mn^+H_2O$. The stretches for the other isomer $Ar_2Mn^+OH_2Ar_2$ are predicted at 3537 and 3607 cm^{-1}. Therefore, the 3614 cm^{-1} peak in the observed spectrum is assigned to the asymmetric O-H stretch of $Ar_2Mn^+OH_2Ar_2$. The symmetric stretch for this complex is probably close to the 3540-3550 cm^{-1} region, where there is an intense peak corresponding to another isomer. The relative abundance is again more for $Ar_3Mn^+OH_2Ar$ isomer, but the other isomer $Ar_2Mn^+OH_2Ar_2$ is also produced in a small amount.

To illustrate the effect of argon isomers in assigning the peaks for manganese-water-argon complexes, we selected $Mn^+(H_2O)Ar_3$ as an example. The upper trace of Figure 3.5 shows the experimental spectrum and three lower traces show the spectra for three different isomers corresponding to $Ar_3Mn^+OH_2$ (3a), $Ar_2Mn^+OH_2Ar$ (3b), and $Ar_2Mn^+OH_2Ar$ (3c). The infrared spectrum of the $Mn^+(H_2O)Ar_3$ complex is best described by the predicted spectra corresponding to the isomers (3a) and 3(b). The two intense bands at 3554 and 3644 cm^{-1} correspond to the symmetric and asymmetric stretches of isomer (3b) predicted at 3540 and 3638 cm^{-1}. The other two less intense bands at 3586 and 3665 cm^{-1} correspond to the O-H stretches predicted for isomer 3(a) at 3577 and 3659 cm^{-1}. There is a small peak at 3607 cm^{-1} observed in the spectrum which corresponds to the asymmetric O-H stretch of isomer (3c) predicted at 3594 cm^{-1}. The symmetric stretch for this complex is not detected, probably because of the low abundance of this isomer. In the experimental spectrum, this stretch may also be hidden beneath the intense 3554 cm^{-1} band.

Figure 3.6 shows the spectra of the $Zn^+(H_2O)_nAr$ complexes. The spectrum of $Zn^+(H_2O)Ar$ has three main peaks at 3565, 3644 and 3726 cm^{-1}. The computed structure for this complex shows that argon binds to the side of Zn^+ similar to that of $Mn^+(H_2O)Ar$. Therefore, the two peaks at 3565 and 3644 cm^{-1} are assigned to the O-H stretches for this complex. The predicted vibrations at 3579 and 3666 cm^{-1} also agree well with this assignment. The other intense peak at 3726 cm^{-1} is assigned to a combination band. This type of combination band has been studied previously by theoretical calculations in the case of $Cu^+(H_2O)Ar_2$.[41f] The spectrum of $Zn^+(H_2O)_2Ar$ has two sets of doublet peaks at 3547, 3578, 3652 and 3668 cm^{-1}. $Zn^+(H_2O)_3Ar$ shows similar doublet peaks roughly at the same positions (3567, 3585, 3657, 3672 cm^{-1}). This spectrum also has some weaker peaks at 3386, 3481, 3626 and 3813 cm^{-1}. In the spectrum of

$Zn^+(H_2O)_4Ar$, an intense band at 3428 cm^{-1} appears abruptly. The spectrum also has two other intense peaks at 3664 and 3682 cm^{-1} along with some weaker features at 3493, 3522 and 3593 cm^{-1}.

The assignments of the peaks observed for the $Zn^+(H_2O)_{2-4}Ar$ complexes can be done with the help of theoretical calculations. For all the sizes DFT finds low energy isomers. The upper trace of Figure 3.7 shows the spectrum of $Zn^+(H_2O)_2Ar$ and the lower traces show the predicted spectra corresponding to two different isomers. As shown in the inset structures, argon binds either to Zn^+ or to water and the relative energies of these two isomers are only 0.5 kcal/mol. The peak corresponding to the $ArZn^+(H_2O)_2$ (isomer 2a) structure (argon on Zn^+) is predicted at 3590 and 3679 cm^{-1}. For $Zn^+(H_2O)_2Ar$ (isomer 2b), argon binding to water breaks the symmetry of this complex and the O-H stretches are shifted to the lower frequencies. The argon bound symmetric stretch is predicted at 3569 cm^{-1} and the same stretch corresponding to free O-H is predicted at 3585 cm^{-1}. The observed spectrum has four peaks at 3547, 3578, 3652 and 3668 cm^{-1}. The set of peaks at 3547/3652 cm^{-1} is then can be assigned to the symmetric and asymmetric O-H stretches of isomer 2b and the set of peaks at 3578/3668 cm^{-1} corresponds to the O-H stretches of isomer 2a.

The $Zn^+(H_2O)_3Ar$ complex is also found to have three lowest energy isomers. Similar to $Zn^+(H_2O)_2Ar$, the two isomers corresponding to the $ArZn^+(H_2O)_3$ structure (isomer 3a, argon on Zn^+) and $Zn^+(H_2O)_3Ar$ (isomer 3b, argon on OH) have a small energy difference. The other isomer has the third water molecule hydrogen bonded to the O-H bonds of two other water molecules which are bound to Zn^+ (isomer 3c). Figure 3.8 shows the predicted spectra corresponding to each isomer and the upper trace shows the spectrum of $Zn^+(H_2O)_3Ar$. The observed spectrum is best described by the predicted spectra corresponding to the isomer 3a and

3b. The assignments of the peaks in the 3500-3700 cm^{-1} region is similar to that of $Zn^{+}(H_2O)_2Ar$. The set of peaks at 3567/3657 cm^{-1} is the argon bound O-H stretches of isomer 3b and 3585/3672 cm^{-1} set is the O-H stretches of isomer 3a. The weak peaks observed at 3386, 3481 and 3626 cm^{-1} correspond to the stretches of isomer 3c. The predicted spectrum for this complex shows an intense band at 3432 cm^{-1} which corresponds to the hydrogen bonded O-H stretches of water. However, the detected stretches are weak probably due to the low abundance of this isomer.

The upper trace of Figure 3.9 shows the spectrum of $Zn^{+}(H_2O)_4Ar$. The bottom three traces show the predicted spectra for three different isomers computed by theory. For the $Zn^{+}(H_2O)_4$ complex, theory finds that the fourth water does not tend to bind to Zn^{+}, rather it prefers to go to the second solvation sphere accepting one hydrogen bond each from the two other water molecules in a double-acceptor configuration. In the $Zn^{+}(H_2O)_4Ar$ complex, argon binds either to Zn^{+} or to the O-H bond of the second sphere water molecule. Both of these isomers are separated from each other by only 0.5 kcal/mol energy. The observed spectrum is best described by the predicted spectra for these two isomers. The hydrogen bonded O-H stretches are predicted at 3414/3450 and 3424/3461 cm^{-1} corresponding to these two isomers. The observed spectrum has an intense band at 3428 cm^{-1} which is assigned to the hydrogen bonded O-H stretch for this complex. The free O-H stretches are observed at 3664 and 3682 cm^{-1}. The argon bound stretches are observed at 3593 cm^{-1}. Even though single-acceptor isomer is only 1.6 kcal/mol higher in energy, it is apparently not formed.

3.4 Conclusions

Singly charged metal cation-water complexes are produced in a pulsed laser vaporization source and studied via infrared photodissociation spectroscopy in the O-H stretching region. For $Sc^+(H_2O)Ar$ and $Cr^+(H_2O)Ar$, argon binds to the metal ion on the C_2 axis opposite to water. The spectra for these complexes show multiplet band structures in the O-H stretch region. Simulation of these spectra provides structural parameters for $M^+(H_2O)Ar$. For $Mn^+(H_2O)Ar$ and $Zn^+(H_2O)Ar$, the valence shell s^1 electron of M^+ is back polarized by water leading to a negative lobe around the metal ion. Therefore, the argon atom binds to M^+ off the C_2 axis and partially resolved rotational structure is lost in the spectra of the $Mn^+(H_2O)Ar$ and $Zn^+(H_2O)Ar$ complexes. The symmetric and asymmetric O-H stretches for $Zn^+(H_2O)Ar$ show 92 and 113 cm^{-1} red shifts compared to the corresponding stretches of free water. The red shifts for $Sc^+(H_2O)Ar$ (77 and 101 cm^{-1}) are close to those observed for $Mn^+(H_2O)Ar$ (73 and 107 cm^{-1}). The magnitude of the red shift for $Cr^+(H_2O)Ar$ is much smaller than those observed for Zn^+, Mn^+ and Sc^+. For $Mn^+(H_2O)Ar_n$ and $Zn^+(H_2O)_nAr$, different binding sites of argon and water give rise to multiple low energy isomers.

Table 3.1: Relative energetics and vibrational frequencies (cm^{-1}) computed for manganese-water-argon structures. IR intensities (km/mol) are in parentheses, and frequencies are scaled by a factor of 0.9575 for comparison to the experiments.

Molecule	Rel. Energy	OH stretches (theory)	OH stretches (exp)
$Mn^+(H_2O)$	0.0	3570 (84), 3651(209)	-
$Mn^+(H_2O)Ar$			
$^7A'$ (C_s) (Ar on H)	0.0	3524(314), 3626(258)	3584, 3660
^7A (C_1)(Ar on Mn^+)	+0.2	3572(78), 3653(206)	
$Mn^+(H_2O)Ar_2$			
$^7A'$ (C_s) (2Ar on H)	0.0	3518(280), 3586(532)	3549, 3584,
^7A (C_1)	+0.2	3535(282), 3633(257)	3643, 3662
(1Ar on Mn^+; 1Ar on H)			
^7A (C_1) (2Ar on Mn^+)	+0.4	3575(74), 3657(207)	
$Mn^+(H_2O)Ar_3$			
^7A (C_1)	0.0	3524(269), 3594(506)	3554, 3586,
(1Ar on Mn^+ ; 2Ar on H)			3644, 3665
^7A (C_1)	+0.3	3540(280), 3638 (248)	
(2 Ar on Mn^+ ; 1Ar on H)			
^7A (C_1) (3Ar on Mn^+)	+0.5	3577(71), 3659 (203)	
Mn^+ $(H_2O)Ar_4$			
^7A (C_1)	0.0	3537(270), 3606(409)	3557, 3614, 3648
(2Ar on Mn^+ ; 2Ar on H)			
^7A (C_1)	+0.3	3548 (242), 3642 (247)	
(3Ar on Mn^+ ; 1Ar on H)	+0.7	3578(68), 3662(201)	
^7A (C_1)(4Ar on Mn^+)			

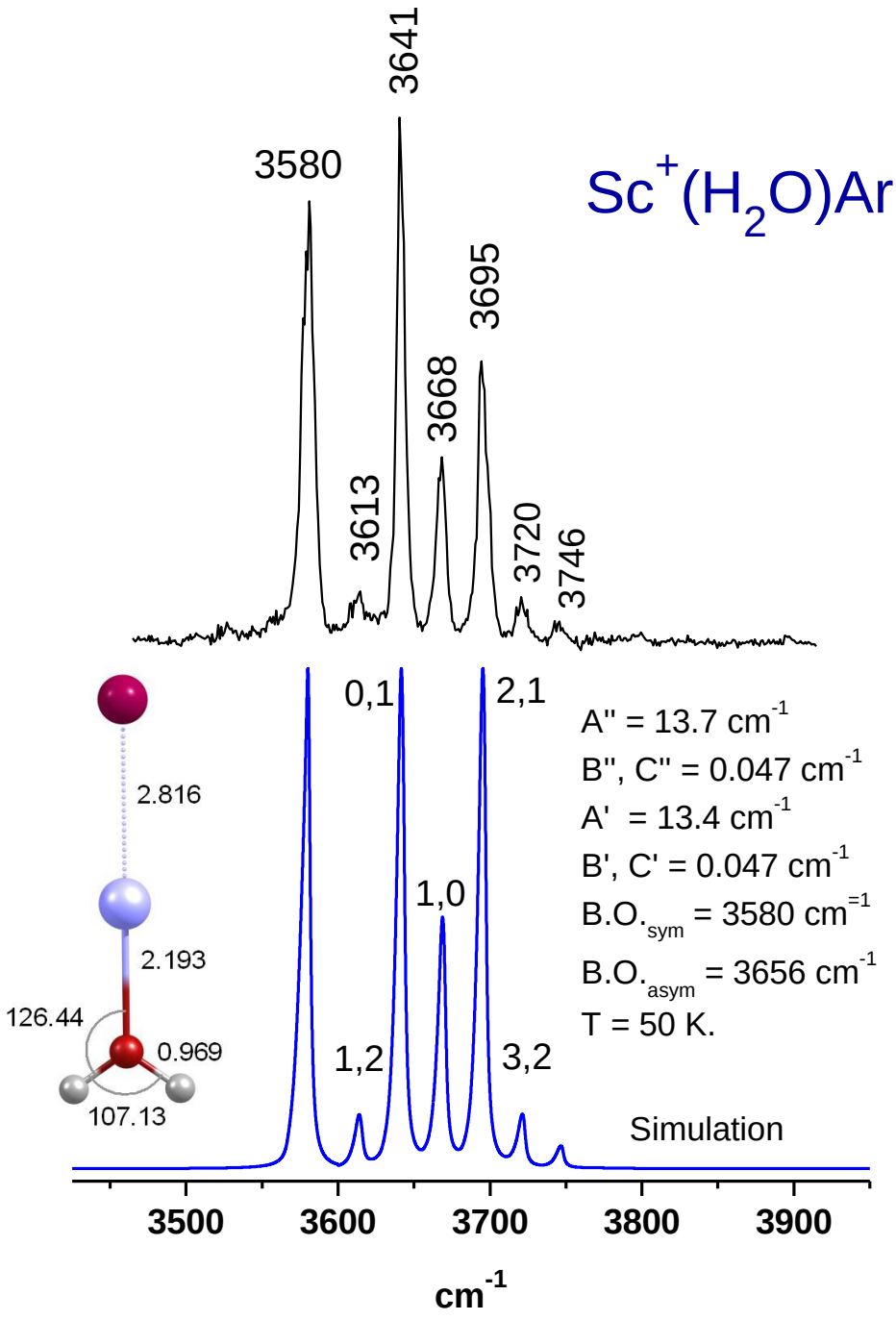

Figure 3.1: The infrared photodissociation spectrum measured for the $Sc^+(H_2O)Ar$ complex (upper trace). The lower trace shows the simulated spectrum. The inset structure of $Sc^+(H_2O)Ar$ is obtained from theory. Rotational constants, band origins for the symmetric and asymmetric stretches and rotational temperature obtained from the observed and simulated spectra are also shown in the inset.

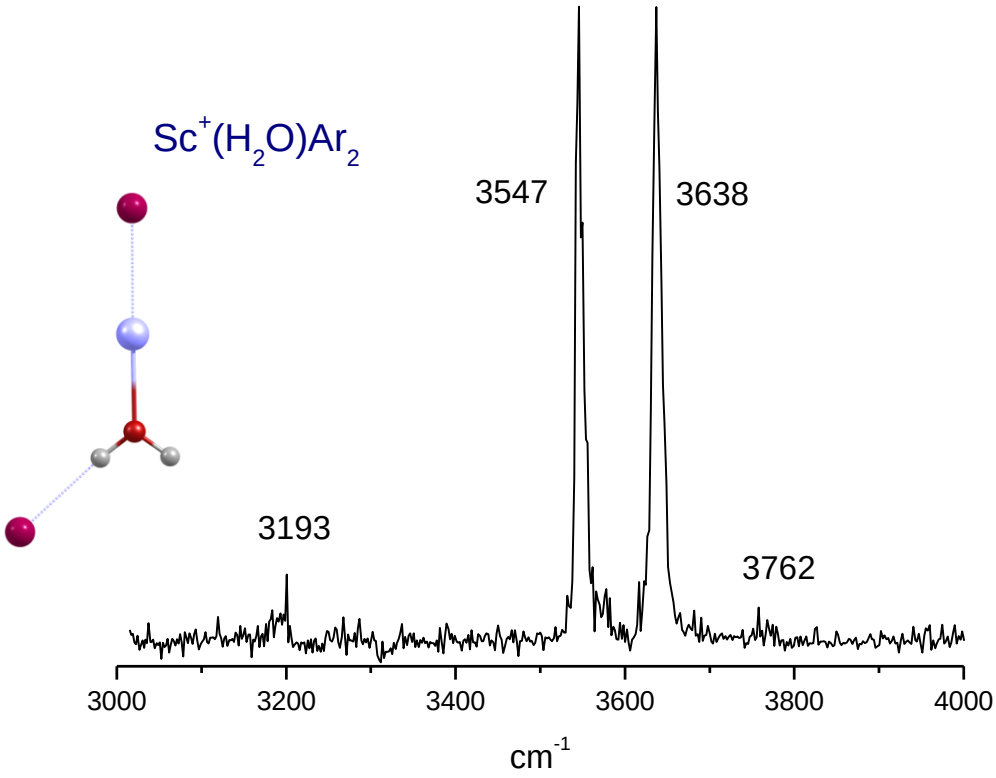

Figure 3.2: The spectrum of $Sc^{+}(H_2O)Ar_2$. Partially resolved rotational structure is lost because heavy atom argon binds to water.

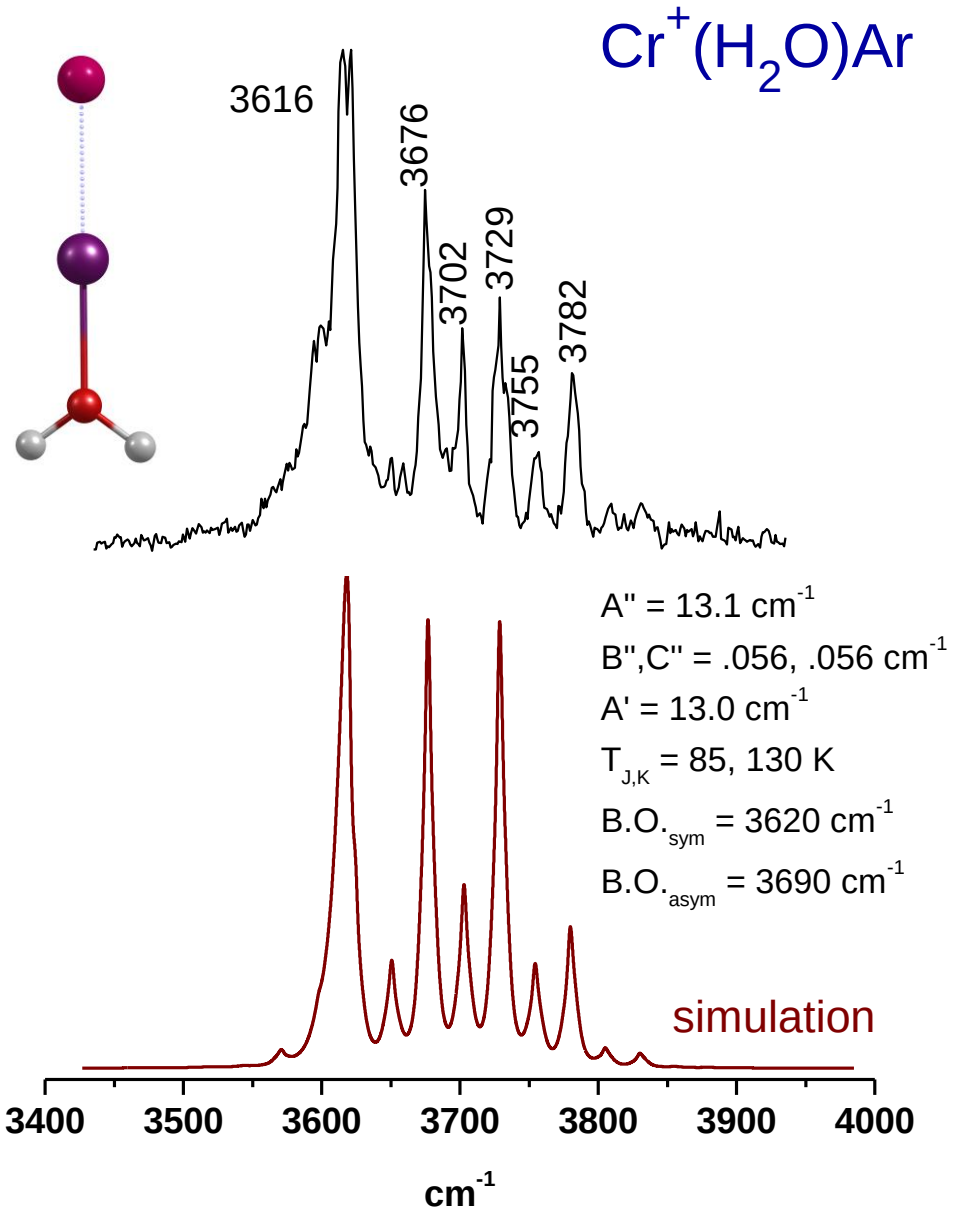

Figure 3.3: The photodissociation spectrum measured for the $Cr^+(H_2O)Ar$ complex (upper trace). The lower trace shows the simulated spectrum. Rotational constants, band origins of the symmetric and asymmetric stretches and rotational temperature obtained from the observed and simulated spectra are also shown in the inset.

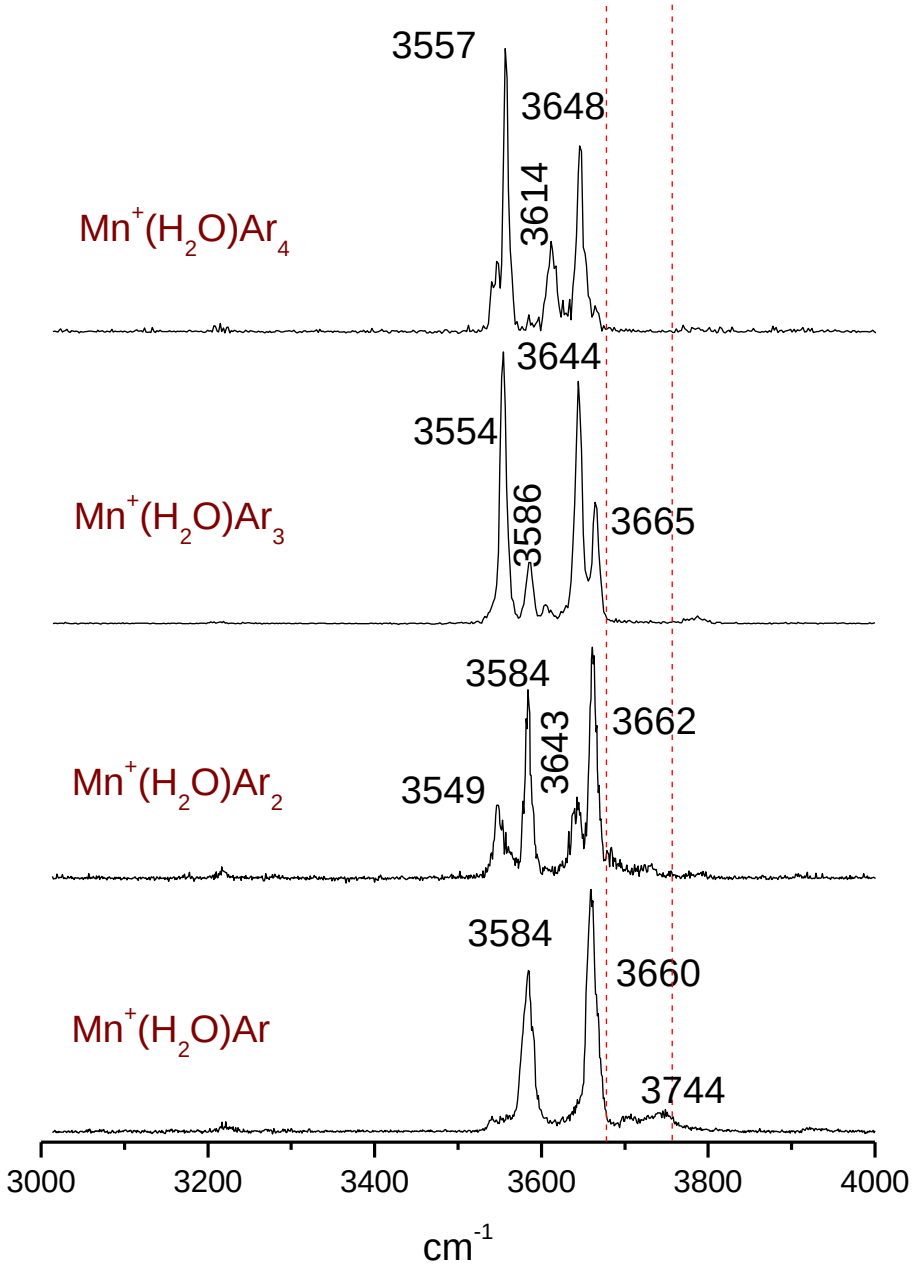

Figure 3.4: The infrared spectra of the $Mn^+(H_2O)Ar_n$ complexes. The red dashed lines correspond to the symmetric and asymmetric stretches of the isolated water molecule (3657 and 3756 cm^{-1} respectively).

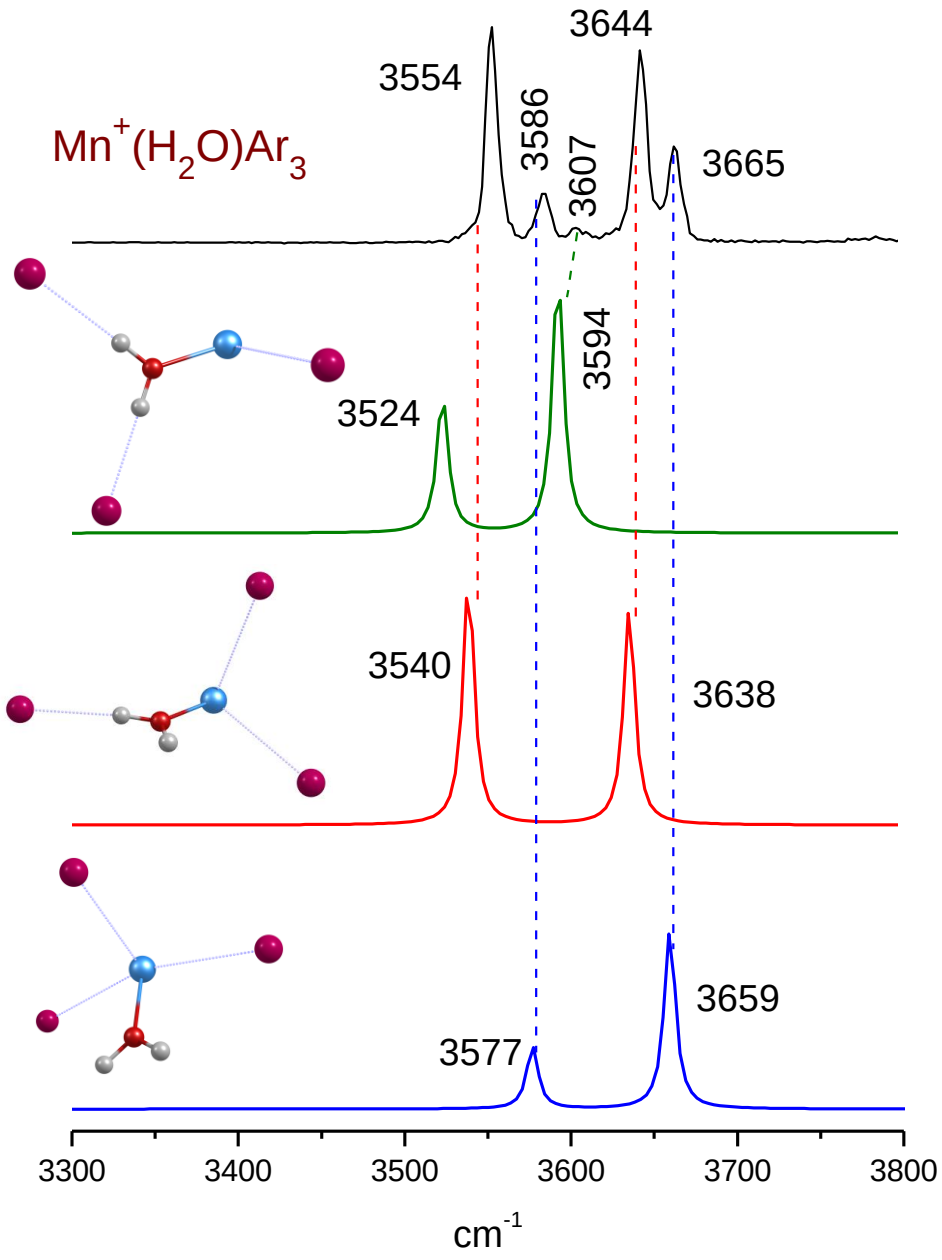

Figure 3.5: The spectrum of the $Mn^+(H_2O)Ar_3$ complex (upper trace). The lower three traces are predicted spectra for $Ar_3Mn^+(H_2O)$ (isomer 3a), $Ar_2Mn^+(H_2O)Ar$ (isomer 3b) and $ArMn^+(H_2O)Ar_2$(isomer 3c). The correspondence between peaks is shown with dashed lines (blue, red and green).

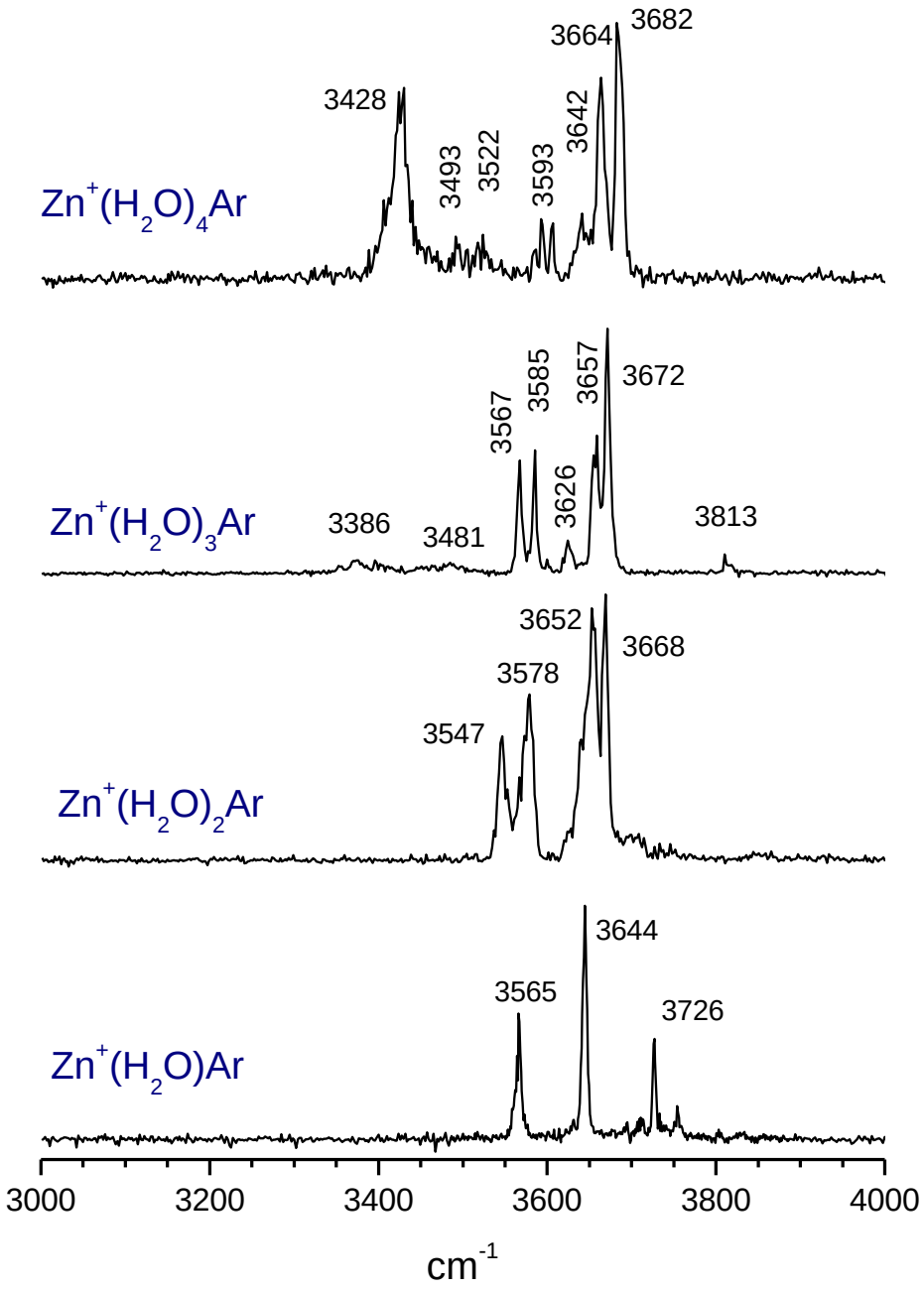

Figure 3.6: The photodissociation spectra measured for the $Zn^+(H_2O)_nAr$ complexes (n = 1-4) in the mass channel corresponding to the elimination of argon.

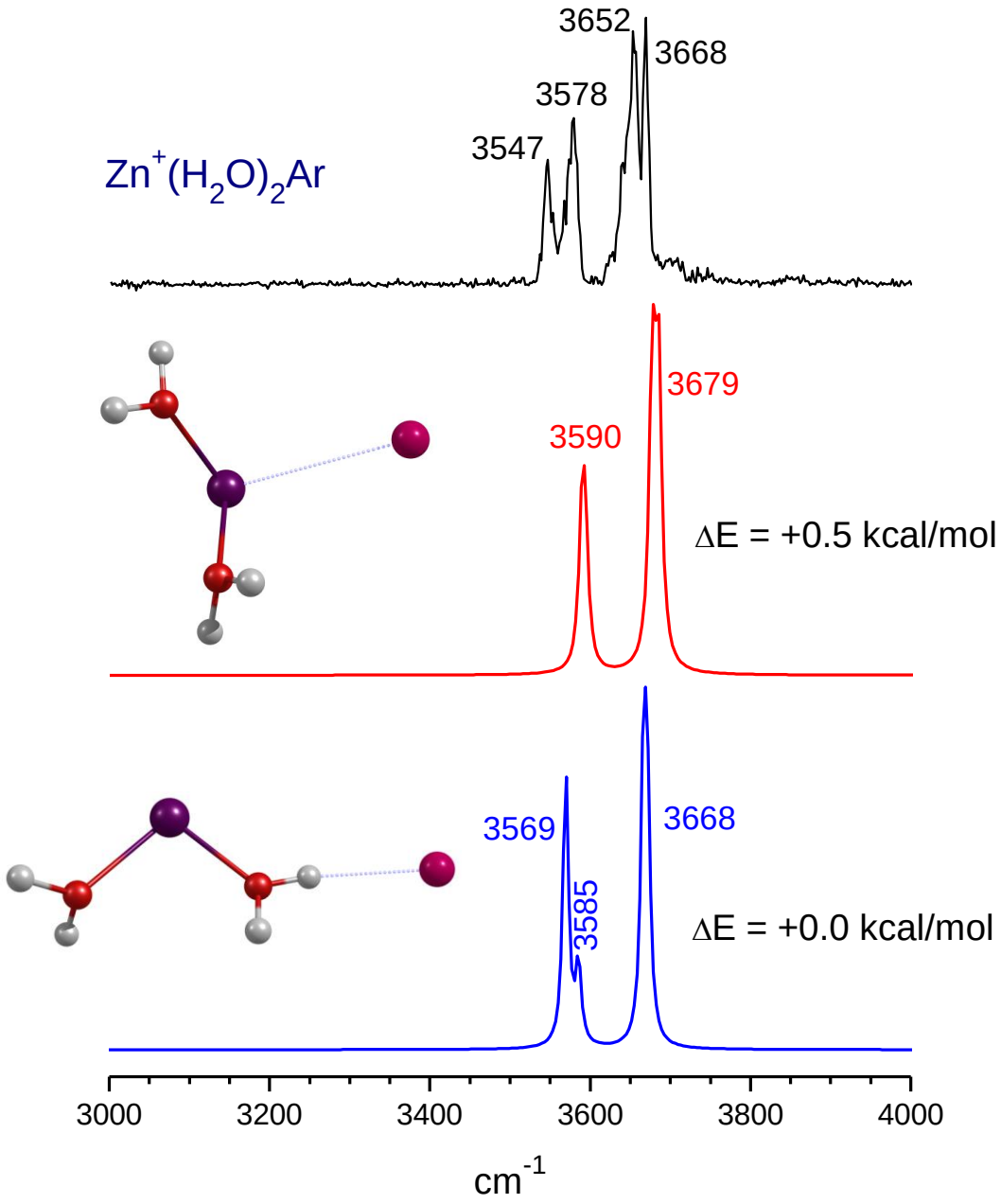

Figure 3.7: The upper trace shows the spectrum of $Zn^{+}(H_2O)_2Ar$. The lower two traces show the predicted spectra corresponding to the different isomers. The structures and relative energies of the isomers are shown in the inset.

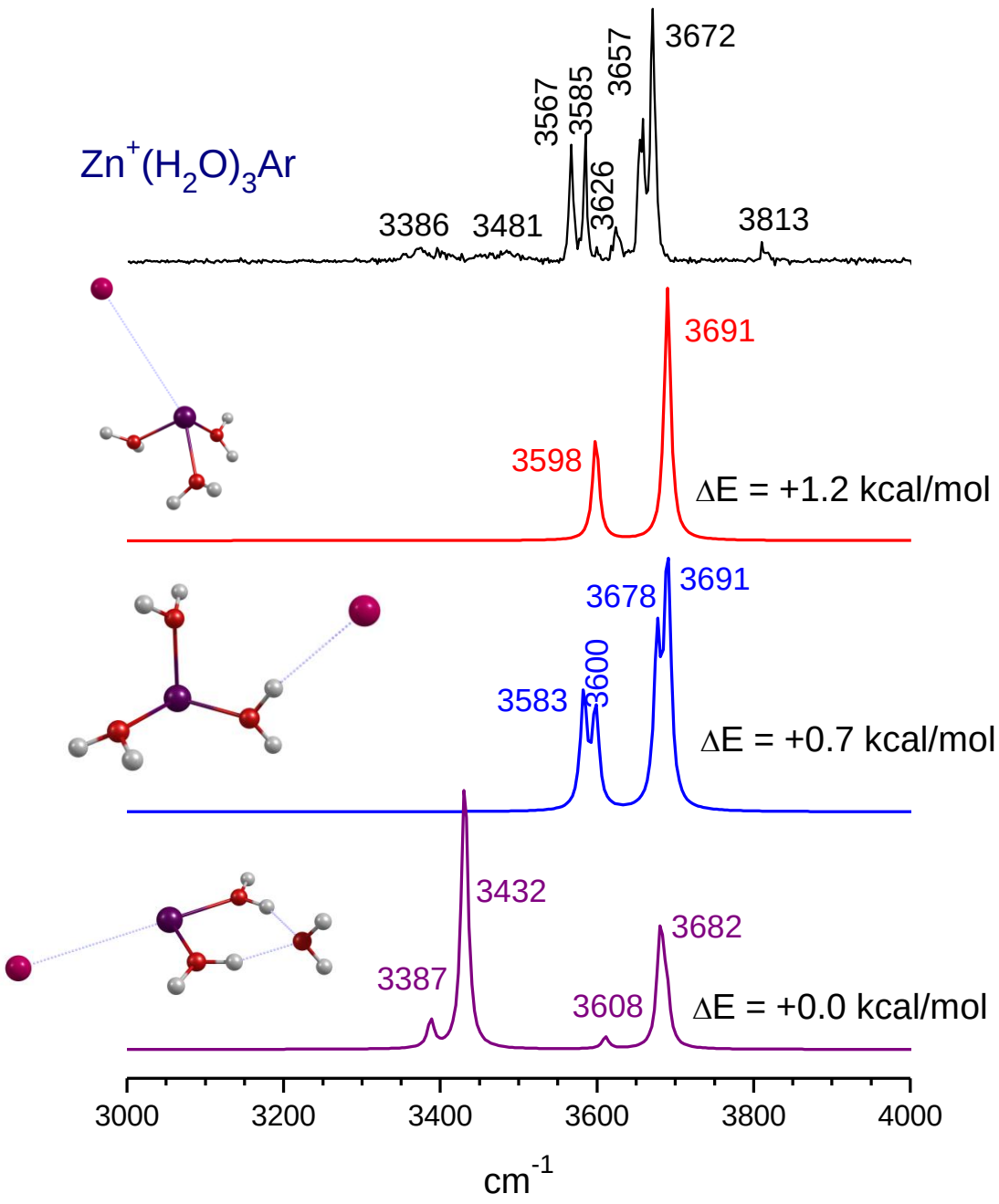

Figure 3.8: The spectrum measured for the $Zn^{+}(H_2O)_3Ar$ complex (upper trace). Lower three traces show the predicted spectra for three low energy isomers. The structures and relative energies of different isomers are shown in the inset.

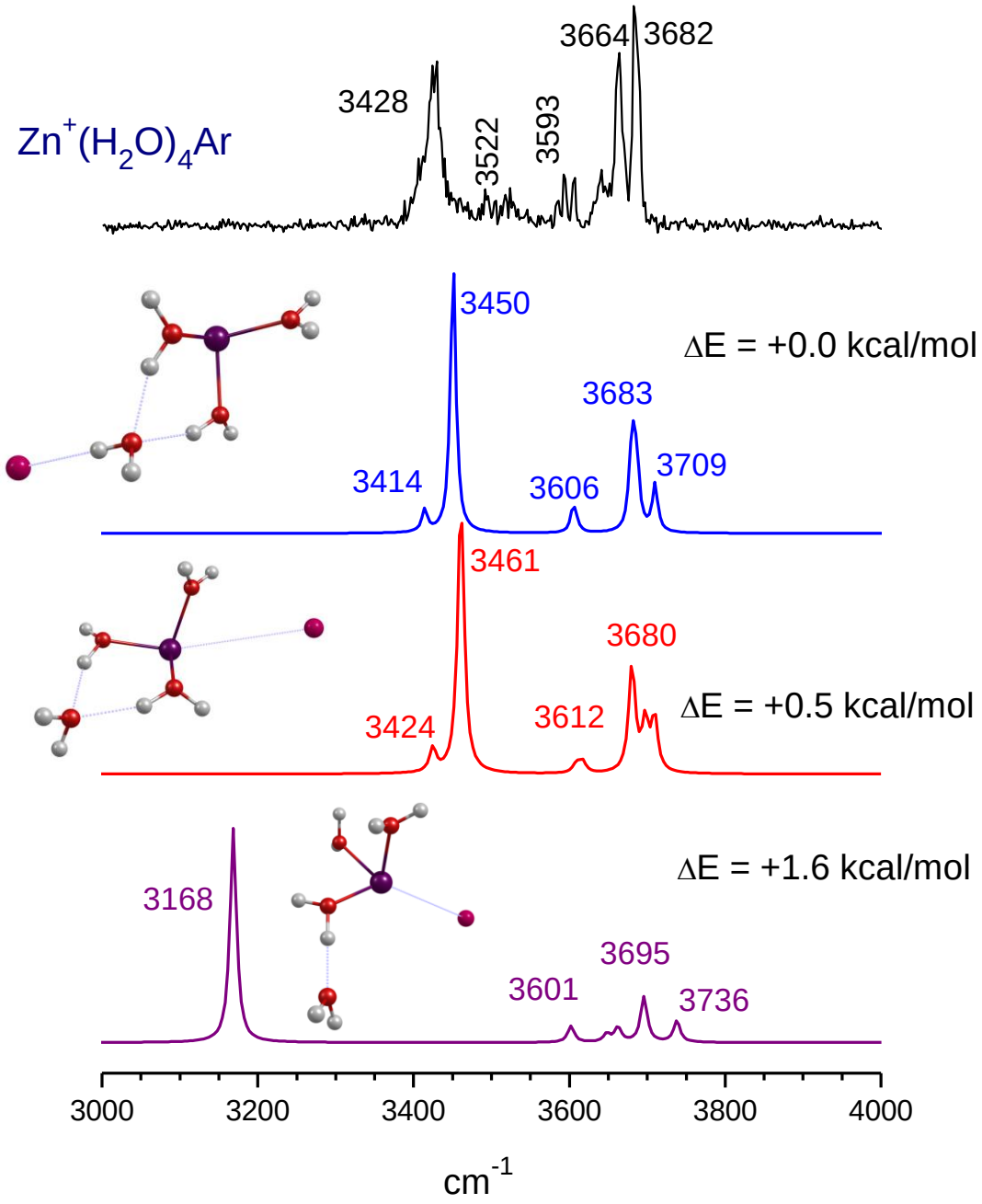

Figure 3.9: The upper trace shows the spectrum of $Zn^{+}(H_2O)_4Ar$. The lower traces show the predicted spectra corresponding to the different isomers. The structures and relative energies of the isomers are shown in the inset.

CHAPTER 4

DOUBLY CHARGED EARLY TRANSITION METAL ION-WATER COMPLEXES

4.1 Introduction

Multiply charged ion-molecule complexes are more difficult to produce in the gas phase due to their intrinsic instability with respect to charge transfer. The second ionization energy of the metal atom is often greater than the first ionization energy of water (12.6 eV).[66] Therefore, charge transfer from the doubly charged metal to the water molecule can occur producing two singly charged ions which repel each other. Metal ions in higher charge states also have this critical problem. However, asymptotically unstable complexes may be stabilized by the strong Coulombic attraction which dominates at short bonding distances. Under some conditions the ions can be trapped in the potential energy surface relative to the curve crossing between the $M^{2+} + H_2O$ and $M^+ + H_2O^+$ potentials.[60, 62-64] One of the widely applied methods used to produce multiply charged ions in the gas phase is electrospray ionization, where $M^{n+}(H_2O)_m$ ions in solution are taken directly into the gas phase to avoid charge transfer.[35,61,67] The laser vaporization technique also has proven to be useful to produce doubly charged metal ion complexes under certain conditions, including asymptotically unstable systems.[60,63,64,68] The advantage of the laser vaporization source over electrospray ionization is that M^{2+}-(H_2O) complexes can be produced directly in the gas phase without any desolvation process. This makes it possible to study the interactions of a metal ion with a single water molecule.

With any of these sources, though, ion densities of multiply charged complexes are much lower than those available for singly charged species, and therefore spectroscopic measurements on these systems are more challenging. In the present work, we describe the infrared photodissociation spectroscopic studies of argon "tagged" $M^{2+}(H_2O)$ complexes (M = Sc, V, Cr, Mn) produced by laser vaporization. A comparative study investigating the effect of different metal ions in these complexes will be discussed. A comparison between singly and doubly charged metal-water complexes will also be discussed investigating the role of charge in ion solvation.

4.2 Experimental

$M^{2+}(H_2O)Ar_n$ complexes are produced in a pulsed-nozzle laser vaporization source which has been described in detail in Chapter 2. In the supersonic expansion, argon is used as buffer gas and a few drops of water are added into the gas flow to produce mixed complexes. The metal rod is vaporized by the third harmonic (355 nm) of a Nd:YAG laser. Mass-selected ions are investigated with infrared photodissociation spectroscopy in the O-H stretching region using an infrared optical parametric oscillator/amplifier laser system (OPO/OPA; LaserVision, Inc.) pumped by a Nd:YAG laser (Continuum 8010). Laser excitation occurs in the turning region of the reflectron field, where ion optics and pulse timing are adjusted to obtain optimized spatial and temporal overlap between the laser and the ion beam. Resonant single photon absorption leads to elimination of argon from $M^{2+}(H_2O)Ar_n$ species. The fragment ion intensity is recorded as a function of the infrared laser frequency using a digital oscilloscope connected to a computer.

Density functional theory (DFT) is employed to investigate the structures and vibrational spectra of the $M^{2+}(H_2O)Ar_n$ (n=0-7) complexes for comparison to the experiment. These computations use the B3LYP functional in the Gaussian 03W package and the 6-311+G(d,p) basis set.[138] The computed vibrational frequencies are scaled by a factor of 0.9575, which is the recommended value for the B3LYP/6-311+G (d, p) method.[139]

4.3 Results and Discussion

In this section, we first discuss the infrared spectroscopy of the $V^{2+}(H_2O)Ar_n$ complexes as a prototype, which is helpful to describe the spectra of other $M^{2+}(H_2O)Ar_n$ systems. One of the main goals of studying doubly charged metal-water complexes is to compare the properties of these systems with those of singly charged species. In order to do a comparison between singly and doubly charged ions we also show the infrared spectrum of the $V^{+}(H_2O)Ar_2$ complex. Infrared photodissociation studies of first row transition metal cation-water complexes have been described in detail in Chapter 3. We typically use slightly different experimental conditions for producing doubly charged complexes than those for singly charged ions. Figure 4.1 shows the mass spectrum of $V^{+}(H_2O)Ar_n$ produced in the laser vaporization source optimizing the conditions for singly charged ions. The most intense peak in the mass spectrum corresponds to the V^+ and the progression of $V^{+}(Ar)_n$ and $V^{+}(H_2O)Ar_n$ are also shown. Figure 4.2 shows the mass spectrum of singly and doubly charged vanadium-water-argon complexes in the same source, but now the conditions are optimized for doubly charged complexes. The crucial change in the experimental condition is higher vaporization laser power. This is typically 5-10 mJ/pulse for doubly charged ions, compared to 1-3 mJ/pulse for singly charged species. The backing pressure of the buffer gas was also higher, typically 200 p.s.i., whereas 50-100 p.s.i was used for

singly charged ions. The higher backing pressure of the buffer gas partially compensates for the higher internal energies of the ions resulting from the higher vaporization laser power. Another key factor for efficient production of doubly charged complexes is the vaporization laser timing with respect to the gas pulse. This timing is also significantly different from that used to produce singly charged ions. It is clearly seen from Figure 4.2 that the ion densities of $V^{2+}(H_2O)Ar_n$ are much smaller than those of $V^{+}(H_2O)Ar_n$.

Since the ion densities are too low to perform absorption spectroscopy, these ions are probed with infrared photodissociation spectroscopy. The binding energy of $V^{+}(H_2O)$ was measured by Armentrout and co-workers to be 35.8 kcal/mol.[28] Since the binding energy is more than the photon energy in the O-H stretch region (3000-4000 cm^{-1}), photodissociation is not possible with a single photon. To our knowledge, the binding energy of the $V^{2+}(H_2O)$ complex has not been measured. We compute this value to be +82.0 kcal/mol which is much greater than that of the $V^{+}(H_2O)$ complex. The argon binding energy to the $V^{2+}(H_2O)$ has also not been measured. We compute these values for the $V^{2+}(H_2O)Ar_{1-7}$ complexes to be 17.6, 16.0, 15.6, 10.9, 9.4, 2.8 and 2.7 kcal/mol respectively. Although the computed binding energies are not expected to be quantitative, we assume that the binding energies of first one or two argon atoms to the metal dication-water complex is too high to observe any photofragmentation because we only begin to detect fragmentation from the $V^{2+}(H_2O)Ar_2$ complex.

Figure 4.3 shows the infrared spectrum of $V^{+}(H_2O)Ar_2$ (upper trace) and $V^{2+}(H_2O)Ar_4$ (lower trace) obtained by monitoring the mass channel corresponding to argon elimination. The inset structures are those obtained from theory and the red dashed lines correspond to the symmetric and asymmetric stretches of the free water molecule (3657 and 3756 respectively).[66] The spectrum of $V^{+}(H_2O)Ar_2$ has two peaks at 3611 and 3683 cm^{-1} corresponding to the

symmetric and asymmetric O-H stretches. Theory for this complex predicts these stretches at 3597 and 3668 cm^{-1}, which is in good agreement with the observed frequencies. For the $V^{2+}(H_2O)Ar_4$ complex, these stretches are shifted to lower frequencies, at 3546 and 3600 cm^{-1} respectively, with a different relative intensity pattern. In both the vanadium cation- and dication-water systems the O-H stretches shift to lower frequencies compared to the free water stretches. The red shifts in O-H stretching frequencies in a metal ion-water complex have been discussed in detail in chapter 3 and it is one of the general features of these systems.[41] The red shift is caused by polarization of the lone pair of electrons on the oxygen induced by the metal cation. The non-bonding molecular orbital of the water accommodating the lone pair has some partial bonding character along the O-H bonds. Polarization of the electron density from this orbital also removes some density from the O-H bonds resulting in longer and weaker O-H bonds. This accounts for the red shifts in O-H stretching frequencies. As these red shifts are essentially an effect due to the polarization of water, doubly charged ions shift the O-H stretching frequencies more than singly charged ions.

Another interesting feature of the spectra of cation-water systems is that the intensity pattern for the symmetric and asymmetric stretches in these systems is different from those in the isolated water molecule. The intensity ratio of these stretches in the free water molecule is roughly 1:18, whereas for cation-water systems this ratio is close to 1:1 or 1:2. The intensity of an infrared vibrational band depends on the dipole moment derivative. The symmetric stretch in a cation-water system is a parallel type vibration which modulates the charge density more effectively along the C_2 axis than the perpendicular type asymmetric stretch. This greater modulation of charge density in the symmetric stretch leads to a larger change in dynamical dipole moment than that of the asymmetric stretch. Therefore, in a cation-water system the

symmetric stretch gains more intensity than the asymmetric stretch. For doubly charged complexes the symmetric stretch is twice as strong as the asymmetric stretch because the extent of the polarization is even greater, which leads to an even greater change in dynamic dipole for the symmetric stretch. Figure 4.3 shows a nice example comparing the general features of spectra of cation- and dication-water systems. As shown, the O-H stretches are 111 and 157 cm^{-1} red shifted for the $V^{2+}(H_2O)Ar_4$ complex compared to the free water stretches, whereas these shifts are 46 and 73 cm^{-1} respectively for $V^{+}(H_2O)Ar_2$. The intensity ratio of the symmetric and asymmetric stretches also switches from 1:2 for $V^{+}(H_2O)Ar_2$ to 2:1 for $V^{2+}(H_2O)Ar_4$.

Figure 4.4 and 4.5 show the spectra of the $V^{2+}(H_2O)Ar_n$ (n=2-7) complexes in the O-H stretch region. The inset structures are those obtained from theory. Table 4.1 lists observed vibrational frequencies and scaled harmonic frequencies along with intensities predicted by theory. As shown in Figure 4.4, the spectrum of $V^{2+}(H_2O)Ar_2$ has a peak around 3501 cm^{-1} with an indication of a couple of small peaks in the high frequency region on top of an overall noisy feature. The spectrum is noisier than those of other sizes since the argon binding is probably still more than the single photon energy, which leads to an overall poor dissociation yield from this species. $V^{2+}(H_2O)Ar_3$ shows two distinct peaks with roughly a 2:1 intensity ratio. The intense peak at 3524 cm^{-1} is blue shifted from the peak observed for the $V^{2+}(H_2O)Ar_2$ complex. The other less intense peak for $V^{2+}(H_2O)Ar_3$ is observed at 3582 cm^{-1}. The peaks are again shifted to the blue at 3546 and 3600 cm^{-1} in the spectrum of $V^{2+}(H_2O)Ar_4$.

The spectrum of $V^{2+}(H_2O)Ar_5$ is more complicated than those of the all other sizes (Figure 4.5). It has a strong peak at 3561 cm^{-1} and three less intense and broad peaks are observed at 3598, 3694 and 3713 cm^{-1}. For the $V^{2+}(H_2O)Ar_6$ species, two sharp peaks are observed, one at 3448 cm^{-1} and another at 3604 cm^{-1}. The spectrum also shows a weak band

near 3280 cm^{-1}. There are no high frequency peaks observed for the $V^{2+}(H_2O)Ar_7$ complex. The spectrum shows three distinct peaks at 3456, 3497 and 3521 cm^{-1} on top of a broad resonance ranging from 3430-3530 cm^{-1}.

The assignments of the peaks can be done with the help of theoretical calculations for the $V^{2+}(H_2O)Ar_{1-7}$ complexes. It is straightforward now that the two peaks at 3524 and 3582 cm^{-1} in the spectrum of $V^{2+}(H_2O)Ar_3$ are the symmetric and asymmetric O-H stretches respectively, where 3524 cm^{-1} peak is roughly twice as intense as the 3582 cm^{-1} peak, consistent with the general feature of these systems. Evidently, these peaks are red shifted by an amount of 133 and 174 cm^{-1} respectively from the free water stretches (3657 and 3756 cm^{-1} respectively). Theory predicts two peaks at 3522 and 3577 cm^{-1} which are within ~10 cm^{-1} of the experimental frequencies. The O-H stretches for $V^{2+}(H_2O)Ar_4$ are observed at 3546 and 3600 cm^{-1}, which are less red shifted relative to the corresponding stretches for $V^{2+}(H_2O)Ar_3$. The O-H bonds regain some of the electron density due to the presence of extra argon which reduces the charge-induced dipole interactions between the metal ion and water. The computed O-H bond lengths in the $V^{2+}(H_2O)Ar_4$ complex (0.973 Å) are slightly shorter than those of the $V^{2+}(H_2O)Ar_3$ complex (0.974 Å). Predicted frequencies for those stretches of the $V^{2+}(H_2O)Ar_4$ system are 3537 and 3593 cm^{-1} respectively, which again agree quite well with the experiment.

Having assigned the spectra of these two cluster sizes, we can now go back and assign the relatively complicated spectra of $V^{2+}(H_2O)Ar_2$ and $V^{2+}(H_2O)Ar_5$. For both the species, there are strong peaks at 3501 and 3561 cm^{-1}, roughly where the symmetric stretches are predicted and we assign these peaks to the symmetric stretches. The asymmetric stretches are predicted at 3531 cm^{-1} for $V^{2+}(H_2O)Ar_2$ and 3612 cm^{-1} for $V^{2+}(H_2O)Ar_5$ respectively, but for the $V^{2+}(H_2O)Ar_2$ complex no clear peak is observed and the spectrum of $V^{2+}(H_2O)Ar_5$ shows three broad bumps

in the high frequency region. Fortunately this pattern is not totally unfamiliar to us. The spectra of singly charged metal-water-argon complexes often show several peaks in the high frequency region instead of two peaks corresponding to symmetric and asymmetric stretches and this pattern was described in detail in chapter 3. These bands arise from the two vibrational bands and their partially resolved rotational structure.[40, 41] In these cation-water systems, argon lies on the C_2 axis giving the overall structure a C_{2v} symmetry, where only the light hydrogen masses are off the C_2 axis and contribute to the moment of inertia along this axis. As a result, the rotational constant along this axis is close to 13-14 cm^{-1} and partially resolved rotational bands can be seen in our low resolution spectra. The peaks observed in these spectra have roughly a 1:3 for K= even:odd intensity ratio following the nuclear spin statistics due to the presence of two identical hydrogen atoms. Simulation of these bands also provides us a rough idea about the rotational temperature, which is typically 15-50 K for cation-water systems.[41] However, doubly charged complexes are produced with greater internal energies since we have to use warmer experimental conditions than those used for singly charged ions. The intensities of the bands are largely influenced by the temperature of the ions produced and therefore the 3:1 intensity alteration can be lost. For some other metal cation water argon complexes, if argon is off the C_2-axis, rotational constant is much smaller and the asymmetric stretch appear as a single band. In some cases, low frequency torsional vibration arising from hydrogen motion can combine with the asymmetric stretch which appears just above the O-H stretches.[41g] In some other scenario, where multiple argon is present and the angular potential is smooth, internal rotation of water with respect to the whole complex can give rise to rotational structure. If the internal rotation is hindered, an intermediate rotation/torsion may produce irregular structure for the asymmetric stretch. Therefore, it makes sense that the three peaks at 3598, 3663 and 3713 cm^{-1} for

$V^{2+}(H_2O)Ar_5$ arise due to the hindered internal rotation. The spectrum of $V^{2+}(H_2O)Ar_2$ shows a slight indication of similar structure in the high frequency region, but asymmetric stretch is not clearly seen because of the poor signal to noise.

The spectrum of the $V^{2+}(H_2O)Ar_6$ complex changes abruptly from that of $V^{2+}(H_2O)Ar_5$, and two intense sharp peaks are observed at 3448 and 3604 cm^{-1}. The computed structure for $V^{2+}(H_2O)Ar_6$ predicts that the first coordination shell of V^{2+} is filled with one water and five argons and the remaining argon interacts with one of the O-H bonds. This argon interaction shifts both the O-H stretches towards lower frequencies. The symmetric and asymmetric stretches are predicted at 3419 and 3593 cm^{-1} respectively, which agrees well with the observed frequencies. The argon interaction with water also restricts its internal rotation and therefore the partially resolved rotational structure is not seen in the spectrum. A relatively weak band at 3281 cm^{-1} was also observed for this species and we believe that this peak arises from an $H\text{-}V^{3+}\text{-}OH^-$ species resulting from an insertion reaction. The overall charge for this complex is still +2 and a small amount of this reaction product may be produced together with the $V^{2+}(H_2O)Ar_6$. Theory predicts that the anionic O-H stretch of the $H\text{-}V^{3+}\text{-}OH^-$ complex should appear at 3263 cm^{-1}, which is in the neighborhood of the observed band. The spectrum of $V^{2+}(H_2O)Ar_7$ again abruptly changes from that of the $V^{2+}(H_2O)Ar_6$ complex. It does not have a free O-H peak in the high frequency region but there are three or four peaks observed on top of a broad resonance ranging from 3440-3540 cm^{-1}. This indicates that both the O-H bonds interact with argons resulting in red shifts in the O-H frequencies.

Having discussed the spectra of the $V^{2+}(H_2O)Ar_n$ complexes, we can now describe the spectra of the other $M^{2+}(H_2O)Ar_n$ complexes where M^{2+}= Sc, Cr and Mn. In order to compare these species the spectra of $M^{2+}(H_2O)Ar_n$ complexes are shown in Figures 4.5, 4.6, 4.8 and 4.9.

Figures are made keeping the number of argon atoms constant in each case and varying the metal to show the effect of different metals in the spectra of these complexes. However, we do not have spectra for all the argon sizes for $Mn^{2+}(H_2O)$ due to mass coincidences with some prominent peaks. Table 4.2 and 4.3 list the observed and computed frequencies for $Cr^{2+}(H_2O)Ar_n$ and $Sc^{2+}(H_2O)Ar_n$ complexes. These tables also list the frequencies of corresponding singly charged ions for a comparison. Figure 4.5 shows the spectra of $M^{2+}(H_2O)Ar_3$. The inset structures are those obtained from theory and the red dashed lines correspond to the symmetric and asymmetric stretches of free water. The computed structures show that argon atoms prefer to bind to the metal ion rather than to the O-H bonds. On the other hand, in some singly charged metal-water systems argon binds to the O-H bond and these isomers are found to have lower energy than the one in which argon binds to the metal ion.[51c] As shown in figure 4.5, $V^{2+}(H_2O)Ar_3$ shows two peaks at 3524 and 3584 cm^{-1} corresponding to the symmetric and asymmetric stretches, whereas $Sc^{2+}(H_2O)Ar_3$ and $Cr^{2+}(H_2O)Ar_3$ complexes each have only one strong band at 3528 and 3512 cm^{-1} respectively. These bands are assigned to the symmetric O-H stretches. The asymmetric stretches are not well resolved since the argon binding energy to these metal ions is still too high and only ions with higher internal energies can fragment giving a overall poor dissociation yield. A similar situation was described in detail previously for the spectrum of $V^{2+}(H_2O)Ar_2$. Although the asymmetric stretches are not well resolved to compare the red shifts among those complexes, we note that the relative red shift in the symmetric stretches for these three metal ions are within 15 cm^{-1} of each other. In other words, O-H stretching frequencies are about the same for these three different metal ions. This is a very different result than that obtained for singly charged complexes, where Sc^{+}, which has the lowest number of valence shell electrons, shifts the O-H stretching frequencies the most.[51b]

Figure 4.6 shows the infrared spectra of $M^{2+}(H_2O)Ar_4$. The interesting feature to note here is that except for Cr^{2+}, all the metal ions show two clear peaks corresponding to the symmetric and asymmetric stretches. The peaks in the high frequency region of $Cr^{2+}(H_2O)Ar_4$ complex arise from the partially resolved rotational structures of the asymmetric stretch vibrational band associated with internal rotation of water. For the $Cr^{2+}(H_2O)Ar_4$ complex the spectrum is simulated using a program *Asyrotwin* and Figure 4.7 shows the comparison between simulated and observed spectrum. The rotational constants and temperatures obtained from the simulation and the experiment are also shown in the inset. These rotational constants do not correspond to the rotation of the whole complex, but from the internal rotation of water. The structural parameters obtained from the simulation are again shown in Table 4.4 compared to those obtained for the $Cr^{+}(H_2O)Ar$ complex (discussed in detail in chapter 3). As shown in Table 4.4, doubly charged complexes have lower rotational constants than those of singly charged complexes. The simulation of the spectrum of $Cr^{2+}(H_2O)Ar_4$ also provides us with a rough estimate of the temperature of the ions produced. For the doubly charged chromium-water complex this is 250K, while for the singly charged ion it is 130 K. With the help of observed and simulated spectra we can also calculate the H-O-H bond angle (detailed procedure discussed in chapter 3) and this angle is larger for $Cr^{2+}(H_2O)Ar_4$ (113.5^{o}) than it is for $Cr^{+}(H_2O)Ar$ (111.1^{o}). This is consistent with the fact that the lone pair of water is more polarized by the doubly charged metal leading to a greater H-O-H bond angle.

Figure 4.8 shows the spectra of $M^{2+}(H_2O)Ar_5$. For all these complexes the symmetric stretches appear as single bands and the asymmetric stretches appear as unresolved rotational bands in the high frequency region. Again all the red shifts are within a few wavenumbers of

each other. The relative red shifts for Sc^{2+} and Cr^{2+} is 2 cm^{-1}, and V^{2+} shows ~10 cm^{-1} relative shift compared to those for Sc^{2+} and Cr^{2+}.

Figure 4.9 shows the spectra of $M^{2+}(H_2O)Ar_6$ complexes where M= Sc, V and Cr. The spectra for all these $M^{2+}(H_2O)Ar_6$ complexes change abruptly from those of the $M^{2+}(H_2O)Ar_5$ species. Computed structures for these complexes are shown in the insets of Figure 4.9 and it is clear from these that the coordination of M^{2+} is filled up with six ligands (one water and five argons) and the remaining argon is interacting with the O-H. The argon interaction with the O-H shifts stretching frequencies to the red and also restricts the internal rotation of water, causing the rotational structure to disappear. The other interesting aspect of these spectra is that all the $M^{2+}(H_2O)Ar_n$ complexes show a small peak near 3265-3280 cm^{-1}. These peaks are believed to arise from a small amount of reaction product between M^{2+} and H_2O forming an $H\text{-}M^{3+}\text{-}OH^-$ species. The reactions of early transition metals with water are well known, and theory predicts that the anionic OH stretches of $H\text{-}M^{3+}\text{-}OH^-$ complexes should appear very close to the observed peak. However, we note that these reaction products are only seen in higher cluster sizes. Solvation of the metal with a larger number of argons apparently causes the reaction.

Having described the spectra of $M^{2+}(H_2O)Ar_n$ complexes, we can now consider the effect of the number of argon atoms on the red shifts of stretching frequencies for different metals. However, it is not possible to do so for both the symmetric and asymmetric stretches since for some of the argon sizes the asymmetric stretches do not appear. Figure 4.10 shows a plot describing the red shifts of the symmetric stretches that we observed in our spectra for different metal dication water–$(argon)_n$ systems where n=3, 4 and 5. As shown, more argon on a metal ion center dilutes the charge on it and smaller red shifts in the O-H frequencies are observed.

We also notice that the difference in red shifts in different $M^{2+}(H_2O)Ar_n$ systems where M= Sc, V, and Cr and Ar = 3-5 are within 10 cm^{-1} of each other.

The discussion above provides us with an idea about the shifts in O-H stretches influenced by the number of argon atoms. For the $M^{2+}(H_2O)Ar_n$ complexes, argons prefer to bind to the metal center and the O-H stretching frequencies are not directly perturbed. However, it is useful to compare the red shifts in these dication-water complexes without the influence of argon atoms. Since we have to tag our complexes in order for photodissociation to occur, it is not possible to do this comparison directly from our spectra. The other way to do this is to compare the theoretically obtained frequencies for these metal-water systems. Therefore, we use theory to validate our available experimental results, and with the help of theory we can compare the red shifts in stretching frequencies for metal dication-water complexes. Table 4.4 lists the symmetric and asymmetric stretch shifts obtained from theory for M^{n+}-(H_2O) complexes where M= Sc, V, Cr and Mn and n=1, 2. This table also contains M^{n+}-O bond lengths as well as O-H bond lengths computed from theory. We note that the red shifts are larger for dication-water systems than those for mono-cation-water systems since the extent of polarization induced by the metal dication is greater. As a result, M^{2+}-O bond lengths are shorter and O-H bond lengths are longer for the doubly charged ions. The red shifts for transition metal cation-water systems are typically 30-100 cm^{-1},[41] where dication-water systems show red shifts ranging from 190-280 cm^{-1}. However, for singly charged systems the red shifts depend on the number of valence electrons on the metals, i.e. scandium cation-water system shows one of the largest red shifts among first row transition metal-water systems since it has fewer number of valence shell electrons. On the other hand, for the doubly charged systems, removing one extra electron form the valence shell

and orbital contraction resulting from greater charge makes these systems almost identical. Therefore, the red shifts for these complexes are remarkably similar to each other.

4.4 Conclusions

$M^{2+}(H_2O)Ar_n$ complexes **(**M = Sc, V, Cr and Mn) are produced in a pulsed laser vaporization source. Mass-selected ions are analyzed with infrared photodissociation spectroscopy in the O-H stretching region. Doubly charged ions shift the O-H stretches to lower frequencies than those of the corresponding singly charged complexes. The symmetric O-H stretch gains more intensity than that of the asymmetric stretch due to greater change in dynamical dipole. The intensity ratio of these two stretches becomes ~1:1 for singly charged complexes and ~2:1 for doubly charged species. Partially resolved spectra for some singly and doubly charged complexes provide rotational constants and doubly charged complexes are found to have lower rotational constants than those of the singly charged complexes. The H-O-H bond angle is also greater for $M^{2+}(H_2O)$ complexes due to more polarization caused by the metal dications. The relative red shifts in stretching frequencies for $M^{2+}(H_2O)Ar_n$ complexes for different metals are within a few wavenumbers of each other as opposed to corresponding $M^{+}(H_2O)Ar_n$ systems where the metals having a fewer number of valence shell electrons shift the O-H stretching frequencies the most. The shifts in O-H stretching frequencies for $M^{2+}(H_2O)Ar_n$ complexes are influenced by the number of argon atoms. Polarization of electrons from argon to metal reduces the partial charge on metal and causing smaller red shifts in the O-H stretching frequencies. For all the $M^{2+}(H_2O)Ar_n$ complexes a coordination number six (one water, five argons) was observed. Doubly charged metal-water complexes with larger number of argon atoms show evidence of an insertion product of the form $H\text{-}M^{3+}\text{-}\ OH^{-}$.

Table 4.1: O-H stretch frequencies (cm^{-1}) computed and measured for doubly-charged vanadium-water-argon complexes. IR intensities (km/mol) are in parentheses, and frequencies are scaled by a factor of 0.9575 for comparison to the experiments.

Complex	OH stretches (theory)	OH stretches (exp)
$V^{2+}(H_2O)$	3587 (154), 3658 (227)	-
$V^{+}(H_2O)Ar_2$	3597 (134), 3668 (230)	3611, 3683
$V^{2+}(H_2O)$	3450 (383), 3496 (402)	-
$V^{2+}(H_2O)Ar$	3448 (411), 3498 (355)	-
$V^{2+}(H_2O)Ar_2$	3479 (349), 3531 (326)	3501, -
$V^{2+}(H_2O)Ar_3$	3522 (308), 3577 (300)	3524, 3582
$V^{2+}(H_2O)Ar_4$	3537 (288), 3593 (275)	3546, 3600
$V^{2+}(H_2O)Ar_5$	3554 (253), 3612 (259)	3561, -
$V^{2+}(H_2O)Ar_6$	3419 (870), 3593 (257)	3448, 3604
$V^{2+}(H_2O)Ar_7$	3426 (811), 3462 (829)	3456, 3521

Table 4.2: O-H stretch frequencies (cm^{-1}) computed and measured for singly and doubly charged chromium-water-argon complexes. IR intensities (km/mol) are in parentheses, and frequencies are scaled by a factor of 0.9575 for comparison to the experiments.

Complex	OH stretches (theory)	OH stretches (exp)
$Cr^{+}(H_2O)$	3624(143), 3696(233)	
$Cr^{+}(H_2O)Ar$	3628(145),3700(228)	3620,-
$Cr^{+}(H_2O)Ar_2$	3631(139),3703(224)	3621, 3687
$Cr^{2+}(H_2O)$	3460(378)/3506(403)	
$Cr^{2+}(H_2O)Ar$	3454(429)/3507(409)	
$Cr^{2+}(H_2O)Ar_2$	3486(417)/3539(368)	
$Cr^{2+}(H_2O)Ar_3$	3515(360)/3572(341)	3512, -
$Cr^{2+}(H_2O)Ar_4$	3528(308)/3587(315)	3531,3586
$Cr^{2+}(H_2O)Ar_5$	3539(308)/3600(296)	3546, -
$Cr^{2+}(H_2O)Ar_6$	3351(1133)/ 3580(290)	3380, 3578

Table 4.3: O-H stretch frequencies (cm^{-1}) computed and measured for singly and doubly charged scandium-water-argon complexes. IR intensities (km/mol) are in parentheses, and frequencies are scaled by a factor of 0.9575 for comparison to the experiments.

Complex	Rel. Energy	OH stretches (theory)	OH stretches (exp)
$Sc^+(H_2O)$	0.0	3589 (122), 3659(209)	-
$Sc^+(H_2O)Ar$			
$^3A_1$ (C_{2v})	0.0	3597(102), 3670(192)	3580, 3656
$^3A_1$ (C_s)	+7.0	3556(340), 3642(256)	
$Sc^+(H_2O)Ar_2$			
$^3A'$ (C_s) (Ar on H)	0.0	3560(317), 3652(228)	3546, 3637
$^3A'$ (C_s) (2Ar on M^+)	+5.3	3607(62), 3679(273)	
$Sc^{2+}(H_2O)$			
$^2A_1$ (C_{2v})	0.0	3465(354), 3506(366)	-
$Sc^{2+}(H_2O)Ar$			
$^2A_1$ (C_{2v})	0.0	3488 (356), 3531 (341)	-
$^2A_1$ (C_s) (Ar on H)	+9.4	3142 (1562), 3497 (341)	
$Sc^{2+}(H_2O)Ar_2$			
(2Ar on Sc^{2+})	0.0	3501 (338), 3548 (319)	3513, -
(1Ar on Sc^{2+}; 1Ar on H)	+6.9	3223 (1387), 3519 (337)	
$Sc^{2+}(H_2O)Ar_3$			
(3Ar on Sc^{2+})	0.0	3517 (324), 3565 (301)	3528, -
$Sc^{2+}(H_2O)Ar_4$			
(4Ar on Sc^{2+})	0.0	3545 (260), 3597 (262)	3539, 3590
$Sc^{2+}(H_2O)Ar_5$			
(5Ar on Sc^{2+})	0.0	3557 (224), 3610 (247)	3548, -
$Sc^{2+}(H_2O)Ar_6$			
(5Ar on Sc^{2+}; 1Ar on H)	0.0	3441 (772), 3591 (242)	3425, 3587
$Sc^{2+}(H_2O)Ar_7$			
(5Ar on Sc^{2+}; 2Ar on H)	0.0	3440 (708), 3472 (775)	3431, 3444

Table 4.4: Ground and excited state rotational constants (A″, A′) of $Cr^{+}(H_2O)Ar$ and $Cr^{2+}(H_2O)Ar_4$ complexes, Rotational temperatures (J, K) obtained from simulated and observed spectra. H-O-H bond angles are calculated from rotational constants assuming that the O-H bond lengths do not change.

Complex	(A″)	(A′)	T (J, K)	H-O-H bond angle
$Cr^{+}(H_2O)Ar$	13.1	13.0	85,130	111.1^{o}
$Cr^{2+}(H_2O)Ar_4$	12.6	12.8	250	113.5^{o}

Table 4.5: The symmetric and asymmetric stretches (cm^{-1}), M^{n+}-O and O-H bond lengths (Å) of M^{n+}-(H_2O) complexes where M = Sc, V, Cr and Mn and n=1, 2 obtained from DFT-B3LYP calculations. The red shifts from free water stretches are shown in parentheses.

Complex	sym str. (Shift)	asym str. (Shift)	M^{n+}-O bond length	O-H bond length
H_2O	3657 (0)	3756(0)		0.962
$Sc^{+}(H_2O)$	3580 (77)	3649(107)	2.200	0.969
$Sc^{2+}(H_2O)$	3465(192)	3506(250)	2.106	0.981
$V^{+}(H_2O)$	3587 (70)	3659(97)	2.077	0.969
$V^{2+}(H_2O)$	3450(207)	3496(260)	2.012	0.981
$Cr^{+}(H_2O)$	3615 (42)	3686 (70)	2.089	0.967
$Cr^{2+}(H_2O)$	3460(197)	3506(250)	2.038	0.981
$Mn^{+}(H_2O)$	3570 (87)	3651(106)	2.191	0.970
$Mn^{2+}(H_2O)$	3433(224)	3479(277)	1.987	0.982

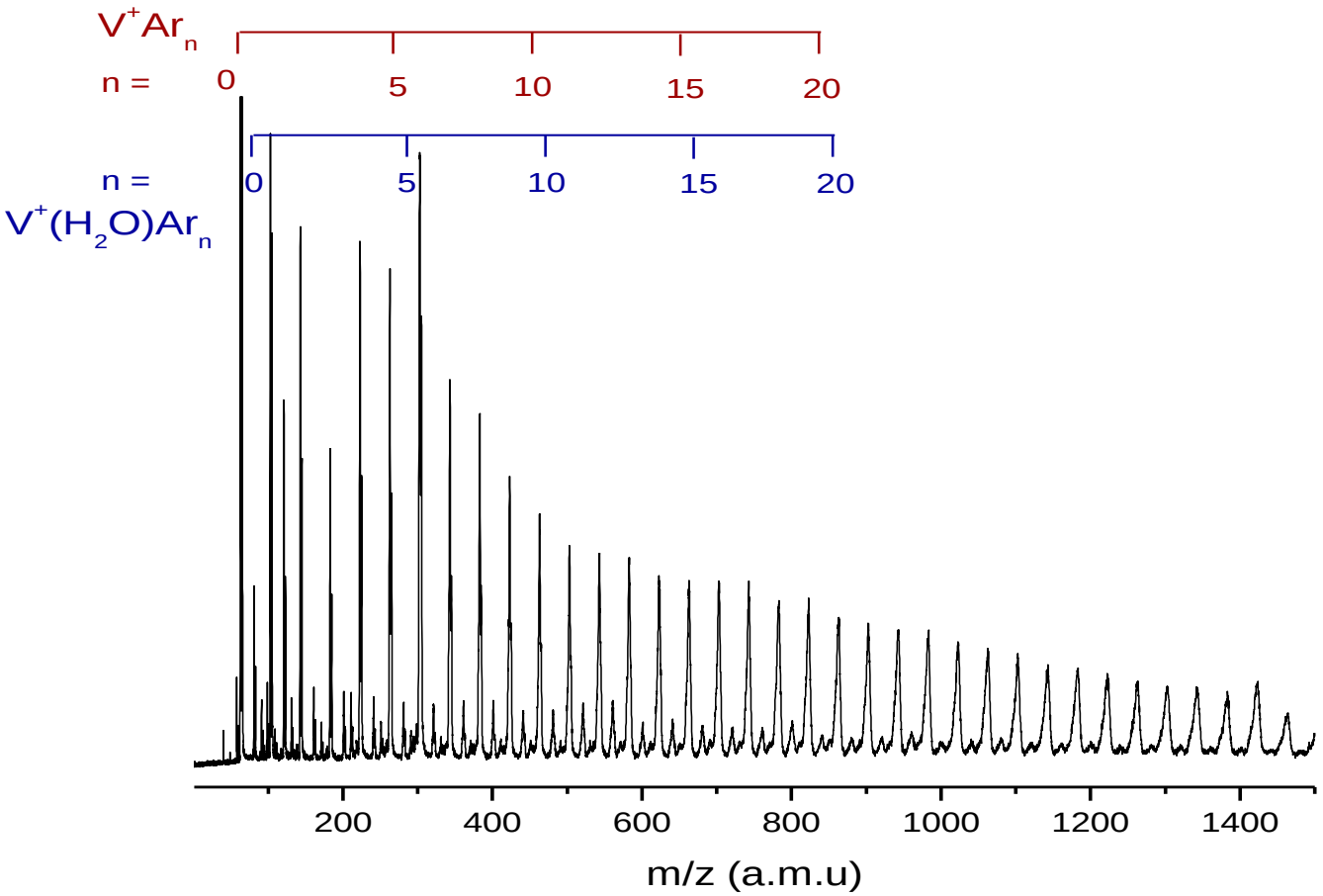

Figure 4.1: The mass spectrum of the $V^+(H_2O)Ar_n$ complexes produced by the laser vaporization source, optimizing the conditions for singly charged ions. The biggest peak corresponds to V^+ and the progression of $V^+(Ar)_n$ and $V^+(H_2O)Ar_n$ are shown in red and blue .

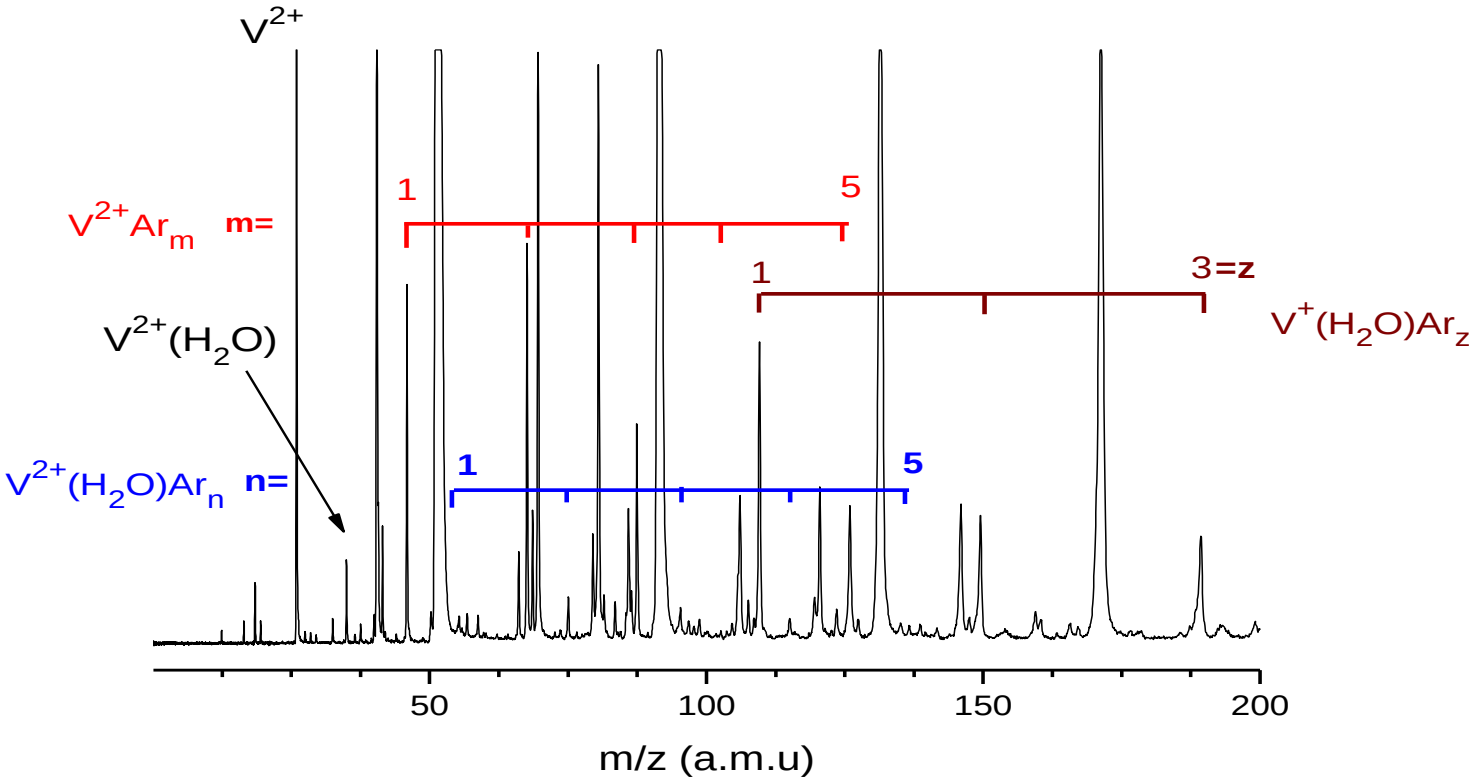

Figure 4.2: The mass spectrum of the $V^{m+}(H_2O)Ar_n$, (m=1,2) complexes produced by the laser vaporization cluster source, optimizing the conditions for doubly charged ions. The progression of $V^{+}(H_2O)Ar_n$, $V^{2+}(Ar)_n$ and $V^{2+}(H_2O)Ar_n$ are shown in different colors . The abundance of doubly charged ions is significantly lower than that of the singly charged complexes.

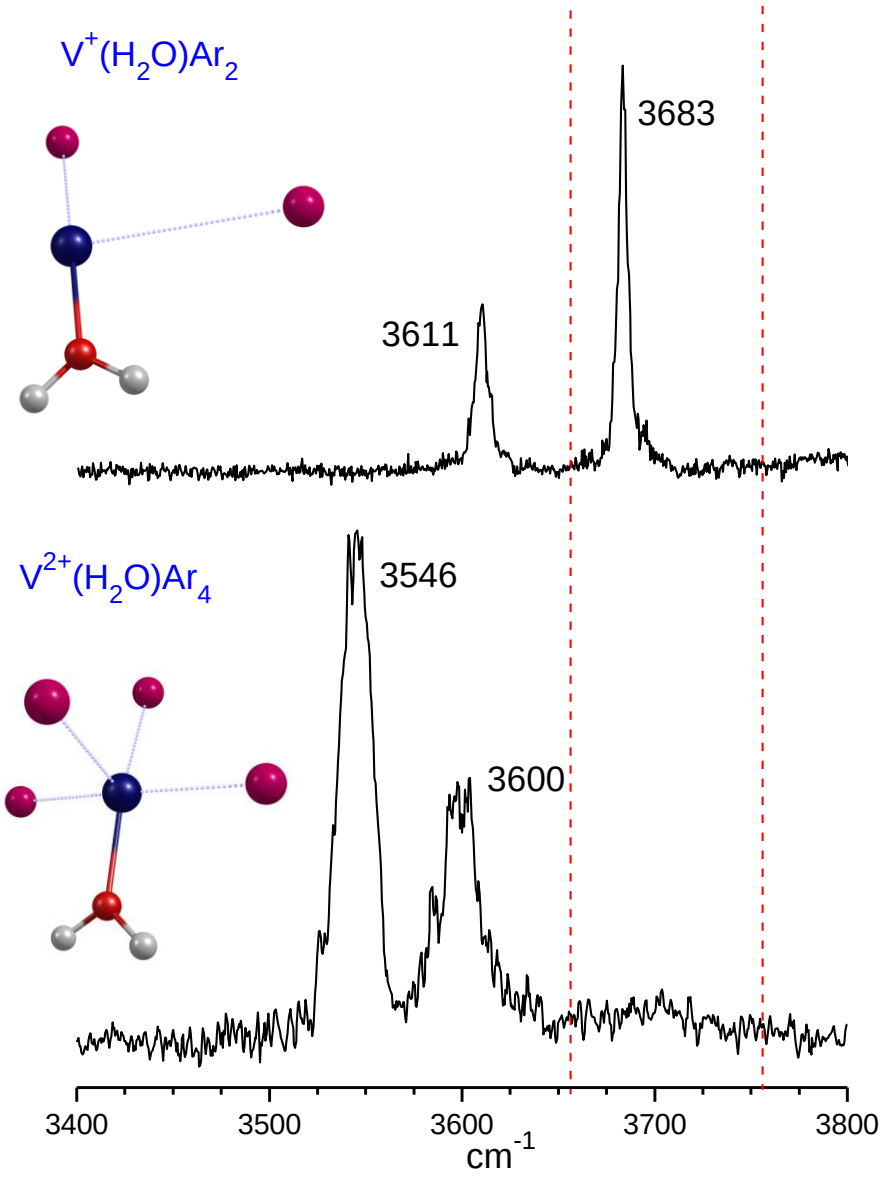

Figure 4.3: The infrared photodissociation spectrum measured for the $V^+(H_2O)Ar_2$ complex in the mass channel corresponding to the elimination of argon (upper trace). The lower trace shows the spectrum of the $V^{2+}(H_2O)Ar_4$ complex for a comparison. The vertical dashed lines show the positions of the vibrations in the isolated water molecule (3657 and 3756 cm^{-1} respectively). The inset structures are computed from theory, and their vibrations also agree best with the observed bands.

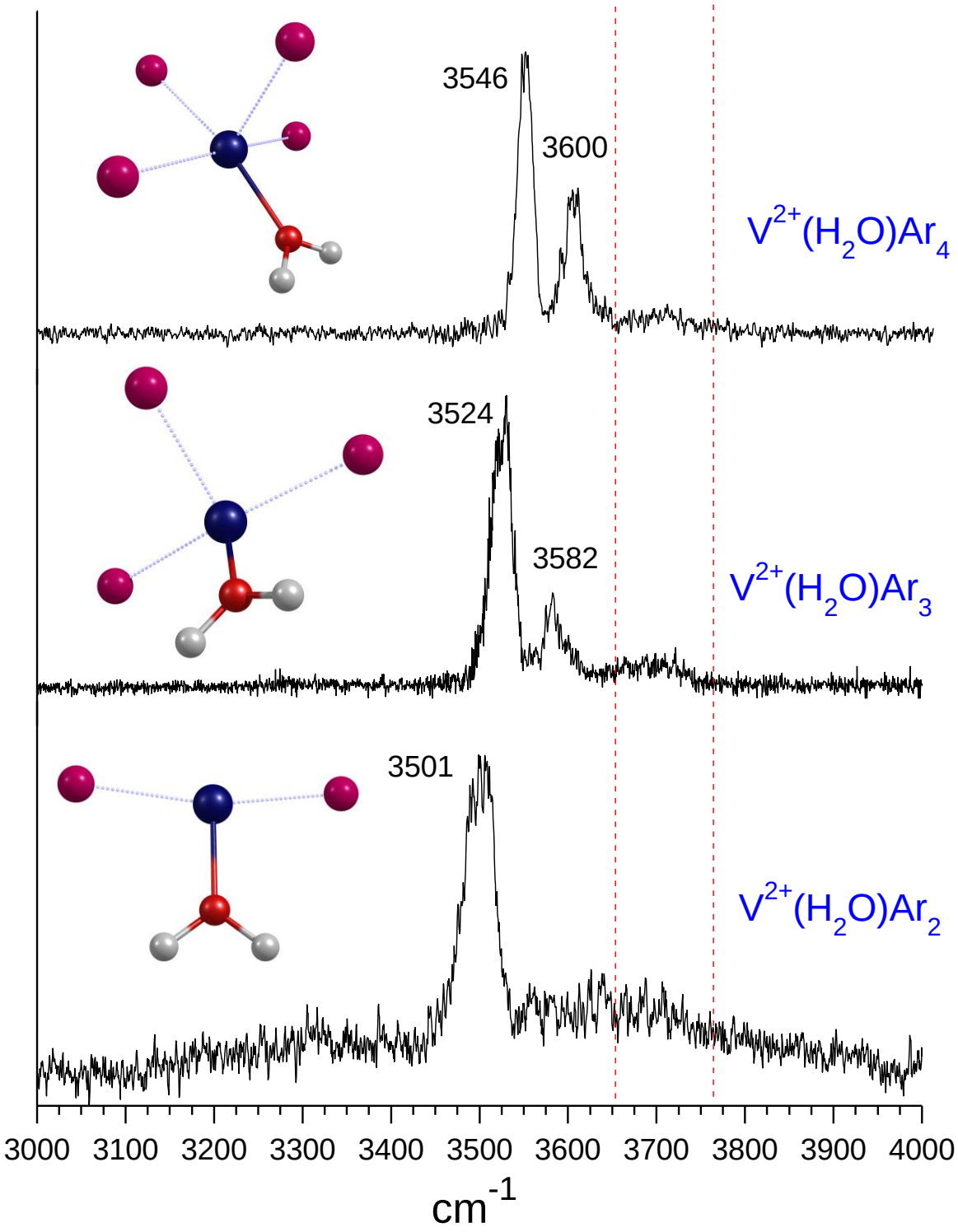

Figure 4.4: The spectra measured for the $V^{2+}(H_2O)Ar_{2\text{-}4}$ complexes in the mass channel corresponding to the elimination of argon. The inset structures are computed by DFT.

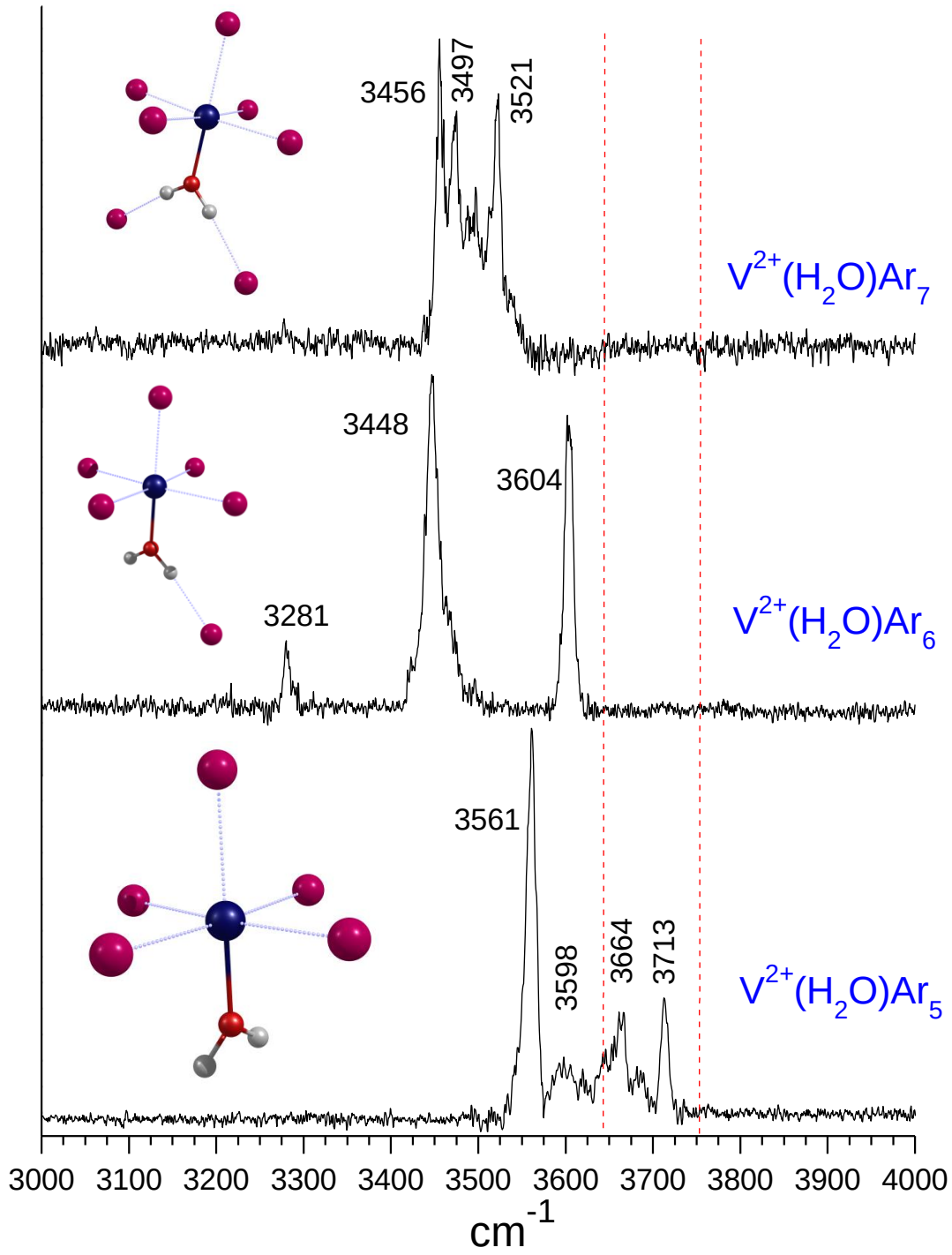

Figure 4.5: The photodissociation spectra measured for the $V^{2+}(H_2O)Ar_{5-7}$ complexes in the mass channel corresponding to the elimination of argon. The inset structures are computed by theory.

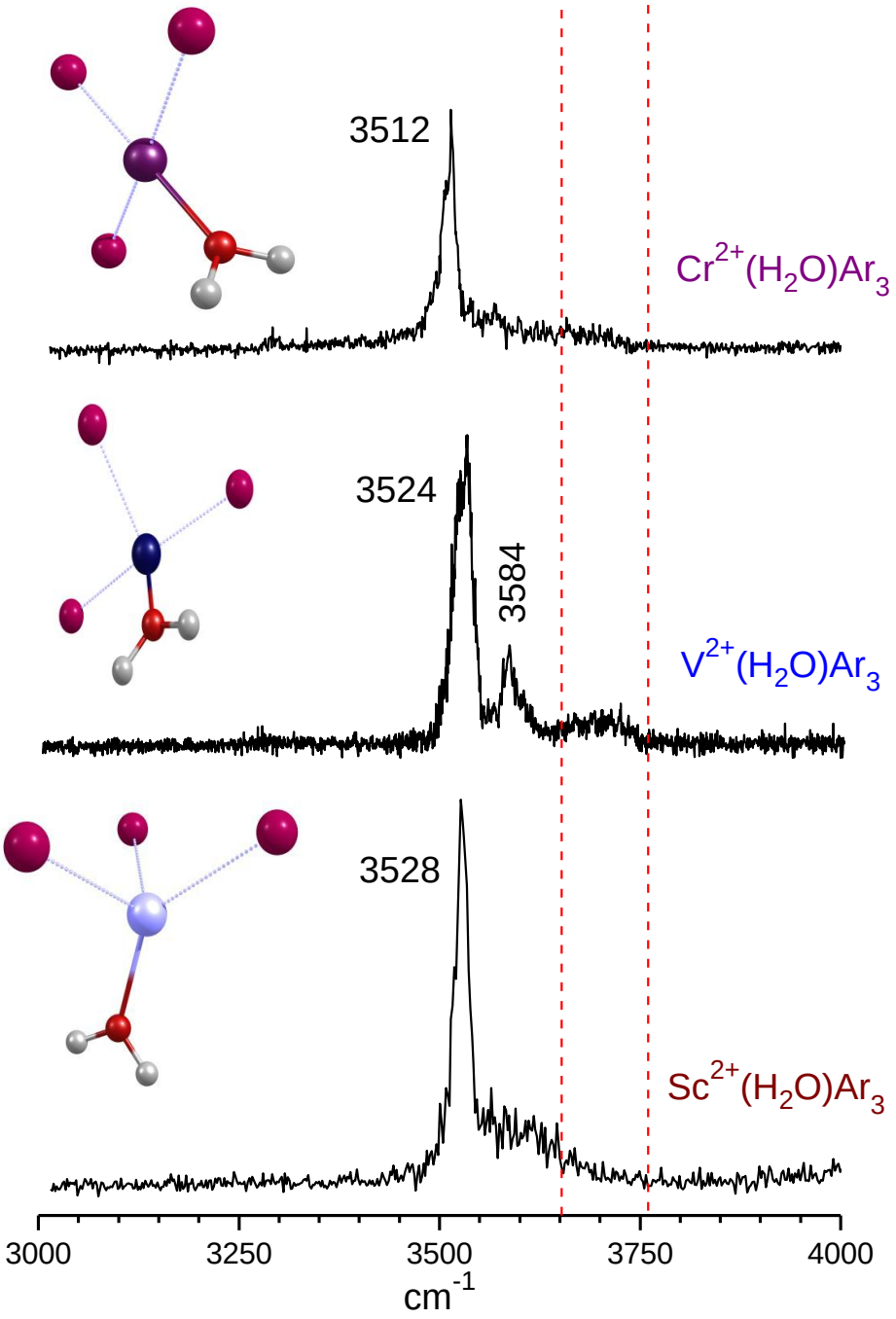

Figure 4.5: The spectra of the $M^{2+}(H_2O)Ar_3$ (where M = Sc, V and Cr) complexes comparing the relative red shifts in the O-H stretching frequencies. The inset structures show that argons bind to the metal ion sites.

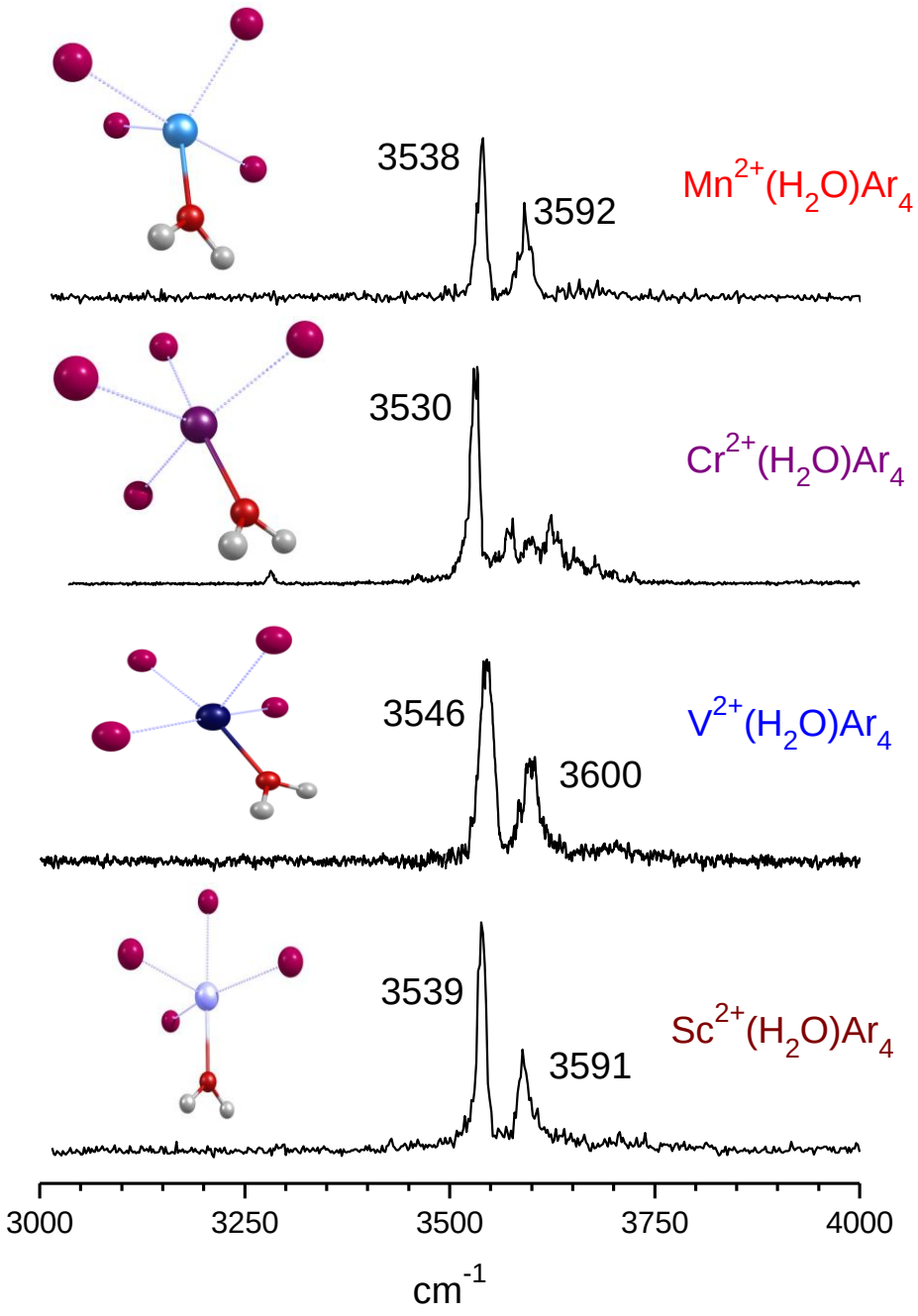

Figure 4.6: The spectra measured for the $M^{2+}(H_2O)Ar_4$ (where M = Sc, V, Cr and Mn) complexes in the O-H stretch region. The asymmetric O-H stretch of $Cr^{2+}(H_2O)Ar_4$ shows multiplet band structures. The inset structures are computed by DFT.

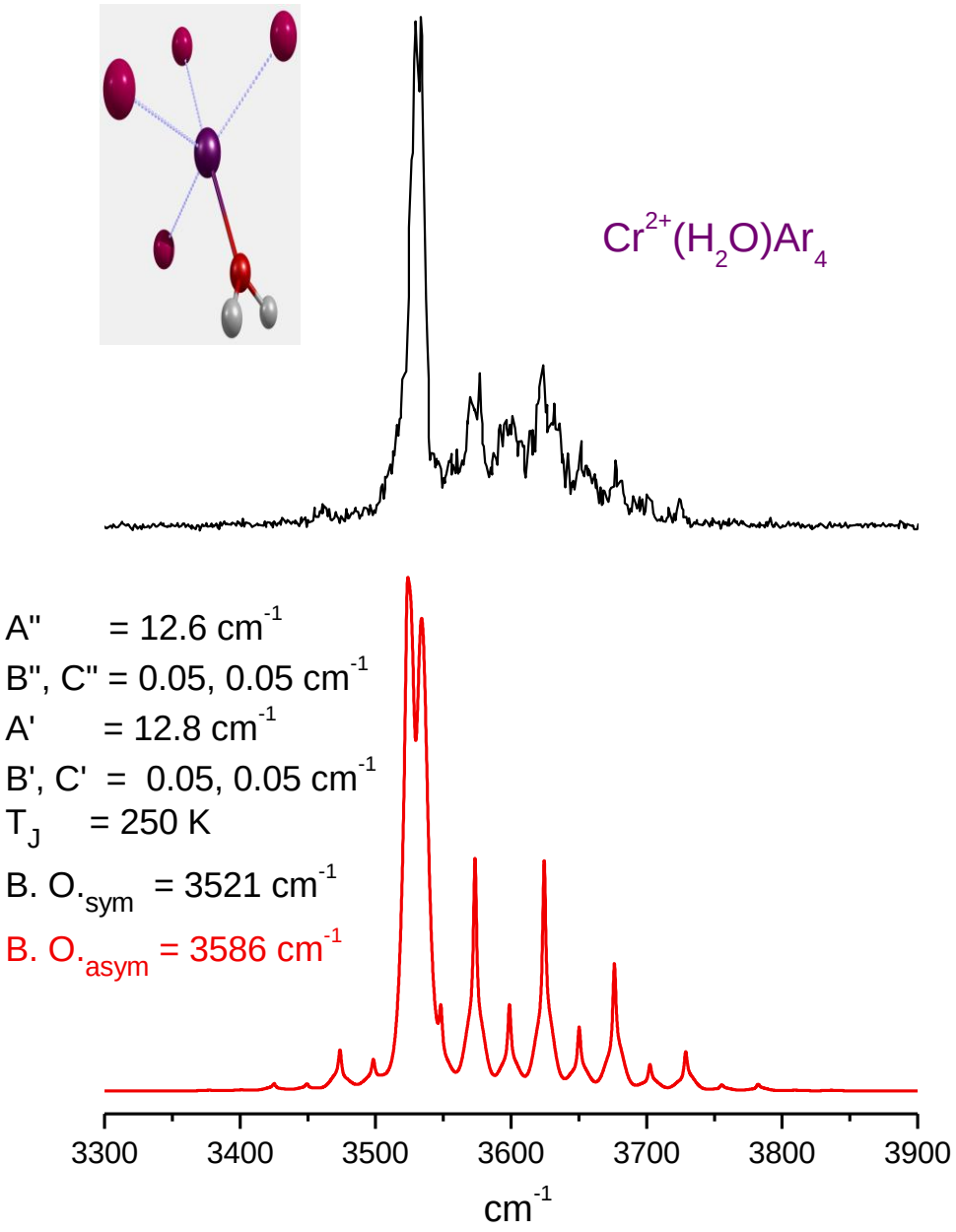

Figure 4.7: The infrared photodissociation spectrum measured for the $Cr^{2+}(H_2O)Ar_4$ complex in the mass channel corresponding to the elimination of argon (upper trace). The lower trace shows a simulation of the vibrational bands and their partially resolved rotational structure. The inset structure is that computed with density functional theory. The structural parameters obtained from the observed and simulated spectra are also shown in the figure.

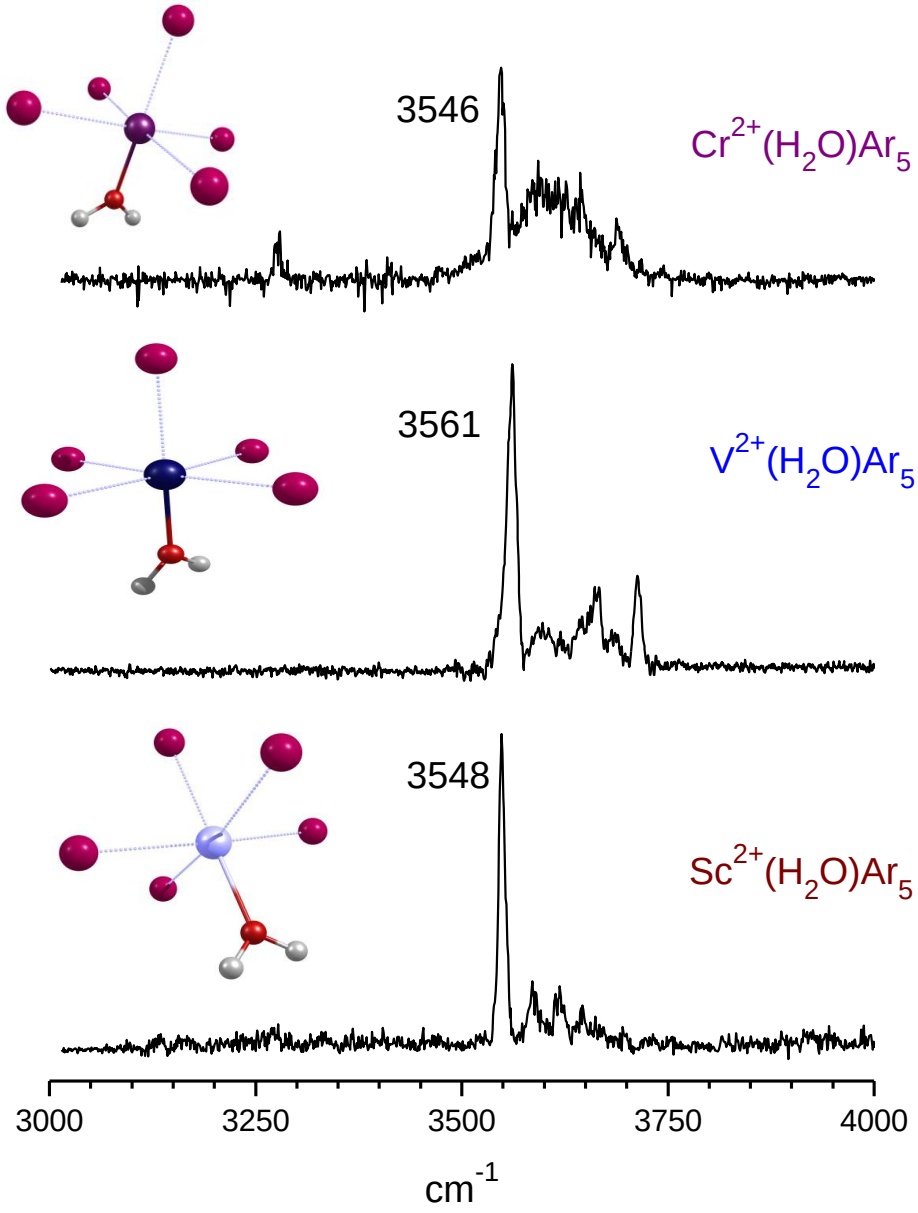

Figure 4.8: The photodissociation spectra measured for the $M^{2+}(H_2O)Ar_5$ (where M = Sc, V and Cr) complexes in the O-H stretch region. The inset structures are those from theory.

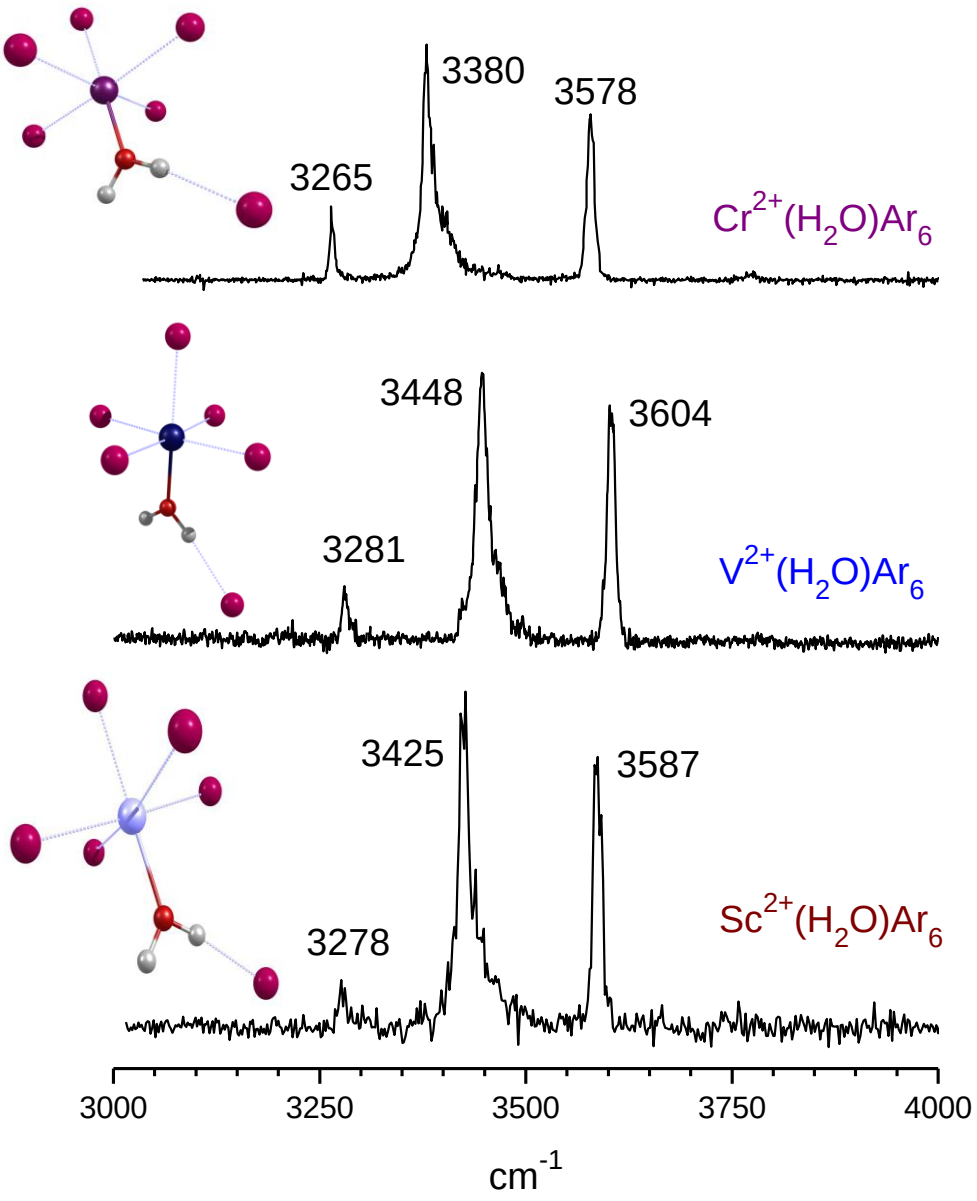

Figure 4.9: The spectra of the $M^{2+}(H_2O)Ar_6$ (where M = Sc, V and Cr) complexes. The inset structures show that the coordination of M^{2+} is filled up with five argons and one water. The other argon binds to water, which shifts the O-H stretches to the red.

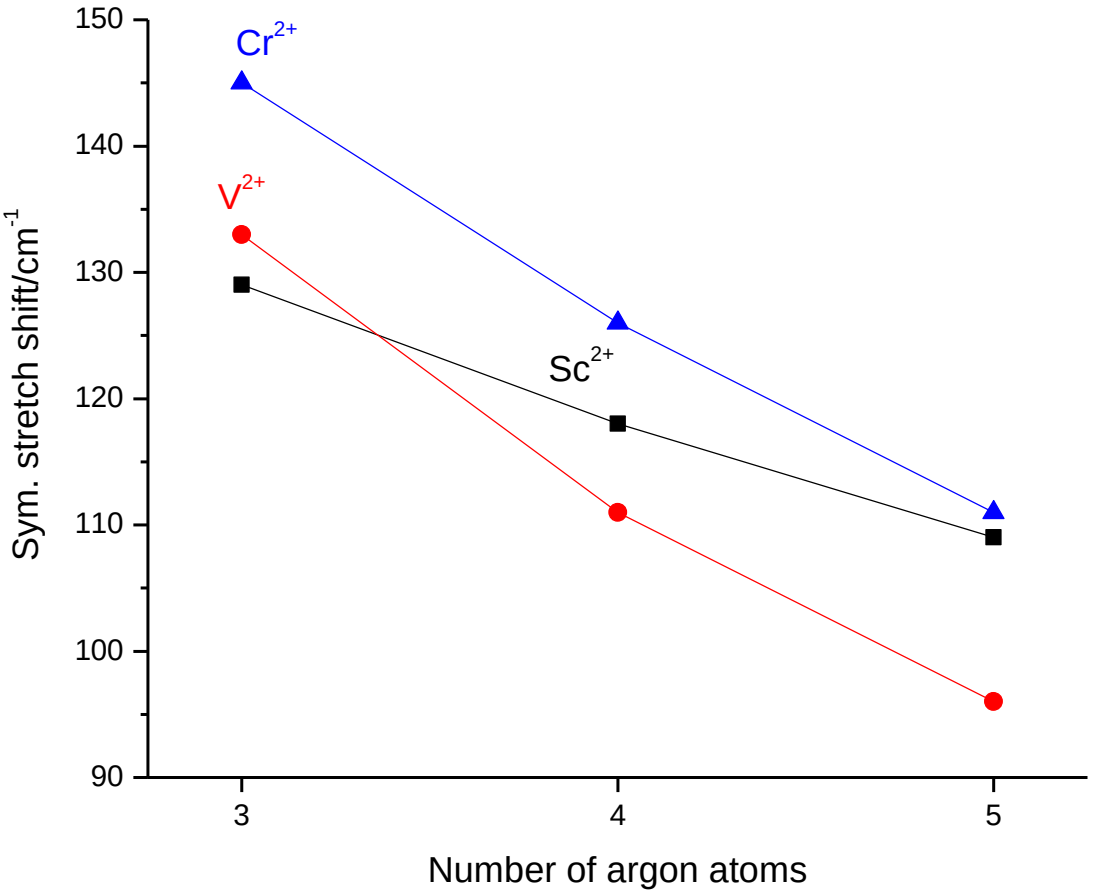

Figure 4.10: Observed red shifts in the symmetric stretches of the $M^{2+}(H_2O)Ar_n$ complexes where M= V, Sc, Cr, and n=3-5. $M^{2+}(H_2O)Ar_3$ complexes have red shifts ranging from 128-145cm^{-1} compared to the O-H stretches of free water. Addition of more argon leads to lower red shifts in the stretching frequencies compared to the free water stretches.

CHAPTER 5

HYDROINUM-NITROGEN COMPLEXES

5.1 Introduction

Protonation and proton transfer processes are ubiquitous throughout chemistry and biology.[69-72] The detailed mechanisms of these processes have been studied for many years.[75-78] The proton transfer processes involve ionic intermediates in which protons are bound or shared between the molecular components. Mass spectrometric studies have extensively investigated these intermediates.[79-91] In recent years, infrared spectroscopic studies have been employed to investigate the structures of the proton bridged dimer complexes.[7-23] Many of these studies have focused on protonated water and its proton sharing interactions with other molecules.[12a,13,15,17] More recent infrared experiments have shown that the proton sharing depends on the difference in proton affinity values of two components competing for the proton.[17] In some cases dipole moments and polarizabilities also play significant role in determining the protonation site.[15f]

Protonated water dimer and its shared proton interactions have been reported by Asmis and coworkers using the free electron laser "FELIX".[12a] In a collaborative work between our group and Johnson group, the small protonated water clusters have been studied using an infrared parametric oscillator/amplifier (IR-OPO/A) laser system.[14] More recent studies by Johnson and coworkers have investigated protonated water dimer with isotopic substitution.[15d,e] A number of theoretical studies employing reduced dimensional and full dimensional anharmonic calculations have investigated the protonated water dimer.[100,102] Shared proton

interactions of symmetric dimers of different molecules such as CH_3OH, NH_3, CO_2, acetylene, acetone and N_2 have been explored by recent infrared experiments.[13c,18-22] Johnson and coworkers have reported a study examining the shared proton stretch vibrations of a number of asymmetric proton bound dimers.[17] This study showed that the shared proton stretch can be linearly correlated to the difference in the proton affinity values (ΔPA) of the molecular components. Based on their measured spectra for a number of species, they made a linear plot of shared proton stretch vs. ΔPA. This plot should predict the shared proton stretch of a complex with a known ΔPA. Fridgen and coworkers have suggested that the dipole moment also affects the accommodation of protons in mixed proton-bound dimers. Johnson and coworkers have studied such an example with protonated acetonitrile-water complex.[15f]

The hydronium cation was studied by Saykally, Oka and others using high resolution infrared spectroscopy.[7-9] The double-well potential energy surface of this ion has been investigated by state-of-the-art theories.[99,101,102c] Protonated nitrogen ion, N_2H^+, has been studied using high resolution spectroscopy.[140] Linnartz et al. and our research group have reported the spectroscopy of protonated nitrogen dimer ($N_2H^+N_2$).[141,22] The proton affinity of water (691.0 kJ/mol) is much greater than that of the nitrogen (493.8 kJ/mol).[66] Therefore, in a mixed protonated complex of water and nitrogen proton is expected to mostly reside on water. In the present work, we describe the infrared spectroscopy of the $H_3O^+(N_2)_n$ complexes, for n = 1-3, describing the effect of nitrogen solvation and related shared proton interactions.

5.2 Experimental

Mixed complexes of protonated water and nitrogen of the form $H_3O^+(N_2)_n$, are produced in a pulsed supersonic expansion source employing the needle electric discharge method that has

been described in detail in Chapter 2. Mass-selected ions are probed with infrared photodissociation spectroscopy (IRPD) with the tunable output of an infrared optical parametric oscillator/amplifier (IR- OPO/OPA) system pumped by an Nd:YAG laser (Spectra Physics model Pro-230). IRPD is carried out in the turning region of the reflectron field, where ion optics and pulse timing are adjusted to obtain optimized spatial and temporal overlap between the laser and the ion beam. Resonant absorption leads to the fragmentation of $H_3O^+(N_2)_n$ complexes by eliminating a nitrogen molecule in each case. The intensities of fragment ions resulting from IR excitation are recorded as a function of the photon energy to obtain a spectrum. The signal is collected with a digital oscilloscope interfaced to a computer.

Density functional theory (DFT) is employed to investigate the structures, energetics and vibrational spectra of the $H_3O^+(N_2)_n$ complexes for comparison to the experiment. These computations use the Gaussian 03W package and the 6-311+G (d, p) basis set.[138] The computed vibrational frequencies are scaled by a factor of 0.961 which is the recommended values for these levels of theory and basis sets.[139]

5.3 Results and discussion

The measured binding energies of $H_3O^+(N_2)_n$ complexes are 7.8, 7.3 and 6.3 kcal/mol (2730, 2550 and 2200 cm^{-1}) respectively for the n=1, 2, 3 species.[143] The infrared photoexcitation in the 2000-4500 cm^{-1} region leads to efficient fragmentation of $H_3O^+(N_2)_n$ systems by eliminating a nitrogen molecule. However, we do not observe any fragmentation at 2330 cm^{-1}, where the N-N stretch for the isolated nitrogen molecule is expected.[22] Therefore, probably the binding energies of these complexes are greater than 2330 cm^{-1}.

Figure 5.1 shows the photodissociation spectra measured for the $H_3O^+(N_2)_n$ complexes in the 2600-4000 cm^{-1} region. Each spectrum is obtained by monitoring the mass channel corresponding to the elimination of a nitrogen molecule. The spectrum of $H_3O^+(N_2)$ has two broad bands centered at 2787 and 3031 cm^{-1}, where the second band is less intense than that of the first. The spectrum also has several sharp peaks in the O-H stretch region (3519, 3580, 3620 cm^{-1}) and some weaker features to both side of the 3580 and 3620 cm^{-1} peaks. The $H_3O^+(N_2)_2$ complex shows an intense but somewhat broader peak at 2957 cm^{-1} and three weaker peaks at 3208, 3284, 3585 cm^{-1}. The spectrum of $H_3O^+(N_2)_3$ has an intense peak at 3110 cm^{-1} and a less intense one at 3347 cm^{-1}. DFT computed structures for the $H_3O^+(N_2)_n$ complexes are shown in the insets of Figure 5.1 and the red solid lines correspond to the predicted vibrations of each complex. The neat H_3O^+ ion has symmetric and asymmetric O-H stretches at 3441/3491 and 3514/3530 cm^{-1} (inversion doublets).[7-9] Interaction with N_2 shifts the solvated O-H stretch of H_3O^+ towards lower frequency. Therefore, the band at 2787 cm^{-1} is assigned to the N_2 bound O-H stretch of the $H_3O^+(N_2)$ complex. This band is broad because of the hydrogen bonding interaction of N_2-HOH_2^+. The pattern of peaks in the lower frequency region is similar to those observed for metal cation-water-argon systems. The multiplet band structure arises due to the symmetric and asymmetric O-H stretches and their partially resolved rotational structure as discussed in Chapters 3 and 4.

Figure 5.2 shows an expanded view of peaks observed in the high frequency region for the $H_3O^+(N_2)$ complex (upper trace). The symmetric stretch is a parallel type band with unresolved rotational structure appearing as a broad band at 3519 cm^{-1}. For the asymmetric stretch K-type rotational sub bands are partially resolved and observed as two intense bands (3579 and 3620 cm^{-1}) and a weaker central one (3600 cm^{-1}). There are some weaker higher order

(K″, K′) type sub bands are observed both side of the two intense peaks at 3579 and 3620 cm^{-1}. To confirm this assignment we have simulated the spectrum with the program *Asyrotwin*, as shown in the lower trace of Figure 5.2. For this simulation we use the rotational constants from the computed structure. The simulation includes the 3:1 intensity alterations of K = odd: even for the two identical hydrogens. The observed spectrum is best described by two different temperatures, i.e. T_J = 25K and T_K = 40 K. The J temperature affects the width of the J type unresolved rotational structure and the K temperature affects the width and intensities of the partially resolved K type sub bands. This behavior has also been seen previously for metal-water complexes and was attributed to the different rates of cooling of J and K levels.[41] The K levels are widely spaced and so do not relax as efficiently as the J levels in the supersonic expansion. Another important aspect of this simulation involves the 3:1 statistical weight which should only be applied to planar C_{2v} systems. The computed lowest energy structure of $H_3O^+(N_2)$ is not planar. However, we have computed the H-O-H bending potential using the MP2/aug-cc-pVDZ theory, keeping all the other atoms of this complex fixed at their equilibrium positions. The barrier to planarity is found to be low (2.0 kcal/mol, 700 cm^{-1}) and the zero point vibrational energy (741 cm^{-1}) also lies close to this barrier. Therefore, this complex may be vibrationally averaged to be planar.

The weaker band observed at 3031 cm^{-1} for the $H_3O^+(N_2)$ complex is assigned to a combination band involving a hydrogen bonded stretch band and a low frequency vibrational mode. The difference between hydrogen bonded stretch (2787 cm^{-1}) and the 3031 cm^{-1} band is 244 cm^{-1} and the predicted vibrations for this complex has an intermolecular $(H_3O)^+$-N_2 stretch vibration at 246 cm^{-1}, which lies on the same axis as the hydrogen bond. Therefore, this mode

can strongly couple with the hydrogen bonded stretch. We can then assign the 3031 cm^{-1} band to the combination band of the intermolecular stretch and the proton stretch.

The $H_3O^+(N_2)_2$ complex has a structure with two N_2 bound to the two O-H bonds of hydronium (structure is shown in the inset of Figure 5.1). In this structure, there should be only one free O-H and the partially resolved rotational structure is not expected. The 3585 cm^{-1} band is then assigned to the free O-H stretch for this complex and the predicted vibration (3585 cm^{-1}) also matches with the experiment. In the hydrogen bonding region, the broad band at 2957 cm^{-1} is assigned to the symmetric and asymmetric O-H stretches towards the nitrogens. Theory predicts these stretches at 2999 and 3039 cm^{-1}. The other weaker bands observed at 3208 and 3284 cm^{-1} are not predicted by theory. These bands are believed to be arise from some kind of combination of a hydrogen bonded stretch with a low frequency intremolecular vibration. The 3208 and 3284 cm^{-1} bands are 251 and 327 cm^{-1} above the main hydrogen bonded stretch band. The computed vibrational frequencies for this complex has a vibration corresponding to the asymmetric N_2-$(H_3O)^+$-N_2 intermolecular stretch at 236 cm^{-1}. There is one more low frequency mode corresponding to the free O-H bending vibration predicted at 338 cm^{-1}. Assuming that the coupling of vibrational bands is not associated with high anharmonicities, we can assign the 3208 and 3284 cm^{-1} bands to the combination of hydrogen bonded stretch band with the low frequency vibrational modes mentioned above.

The first coordination sphere of hydronium is filled with three nitrogens in the $H_3O^+(N_2)_3$ complex. Subsequently, there is no free O-H stretches and due to the symmetric structure the symmetric and asymmetric stretches are expected to appear roughly at the same positions in the experimental spectrum. Indeed an intense band is observed at 3110 cm^{-1} and this is assigned to

the hydrogen bonded stretch. Similar to the $H_3O^+(N_2)_{1,2}$ complexes, in this spectrum a combination band is observed at 3347 cm^{-1}.

Having assigned the spectra of the $H_3O^+(N_2)_n$ species, it is interesting to investigate the nature of the shared proton in these system. The hydrogen bonded stretch of $H_3O^+(N_2)$ is observed at 2787 cm^{-1} which is ~700 cm^{-1} red shifted from the corresponding stretch of neat hydronium cation (3445/3491, 3515/3530 cm^{-1}). This large red shift indicates that this complex has a shared proton interaction rather than a complex where N_2 is weakly bound to hydronium. The amount of red shift is less (500 cm^{-1}) for $H_3O^+(N_2)_2$ because the shared proton interaction is distributed over two N_2 binding sites and each of this interaction is less than that of the $H_3O^+(N_2)$ complex. Consistent with this same logic $H_3O^+(N_2)_3$ shows the smallest red shift from the free O-H stretches of hydronium.

5.4 Conclusions

$H_3O^+(N_2)_n$ complexes are produced in pulsed nozzle source and investigated with infrared laser spectroscopy in the 2000-4000 cm^{-1} region. The hydrogen bonded stretch of the $H_3O^+(N_2)$ complex shows a large red shift compared to the free O-H stretches of hydronium. In the high frequency region partially resolved rotational structure is also observed for this complex. Higher cluster sizes show smaller red shifts for the hydrogen bonded stretches due to the effect of nitrogen solvation. The spectra of $H_3O^+(N_2)_n$ show combination bands between hydrogen bonded stretches and the low frequency intermolecular stretches.

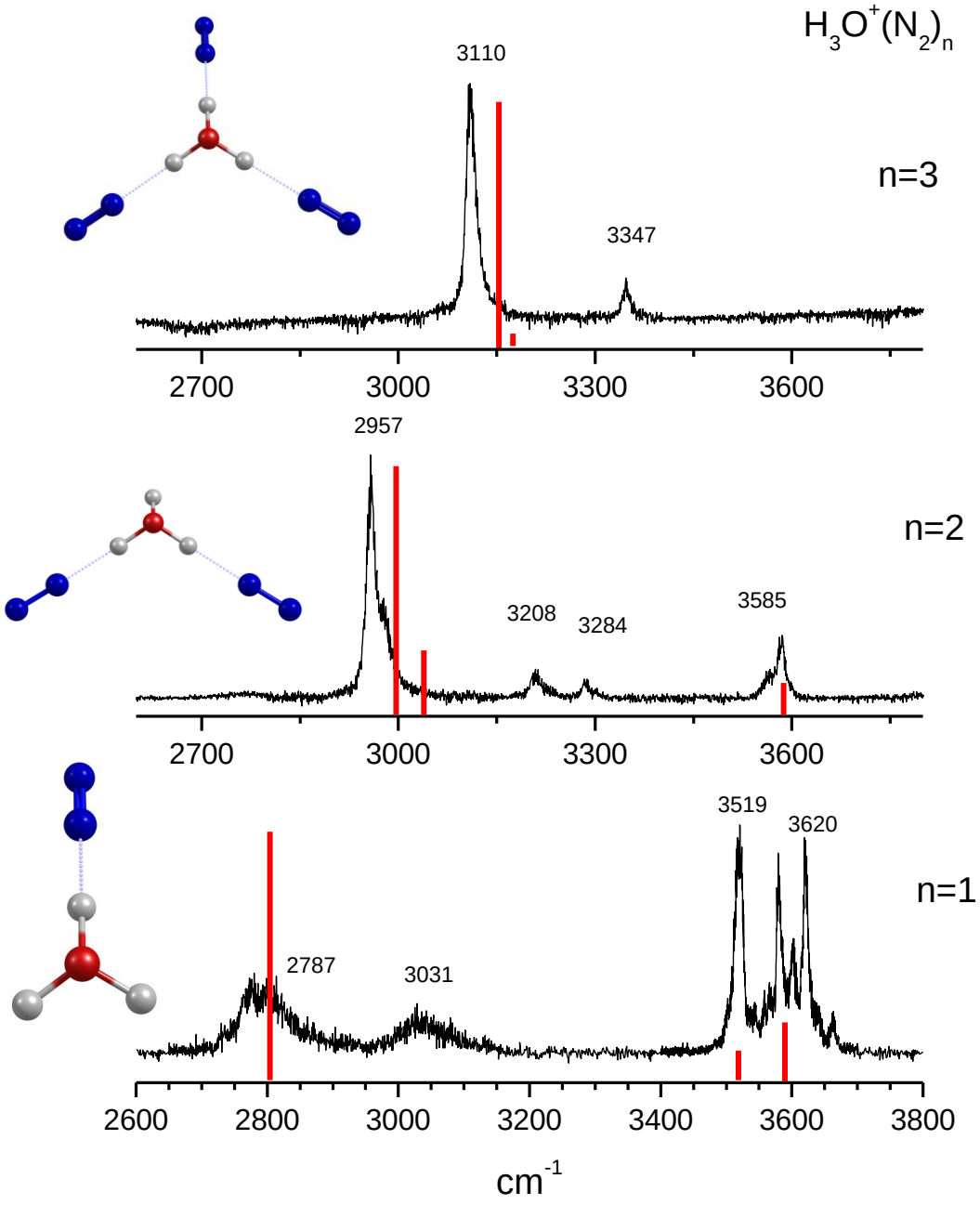

Figure 5.1: The photodissociation spectra of the $H_3O^+(N_2)_n$ complexes, for n=1-3. The red solid lines indicate the computed vibrational bands, which are scaled by factor of 0.961.

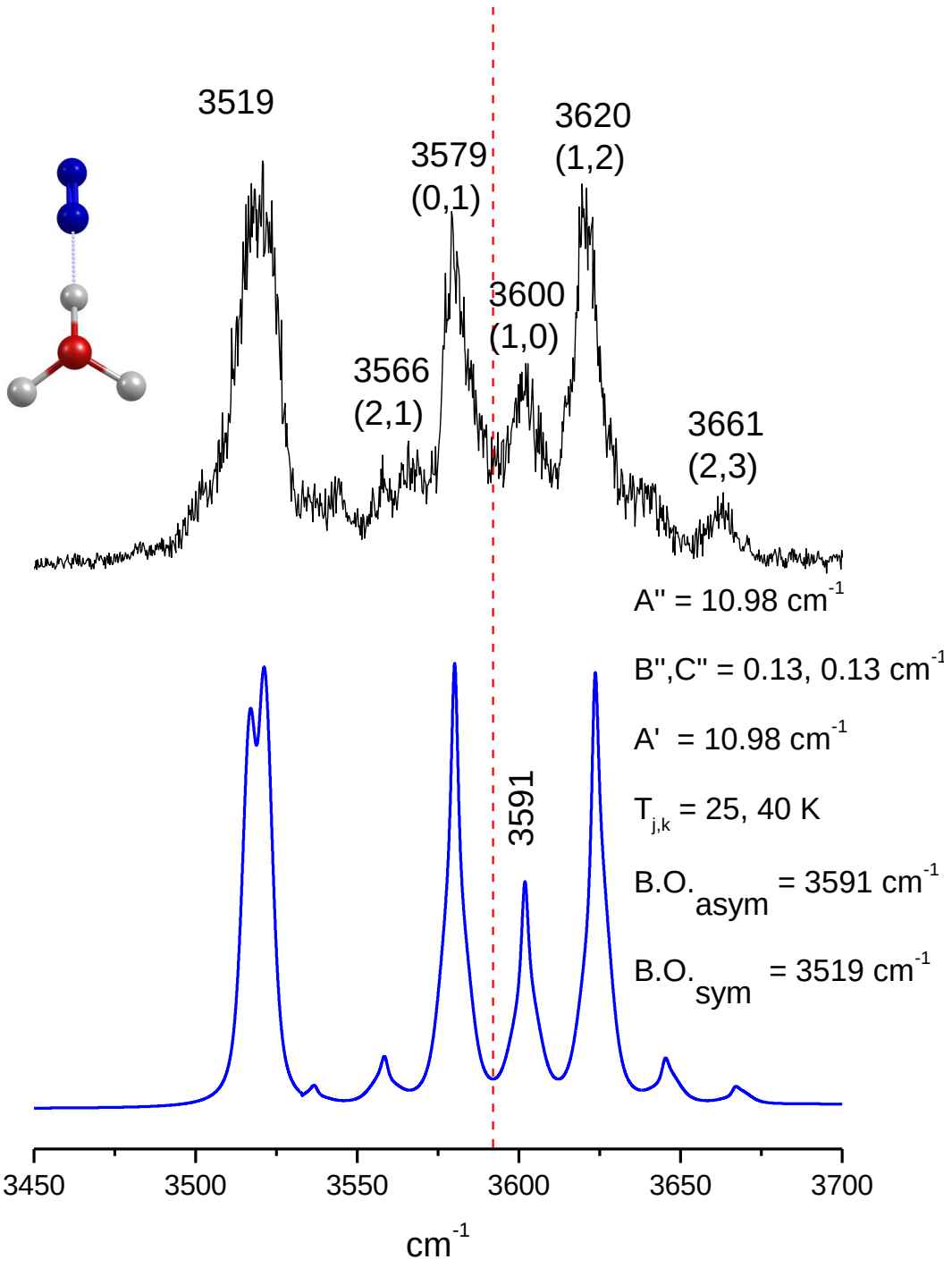

Figure 5.2: An expanded view of the spectrum of $H_3O^+(N_2)$ in the free O-H stretch region, showing the partially resolved rotational structure in this region. The lower trace shows the simulated spectrum.

CHAPTER 6

MIXED PROTONATED COMPLEXES OF BENZENE AND WATER

6.1 Introduction

The mechanistic details involving the unusual rates of proton transfer in aqueous solutions has gained much attention for many years.[69-72, 75-78] In an aqueous solution, rapid transfer of proton is believed to occur between two limiting structures. First is the "Eigen" ion, where hydronium (H_3O^+) is symmetrically solvated by three other water molecules and second is the "Zundel" ion, where the proton is symmetrically solvated between two water molecules.[75, 76] The structures of the solvated proton are difficult to characterize from condensed phase studies. Therefore, these structures have been investigated by infrared experiments and theoretical studies.[11-15, 17, 23, 92-111] Many of the infrared experiments have also explored the proton sharing interactions of water with other molecules.[13,15,17] More recently, understanding the behavior of protons at the interface of water and hydrophobic media has been an active area of research.[112-117] These studies show that the surface charge density plays a crucial role in stabilizing ions at hydrophobic interfaces.[115-117] Therefore, a molecular level understanding of the interaction between charged species, such as protonated water clusters, and a hydrophobic molecule is required to elucidate the behavior of protons at interfaces. In this present work, we describe the infrared photodissociation spectroscopy of mixed complexes of protonated water and benzene which can be viewed as a simple model system to study hydrophilic-hydrophobic interactions.

The shared proton stretch vibrations have been a central focus in studying small protonated systems in which the components are either homo-molecular or hetero-molecular.[17] Since the proton has low mass, it can undergo high amplitude motion in a complex of two constituents having the same or a low difference in proton affinity values (ΔPA). Protonated water dimer has a shared proton stretch at ~1000-1200 cm^{-1} while this stretch is observed at ~750 cm^{-1} for the protonated nitrogen dimer.[12a,22] Apart from these two symmetric proton-bound dimers, a number of other proton-bound systems including CH_3OH, NH_3, CO_2, acetylene and acetone have been studied using vibrational spectroscopy.[12b,13c,18-20,22] Johnson and coworkers have done a systematic study of proton-bound dimers of hetero-molecular species having different ΔPA values, which shows that the shared proton stretch appears at wide range of frequencies, and a linear plot of ΔPA vs. shared proton stretch can be used to predict this vibration of a mixed complex.[17] Fridgen and coworkers suggested that if one of the components has a high dipole moment the shared proton stretch may not follow the ΔPA trend. Johnson and coworkers studied such an example in the case of the protonated complex of water and acetonitrile.[15f] Acetonitrile has much higher proton affinity (788 kJ/mol)[66] than that of water (691.0 kJ/mol), but in the proton-bound dimer the proton is closer to water since acetonitrile also has much higher dipole moment (3.84D) than that of water (1.85D). The proton affinity of benzene (750.4 kJ/mol) is higher than that of water but benzene has no dipole moment. Previous theoretical work by Nguyen and coworkers predicted that in the $[(bz)HH_2O]^+$ complex, proton transfer occurs from bzH^+-H_2O to $bz(H_3O)^+$ via a transition state of the form $[bz\ldots H\ldots H_2O]^+$ with a low energy barrier (2.5 kcal/mol).[144]

Our research group has studied protonated benzene complex employing infrared spectroscopy and the method of rare gas tagging.[125] Mikami and coworkers have studied benzene

cation-(water)$_n$ systems, $[(C_6H_6)(H_2O)_n]^+$ where n = 1-6, using infrared spectroscopy and they have investigated the structural changes upon photoionization and resulting proton transfer reaction.[126] Chang and coworkers have employed infrared spectroscopy along with theoretical calculations to study protonated benzene-(water)$_2$, $[H(C_6H_6)(H_2O)_2]^+$.[127] However, they could only study this complex in the high frequency region (3600-3800 cm^{-1}). In this present work, we describe the infrared spectroscopic studies of mixed complexes of protonated benzene and water, $[H(C_6H_6)_m(H_2O)_n]^+$,where m=1, 2 and n=1- 4, examining the preferential sites of protonation and the role of solvation.

6.2 Experimental

Mixed complexes of protonated benzene and water of the form $[H(C_6H_6)_m(H_2O)_n]^+$ are produced in a pulsed supersonic expansion source employing the needle electric discharge method that has been described in detail in Chapter 2. The expansion consists of a gas mixture of 20% H_2 and 80% Ar with a small amount of ice-cooled benzene and water is seeded in it. The molecular beam is collimated with a skimmer, and cations are pulsed extracted into a reflectron time-of-flight mass spectrometer where they are mass-analyzed and size-selected. Mass-selected ions are probed with infrared photodissociation spectroscopy (IRPD) with the tunable output of an infrared optical parametric oscillator/amplifier (IR- OPO/OPA) system. The IR-OPO/OPA laser system is pumped by a Nd:YAG laser (Spectra Physics model Pro-230) producing radiation between 600-4500 cm^{-1} with a linewidth of 1-2 cm^{-1}. IRPD is carried out in the turning region of the reflectron field, where ion optics and pulse timing are adjusted to obtain optimized spatial and temporal overlap between the laser and the ion beam. For the smaller systems, the rare gas tagging method is applied for efficient photofragmentation while larger clusters are

photodissociated by the elimination of weakly bound benzene. The intensities of fragment ions resulting from IR excitation are recorded as a function of the IR photon energy to obtain a spectrum. The signal is collected with a digital oscilloscope (LeCroy) interfaced to a computer.

Density functional theory (DFT) and second order Moller-Plesset perturbation theory (MP2) calculations are employed to investigate the structures, energetics and vibrational spectra of the $[H(C_6H_6)_m(H_2O)_n]^+$ Ar complexes where m=1 and n=1, 2 for comparison to the experiment. DFT is used for the larger systems in order to minimize the computational cost. These computations use the Gaussian 03W package and the 6-311+G (d, p) basis set.[138] The computed vibrational frequencies are scaled by a factor of 0.9575 for DFT and 0.9523 for MP2, which are the recommended values for these levels of theory and basis sets.[139]

6.3 Results and discussion

The potential energy surface of the $[bz\text{-}H_2O]H^+$ complex has been calculated by Nguyen and coworkers using the MP2/6-31+G (d, p) level of theory, which predicted two low lying isomers corresponding to the $bz(H_3O)^+$ and $bzH^+\text{-}H_2O$ structures. This MP2 calculation showed that the energy difference between these two isomers is 2.62 kcal/mol and the barrier to proton transfer is 2.5 kcal/mol.[144] We have obtained the same structures using DFT-B3LYP and MP2 levels of theory and the 6-311+G (d, p) basis set. The binding energies and relative energetics of various isomers calculated using these two different theories are shown in Table 6.1. The main difference between DFT and MP2 is that DFT finds $bzH^+\text{-}H_2O$ as the lowest energy isomer (3.5 kcal/mol lower energy than $bz(H_3O)^+$), while MP2 finds $bz(H_3O)^+$ as the lowest energy isomer (6.2 kcal/mol lower than $bzH^+\text{-}H_2O$) on the potential energy surface. To our knowledge, the binding energies of these complexes have not been measured. The computed binding energies of

the bz$(H_3O)^+$ and bzH^+-H_2O complexes (25.0 and 11.4 kcal/mol) are much greater than the available infrared photon energies and therefore it is not possible to study these species directly via single photon photodissociation spectroscopy in the infrared. We must use rare gas atom predissociation, also known as rare gas tagging, in order for fragmentation to occur. The binding energies of argon to any of these ions have also not been measured to our knowledge, and we calculated these energies to be low (~300-400 cm^{-1}). Therefore, photodissociation is expected to occur efficiently for these weakly bound complexes and indeed we see photofragmentation even in the low frequency region.

Figure 6.1 shows the infrared spectrum measured for the [(bz)H^+(H_2O)Ar] complex by monitoring the mass channel corresponding to the elimination of argon (middle trace). The lower and upper traces show the spectra of the bzH^+-Ar and H_3O^+-Ar_2 species for a comparison with the spectrum of [(bz)H^+(H_2O)Ar]. The inset structures corresponding to each complex are obtained from theory. The infrared spectroscopy of argon tagged protonated benzene has been described by our research group in detail.[125] Here we show the spectrum measured previously in order to explain the spectroscopy of the [(bz)H^+(H_2O)Ar] system. The main structural information obtained from the IR study of bzH^+-Ar was that protonation occurs on one of the carbon atoms of the benzene ring changing the hybridization of that carbon from sp^2 to sp^3. The high proton affinity of benzene compensates for the loss of resonance energy to make protonation favorable for this system. The overlapping symmetric and asymmetric sp^3 CH_2 stretches of benzene are observed at ~2820 cm^{-1} as a set of intense peaks. As an effect of protonation, charge delocalizes in the pi-system and part of the ring opposite the protonation site acquires a partial positive charge. Therefore, the ring modes of "charged" benzene turn on appearing as strong peaks in the low frequency region. The two intense peaks at 1456 and 1607

cm^{-1} in the spectrum of bzH^+-Ar are assigned to the asymmetric stretches involving the CCC framework of protonated benzene. These low frequency peaks along with the 2820 cm^{-1} peak corresponding to the sp^3 CH_2 stretch are considered as spectral signatures of protonated benzene.

The IRPD spectrum of the $H_3O^+Ar_2$ complex is shown in the upper trace of Figure 6.1, obtained by monitoring the mass channel corresponding to the elimination of argon. The vibrational spectroscopy of $H_3O^+Ar_2$ has been studied by our group[142] and also that of Johnson and coworkers.[15g] The spectrum of the neat hydronium cation has the symmetric and asymmetric O-H stretch vibrations at 3445/3491 and 3514/3530 cm^{-1} (inversion doublets).[7-9] In the $H_3O^+Ar_2$ complex, two O-H bonds of hydronium are solvated by the two argon atoms leaving only one free O-H bond. Therefore, three bands are expected in the O-H stretch region. The free O-H stretch is observed at 3540 cm^{-1} which is close to the corresponding stretch of the neat hydronium ion. The argon bound symmetric and asymmetric O-H stretches are shifted to the red at 3187 and 3266 cm^{-1} respectively. The low frequency peaks (1613 and 1876 cm^{-1}) are assigned to the hydronium bending mode (1613 cm^{-1}) and a combination band of the bending mode with one of the low frequency vibrational modes (1876 cm^{-1}).[15g] The umbrella or inversion vibration of the isolated hydronium ion is expected below 1000 cm^{-1},[8] and not detected probably because of the higher argon binding energy.

Having described the spectra of the bzH^+-Ar and $H_3O^+Ar_2$ complexes, we can now discuss the spectrum of $[(bz)H^+(H_2O)Ar]$. The first noticeable feature is that there are no peaks observed in the 2800-2850 cm^{-1} region. If protonation occurs to benzene making a bzH^+-H_2O structure, there should be a peak around this region, which would correspond to the spectral signature of the sp^3 CH_2 stretch. DFT predicts this stretch at 2433 cm^{-1} (see Figure S1 in Appendix). As shown in the spectrum of $[(bz)H^+(H_2O)Ar]$, there is no peak observed in the

2400-2800 cm^{-1} region. The other strong peaks at 1239, 1456 and 1607 cm^{-1},which turn on as an effect of benzene protonation, are also not observed in the spectrum of [bz-H_2O]H^+-Ar . The other possible structure bz$(H_3O)^+$-Ar resembles that of $H_3O^+Ar_2$, with a hydronium core and one of the argon atoms is replaced by benzene. In that case, there are three main vibrations expected - a free O-H stretch, an argon-bound O-H stretch and an O-H stretch towards benzene. The free O-H stretch should be very close to the corresponding stretch of $H_3O^+Ar_2$ and indeed a peak at 3555 cm^{-1} is observed for the bz$(H_3O)^+$-Ar complex, which is close to the free O-H stretch observed at 3540 cm^{-1} for $H_3O^+Ar_2$. The other peak at 3395 cm^{-1}, which is more intense than the 3555 cm^{-1} peak, can then be assigned to the O-H stretch attached to the argon atom. Theory predicts this argon-bound O-H stretch at 3398 cm^{-1}, which agrees well with this assignment. This peak is more intense than that of the free O-H stretch since the argon interaction with O-H enhances the intensity of this stretch band. The remaining O-H stretch towards benzene is one of the most interesting aspects of the spectrum of the bz$(H_3O)^+$-Ar complex. DFT and MP2 predict this stretch at two significantly different frequencies, at 2247 and 2635 cm^{-1} respectively (see Figure S2 in Appendix). These predicted stretches are more red shifted than the free O-H stretches of hydronium by an amount of ~1000-1300 cm^{-1}. This large red shift is consistent with the ionic-π type of hydrogen bonded interaction, and it is known that the amount of red shift corresponds to the strength of the hydrogen bond.[90, 118, 119, 126] However, since the proton affinity difference between benzene and water is small, this hydrogen bonded stretch can also be considered as a shared proton stretch between benzene and water, rather than an oxonium O-H stretch towards benzene. In a protonated complex, if the proton affinity difference (ΔPA) between the constituents is small, the proton does not tend to localize on any of these constituents, but instead is shared between them. In such complexes, the proton can undergo

high amplitude motion due to its low mass and therefore this stretch is highly anharmonic in nature. The shared proton stretch vibration can also couple strongly with low frequency vibrational modes which results in combinations bands, Fermi resonances and overtones. Therefore, harmonic calculations have often been unsuccessful in predicting the frequency of the shared proton stretch. However, the high amplitude motion of a charged species leads to a greater change in dipole moment derivative, and as a result an extremely high oscillator strength is associated with this stretch. With the recent availability of new infrared laser systems which can go as low as 600 cm^{-1}, these stretches have been probed by vibrational spectroscopy and are known to appear in a wide range of frequencies depending on ΔPA of the two constituents competing for the proton.[17] For example, the symmetrically shared proton has stretch at ~750 cm^{-1} for the protonated nitrogen dimer (ΔPA = 0),[22] whereas the asymmetrically shared proton stretch in the H_3O^+-N_2 complex (ΔPA = 197 kJ/mol) is observed at ~2800 cm^{-1}.[145] In the IR spectrum of bz$(H_3O)^+$-Ar, two peaks in the low frequency region are observed at 1639 and 1949 cm^{-1}, where the 1949 cm^{-1} peak is more intense. The peak at 1639 cm^{-1} is close to the hydronium bending mode, which is observed at 1613 cm^{-1} for the $(H_3O)^+Ar_2$ complex. Therefore, it makes sense that 1639 cm^{-1} band is the hydronium bending mode of the bz$(H_3O)^+$-Ar species. The only remaining strong peak observed at 1949 cm^{-1} is then assigned to the shared proton stretch between benzene and water. This peak is significantly shifted to the red from the free O-H stretch of $(H_3O)^+$-Ar_2 (3540 cm^{-1}) and also from the argon-bound O-H stretches (3187 and 3266 cm^{-1}). This makes sense because benzene is more polarizable than argon. The 1949 cm^{-1} peak is intense because of the high oscillator strength associated with the proton stretch. This peak also appears 73 cm^{-1} higher than the combination band observed for $(H_3O)^+$-Ar_2 at 1876 cm^{-1}. Therefore, the 1949 cm^{-1} peak is probably not a combination band.

Further confirmation regarding the assignment of this peak can be obtained using a spectroscopic study done by Johnson and coworkers.[17] They have shown that the proton stretch has a nearly linear correlation with ΔPA values between the species competing for proton. Based on their measured spectra for a number of complexes with different ΔPA values, they made a plot of ΔPA vs. frequencies of the observed shared proton stretch. Ideally this plot should predict the shared proton stretch of a complex if ΔPA of the constituents is known. According to this analysis, since the ΔPA between benzene and water is ~60 kJ/mol, the shared proton stretch for the $bz(H_3O)^+$ complex should appear at ~1950 cm^{-1}. In our spectrum of $bz(H_3O)^+$-Ar, this is indeed exactly where we observe the band.

Although infrared spectroscopy of $[bz\text{-}H_2O]H^+$-Ar proves that the $bz(H_3O)^+$ isomer is preferred over the $bzH^+\text{-}H_2O$ isomer, it does not provide information about why the preferential site of protonation is water even though benzene is more basic. The preferential protonation site of a complex depends on the overall complexation energy, and so this information can only be obtained from the energetics of these two isomers. As shown in Table 6.1, both DFT and MP2 calculations show that the complexation energy of $bz(H_3O)^+$ (25.0 and 28.7 kcal/mol respectively) is much greater than that of $bzH^+\text{-}H_2O$ (11.4 and 13.6 kcal/mol respectively). Although both the isomers are found to reside in the potential energy surface as stable minima having a low barrier for proton transfer, protonation certainly favors $bz(H_3O)^+$ over $bzH^+\text{-}H_2O$. The structural parameters (bond lengths and angles) of different isomers of the $[(bz)H(H_2O)Ar]^+$ complex, predicted frequencies corresponding to these isomers, and the binding energies are shown in Appendix. Here it is worth discussing the structural details obtained for the $[(bz)H(H_2O)]^+$ complex using two level of theories (DFT and MP2). MP2 finds the $bz(H_3O)^+$ isomer to be more stable by 6.2 kcal/mol than the $bzH^+\text{-}H_2O$ isomer. In the $bz(H_3O)^+$ complex,

hydronium forms a nearly symmetrical bifurcated hydrogen bond of the ionic H…C type with two adjacent C atom of benzene. The structure in which the O-H of oxonium ion directly interacts with one of the C atoms of benzene is found as a transition state between the $bz(H_3O)^+$ and bzH^+-H_2O isomers. DFT, as opposed to MP2, finds bzH^+-H_2O as the lowest energy isomer and in the $bz(H_3O)^+$ complex, the O-H of hydronium forms a hydrogen bond with one of the carbon atoms of the benzene ring. This O-H bond length (1.051 Å) calculated using DFT is also longer than the corresponding bond length (1.026 Å) calculated using MP2. The predicted spectra for these slightly different structures obtained from different theories are compared to the observed spectrum in Figures S1 and S2 of Appendix. MP2 predicts the hydronium stretch to appear at 2635 cm^{-1}, while DFT predicts this at 2247 cm^{-1}. Comparing the predicted frequencies with the observed frequency of the shared proton stretch and the benzene bound O-H bond lengths of hydronium calculated using two different theories, it is apparent that although theory indicates more hydronium character than the experiment, the description of the delocalized proton is better obtained by DFT than MP2.

The spectroscopy of $[bz\text{-}H_2O]H^+$-Ar shows that the preferential protonation site is water although benzene is more basic. The next step was to add more water to study the solvation effect in a systematic manner. The second trace of Figure 6.2 shows the photodissociation spectrum measured for $[(bz)H(H_2O)_2]^+$-Ar by monitoring the mass channel corresponding to the elimination of argon. The upper trace shows the spectrum of the $H_5O_2^+$-Ar complex for a comparison. The lower trace shows the predicted spectrum for $bz(H_5O_2)^+$-Ar. Protonated water dimer ($H_5O_2^+$), also known as the "Zundel" ion, has a symmetric structure with the proton equally shared between the two water molecules and therefore only two stretches corresponding to the symmetric and asymmetric O-H stretches are expected in the high frequency region. The

binding energy of $H_5O_2^+$ with respect to elimination of water is over 30 kcal/mol (~10500 cm^{-1})[82] and so photodissociation is not possible without tagging. The argon atom attaches to the one of the terminal O-H bonds making this molecule asymmetric and so there are four stretches (3523, 3616, 3658 and 3696 cm^{-1}) in the high frequency region. The two peaks at 3616 and 3696 cm^{-1} are assigned to the stretches of the water molecule remote from the argon atom. The other two peaks at 3523 and 3658 cm^{-1} are more intense and these are assigned to the symmetric and asymmetric stretches of the water molecule bound to the argon atom. These stretches are shifted to the red from the corresponding vibrations of free water molecules (3657 and 3756 cm^{-1} respectively). In the neat $H_5O_2^+$ ion, since a proton is equally shared between the two water molecules ($\Delta PA = 0$), this shared proton stretch is shifted to lower frequencies. Recent vibrational spectroscopic studies along with anharmonic calculations assigned the peak at 1073 cm^{-1} to the shared proton stretch for $H_5O_2^+$-Ar.[15b, c, d] The other remaining peak at 1764 cm^{-1} is assigned to a bending mode. The spectrum of bz$(H_5O_2)^+$-Ar has three sharp peaks (3523, 3634 and 3718 cm^{-1}) and one relatively broad peak (2970 cm^{-1}) in the high frequency region. The computed lowest energy structure shows that benzene binds to the same water molecule as argon in a "cis" position, i.e. to the other free O-H bond of the argon-bound water molecule, forming a π-hydrogen bond. The O-H bonds of the other water remote from benzene are free and so the peaks at 3634 and 3718 cm^{-1} are assigned to the symmetric and asymmetric stretches of this free water molecule. These stretches are shifted ~20 cm^{-1} to higher frequencies from the corresponding free O-H stretches of $(H_5O_2)^+$-Ar. Apparently, the polarization effect of benzene is transferred even to remote water through the molecular framework. The O-H bond lengths of the free water molecule are shorter in bz$(H_5O_2)^+$-Ar (0.965 Å) than those of $(H_5O_2)^+$-Ar (0.967 Å). The peak at 3523 cm^{-1} is assigned to the symmetric stretch of argon-bound O-H. This peak

position is exactly the same as the corresponding stretch of $(H_5O_2)^+$-Ar. Apart from these three sharp peaks in the high frequency region, one additional O-H stretch towards benzene is expected. Indeed, this π-hydrogen bonded band, which is somewhat broader, is observed at 2970 cm^{-1} in the spectrum of $bz(H_5O_2)^+$-Ar. Theory predicts this stretch at 2978 cm^{-1}, which is less than 10 cm^{-1} from the observed band. In the low frequency region, the spectrum has two strong peaks at 1488 and 1820 cm^{-1} along with a weak feature at 1928 cm^{-1}. We notice that the set of peaks at 1488 and 1820 cm^{-1} are shifted to higher frequencies from those observed for $(H_5O_2)^+$-Ar (1073 and 1764 cm^{-1}). The 1073 cm^{-1} peak is assigned to the "Zundel"-ion stretch and since $bz(H_5O_2)^+$-Ar has the same core, a stretch corresponding to this unit is expected. We have discussed before that the polarization effect of benzene shifts the O-H stretches of remote water to higher frequencies. Therefore, it makes sense that the water molecule adjacent to benzene feels this effect more, and the proton moves closer to this water. The distance of the proton from the oxygen in the water molecule interacting with argon in the $(H_5O_2)^+$-Ar complex is 1.140 Å, whereas this distance in $bz(H_5O_2)^+$-Ar is significantly shorter (1.052 Å). As a result, this unequally shared proton stretch shifts to a higher frequency. This stretch band is actually shifted 415 cm^{-1} to the blue compared to the corresponding stretch for the $(H_5O_2)^+$-Ar complex. For the same reason the bending mode at 1820 cm^{-1} is also shifted to a higher frequency compared to the corresponding mode of $(H_5O_2)^+$-Ar (1764 cm^{-1}).

Figure 6.3 shows the spectrum of $[(bz)H(H_6O_3)]^+$ (second trace from the top) obtained by monitoring the mass channel corresponding to elimination of benzene. Apparently, the binding energy of this complex with respect to the elimination of benzene is less than the infrared photon energy, and we see photofragmentation without argon tagging. The lower two traces show the predicted spectra for the $bz(H_7O_3)^+$ and $bzH^+(H_2O)_3$ complexes and the corresponding structures

are shown in the inset. The top trace shows the spectrum of $(H_7O_3)^+$-Ar and the inset structure is obtained from theory. Comparing the predicted spectra corresponding to the two isomers of $[(bz)H(H_6O_3)]^+$, the observed spectrum is best described by that of $bz(H_7O_3)^+$. A comparison of the spectra of $(H_7O_3)^+$-Ar and $bz(H_7O_3)^+$ also shows that the protonation occurs on the water making it a $(H_7O_3)^+$ ion solvated by benzene. In the spectrum of $(H_7O_3)^+$-Ar, three intense peaks are observed at 3577, 3638 and 3722 cm^{-1}. As shown in the inset structure, $(H_7O_3)^+Ar$ has a hydronium core with two water molecules interacting with two of the O-H bonds and the other O-H binds to the argon atom. Therefore, the assignments of these three peaks in the high frequency region are relatively straightforward. The 3638 and 3722 cm^{-1} peaks are the O-H stretches of free water. The other stretch at 3577 cm^{-1} is the argon-bound O-H stretch. In the spectrum of $bz(H_7O_3)^+$ the free water stretches are shifted to higher frequencies. These peaks are observed at 3641 and 3732 cm^{-1}, whereas the spectrum of $(H_7O_3)^+$-Ar has the corresponding stretches at 3638 and 3722 cm^{-1}. The hydrogen bonded stretch for $bz(H_7O_3)^+$ is observed at 3192 cm^{-1}. This band is shifted 331 cm^{-1} to the red compared to the argon-bound O-H stretch of $(H_7O_3)^+$-Ar, consistent with the greater polarization effect of benzene. There is no evidence for the $bzH^+(H_2O)_3$ isomer in the experimental spectrum.

Infrared spectroscopy of the $[bzH(H_2O)_n]^+$ complexes, where n=1-3, show that the preferential site of protonation is water making the structures that of protonated water clusters solvated by benzene. The second trace of Figure 6.4 shows the infrared spectrum measured for the $[bzH(H_2O)_4]^+$ complex by monitoring the mass channel corresponding to the elimination of benzene. The spectrum of the $H(H_2O)_4^+$-Ar complex is shown in the upper trace for comparison. The bottom trace shows the predicted spectrum for the lowest energy isomer of $[bzH(H_2O)_4]^+$. The structures shown in the insets are computed from theory. The spectroscopy of $H(H_2O)_4^+$-Ar

has been described by our group in detail.[62] The spectrum has two sharp peaks (3646 and 3732 cm^{-1}) in the high frequency region and two broad bands (centered at 2670 and 3053 cm^{-1}) in the hydrogen bonding region. The neat $H(H_2O)_4^+$ ion, also known classically as the "Eigen" ion, where a hydronium core is solvated by three water molecules each hydrogen bonded to a single O-H. Theory for the $H(H_2O)_4^+$-Ar complex finds a couple of low energy isomers, but the spectrum suggests the presence of a symmetrical "Eigen" core with a weakly interacting argon. Therefore, only two peaks at 3646 and 3732 cm^{-1} are observed, consistent with a symmetrical structure and these peaks are assigned to the free symmetric and asymmetric O-H stretches of $H(H_2O)_4^+$-Ar. The broad band in the hydrogen bonding region is associated with the symmetric "Eigen" ion stretch. The mechanism of broadening of hydrogen bonded peaks is not well understood. However, some possible explanations have been proposed such as an inhomogeneous effect from different isomeric species, a temperature effect, a predissociation lifetime effect or a lifetime effect from the relative rates for intramolecular vibrational relaxation (IVR). As discussed previously for the $H(H_2O)_4^+$-Ar complex, although there are some low lying isomers possible, the observed spectrum suggests that only one isomer is present corresponding to a more symmetrical structure.[21] This rules out the possibility of an inhomogeneous effect arising from different isomers. The line widths of the high frequency peaks are much sharper, which suggests that the temperature does not affect the broadening. The predissociation lifetime should be longer at lower energy and as the high frequency peaks are sharper than the hydrogen bonded peaks observed at the low frequency. Therefore, this cannot be the source of this broadening. However, the relative rates of IVR can be different for different vibrational modes with different coupling strength. Apparently, the free O-H stretches are less well-coupled to the molecular framework than that of the hydrogen bonding modes.

This makes sense because the core ion is bonded to three other water molecules which make the coupling stronger.

The interaction of benzene with $H(H_2O)_4^+$ is expected to have a greater perturbation on the core hydronium stretch and in the spectrum of bz-$H(H_2O)_4^+$ indeed we see that this band is shifted to higher frequencies. The hydrogen bonded peaks are observed at 2830 cm^{-1}, which is 160 cm^{-1} blue shifted compared to the corresponding stretch of $H(H_2O)_4^+$-Ar. The symmetric O-H stretch towards benzene is observed at 3473 cm^{-1} and this peak is also broad, consistent with the π-hydrogen bonding interaction. The spectrum also has three sharp peaks at 3645, 3700 and 3734 cm^{-1}. The peaks at 3645 and 3734 cm^{-1} are observed at about the same positions as the free O-H symmetric and asymmetric stretches of $H(H_2O)_4^+$-Ar (3645 and 3732 cm^{-1} respectively). Therefore, we assign these peaks to the symmetric and asymmetric free O-H stretches. Apparently, the polarization effect of benzene does not change these remote O-H stretches. The other relatively broad peak at 3700 cm^{-1} is assigned to the asymmetric O-H stretch towards benzene. The predicted spectrum corresponding to the computed structure agrees well with the experiment.

The spectroscopic study so far shows that the progressive addition of water to the $[bzH(H_2O)]^+$ species produces protonated water clusters solvated by benzene. The other interesting aspect of this work is the effect of multiple benzenes on the $[bzH(H_2O)]^+$ complex. To start this discussion in a simple way, we first show the spectrum of $[bz_2H(H_2O)]^+$. The upper trace of Figure 6.5 shows the infrared spectrum measured for $[bz_2H(H_2O)]^+$-Ar obtained by monitoring the mass channel corresponding to the elimination of argon. The neat $[bz_2H(H_2O)]^+$ species has two low energy isomers corresponding to the $bz_2(H_3O)^+$ and bz_2H^+-H_2O structures. The predicted vibrational spectra corresponding to these isomers are shown in the bottom two

traces of Figure 6.5. The most stable isomer $bz_2(H_3O)^+$ has a 6.6 kcal/mol lower energy than that of bz_2H^+-H_2O. The calculated binding energies for these two complexes are 41.1 and 17.3 kcal/mol respectively, and therefore photodissociation is not possible without tagging. As shown in Figure, the observed spectrum is best described by that predicted for $bz_2(H_3O)^+Ar$ (second trace from the top). In the $bz_2(H_3O)^+Ar$ complex, the coordination of H_3O^+ is filled with two benzenes and one argon. Therefore, two main vibrational bands are expected. The argon-bound O-H stretch is observed at 3457 cm^{-1} and this peak is shifted 62 cm^{-1} to the blue from the corresponding stretch of $bz(H_3O)^+Ar$. The polarization effect of benzene apparently shifts this stretch to a higher frequency. The symmetric and asymmetric π-hydrogen bonded stretches appear as a broad resonance centered at 2740 cm^{-1}. Comparing the predicted spectra for the two isomers with the observed spectrum, it is clear that even though the bz_2H^+-H_2O isomer has only a 6.6 kcal/mol higher energy than that of $bz_2(H_3O)^+Ar$, the latter is preferred over the former. Apparently, the preferential protonation site is still water in a complex in which more than one benzene is present.

We extend this study to protonated water dimer ($H_5O_2^+$) by progressively adding multiple benzenes. The bottom trace of Figure 6.6 shows the infrared spectrum of the $(H_5O_2)^+$-Ar complex and the ascending traces show the spectra of $bz_n(H_5O_2)^+$-Ar, where n=1-2 and $bz_m(H_5O_2)^+$, where m=3-4. The spectra of $(H_5O_2)^+$-Ar and $bz(H_5O_2)^+$-Ar were described in detail before and we have seen that the addition of benzene to $(H_5O_2)^+$-Ar shifts both the shared proton and O-H stretching bands to higher frequencies due to the greater polarization effect. The spectrum of $bz_2(H_5O_2)^+$-Ar shows the hydrogen bonded stretch at 3110 cm^{-1} which is 140 cm^{-1} shifted to the blue compared to the corresponding stretch for $bz(H_5O_2)^+$-Ar at 2970 cm^{-1}. The free O-H stretches are observed (3636 and 3717 cm^{-1}) at about the same positions as the

corresponding stretches (3634 and 3718 cm^{-1}) of $bz(H_5O_2)^+$-Ar. However, these peaks for $bz_2(H_5O_2)^+$-Ar are not as sharp as those for $bz(H_5O_2)^+$-Ar. The peaks in the low frequency region are observed at slightly different positions (1462 and 1788 cm^{-1}) than the corresponding stretches of $bz(H_5O_2)^+$-Ar (1488 and 1820 cm^{-1}). The photodissociation spectrum of $bz_3(H_5O_2)^+$ is obtained by monitoring the benzene elimination channel because apparently the third benzene is weakly bound. In the spectrum of $bz_3(H_5O_2)^+$, the hydrogen bonded stretch is observed at 3129 cm^{-1}, which is again blue shifted from the corresponding stretch of $bz_2(H_5O_2)^+$-Ar . The free O-H stretches for this complex are observed at 3621 and 3706 cm^{-1} respectively. For $bz_4(H_5O_2)^+$, each of the four O-H bonds of the two water molecules are hydrogen bonded to benzene. Therefore, no free O-H stretch is observed for this complex. However, the hydrogen bonded peak is broader than those observed for other sizes. This spectrum also has three weak peaks at 3049, 3075 and 3100 cm^{-1} which correspond to the well known "Fermi triad" of isolated benzene.[146]

Having assigned the vibrational spectra for the $bz_n(H_5O_2)^+$-Ar complexes, it is interesting to consider how shared proton and π-hydrogen bonded interactions change with benzene solvation. The π-hydrogen bonded stretch for $bz(H_5O_2)^+$-Ar is shifted to a lower frequency (2970 cm^{-1}) than the free O-H stretches (3658, 3696 cm^{-1}) or from the argon-bound stretch (3523 cm^{-1}) of $(H_5O_2)^+$-Ar. It is known that this red shift corresponds to the strength of the hydrogen bond.[90, 118, 119, 126] Then it makes sense that this stretch is less red shifted for $bz_2(H_5O_2)^+$-Ar because in this case there are two π-hydrogen bonds and the strength of each of these two interactions is less than the single interaction of one hydrogen bond in the $bz(H_5O_2)^+$-Ar species. For the same reason, the hydrogen bonded stretches for the higher cluster sizes are less red shifted compared to the free O-H stretches. The $bz_4(H_5O_2)^+$ complex has a completed

coordination with each benzene interacting with one O-H bond, which makes a symmetrical environment around $(H_5O_2)^+$. Therefore, there is no free O-H stretch observed and all four hydrogen bonded stretches appear around the same position making this peak broader than those observed for all the other sizes.

The effect of solvation by benzene is relatively subtle on the shared proton stretch. We have discussed before that due to the polarization effect the proton moves closer to benzene and therefore this proton stretch is 415 cm^{-1} shifted to the blue for $bz(H_5O_2)^+$-Ar compared to that of $(H_5O_2)^+$-Ar. However, for the $bz_2(H_5O_2)^+$-Ar complex the observed band is less blue shifted (26 cm^{-1}) than that of $bz(H_5O_2)^+$-Ar. We also notice that this peak at 1462 cm^{-1} for $bz_2(H_5O_2)^+$-Ar is relatively weaker than the 1488 cm^{-1} peak observed for $bz(H_5O_2)^+$-Ar. In order to explain this apparent anomaly we look closely at the spectrum of the $bz_2(H_5O_2)^+$-Ar complex. DFT predicts that this complex has two low lying isomers. In the first, benzene attaches to the same water molecule as the other benzene in a "cis" structure. In the other isomer, benzene binds to the free water molecule in a "trans" structure. The energy difference between these two isomers is low (~300 cm^{-1}). Figure 6.7 shows the predicted spectrum corresponding to these isomers along with that spectrum for $bz_2(H_5O_2)^+$-Ar . For the "cis" and "trans" isomers the symmetric and asymmetric free O-H stretches are predicted at 3583/3668 and 3598/3771 cm^{-1} respectively. The observed spectrum does not have sharp peaks in this region, but rather the peak observed at 3636 and 3717 cm^{-1} are broad and noisy. The hydrogen bonded peaks are broad and stretches predicted for these two isomers are roughly at the same position. Therefore, it is hard to decide if one isomer is preferred over the other by looking at the peaks in the high frequency region. However, for these two different isomers the shared proton stretch frequency is predicted to be significantly different. In the "cis" isomer, one water molecule is polarized by two benzenes,

and so the proton is more localized on this water compared to water molecules in the "trans" isomer, where each water is polarized by benzene to the same extent. The proton stretch for the "cis" isomer is predicted at 2124 cm^{-1} indicating a hydronium like character, whereas for the "trans" isomer this stretch is predicted at 997 cm^{-1} indicating a shared proton character. Although it is known that harmonic calculations have often been unsuccessful in predicting the shared proton stretch, but it seems that we detect only the shared proton stretch of the "cis" isomer at 1462 cm^{-1} which is close to the corresponding stretch of $bz(H_5O_2)^+$-Ar. The same stretch of the "trans" isomer is probably shifted down to an even lower frequency and we probably could not detect it because of low laser power in the low frequency region as well as the relative abundance of the "trans" isomer.

6.4 Conclusions

Mixed complexes of protonated benzene and water are studied via infrared photodissociation spectroscopy in a pulsed supersonic expansion source employing an electric discharge. Although benzene is more basic than water, the preferential site of protonation is water in the $[(bz)_nH(H_2O)_m]^+$ complexes due to the greater solvation energy. In the $[Hbz(H_2O)]^+$ system, the proton is unequally shared between benzene and water (the proton is closer to water). This shared proton stretch vibration can be predicted based on the relative proton affinity values of benzene and water. The shared proton stretch of protonated water dimer shifts to a higher frequency in the $[Hbz(H_2O)_2]^+$ complex because of the polarization effect induced by benzene. This effect is also transferred to the free O-H stretches of remote water. For $[Hbz(H_2O)_4]^+$, the "Eigen" ion stretch shifts to higher frequencies but the remote water molecules apparently do not experience the same polarization effect. The solvation of protonated water dimer with multiple

benzenes shifts the π-hydrogen bonded stretches towards higher frequencies due to a charge redistribution in the cluster. The spectrum of $bz_2(H_5O_2)^+$ indicates a symmetrical environment around $H_5O_2^+$, which shows that the coordination of $H_5O_2^+$ is completed with four benzene molecules. The shared proton stretches are also affected by the solvation.

Table 5.1: Computed binding energies and relative energies (with respect to the most stable isomer) of [(benzene)$H^+(H_2O)]Ar_n$ in kcal/mol. Calculations are done using MP2 and/or B3LYP levels of theory with 6-311+G (d, p) basis set. Energies are not ZPVE or BSSE corrected.

	DFT		MP2	
Complex	B.E.	ΔE	B.E.	ΔE
BW-1, 1 isomer-a $(bz\text{-}H_3O)^+$	25.0	+3.5	28.7	0.0
BW-1, 1 isomer-b $(bzH\text{-}H_2O)^+$	11.4	0.0	13.6	+6.2
BW-1, 1-Ar isomer-a $(bz\text{-}H_3O\text{-}Ar)^+$	27.0	+1.9	32.3	0.0
BW-1, 1-Ar isomer-b $(bzH\text{-}H_2O\text{-}Ar)^+$	11.8	0.0	15.5	+7.8

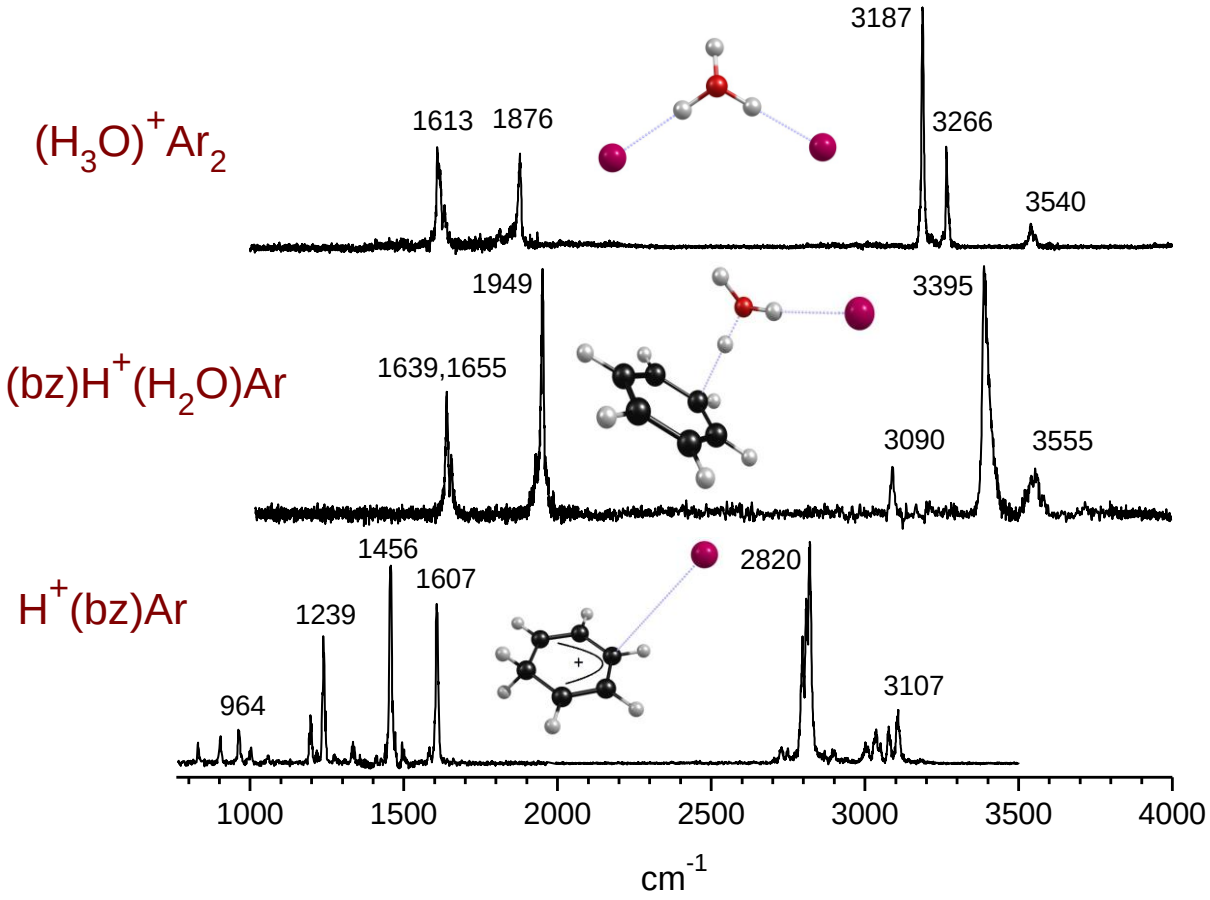

Figure 6.1: The infrared spectrum measured for the $(bz)H^+(H_2O)Ar$ complex by monitoring the mass channel corresponding to the elimination of argon (middle trace). The top and bottom traces show the spectra of $(H_3O)^+Ar_2$ and $H^+(bz)Ar$ in order for a comparison with the spectrum of $(bz)H^+(H_2O)Ar$. Inset structures are obtained from DFT.

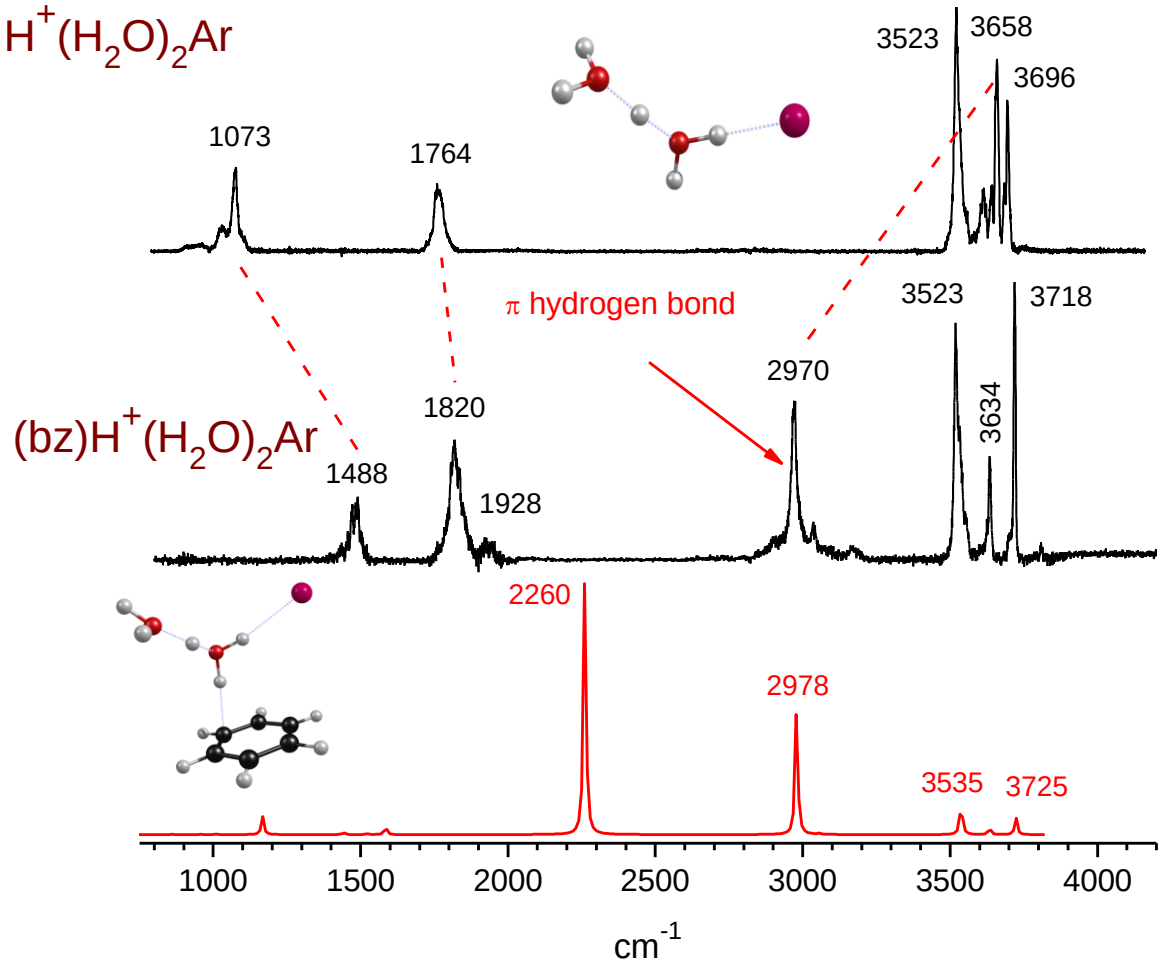

Figure 6.2: The first and second trace from the top show the infrared spectra measured for the $H^+(H_2O)_2Ar$ and $(bz)H^+(H_2O)_2Ar$ complexes by monitoring the mass channel corresponding to the elimination of argon. The bottom trace show the predicted spectrum corresponding to the lowest energy isomer of $(bz)H^+(H_2O)_2Ar$. Inset structures are obtained from DFT.

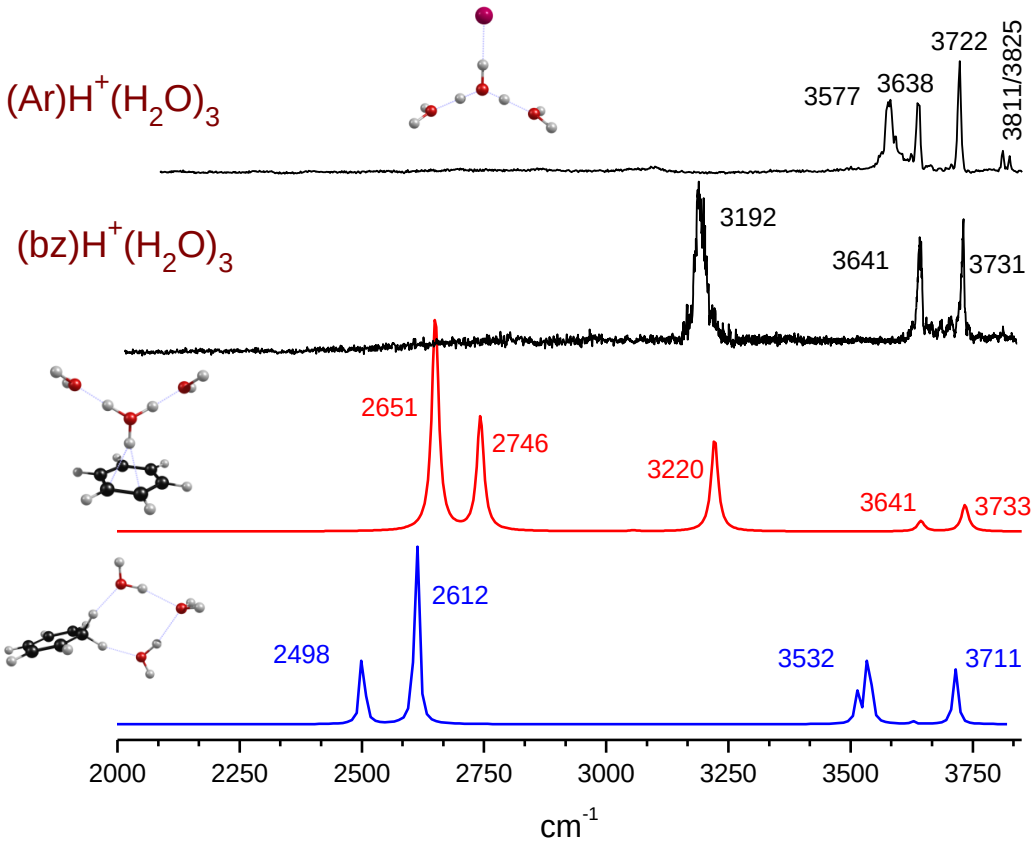

Figure 6.3: The second trace from the top shows the infrared spectrum of $(bz)H^+(H_2O)_3$ obtained by monitoring the mass channel corresponding to the elimination of benzene. The first trace show the spectrum measured for $H^+(H_2O)_3Ar$ by monitoring the argon elimination mass channel. The lower two traces show the predicted spectra for two low energy isomers of $(bz)H^+(H_2O)_3$. Inset structures are computed by DFT.

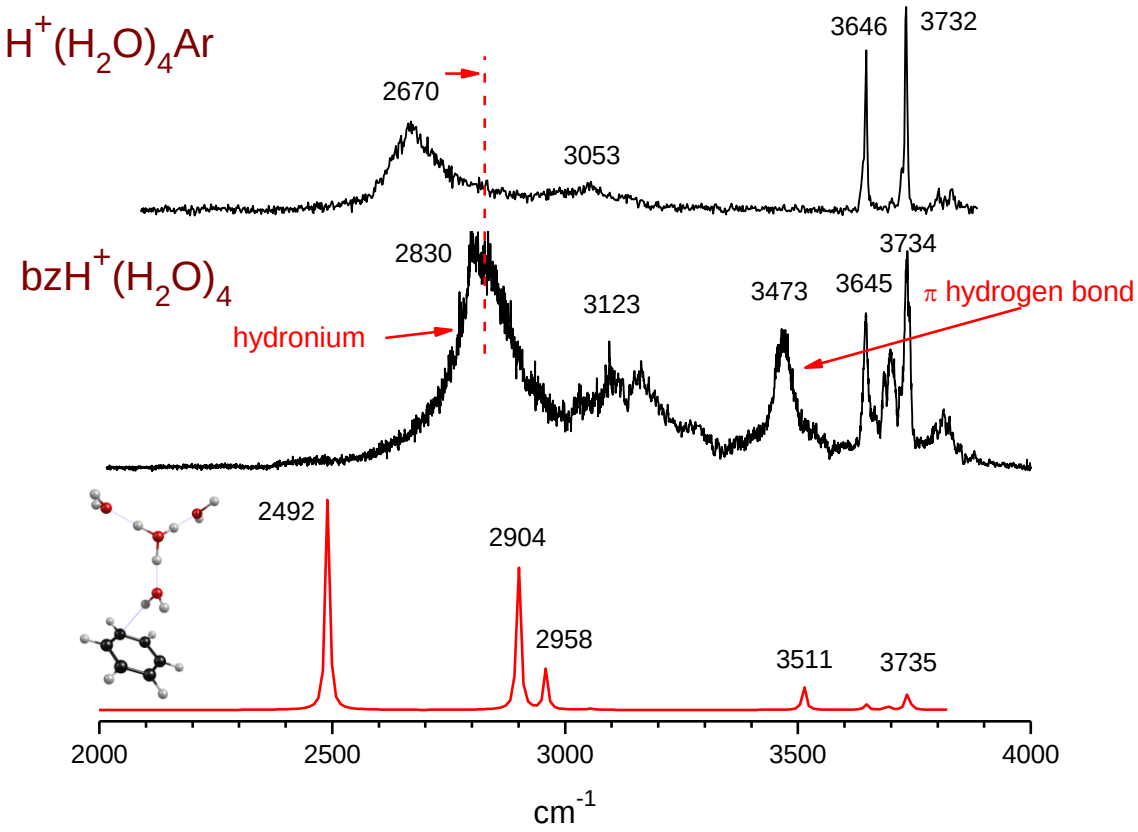

Figure 6.4: The second trace from the top shows the infrared spectrum measured for the $(bz)H^+(H_2O)_4$ complex by monitoring the mass channel corresponding to the elimination of benzene. The top trace shows the spectrum of $H^+(H_2O)_4Ar$ obtained by monitoring the argon elimination channel. The bottom trace shows the predicted spectrum corresponding to the lowest energy isomer of $(bz)H^+(H_2O)_4$. Inset structure is obtained from DFT.

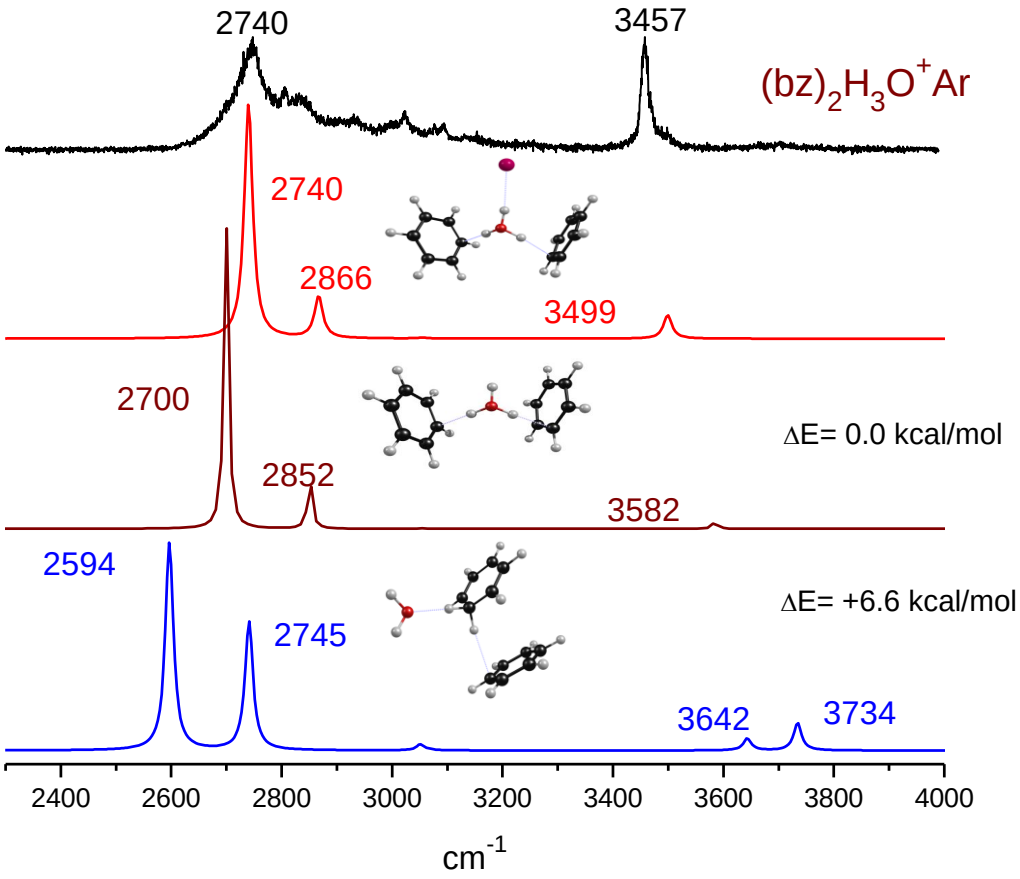

Figure 6.5: The top trace shows the spectrum of $(bz)_2H^+(H_2O)Ar$ obtained by monitoring the argon elimination channel. The second trace from the top shows the predicted vibrational spectrum corresponding to the $(bz)_2(H_3O)^+Ar$ structure. The lower two traces show the predicted spectra for two low energy isomers corresponding to the $(bz)_2(H_3O)^+$ and (bz)bz-H^+-(H_2O) structures. Inset structures are those obtained from DFT.

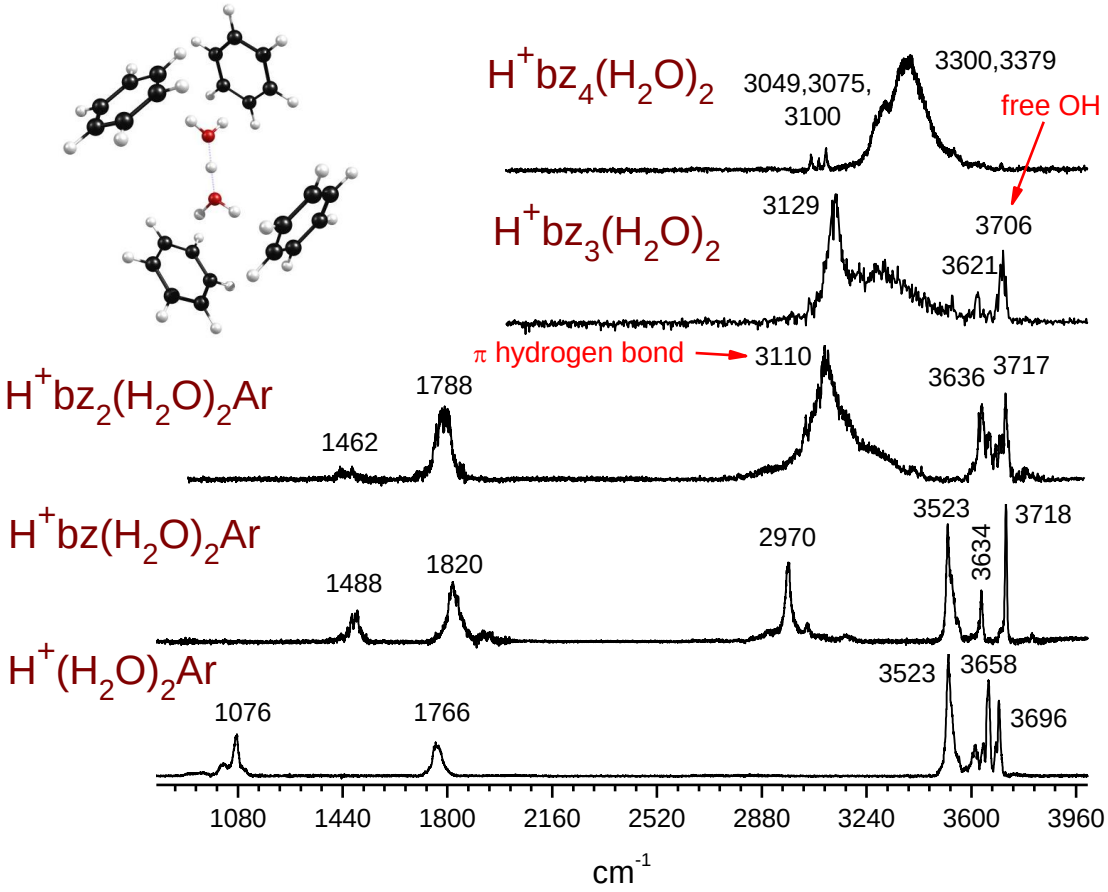

Figure 6.6: The spectra of protonated water dimer ($H_5O_2^+$) solvated by multiple benzenes. The bottom trace shows the infrared spectrum of $(H_5O_2)^+$-Ar and the ascending traces show the spectra of $bz_n(H_5O_2)^+$-Ar (where n=1-2) and $bz_m(H_5O_2)^+$ (where m=3-4).

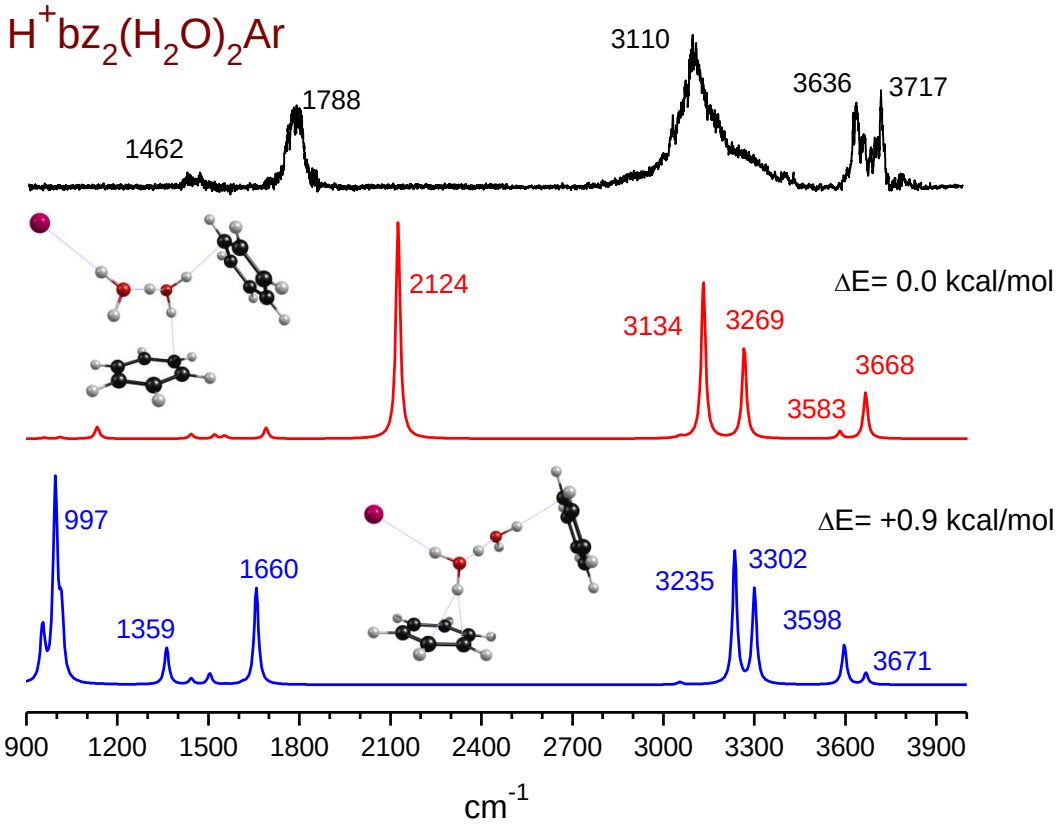

Figure 6.7: The top trace shows the infrared spectrum of $H^+bz_2(H_2O)_2Ar$. The middle trace shows the predicted spectrum corresponding to the "cis" isomer (two benzenes bind to the same water molecule). The bottom trace shows the predicted spectrum corresponding to the "trans" isomer (each water molecule binds to a single benzene). Inset structures are computed by DFT.

CHAPTER 7

CONCLUSIONS

Cation-water complexes are produced in a pulsed nozzle source using laser vaporization and the arc-electric discharge techniques. Mass-selected complexes are investigated with laser photodissociation spectroscopy. The spectra of singly charged metal cation-water-argon complexes show variations in the O-H stretch region depending on the electronic structure of the metal or the location of argon in the complex. For $Sc^+(H_2O)Ar$ and $Cr^+(H_2O)Ar$, argon binds to the C_2 axis opposite to water. Since the heavy atoms lie on the symmetry axis, the rotational constants for these complexes are large. The spectra of these two species show partially resolved rotational structure. However, this multiple band structure in the O-H region is not observed for $Mn^+(H_2O)Ar$ and $Zn^+(H_2O)Ar$ because argon binds to M^+ off the C_2 axis. All of these systems show red shifts in the O-H stretching frequencies. The symmetric stretch gains more intensity than the asymmetric stretch. For $Mn^+(H_2O)Ar_n$, where n=1-4, different binding sites of argon atoms produce low energy isomers. Similarly, the spectra of $Zn^+(H_2O)_nAr$ show evidence of different isomers. Doubly charged metal (Sc^{2+}, V^{2+}, Cr^{2+}, and Mn^{2+})-water complexes show larger red shifts in the O-H stretches than those of the singly charged ions. The intensity pattern of the symmetric and asymmetric stretches also switches in the doubly charged systems. The fragmentation and spectral patterns for $M^{2+}(H_2O)Ar_n$ show that the coordination of M^{2+} is filled with six ligands (five argons and a water).

The infrared spectroscopy of mixed complexes shed light on the proton sharing interaction of water with nitrogen and benzene. The proton affinity of water is much greater than that of nitrogen. The spectrum of mixed protonated complexes of water and nitrogen shows evidence for the $H_3O^+(N_2)_n$ structures with a partial proton sharing interaction. The proton affinity of benzene is more than that of water, but the preferential site of protonation is on water in the $[(bz)_nH(H_2O)_m]^+$ complexes due to the greater solvation energy. In the $[Hbz(H_2O)]^+$ system, the proton is unequally shared between benzene and water (the proton is closer to water). This shared proton stretch vibration can be predicted based on the relative proton affinity values of benzene and water. The shared proton stretch of protonated water dimer shifts to a higher frequency in the $[Hbz(H_2O)_2]^+$ complex because of the polarization effect induced by benzene. This effect is also transferred to the free O-H stretches of remote water. For $[Hbz(H_2O)_4]^+$, the "Eigen" ion stretch shift to higher frequencies, but the remote water molecules apparently do not experience the same polarization effect. The solvation of protonated water dimer with multiple benzenes shifts the π-hydrogen bonded stretches towards higher frequencies due to a charge redistribution in the cluster. The spectrum of $bz_2(H_5O_2)^+$ indicates a symmetrical environment around $H_5O_2^+$, which shows that the coordination of $H_5O_2^+$ is completed with four benzene molecules. The shared proton stretches are also affected by solvation.

CHAPTER 8

BIBLIOGRAPHY

1) a) J. Burgess, *Metal Ions in Solution* (John Wiley and Sons, New York, 1978). b) J. Burgess, *Ions in Solution* (Horwood Publishing, Chichester, U.K., 1999).

2) Y. Marcus, *Ion Solvation* (John Wiley & Sons, Chichester, U.K., 1985).

3) D. T. Richens, *The Chemistry of Aqua Ions* (John Wiley, Chichester, U.K., 1997).

4) F. A. Cotton, G. Wilkinson, C. A. Murillo and M. Bochmann, *Advanced Inorganic Chemistry*, (6^{th} ed., John Wiley, New York, 1999).

5) a) I. Bertini; A. Sigel; H. Sigel, eds., *Handbook on Metalloproteins*, Marcel Dekker, New York, (2001). b) K. A. Kumpf and D. A. Daugherty, "A mechanism for ion selectivity in potassium channels: computational studies of cation-pi interactions," *Science* **261**, 1708 (1993).

6) a) M. A. Duncan, "Spectroscopy of metal ion complexes: Gas phase models for solvation," *Ann. Rev. Phys. Chem.* **48**, 63 (1997). b) M. A. Duncan, "Frontiers in the spectroscopy of mass-selected molecular ions," *Int. J. Mass Spectrom.* **200**, 545 (2000).

7) a) M. H. Begemann, C. S. Gudeman, J. Pfaff and R. J. Saykally, "Detection of the hydronium ion (H_3O^+) by high-resolution infrared spectroscopy," *Phys. Rev. Lett.* **51**, 554 (1983). b) M. H. Begemann and R. J. Saykally, "A study of the structure, dynamics of the hydronium ion by high-resolution infrared laser spectroscopy - the υ_3 band of $H_3{}^{16}O^+$," *J. Chem. Phys.* **82**, 3570 (1985).

8) a) D.-L. Liu and T. Oka, "Experimental determination of the ground-state inversion splitting in H_3O^+," *Phys. Rev. Lett.* **54**, 1787 (1985). b) J. Tang and T. Oka, "Infrared spectroscopy of H_3O^+: The ν_1 fundamental band," *J. Mol. Spec.* **196**, 120 (1999).

9) F. Dong, D. Uy, S. Davis, M. Child and D. J. Nesbitt, "Supersonically cooled hydronium ions in a slit-jet discharge: High-resolution infrared spectroscopy and tunneling dynamics of HD_2O^+," *J. Chem. Phys.* **122**, 224301 (2005).

10) H. A. Schwarz, "Gas phase infrared spectra of oxonium hydrate ions from 2-5 μ," *J. Chem. Phys.* **67**, 5525 (1977).

11) a) L. I. Yeh, M. Okumura, J. D. Myers, J. M. Price and Y. T. Lee, "Vibrational spectroscopy of the hydrated hydronium cluster ions $H_3O^+(H_2O)_n$ (n=1,2,3)," *J. Chem. Phys.* **91**, 7319 (1989). b) L. I. Yeh, Y. T. Lee and J. T. Hougen, "Vibration-rotation spectroscopy of the hydrated hydronium ions $H_5O_2^+$, $H_9O_4^+$," *J. Mol. Spec.* **164**, 473 (1994). c) Y.-S. Wang, J.-C. Jiang, C.-L. Cheng, S. H. Lin, Y. T. Lee and H.-C. Chang, "Indentifying 2-, 3-coordinated H_2O in protonated ion-water clusters by vibrational pre-dissociation spectroscopy, *ab initio* calculations," *J. Chem. Phys.* **107**, 9695 (1997). d) J.-C. Jiang, Y.-S. Wang, H.-C. Chang, S. H. Lin, Y. T. Lee, G. Niedner-Schatteburg and H.-C. Chang, "Infrared spectra of $H^+(H_2O)_{5-8}$ clusters: Evidence for symmetric proton hydration," *J. Am. Chem. Soc.* **122**, 1398 (2000). e) H.-C. Chang, J.-C. Jiang, I. Hahndorf, S. H. Lin, Y. T. Lee and H.-C. Chang, "Migration of an excess proton upon asymmetric hydration: $H^+[(CH_3)_2O](H_2O)_n$ as a model system," *J. Am. Chem. Soc.* **121**, 4443 (1999).

12) a) K. R. Asmis, N. L. Pivonka, G. Santambrogio, M. Brümmer, C. Kaposta, D. M. Neumark and L. Wöste, "Gas-phase infrared spectrum of the protonated water dimer,"

Science **299**, 1375 (2003). b) K. R. Asmis, Y. Yang, G. Santambrogio, M. Brümmer, J. R. Roscioli, L. R. McCunn, M. A. Johnson and O. Kühn, "Gas phase infrared spectroscopy and multi-dimensional quantum calculations of the protonated ammonia dimer $N_2H_7^+$," *Ang. Chem. Int. Ed.* **46**, 8691 (2007).

13) a) T. D. Fridgen, T. B. McMahon, L. MacAleese, J. Lemaire and P. Maitre, "Infrared spectrum of the protonated water dimer in the gas phase," *J. Phys. Chem. A* **108**, 9008 (2004). b) T. D. Fridgen, L. MacAleese, P. Maitre, T.B. McMahon, P. Boissel and J. Lemaire, "Infrared spectra of homogeneous and heterogeneous proton-bound dimers in the gas phase," *Phys. Chem. Chem. Phys.* **7**, 2747 (2005). c) T. D. Fridgen, L. MacAleese, T. B. McMahon, J. Lemaire and P. Maitre, "Gas phase infrared multiple-photon dissociation spectra of methanol, ethanol, propanol proton-bound dimers, protonated propanol and the propanol/water proton-bound dimer," *Phys. Chem. Chem. Phys.* **8**, 955 (2006).

14) a) J.-W. Shin, N. I. Hammer, E. G. Diken, M. A. Johnson, R. S. Walters, T. D. Jaeger, M. A. Duncan, R. A. Christie and K. D. Jordan, "Infrared signature of structural motifs associated with the $H^+(H_2O)_n$, n=6-27, clusters," *Science* **304**, 1137 (2004). b) J. Headrick, E. G. Diken, R. S. Walters, N. I. Hammer, R. A. Christie, J. Cui, E. M. Myshakin, M. A. Duncan, M. A. Johnson and K. D. Jordan, "Spectral signatures of hydrated proton vibrations in water clusters," *Science* **308**, 1765 (2005**)**.

15) a) J. M. Headrick, J. C. Bopp and M. A. Johnson, "Predissociation spectroscopy of the argon-solvated $H_5O_2^+$ "zundel" cation in the 1000-1900 cm^{-1} region," *J. Chem. Phys.* **121**, 11523 (2004). b) E. G. Diken, J. M. Headrick, J. R. Roscioli, J. C. Bopp, M. A. Johnson and A. B. McCoy, "Fundamental excitations of the shared proton in the $H_3O_2^-$, $H_5O_2^+$

complexes," *J. Phys. Chem. A* **109**, 1487 (2005). c) N. L. Hammer, E. G. Diken, J. R. Roscioli, M. A. Johnson, E. M. Myshakin, K. D. Jordon, A. B. McCoy, X. Huang, J. M. Bowman and S. Carter, "The vibrational predissociation spectra of the $H_5O_2^+RG_n$ (RG=Ar, Ne) clusters: Correlation of the solvent perturbations in the free OH, shared proton transitions of the Zundel ion," *J. Chem. Phys.* **122**, 244301 (2005). d) L. R. McCunn, J. R. Roscioli, M. A. Johnson and A. B. McCoy, "An H/D isotopic substitution study of the $H_5O_2^+Ar$ vibrational predissociation spectra: exploring the putative role of Fermi resonances in the bridging proton fundamentals," *J. Phys. Chem. B.* **112**, 321 (2008). e) L. R. McCunn, J. R. Roscioli, B. M. Elliott, M. A. Johnson and A. B. McCoy, "Why does argon bind to deuterium? Isotope effects, structures of $ArH_5O_2^+$ complexes," *J. Phys. Chem. A* **112**, 6074 (2008). f) G. H. Gardenier, J. R. Roscioli and M. A. Johnson, "Intermolecular proton binding in the presence of a large electric dipole: Ar-tagged vibrational predissociation spectroscopy of the $CH_3CN{\cdot}H^+{\cdot}OH_2$ and $CH_3CN{\cdot}H^+{\cdot}OD_2$ complexes," *J. Phys. Chem. A* **112**, 12022 (2008). g) S.G. Oleson, T.L. Guasco, G.H. Weddle, S. Hammerum and M.A. Johnson, "Vibrational predissociation spectra of the Ar-tagged [$CH_4 \cdot H_3O^+$] binary complex: spectroscopic signature of hydrogen bonding to an alkane," *Mol. Phys.* **108**, 1191 (2010).

16) O. Dopfer, R. V. Olkhov, D. Roth and J. P. Maier, "Intermolecular interaction in proton-bound dimers. Infrared photodissociation spectra of Rg-HOCO+ (Rg=He, Ne, Ar) complexes," *Chem. Phys. Lett.* **296**, 585 (1998).

17) J. R. Roscioli, L. R. McCunn and M. A. Johnson, "Quantum structure of the intermolecular proton bond," *Science* **316**, 249 (2007).

18) G.E. Douberly, A.M. Ricks, B.W. Ticknor and M.A. Duncan, "Infrared spectroscopy of protonated acetone and its dimer," *Phys. Chem. Chem. Phys.* **10**, 77 (2008).

19) G.E. Douberly, A.D. Ricks, B.W. Ticknor and M.A. Duncan, "The structure of protonated carbon dioxide clusters: Infrared photodissociation spectroscopy and ab initio calculations," *J. Phys. Chem. A* **112**, 950 (2008).

20) G.E. Douberly, A.M. Ricks, B.W. Ticknor, W.C. McKee, P.v.R. Schleyer and M.A. Duncan, "Infrared photodissociation spectroscopy of protonated acetylene and its clusters," *J. Phys. Chem. A* **112**, 1897 (2008).

21) G.E. Douberly, A.M. Ricks and M.A. Duncan, "Infrared spectroscopy of predeuterated protonated water clusters in the vicinity of the clathrate cage structure," *J. Phys. Chem. A* **113**, 8449 (2009).

22) G.E. Douberly, A.M. Ricks and M.A. Duncan, "Infrared spectroscopy of proton-bridged nitrogen dimers: Complex vibrational dynamics of the shared proton," *J. Chem. Phys.* **131**, 104312 (2009).

23) G. E. Douberly, R. S. Walters, J. Cai, K. D. Jordan and M. A. Duncan, "Infrared spectroscopy of small protonated water clusters and their deuterated analogues: The role of argon tagging," *J. Phys. Chem. A* **114**, 4570 (2010).

24) P. Kebarle, "Ion thermochemistry and solvation from gas-phase ion equilibria," *Ann. Rev. Phys. Chem.* **28**, 445 (1977).

25) P. M. Holland and A. W. Castleman, Jr., "The thermochemical properties of gas-phase transition metal ion complexes," *J. Chem. Phys.* **76**, 4195 (1982).

26) T. F. Magnera, D. E. David and J. Michl, "Gas-phase water and hydroxyl binding-energies for monopositive first row transition-metal ions," *J. Am. Chem. Soc.* **111**, 4100 (1989).

27) P. J. Marinelli and R. R. Squires, "Sequential solvation of atomic transition metal ions - the second solvent molecule can bind more strongly than the first," *J. Am. Chem. Soc.* **111**, 4101 (1989).

28) a) N. F. Dalleska, K. Honma, L.S. Sunderlin and P. B. Armentrout, "Solvation of transition-metal ions by water - sequential binding energies of $M^+(H_2O)_x$, (x=1-4) for M=Ti to Cu determined by collision-induced dissociation," *J. Am. Chem. Soc.* **116**, 3519 (1994). b) N. F. Dalleska, B. L. Tjelta and P. B. Armentrout, "Sequential bond energies of water to Na^+ ($3s^0$), Mg^+ ($3s^1$) and Al^+ ($3s^2$)," *J. Phys. Chem.* **98**, 4191 (1994). c) T. Cooper and P. B. Armentrout, "Threshold collision induced dissociation of hydrated cadmium (II): Experimental and theoretical investigation of the binding energies for $Cd^{2+}(H_2O)_n$ complexes (n=4-11)," *Chem. Phys. Lett.* **486**, 1 (2010). d) D. R. Carl, B. K. Chatterjee and P. B. Armentrout, "Threshold collision induced dissociation of $Sr^{2+}(H_2O)_x$ complexes (x=1-6): An experimental and theoretical investigation of the complete inner shell hydration energies of Sr^{2+}," *J. Chem. Phys.* **132**, 044303 (2010).

29) a) M. Beyer, C. Berg, H. W. Gorlitzer, T. Schindler, U. Achatz, G. Albert, G. Niedner-Schatteburg and V. E. Bondybey, "Fragmentation and intracluster reactions of hydrated aluminum cations $Al^+(H_2O)_n$, n=3-50," *J. Am. Chem. Soc.* **118**, 7386 (1996**)**. b) C. Berg, M. Beyer, U. Achatz, S. Joos, G. Niedner-Schatteburg and V. E. Bondybey, "Stability and reactivity of hydrated magnesium cations," *Chem. Phys.* **239,** 379 (1998). c) M. Beyer, E. R. Williams and V. E. Bondybey, "Unimolecular reactions of dihydrated

alkaline earth metal dications $M^{2+}(H_2O)_2$, M = Be, Mg, Ca, Sr, and Ba: Salt-bridge mechanism in the proton-transfer reaction $M^{2+}(H_2O)_2 \rightarrow MOH^+ + H_3O^+$," *J. Am. Chem. Soc.* **121**, 1565 (1999).

30) a) L. Poisson, P. Pradel, F. Lepetit, F. Reau, J. M. Mestdagh and J. P. Visticot, "Binding energies of first and second shell water molecules in the $Fe(H_2O)_2^+$, $Co(H_2O)_2^+$ and $Au(H_2O)_2^+$ cluster ions," *Eur. Phys. J. D* **14**, 89 (2001). b) L. Poisson, L. Dukan, O. Sublemontier, F. Lepetit, F. Reau, P. Pradel, J. M. Mestdagh and J. P. Visticot, "Probing several structures of $Fe(H_2O)_n^+$ and $Co(H_2O)_n^+$ (n=1,...,10) cluster ions," *Int. J. Mass Spectrom.* **220**, 111 (2002). c) S. le Caer, M. Heninger, P. Maitre and H. Mestdagh, "Accurate measurement of the relative bond energies of CO and H_2O ligands in Fe^+ mono- and bis-ligated complexes," *Rapid Comm. Mass Spectrom.* **17**, 351 (2003).

31) D. E. Lessen, R. L. Asher and P. J. Brucat, "Vibrational Structure of an Electrostatically Bound Ion-Water Complex," *J. Chem. Phys.* **93**, 6102 (1990).

32) M. H. Shen and J. M. Farrar, "Absorption-Spectra of Size-Selected Solvated Metal-Cations - Electronic States, Symmetries, and Orbitals in $Sr^+(NH_3)_{1,2}$ and $Sr^+(H_2O)_{1,2}$," *J. Chem. Phys.* **94**, 3322 (1991).

33) a) K. F. Willey, C. S. Yeh, D. L. Robbins, J. S. Pilgrim and M. A. Duncan, "Photodissociation Spectroscopy of Mg^+H_2O and Mg^+D_2O," *J. Chem. Phys.* **97**, 8886 (1992). b) C. S. Yeh, J. S. Pilgrim, K. F. Willey, D. L. Robbins and M. A. Duncan, "Spectroscopy of Weakly-Bound Magnesium-Ion Complexes," *Int. Rev. Phys. Chem.* **13**, 231 (1994). c) C. T. Scurlock, S. H. Pullins, J. E. Reddic and M. A. Duncan, *J. Chem. Phys.* **104**, 4591 (1996**)**. d) C. T. Scurlock, S. H. Pullins, J. E. Reddic and M. A. Duncan,

"Photodissociation spectroscopy of Ca^+-H_2O and Ca^+-D_2O, *J. Chem. Phys.* **104**, 4591 (1996).

34) a) F. Misaizu, M. Sanekata, K. Tsukamoto, K. Fuke and S. Iwata, "Photodissociation of Size-Selected $Mg^+(H_2O)_n$ Ions for n=1 and n=2," *J. Phys. Chem.* **96**, 8259 (1992). b) F. Misaizu, M. Sanekata, K. Fuke and S. Iwata, "Photodissociation Study on $Mg^+(H_2O)_n$, n=1-5 - Electronic-Structure and Photoinduced Intracluster Reaction," *J. Chem. Phys.* **100**, 1161 (1994**)**. c) F. Misaizu, K. Tsukamoto, M. Sanekata and K. Fuke, "Photoelectron-Spectroscopy of Mass-Selected Copper-Water Cluster Negative-Ions," *Laser Chemistry* **15,** 195 (1995). d) M. Sanekata, F. Misaizu, K. Fuke , S. Iwata and K. Hashimoto, "Reactions of Singly Charged Alkaline-Earth Metal-Ions with Water Clusters - Characteristic Size Distribution of Product Ions," *J. Am. Chem. Soc.* **117**, 747 (1995). e) M. Sanekata, F. Misaizu and K. Fuke, "Photodissociation study on $Ca^+(H_2O)_n$, n=1-6: Electron structure and photoinduced dehydrogenation reaction," *J. Chem. Phys.* **104**, 9768 (1996).

35) a) C. J. Thompson, F. Aguirre, J. Husband and R. B. Metz, "Photofragment spectroscopy and dynamics of $NiOH^+$ and $NiOH^+(H_2O)$," *J. Phys. Chem. A* **104**, 9901 (2000). b) C. J. Thompson, J. Husband, F. Aguirre and R. B. Metz, "Photodissociation dynamics of hydrated Ni^{2+} Clusters: $Ni^{2+}(H_2O)_n$(n = 4 – 7)," *J. Phys. Chem. A* **104,** 8155 (2000). c) K. P. Faherty, C. J. Thompson, J. M. Aguirre and R. B. Metz, "Electronic spectroscopy and photodissociation dynamics of hydrated Co^{2+} Clusters: $Co^{2+}(H_2O)_n$(n = 4-7)," *J. Phys. Chem. A* **105**, 10054 (2001); M. K. Beyer and R. B. Metz, "Salt-bridge transition state for the charge separation $Co(H_2O)_4^{2+} \rightarrow CoOH(H_2O)_2^+ + H_3O^+$," *J. Phys. Chem. A* **107**, 1760

(2003). d) R. B. Metz, "Optical spectroscopy and photodissociation dynamics of multiply charged ions," *Int. J. Mass. Spectrom.* **235**, 131 (2004).

36) Y. Abate and P. D. Kleiber, "Photodissociation spectroscopy of $Zn^+(H_2O)$ and $Zn^+(D_2O)$,"*J. Chem. Phys.* **122**, 084305 (2005).

37) K. H. Wang, D. A. Rodham, V. McKoy and G. A. Blake, "High-resolution zero-kinetic-energy pulsed field ionization, photoelectron spectra of the Na(H_2O) complex," *J. Chem. Phys.* **108**, 4817 (1998).

38) J. K. Agreiter, A. M. Knight and M. A. Duncan, "ZEKE-PFI spectroscopy of the Al-(H_2O) and Al-(D_2O) complexes," *Chem. Phys. Lett.* **313**, 162 (1999).

39) a) F. Muntean, M. S. Taylor, A. B. McCoy and W. C. Lineberger, "Femtosecond study of Cu(H_2O) dynamics," *J. Chem. Phys.* **121**, 5676 (2004). b) T. Sandford, D. Andrews, J. Rathbone, M. Taylor, F. Muntean, M. Thompson, A. B. McCoy, R. Parson and W. C. Lineberger, "Time resolved solvent rearrangement dynamics," *Faraday Discuss.* **127**, 383 (2004).

40) a) C. J. Weinheimer and J. M. Lisy, "Vibrational predissociation spectroscopy of $Cs^+(H_2O)_{1-5}$," *J. Chem. Phys.* **105**, 2938 (1996). b) J. M. Lisy, "Spectroscopy and structure of solvated alkali-metal ions," *Int. Rev. Phys. Chem.* **16**, 267 (1997). c) O. M. Cabarcos, C. J. Weinheimer and J. M. Lisy, "Competitive solvation of K^+ by benzene and water: Cation-π interactions and pi-hydrogen bonds," *J. Chem. Phys.* **108**, 5151 (1998). d) O. M. Cabarcos, C. J. Weinheimer and J. M. Lisy, "Size selectivity by cation-pi interactions: Solvation of K^+ and Na^+ by benzene and water," *J. Chem. Phys.* **110**, 8429 (1999). e) T. D. Vaden, B. Forinash and J. M. Lisy, "Rotational structure in the asymmetric OH stretch of $Cs^+(H_2O)$Ar," *J. Chem. Phys.* **117**, 4628 (2002). f) G. N.

Patwari and J. M. Lisy, "Mimicking the solvation of aqueous Na^+ in the gas phase." *J. Chem. Phys.* **118**, 8555 (2003). g) T. D. Vaden, C. J. Weinheimer and J. M. Lisy, "Evaporatively cooled $M^+(H_2O)Ar$ cluster ions: Infrared spectroscopy and internal energy simulations," *J. Chem. Phys.* **121**, 3102 (2004).

41) a) N. R. Walker, R. S. Walters, E. D. Pillai and M. A. Duncan, "Infrared spectroscopy of $V^+(H_2O)$ and $V^+(D_2O)$ complexes: Solvent deformation and an incipient reaction," *J. Chem. Phys.* **119**, 10471 (2003). b) R. S. Walters and M. A. Duncan, "Infrared spectroscopy of solvation and isomers in $Fe^+(H_2O)_{1,2}Ar_m$ complexes," *Aust. J. Chem.* **57**, 1145 (2004). c) N. R. Walker, R. S. Walters and M. A. Duncan, "Frontiers in the infrared spectroscopy of gas phase metal ion complexes," *New J. Chem.* **29**, 1495 (2005). d) N. R. Walker, R. S. Walters, M. K. Tsai, K. D. Jordan and M. A. Duncan, "Infrared photodissociation spectroscopy of $Mg^+(H_2O)Ar_n$ complexes: Isomers in progressive microsolvation," *J. Phys. Chem. A* **109**, 7057 (2005). e) R. S. Walters, E. D. Pillai and M. A. Duncan, "Solvation dynamics in $Ni^+(H_2O)_n$ clusters probed with infrared spectroscopy," *J. Am. Chem. Soc.* **127**, 16599 (2005). f) T. D. Vaden, J. M. Lisy, P. D. Carnegie, E. D. Pillai and M. A. Duncan, "Infrared spectroscopy of the $Li^+(H_2O)Ar$ complex: the role of internal energy and its dependence on ion preparation," *Phys. Chem. Chem. Phys.* **8**, 3078 (2006). g) P. D. Carnegie, A. B. McCoy and M. A. Duncan, "Infrared spectroscopy and theory of $Cu^+(H_2O)Ar_2$ and $Cu^+(D_2O)Ar_2$: Fundamentals and combination bands," *J. Phys. Chem. A* **113**, 4849 (2009).

42) a) Y. Inokuchi, K. Ohshimo, F. Misaizu and N. Nishi, "Infrared photodissociation spectroscopy of $[Mg(H_2O)_{1-4}]^+$ and $[Mg(H_2O)_{1-4}Ar]^+$," *J. Phys. Chem. A* **108**, 5034 (2004). b) Y. Inokuchi, K. Ohshimo, F. Misaizu and N. Nishi, "Structures of

$[Mg(H_2O)_{1,2}]^+$ and $[Al(H_2O)_{1,2}]^+$ ions studied by infrared photodissociation spectroscopy: evidence of $[HO\text{-}Al\text{-}H]^+$ ion core structure in $[Al(H_2O)_2]^+$," *Chem. Phys. Lett.* **390**, 140 (2004). c) T. Iino, K. Ohashi, Y. Mune, Y. Inokuchi, K. Judai, N. Nishi and H. Sekiya, "Infrared photodissociation spectra and solvation structures of $Cu^+(H_2O)_n$ (n = 1-4)," *Chem. Phys. Lett.* **427**, 24 (2006). d) T. Iino, K. Ohashi, K. Inoue, K. Judai, N. Nishi and H. Sekiya, "Infrared spectroscopy of $Cu^+(H_2O)_n$ and $Ag^+(H_2O)_n$: coordination and solvation of noble-metal ions," *J. Chem. Phys.* **126**, 194302 (2007).

43) a) M. Rosi and C. W. Bauschlicher, "The binding energies of one and two water-molecules to the first transition-row metal positive-ions," *J. Chem. Phys.* **90**, 7264 (1989). b) M. Rosi and C. W. Bauschlicher, " binding energies of one and two water-molecules to the first transition-row metal positive-ions 2," *J. Chem. Phys.* **92**, 1876 (1990**).** c) C. W. Bauschlicher, S. R. Langhoff and H. Partridge, "The binding-energies of $Cu^+(H_2O)$n and $Cu^+(NH_3)_n$ (n = 1-4)," *J. Chem. Phys.* **94**, 2068 (1991). d) C. W. Bauschlicher and H. Partridge, "The bonding of multiple ligands to Mg^+ and Al^+," *J. Phys. Chem.* **95**, 9694 (1991). e) C. W. Bauschlicher, M. Sodupe and H. Partridge, "A theoretical study of the positive and dipositive ions of $M(NH_3)_n$ and $M(H_2O)_n$ for M=Mg, Ca, or Sr," *J. Chem. Phys.* **96**, 4453 (1992). f) A. Ricca, and C. W. Bauschlicher, "Successive H_2O binding-energies for $Fe(H_2O)_n^+$," *J. Phys. Chem.* **99**, 9003 (1995). g) A. Ricca and C. W. Bauschlicher, "Theoretical study of the interaction of water and imidazole with Iron and Nickel dications," *J. Phys. Chem. A* **106**, 3219 (2002).

44) a) J. Hrusak, D. Stockigt and H. Schwarz, "Potential-energy surface of the $Al^+(H_2O)$ cluster," *Chem. Phys. Lett.* **221**, 518 (1994). b) J. Hrusak, D. Schröder and H. Schwarz,

"Theoretical prediction of the structure and the bond-energy of the Gold(I) complex $Au^{+}(H_2O)$," *Chem. Phys. Lett.* **225**, 416 (1994).

45) R. Akesson and L. G. M. Petterson, "Theoretical study of the mono- and di-hydrated divalent ions of the first-row transition metals," *Chem. Phys.* **184**, 85 (1994).

46) a) H. Watanabe and S. Iwata, "Molecular orbital studies of the structures and reactions of a singly charged calcium ion with water clusters, $Ca^{+}(H_2O)_n$," *J. Phys. Chem. A* **101**, 487 (1997). b) H. Watanabe and S. Iwata, "Theoretical assignments of the photo-dissociation excitation spectra of Mg^{+} ion complexes with water clusters: Multi-reference Cl studies," *J. Chem. Phys.* **108**, 10078 (1998). c) H. Watanabe, S. Iwata, K. Hashimoto, F. Misaizu and K. Fuke, "Molecular-Orbital Studies of the Structures and Reactions of Singly Charged Magnesium-Ion with Water Clusters, $Mg^{+}(H_2O)_n$," *J. Am. Chem. Soc.* **117**, 755 (1995).

47) a) M. Trachtman, G. D. Markham, J. P. Glusker, P. George and C. W. Bock, "Interactions of metal ions with water: ab initio molecular orbital studies of structure, bonding enthalpies, vibrational frequencies and charge distributions. 1. Monohydrates," *Inorg. Chem.* **37**, 4421 (1998). b) G. D. Markham, J. P. Glusker George and C. W. Bock, "The arrangement of first- and second-sphere water molecules in divalent magnesium complexes: Results from molecular orbital and density functional theory and from structural crystallography," *J. Phys. Chem. B* **106**, 5118 (2002). c) C. W. Bock, G. D. Markham, A. K. Katz and J. P. Glusker, "The arrangement of first- and second-shell water molecules in trivalent aluminum complexes: Results from density functional theory and structural crystallography," *Inorg. Chem.* **42**, 1538 (2003).

48) a) A. Irigoras, J. E. Fowler and J. M. Ugalde, "Reactivity of Sc^+(D-3,D-1) and V^+(D-5,F-3): Reaction of Sc^+ and V^+ with water," *J. Am. Chem. Soc.* **121**, 574 (1999). b) A. Irigoras, J. E. Fowler and J. M. Ugalde, "Reactivity of Cr^+(S-6,D-4), Mn^+(S-7,S-5) and Fe^+(D-6,F-4): Reaction of Cr^+, Mn^+, and Fe^+ with water," *J. Am. Chem. Soc.* **121**, 8549 (1999). c) A. Irigoras, O. Elizalde, I. Silanes, J. E. Fowler and J. M. Ugalde, "Reactivity of Co^+(F-3,F-5), Ni^+(D-2,F-4) and Cu^+(S-1,D-3): Reaction of Co^+, Ni^+ and Cu^+ with water," *J. Am. Chem. Soc.* **122**, 114 **(**2000).

49) D. Feller, E. D. Glendening and W. A. de Jong, "Structures and binding enthalpies of $M^+(H_2O)_n$ clusters, M=Cu, Ag, Au," *J. Chem. Phys.* **110**, 1475 (1999).

50) A. M. El-Nahas, "Thermochemically stable $M^{2+}OH_2$ complexes in the gas phase: M = Mn, Fe, Co, Ni, and Cu," *Chem. Phys. Lett.* **345**, 325 (2001).

51) a) B. M. Reinhard and G. Niedner-Schatteburg, "H_2 elimination from hydrated aluminum clusters: Acid-base reaction mediated by intracluster proton transfer," *J. Phys. Chem. A* **106**, 7988 (2002). b) B. M. Reinhard and G. Niedner-Schatteburg, "Co-existence of hydrated electron and metal di-cation in $[Mg(H_2O)_n]^+$," *Phys. Chem. Chem. Phys.* **4**, 1471 (2002). c) B. M. Reinhard and G. Niedner-Schatteburg, "Ionization energies and spatial volumes of the singly occupied molecular orbital in hydrated magnesium clusters $[Mg,nH_2O]^+$," *J. Chem. Phys.* **118**, 3571 (2003).

52) E. C. Lee, H. M. Lee, P. Tarakeshwar and K. S. Kim, "Structures, energies, and spectra of aqua-silver (I) complexes," *J. Chem. Phys.* **119**, 7725 (2003).

53) M. S. Taylor, F. Muntean, W. C. Lineberger and A. B. McCoy, "A theoretical and computational study of the anion, neutral, and cation $Cu(H_2O)$ complexes," *J. Chem. Phys.* **121**, 5688 (2004).

54) J-M. Ducere, A. Goursot and D. Berthomieu, "Comparative density functional theory study of the binding of ligands to Cu^{+} and Cu^{2+}: Influence of the coordination and oxidation state," *J. Phys. Chem. A* **109**, 400 (2005).

55) J.-G. Han and J. A. Morales, "A theoretical investigation of the $Cr(H_2O)_n^{0,1+}$ (n = 1 – 4) clusters by density functional theory methods," *THEOCHEM* **756**, 55 (2005).

56) V. Kasalova, W. D. Allen, H. F. Schaefer III, E. D. Pillai and M. A. Duncan, "Model systems for probing metal cation hydration: the $V^{+}(H_2O)$ and $ArV^{+}(H_2O)$ complexes," *J. Phys. Chem. A* **111**, 7599 (2007).

57) S. De, S.M. Ali, A. Ali and V. G. Gaikar, "Microsolvation of Zn^{2+} ion- a case study," *Phys. Chem. Chem. Phys.* **11**, 8285 (2009).

58) a) P. Jayaweera, A. T. Blades, M. G. Ikonomou and P. Kebarle, "Production and study in the gas phase of multiply charged solvated or coordinated metal ions," *J. Am. Chem. Soc.* **112**, 2452 (1990). b) A. T. Blades, P. Jayaweera, M. G. Ikonomou and P. Kebarle, "Ion-molecule clusters involving doubly charged metal ions (M^{2+})," *Int. J. Mass Spectrom. Ion Processes* **102**, 251 (1990). c) M. Peschke, A. T. Blades and P. Kebarle, "Hydration energies and entropies for Mg^{2+}, Ca^{2+}, Sr^{2+}, and Ba^{2+} from gas-phase ion-water molecule equilibria determinations," *J. Phys. Chem. A* **102**, 9978 (1998). d) M. Peschke, A. T. Blades and P. Kebarle, "Formation, acidity and charge reduction of the hydrates of doubly charged ions M^{2+} (Be^{2+}, Mg^{2+}, Ca^{2+}, Zn^{2+})," *Int. J. Mass Spectrom.* **185**, 685 (1999). e) M. Peschke, A. T. Blades and P. Kebarle, "Binding energies for doubly-charged ions M^{2+} = Mg^{2+}, Ca^{2+}, and Zn^{2+} with the ligands L = H_2O, Acetone and N-methylacetamide in complexes ML_n^{2+} for n = 1 to 7 from gas phase equilibria determinations and theoretical calculations," *J. Am. Chem. Soc.* **122**, 10440 (2000).

59) a) A. J. Stace, N. R. Walker and S. Firth, "$[Cu(H_2O)_n]^{2+}$ clusters: The first evidence of aqueous Cu(II) in the gas phase," *J. Am. Chem. Soc.* **119**, 10239 (1997**)**. b) N. R. Walker, S Firth and A. J. Stace, "Stable Cu(II) co-ordination complexes in the gas phase," *Chem. Phys. Lett.* **292**, 125 (1998**)**. c) N. R. Walker, M. P. Dobson, R. R. Wright, P. E. Barran, J. N Murrell and A. J. Stace, "A gas-phase study of the coordination of Mg^{2+} with oxygen- and nitrogen-containing ligands," *J. Am. Chem. Soc.* **122**, 11138 (2000**)**. d) L. Puskar and A.J. Stace, "Gas phase ligand field photofragmentation spectroscopy," *J. Chem. Phys.* **114**, 6499 (2001). e) A. J. Stace, "Metal ion solvation in the gas phase: The quest for higher oxidation states," *J. Phys. Chem. A* **106**, 7993 (2002**)**. f) H. Cox, G. Akibo-Betts, R. R. Wright, N. R. Walker, S. Curtis, B. Duncombe and A. J. Stace, "Solvent coordination in gas-phase $[Mn(H_2O)_n]^{2+}$ and $[Mn(ROH)_n]^{2+}$ complexes: Theory and experiment," *J. Am. Chem. Soc.* **125**, 233 (2003**)**. g) G. Wu, D. Chapman and A. Stace, "Trapping and recording the collision- and photo-induced fragmentation patterns of multiply charged metal complexes in the gas phase," *Int. J. of Mass Spec.* **262**, 211 (2007). h) B. J. Duncombe, K. Duale, A. Buchanan-Smith and A. J. Stace, "The solvation of Cu^{2+} with gas-phase clusters of water and ammonia," *J. Phys. Chem.* **111**, 5158 (2007). i) J. Guan, L. Puskar, R. O. Esplugas, H. Cox and A. J. Stace, "Ligand field photofragmentation spectroscopy of $[Ag, L_n]^{2+}$ complexes in the gas phase: Experiment and theory," *J. Chem. Phys.* **127**, 064311 (2007). j) G. Wu, C. Norris, H. Stewart, H. Cox and A. J. Stace, "State-resolved UV photofragmentation spectrum of the metal dication complex [Zn(pyridine)(4)](2+)," *Chem. Comm.* **35**, 4153 (2008). k) B. J. Duncombe, J. O. S. Ryden, L. Puskar, H. Cox and A. J. Stace, "A gas-phase study of the preferential solvation of Mn^{2+} in mixed Water/Methanol clusters," *J. Am. Soc. Mass Spectrom.* **19**,

520 (2008). l) G. Wu, H. Stewart, F. D. Lemon, H. Cox and A. J. Stace, "The UV photofragmentation spectroscopy of the metal dication complex $[Mn(pyridine)_4]^{2+}$," *Mol. Phys.* **108**, 1199 (2010).

60) a) D. Schröder and H. Schwarz, "Generation, stability, and reactivity of small multiply charged ions in the gas phase," *J. Phys. Chem. A* **103**, 7385 (1999**)**. b) D. Schröder, H. Schwarz, J. L. Wu and C. Wesdemiotis, "Long-lived dications of $Cu(H_2O)^{2+}$ and $Cu(NH_3)^{2+}$ do exist!" *Chem. Phys. Lett.* **343**, 258 (2001). c) N. G. Tsierkezos, J. Roithova´, D. Schroeder, I. E. Molinou and H. Schwarz, "Solvation of Copper (II) Sulfate in binary Water/*N*,*N*-Dimethylformamide mixtures: From the solution to the gas phase," *J. Phys. Chem. A* **112**, 4365 (2008).

61) a) S. E. Rodriquez-Cruz, R. A. Jockusch and E. R. Williams, "Binding energies of hexahydrated alkaline earth metal ions, $M^{2+}(H_2O)_6$, M = Mg, Ca, Sr, Ba: evidence of isomeric structures for magnesium," *J. Am. Chem. Soc.* **121**, 1986 (1999). b) S. E. Rodriguez-Cruz, J. S Klassen and E. R. Williams, "Hydration of gas-phase ions formed by electrospray ionization," *J. Am. Soc. Mass Spectrom.* **10**, 958 (1999). c) S. E. Rodriguez-Cruz, R. A. Jockusch and E. R. Williams, "Hydration energies and structures of alkaline earth metal ions, $M^{2+}(H_2O)_n$, n = 5 – 7, M = Mg, Ca, Sr and Ba," *J. Am. Chem. Soc.* **121**, 8898 (1999**)**. d) R. L. Wong, K. Paech and E. R. Williams, "Blackbody infrared radiative dissociation at low temperature: hydration of $X^{2+}(H_2O)_n$, for X = Mg, Ca," *Int. J. Mass Spectrom.* **232**, 59 (2004**)**. e) M. F. Bush, R. J. Saykally and E. R. Williams, "Formation of hydrated triply charged metal ions from aqueous solutions using nanodrop mass spectrometry," *Int. J. Mass Spectrom.* **253**, 256 (2006). f) R. D. Leib, W. A. Donald, M. F. Bush, J. T. O'Brien and E. R. Williams, "Internal energy deposition in

electron capture dissociation measured using hydrated divalent metal ions as nanocalorimeters," *J. Am. Chem. Soc.* **129**, 4894 (2007). g) R. D. Leib, W. A. Donald, M. F. Bush, J. T. O'Brien and E. R. Williams, "Nonergodicity in electron capture dissociation investigated using hydrated ion nanocalorimetry," *J. Am. Soc. Mass. Spectrom.* **18**, 1217 (2007).

62) A. A. Shvartsburg and K. W. M. Siu, "Is there a minimum size for aqueous doubly charged metal cations?" *J. Am. Chem. Soc.* **123**, 10071 (2001).

63) M. Velegrakis and C. Lueder, "Formation and stability of singly and doubly charged $MgAr_n$ clusters," *Chem. Phys. Lett.* **223**, 139 (1994).

64) N. R. Walker, G. A. Grieves, J. B. Jaeger, R. S. Walters and M. A. Duncan, "Generation of "unstable" doubly charged metal ion complexes in a laser vaporization cluster source," *Int. J. Mass Spec.* **228**, 285 (2003).

65) a) T. Shi, G. Orlova, J. Guo, D. K. Bohme, A. C. Hopkinson and K. W. M. Siu, "Existence of doubly charged lead monohydrate: experimental evidence and theoretical examination," *J. Am. Chem. Soc.* **126**, 7975 (2004). b) T. Shi, J. Zhao, A. C. Hopkinson and K. W. M. Siu, "formation of abundant $[Pb(H_2O)]^{2+}$ by ligand-exchange reaction between $[Pb(N_2)_n]^{2+}$ (n=1-3) and H_2O," *J. Phys. Chem. B* **109**, 10590 (2005).

66) E. P. Hunter and S. G. Lias, *NIST Chemistry WebBook*, NIST Standard Reference Database Number 69, February 2010.

67) a) M. F. Bush, R. J. Saykally and E. R. Williams, "Hydration of the calcium dication: direct evidence for second shell formation from infrared spectroscopy," *ChemPhysChem* **8**, 2245 (2007). b) J.T. O'Brien and E. R. Williams, "Hydration of gaseous copper dications probed by IR action spectroscopy," *J. Phys. Chem.* A **112**, 5893 (2008). c) M.

F. Bush, R. J. Saykally and E. R. Williams, "Reactivity and infrared spectroscopy of gaseous hydrated trivalent metal ions," *J. Am. Chem. Soc.* **130**, 9122 (2008). d) M. F. Bush, R. J. Saykally and E. R. Williams, "Infrared action spectroscopy of $Ca^{2+}(H_2O)_{11-69}$ exhibit spectral signatures for condensed phase structures with increasing cluster size," *J. Am. Chem. Soc.* **130**, 15482 (2008). e) M. F. Bush, J. T. O'Brien, J. S. Prell, C.-C. Wu, R. J. Saykally and E. R. Williams, "Hydration of alkaline earth metal dications: Effects of metal ion size determined using infrared action spectroscopy," *J. Am. Chem. Soc.* **131**, 13270 (2009).

68) a) P. D. Carnegie, B. Bandyopadhyay and M. A. Duncan, "Infrared spectroscopy of $Cr^{+}(H_2O)$ and $Cr^{2+}(H_2O)$: The role of charge in cation hydration," *J. Phys. Chem.* A **112**, 6237 (2008). b) P. D. Carnegie, B. Bandyopadhyay and M. A. Duncan, "Infrared spectroscopy of $Sc^{+}(H_2O)$ and $Sc^{2+}(H_2O)$ via argon complex predissociation: The charge dependence of cation hydration," *J. Chem. Phys.***134**, 014302 (2011). c) P. D. Carnegie, B. Bandyopadhyay and M. A. Duncan, "Infrared Spectroscopy of $Mn^{+}(H_2O)$ and $Mn^{2+}(H_2O)$ via Argon Complex Predissociation," *J. Phys. Chem. A* **115**, 7602 (2011).

69) R.P. Bell, *The Proton in Chemistry*, (Chapman & Hall, London, 1973).

70) E. Caldin and V. Gold, eds., *Proton Transfer Reactions*, (Chapman and Hall, London, 1975).

71) J. T. Hynes, J. P. Klinman, H.-H. Limbach, R. L. Schowen, eds., *Hydrogen-Transfer Reactions*, Vols. 1-4, (Wiley-VCH Publishers, Weinheim, 2006).

72) I. Bertini, H. B. Gray, E. I. Stiefel and J. S. Valentine, *Biological Inorganic Chemistry*, (University Science Books, Sausalito, CA, 2007).

73) E. E. Ferguson, F. C. Fehsenfield and D. L. Albritton, "Ion chemistry of the earth's atmosphere," in *Gas Phase Ion Chemistry*, edited by M. T. Bowers, Vol. 1, Academic Press, New York, 1979, p. 45.

74) R. D'Auria and R. P. Turco, "Ionic clusters in the polar winter stratosphere," *Geophys. Res. Lett.* **28**, 3871 (2001).

75) a) C. J. T. de Grotthuss, "Mémoire sur la décomposition de l'eau et des corps qu'elle tient en dissolution à l'aide de l'électricité galvanique," *Ann. Chim.* (Paris) **LVIII**, 54 (1805). b) C. J. T. de Grotthuss, "Memoirs on the decomposition of water and of the bodies that it holds in solution by means of galvanic electricity," *Biochimica & Biophysica Acta* **1757**, 871 (2006) (translation of a)).

76) a) M. Eigen, "Uber die kinetik sehr schnell verlaufender ionen reaktionen in wasseriger losung," *Z. Phys. Chem.* (N.F. Frankfurt) **1**, 176 (1954). b) M. Eigen, "Protonennubertragnung sauer-base-katalyse und enzymatische hydrolyse. I. Elementarvorgange," *Angew. Chem.* **75**, 489 (1963). c) M. Eigen, "Proton transfer acid-base catalysis + enzyme hydrolysis. I. Elementary processes," *Angew. Chem. Int. Ed. Eng.* **3**, 1 (1964). d) M. Eigen, W. Kruse, G. Maass, L. DeMaeyer, "Rate constants of protolytic reactions in aqueous solution," *Prog. Reac. Kinet. & Mech.* **2**, 285 (1964).

77) a) G. Zundel, H. Z. Metzer, "Energy bands of excess tunneling protons in fluid acids. IR spectroscopy of $H_5O_2^+$ groups," *Z. Phys. Chem.* (N.F. Frankfurt) **58**, 225 (1968). b) G. Zundel, "Hydrogen bonds with large proton polarizability and proton transfer processes in electrochemistry and biology," *Adv. Chem. Phys.* **111**, 1 (2000).

78) D. Marx, "Proton transfer 200 years after von Grotthuss: New insights from ab initio simulations," *Chem.Phys.Chem.* **7**, 1848 (2006).

79) Lin, S. S. "Detection of large water clusters by a low rf quadrupole mass filter," *Rev. Sci. Instrum.* **44**, 516 (1973).

80) J. Q. Searcy and J. B. Fenn, "Clustering of water on hydrated protons in a supersonic free jet expansion," *J. Chem. Phys.* **61**, 5282 (1974).

81) G. M. Lancaster, F. Honda, Y. Fukuda and J. W. Rabalais, "Secondary ion spectroscopy of molecular solids. Cluster formation during ion bombardment of frozen water, benzene and cyclohexane," *J. Am. Chem. Soc.* **101**, 1951 (1979).

82) Y. K. Lau, S. Ikuta and P. Kebarle, "Thermodynamics and kinetics of the gas-phase reactions: $H_3O^+(H_2O)_{n-1} + H_2O = H_3O+(H_2O)$," *J. Am. Chem. Soc.* **104**, 1462 (1982).

83) a) V. Hermann, B. D. Kay and A. W. Castleman, Jr. "Evidence for the existence of structures in gas-phase homomolecular clusters of water," *Chem. Phy.* **72**, 185 (1982). b) X. Yang and A. W. Castleman, Jr. "Large protonated water cluster $H^+(H_2O)_N$ (1-60) - The production and reactivity of clathrate-like structure under thermal condition," *J. Am. Chem. Soc.* **111**, 6845 (1989). c) S. Wei, Z. Shi and A. W. Castleman, Jr. "Mixed cluster ions as a structure probe – experimental evidence for clathrate structure of $(H_2O)_{20}H^+$ and $(H_2O)_{21}H^+$," *J. Chem. Phys.* **94**, 3268 (1991).

84) A. J. Stace and C. Moore, "A correlation between structure and reactivity in ion clusters," *Chem. Phys. Lett.* **96**, 80 (1983).

85) O. Echt, D. Kreisle, M. Knapp and E. Recknagel, "Evolution of magic numbers in mass-spectra of water clusters," *Chem. Phys. Lett.* **108**, 401 (1984).

86) U. Nagashima, H. Shinohara, N. Nishi and H. J. Tanaka, "Enhanced stability of ion-clathrate structures for magic number water clusters," *J. Chem. Phys.* **84**, 209 (1986).

87) T. F. Magnera, D. E. David and J. Michl, "The first twenty-eight gas-phase proton hydration energies," *Chem. Phys. Lett.* **182**, 363 (1991).

88) a) T. Schindler, C. Berg, G. Niedner-Schatteburg and V. E. Bondybey, "Protonated water clusters and their black body radiation induced fragmentation," *Chem. Phys. Lett.* **250**, 301 (1996). b) G. Niedner-Schatteburg and V. E. Bondybey," FT-ICR studies of solvation effects in ionic water cluster reactions," *Chem. Re*V. **100**, 4059 (2000).

89) K. Honma and P. B. Armentrout, "The mechanism of proton exchange: Guided ion beam studies of the reactions, $H(H_2O)_n^+$ (n=1-4) + D_2O and $D(D_2O)_n^+$ (n=1-4)+H_2O," *J. Chem. Phys.* **121**, 8307 (2004).

90) M. Meot-Ner, "The ionic hydrogen bond," *Chem. Re*v. **105**, 213 (2005).

91) P. U. Andersson, M. J. Ryding, O. Sekiguchi and E. Uggerud, "Isotope exchange and structural rearrangements in reactions between size-selected ionic water clusters," $H_3O^+(H_2O)_n$ and $NH_4^+(H_2O)_n$, and D_2O," *Phys. Chem. Chem. Phys.* **10**, 6127 (2008).

92) Y. Xie, R. B. Remington and H. F. Schaefer III, "The protonated water dimer: extensive theoretical studies of $H_5O_2^+$," *J. Chem. Phys.* **101**, 4878 (1994).

93) D. Wei and D. R. Saluhub, "Hydrated proton clusters, solvent effects on the proton transfer barrier: a density functional study," *J. Chem. Phys.* **101**, 7633 (1994).

94) G. Corongiu, R. Kelterbaum and E. Kochanski, "Theoretical studies of $H^+(H_2O)_5$," *J. Phys. Chem.* **99**, 8038 (1995).

95) a) D. J. Wales and M. P. Hodges, "Global minima of water clusters $(H_2O)_n$, n<=21, described by an empirical potential," *Chem. Phys. Lett.* **286**, 65 (1998). b) M. P. Hodges and D. J. Wales, "Global minima of protonated water clusters," *Chem. Phys. Lett.* **324**,

279 (2000). c) T. James and D. J. Wales, "Protonated water clusters described by an empirical valence bond potential," *J. Chem. Phys.* **122**, 134306 (2005).

96) M. Svanberg and J. B. C. Pettersson, "Structure, thermodynamics of $H^+(H_2O)_n$ (n=9, 21, 40) clusters between 0, 300 K: A Monte Carlo study," *J. Phys. Chem. A* **102**, 1865 (1998).

97) I. Kusaka and D. W. Oxtoby, "Evaluating free energy, enthalpy, entropy of protonated water clusters by a grand canonical Monte Carlo simulation," *J. Chem. Phys.* **113**, 10100 (2000).

98) S. J. Singer, S. McDonald and L. Ojamae, "Topology versus temperature: Thermal behavior of $H^+(H_2O)_8$, $H^+(H_2O)_{16}$," *J. Chem. Phys.* **112**, 710 (2000).

99) A. L. Sobolewski and W. Domcke, "Ab initio investigation of the structure and spectroscopy of hydronium-water clusters," *J. Phys. Chem. A* **106**, 4158 (2002).

100) X. Huang, H. M. Cho, S. Carter, L. Ojamae, J. M. Bowman and S. J. Singer, "Full dimensional quantum calculations of vibrational energies of $H_5O_2^+$," *J. Phys. Chem. A* **107**, 7142 **(**2003).

101) M. Mella and D. C. Clary, "Zero temperature quantum properties of small protonated water clusters $H^+(H_2O)_n$ (n=1-5)," *J. Chem. Phys.* **119**, 10048 (2003)

102) a) X. Huang, H. M. Cho, S. Carter, L. Ojamae, J. M. Bowman and S. J. Singer, "Full dimensional quantum calculations of vibrational energies of $H_5O_2^+$," *J. Phys. Chem. A* 107**,** 7142 **(**2003). b) J. Dai, Z. Bacic, X. Huang, S. Carter and J. M. Bowman, "A theoretical study of vibrational mode coupling in $H_5O_2^+$," *J. Chem. Phys.* **119**, 6571 (2003). c) X. Huang, S. Carter and J. M. Bowman, "Ab initio potential energy surface and rovibrational energies of H_3O^+ and its isotopomers," *J. Chem. Phys.* **118**, 5431

(2003). d) X. Huang, B. J. Braams and J. M. Bowman, "*Ab initio* potential energy and dipole moment surfaces for $H_5O_2^+$," *J. Chem. Phys.* **122**, 044308 (2005). e) A. B. McCoy, X. Huang, S. Carter, M. Y. Landeweer and J. M. Bowman, "Full-dimensional vibrational calculations for $H_5O_2^+$ using an *ab initio* potential energy surface," *J. Chem. Phys.* **122**, 061101 (2005). f) M. Kaledin, A. L. Kaledin and J. M. Bowman, "Vibrational analysis of $H_5O_2^+$ infrared spectrum using molecular and driven molecular dynamics," *J. Phys. Chem. A* **110**, 2933 (2006). g) M. Kaledin, A. L. Kaledin, J. M. Bowman, J. Ding and K. D. Jordan, "Calculation of the vibrational spectra of $H_5O_2^+$ and its deuterium-substituted isotopologues by molecular dynamics simulations," *J. Phys. Chem. A* **113**, 7671 (2009).

103) R. Ludwig, "Protonated water clusters: the third dimension," *Chem. Phys. Chem.* **5**, 1495 (2004).

104) J.-L. Kuo and M. L. Klein, "Structure of protonated water clusters: low-energy structures, finite temperature behavior," *J. Chem. Phys.* **122**, 024516 (2005).

105) F. C. Pickard, IV, E. K. Pokon, M. D. Liptak and G. C. Shields, "Comparison of CBS-QB3, CBS-APNO, G2, G3 thermochemical predictions with experiment for the formation of ionic clusters of hydronium and hydroxide ions complexed with water," *J. Chem. Phys.* **122**, 024302 (2005).

106) J. P. Devlin, M. W. Severson, F. Mohamed, J. Sadlej, V. Buch and M. Parrinello, "Experimental and computational study of isotopic effects within the Zundel ion," *Chem. Phys. Lett.* **408**, 439 (2005).

107) a) N. J. Singh, M. Park, S. K. Min, S. B. Suh and K. S. Kim, "Magic and antimagic protonated water clusters: exotic structures with unusual dynamics effects," *Angew.*

Chem. Int. Ed. **45**, 3795 (2006). b) I. Shin, M. Park, S. K. Min, E. C. Lee, S. B. Suh and K. S. Kim, "Structure and spectral features of $H^+(H_2O)_7$: Eigen versus Zundel forms," *J. Chem. Phys.* **125**, 234305 (2006). c) M. Park, I. Shin, N. J. Singh and K. S. Kim, "Eigen and Zundel forms of small protonated water clusters: structures, infrared spectra," *J. Phys. Chem. A* **111**, 10692 (2007). d) S. Karthikeyan, M. Park, I. Shin and K. S. Kim, "Structure, stability, thermodynamic properties and infrared spectra of the protonated water octamer $H^+(H_2O)_8$," *J. Phys. Chem. A* **112**, 10120 (2008).

108) Y. Luo, S. Maeda and K. Ohno, "Quantum chemistry study of $H^+(H_2O)_8$: A global search for its isomers by the scaled hypersphere method and its thermal behavior," *J. Phys. Chem. A* **111**, 10732 (2007).

109) H. Yu and Q. Cui, "The vibrational spectra of protonated water clusters: A benchmark for self-consistent-charge density-functional tight binding," *J. Chem. Phys.* **127**, 234504 (2007).

110) a) O. Vendrell, F. Gatti and H. D. Meyer, "Dynamics, infrared spectroscopy of the protonated water dimer," *Angew. Chem. Int. Ed.* **46**, 6918 (2007). b) O. Vendrell and H. D. Meyer, "A proton between two waters: Insight from full-dimensional quantum-dynamics simulations of the $[H_2O\text{-}H^+\text{-}H_2O]$ clusters," *Phys. Chem. Chem. Phys.* **10**, 4692 (2008). c) O. Vendrell, F. Gatti and H. D. Meyer, "Strong isotope effects in the infrared spectrum of the Zundel Cation," *Angew. Chem. Int. Ed.* **48**, 352 (2009).

111) R. Kumar, R. A. Kristie and K. D. Jordan, "A modified MSEVB force field for protonated water clusters," *J. Phys. Chem. B* **113**, 4111 (2009).

112) B. J. Berne, J. D. Weeks and R. Zhou, "Dewetting and hydrophobic interactions in physical and biological systems," *Annu. Rev. Phys. Chem.* **60**, 85 (2009).

113) S. Iuchi, H. Chen, F. Paesani and G. A. Voth, "Hydrated excess proton at water-hydrophobic interfaces," *J. Phys. Chem. B* **113**, 4017 (2009).

114) J. Chowdhary and B. M. Ladanyi, "Hydrogen bond dynamics at the water/hydrocarbon interface," *J. Phys. Chem. B* **113**, 4045 (2009).

115) M. E. Johnson, C. Malardier-Jugroot, R. M. Murarka and T. Head-Gordon, "Hydration water dynamics near biological interfaces," *J. Phys. Chem. B* **113**, 4082 (2009).

116) B. J. -Cwiklik, L. Cwiklik and P. Jungwirth, "Behavior of the Eigen form of hydronium at the Air/Water Interface," *J. Phys. Chem. A* **115**, 5881 (2011).

117) R. Vacha, S. W. Rick, P. Jungwirth, A. G. F. de Beer, H. B. de Aguiar, J.-S. Samson and S. Roke, "The orientation and charge of water at the hydrophobic oil droplet–water interface," *J. Am. Chem. Soc.* **133**, 10204 (2011).

118) G. A. Jeffrey, *An Introduction to Hydrogen Bonding*, (Oxford University Press, Oxford, 1997).

119) G. R. Desiraju and T. Steiner, *The Weak Hydrogen Bond*, (Oxford University Press, Oxford, 1999).

120) a) S. Sun and E. R. Bernstein, "Aromatic van der Waals Clusters: Structure and nonrigidity" *J. Phys. Chem.* **100**, 13348 (1996). b) K. S. Kim, P. Tarakeshwar and J. Y. Lee, "Molecular clusters of ð-Systems: Theoretical studies of structures, spectra, and origin of interaction energies," *Chem. Rev.* **100**, 4145 (2000). c) J. E. Braun, Th. Mehnert and H. J. Neusser, "Binding energy of van der Waals- and hydrogen-bonded clusters by threshold ionization techniques," *Int. J. Mass Spectrom.* **203**, 1 (2000) and references therein.

121) a) R. N. Pribble and T. S. Zwier, "Size-specific infrared-spectra of benzene-$(H_2O)_n$ clusters (n=1 through 7) – evidence for noncyclic $(H_2O)_n$ structures," *Science* **265**, 75 (1994). b) T. S. Zwier, "The spectroscopy of solvation in hydrogen-bonded aromatic clusters," *Annu. Rev. Phys. Chem.* **47**, 205 (1996). c) C. J. Gruenloh, R. J. Carney, C. A. Arrington, T. S. Zwier, S. Y. Fredericks and K. D. Jordan, "Infrared spectrum of a molecular ice cube: The S-4 and D-2d water octamers in benzene-$(water)_8$," *Science* **276**, 1678 (1997).

122) T. Tassaing, "A vibrational spectroscopic study of water confined in benzene from ambient conditions up to high temperature and pressure," *Vib. Spectrosc.* **24**, 15 (2000).

123) R. Souda, "Interactions of water with pyridine and benzene studied by TOF-SIMS," *J. Phys. Chem. B* **108**, 283 (2004).

124) P. M. Maxton, M. W. Schaeffer and P. M. Felker, "Nonlinear Raman-spectroscopy of intermolecular vibrations in benzene-$(water)_n$ clusters," *Chem. Phys. Lett.* **241**, 603 (1995).

125) G.E. Douberly, A.M. Ricks, B.W. Ticknor, P.v.R. Schleyer and M.A. Duncan, "Infrared spectroscopy of gas phase benzenium ions: Protonated benzene and protonated toluene from 750 to 3400 cm^{-1}," *J. Phys. Chem. A* **112**, 4869 (2008).

126) M. Miyazaki, A. Fujii, T. Ebata and N. Mikami, "Infrared spectroscopy of hydrated benzene cluster cations, $[C_6H_6\text{-}(H_2O)_n]^+$ (n=1-6): Structural changes upon photoionization and proton transfer reactions," *Phys. Chem. Chem. Phys.* **5**, 1137 (2003).

127) C. Chaudhuri, C. C. Wu, J. C. Jiang and H. C. Chang, "In comparative studies of $H^+(C_6H_6)(H_2O)_{(1,2)}$ and $H^+(C_5H_5N)(H_2O)_{(1,2)}$ by DFT calculations and IR spectroscopy," *Aus. J. Chem.* **57**, 1153 (2004).

128) K. LaiHingn, P. Y. Cheng, T. G. Taylor, K. F. Wiley, M. Peschke and M. A. Duncan, "Photodissociation in a reflectron time-of-flight mass spectrometer: A novel MS/MS scheme for high mass systems," *Anal. Chem.* **61**, 1458 (1989).

129) D. S. Cornett, M. Peschke, K. LaiHing, P. Y. Cheng, K. F. Wiley and M. A. Duncan, "A reflectron time-of-flight mass spectrometer for laser photodissociation," *Rev. Sci. Instrum.* **63**, 2177 (1992).

130) C. S. Yeh, J. S. Pilgrim, D. L Robbins, K. F. Wiley and M. A. Duncan, "Spectroscopy of weakly-bound magnesium ion complexes," *Int. Rev. Phys. Chem.* **13**, 231 (1994).

131) L. R. Brock, J. S. Pilgrim, D. L. Robbins and M. A. Duncan, "A convenient modification to the Newport pulsed molecular beam valve, *Rev. Sci. Instr.* **67**, 2989 (1996).

132) M. A. Duncan, "Photodissociation and photoionization of metal complexes," *Frontiers in Science Series* **16** (Structures and dynamics of clusters), 227 (1996).

133) M. A. Duncan, *Rev. Sci. Instrum.* Submitted.

134) G. Moreau, L. Helm, J. Purans and A. E. Merbach, "Structural investigation of the aqueous Eu^{2+} ion: Comparison with Sr^{2+} using the XAFS technique," *J. Phys. Chem. A* **106**, 3034 (2002).

135) a) L. X. Dang, G. K. Schenter, V.-A. Glezakou and J. L. Fulton, "Molecular simulation analysis and X-ray absorption measurement of Ca^{2+}, K^{+} and Cl^{-} ions in solution," *J. Phys. Chem. B* **110**, 23644 (2006). b) J. L. Fulton, S. M. Kathmann, G. K. Schenter and M. Balasubramanian, "Hydrated structure of Ag(I) ion from symmetry-dependent, K- and L-edge XAFS multiple scattering and molecular dynamics simulations," *J. Phys. Chem. A* **113**, 13976 (2009).

136) D. T. Bowron and S. Diaz-Moreno, "Solvent structure and the extended range hydration of Cr^{3+} in aqueous solution," *J. Phys. Chem. B* **113**, 11858 (2009).

137) K. J. Tielrooij, N. Garcia-Araez, M. Bonn and H. J. Bakker, "Cooperativity in Ion Hydration," *Science* **328**, 1006 (2010).

138) M. J. Frisch, G. W. Trucks, H. B. Schlegel, G. E. Scuseria, M. A. Robb, J. R. Cheeseman, J. A. Montgomery, Jr., T. Vreven, K. N. Kudin, J. C. Burant, J. M. Millam, S. S. Iyengar, J. Tomasi, V. Barone, B. Mennucci, M. Cossi, G. Scalmani, N. Rega, G. A. Petersson, H. Nakatsuji, M. Hada, M. Ehara, K. Toyota, R. Fukuda, J. Hasegawa, M. Ishida, T. Nakajima, Y. Honda, O. Kitao, H. Nakai, M. Klene, X. Li, J. E. Knox, H. P. Hratchian, J. B. Cross, C. Adamo, J. Jaramillo, R. Gomperts, R. E. Stratmann, O. Yazyev, A. J. Austin, R. Cammi, C. Pomelli, J. W. Ochterski, P. Y. Ayala, K. Morokuma, G. A. Voth, P. Salvador, J. J. Dannenberg, V. G. Zakrzewski, S. Dapprich, A. D. Daniels, M. C. Strain, O. Farkas, D. K. Malick, A. D. Rabuck, K. Raghavachari, J. B. Foresman, J. V. Ortiz, Q. Cui, A. G. Baboul, S. Clifford, J. Cioslowski, B. B. Stefanov, G. Liu, A. Liashenko, P. Piskorz, I. Komaromi, R. L. Martin, D. J. Fox, T. Keith, M. A. Al-Laham, C. Y. Peng, A. Nanayakkara, M. Challacombe, P. M. W. Gill, B. Johnson, W. Chen, M. W. Wong, C. Gonzalez and J. A. Pople, Gaussian 03 (Revision B.02), Gaussian, Inc., Pittsburgh PA, 2003.

139) a) A. P. Scott and L. Radom, "Harmonic Vibrational Frequencies: An evaluation of Hartree-Fock, Møller-Plesset, Quadratic Configuration Interaction, Density Functional Theory, and Semiempirical scale factors," *J. Phys. Chem.* **100**, 16502 (1996). b) J. P. Merrick, D. Moran and L. Radom, "An evaluation of harmonic vibrational frequency scale factors," *J. Phys. Chem. A* **2007**, *111,* 11683.

140) C. Gudeman, M. H. Begeman, J. Pfaff and R.J. Saykally, "Velocity-modulated infrared laser spectroscopy of molecular ions: The ν_1 band of HNN^+," *J. Chem. Phys.* **78**, 5837 (1983).

141) D. Verdes, H. Linnartz, J.P. Maier, P. Botschwina, R. Ostwald, P. Rosumas and P. J. Knowles, "Spectroscopic and theoretical characterization of linear centrosymmetric $NN..H^+..NN$," *J. Chem. Phys.* **111**, 8400 (1999).

142) R.S. Walters, M.A. Duncan, unpublished results.

143) R. Mabourki, Y. Ibrahim, E. Xie, M. Meot-Ner and M. SamyEl-Shall, "Clusters of the hydronium ion (H3O+) with H2, N2 and CO molecules," *Chem. Phys. Lett*. **424**, 257 (2006).

144) E. S. Kryachko and M. T. Nguyen, "Low energy barrier proton transfer in protonated benzene-water complex," *J. Phys. Chem. A* **105**, 153 (2001).

145) B. Bandyopadhyay, T. C. Cheng and M. A. Duncan, "Proton sharing in hydronium-nitrogen clusters probed with infrared spectroscopy," *Int. J. Mass Spectrom.* **297**, 124 (2010).

146) a) T. D. Jaeger, D. van Heijnsbergen, S. Klippenstein, G. von Helden, G. Meijer and M. A. Duncan, "Infrared spectroscopy and Density Functional Theory of transition metal ion-benzene and dibenzene complexes," *J. Am. Chem. Soc.* **126**, 10981 (2004). b) T. D. Jaeger and M. A. Duncan, "Vibrational spectroscopy of $Ni^+(benzene)_n$ complexes in the gas phase," *J. Phys. Chem. A* **109**, 3311 (2005).

APPENDIX

STRUCTURES AND VIBRATIONS OF PROTONATED BENZENE-WATER COMPLEXES[1]

---

[1] All calculations are done with either DFT-B3LYP or MP2 level of theory with 6-311+G (d, p) basis set.

a. Total binding energy in the complex relative to separated molecules as specified (in kcal/mol). The energies are not ZPVE and BSSE corrected.

b. Dissociation energy in kcal/mol for the elimination of benzene, water or argon as specified.

c. Intensities are in Km/mol. Frequencies are scaled by a factor of 0.9575 for DFT and 0.9523 for MP2.

Total energies are in atomic units.

BW-1, 1 isomer-a $(bz\text{-}H_3O)^+$ DFT

State: $^1A(C_1)$ Total Energy = -309.082267 ΔE = +3.5

B.E.[a] = E (complex)-E (H_3O^++bz) = 25.0 D.E[b] (H_3O^+, bz) = 25.0

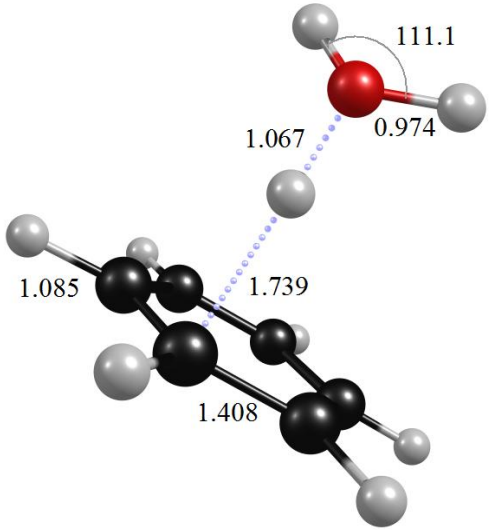

Unscaled Frequency (Intensity) Scaled Frequency /Symmetry of vibration

45 (8.8) 43/a, 62 (5.8) 60/a, 101(52.6) 97/a, 267 (89.8) 255/a, 289 (1.8) 277/a, 407 (0.1) 389/a, 408(10.7) 391/a, 487 (246.6) 467/a, 616(0.1) 589/a, 617 (1.6) 590/a, 683 (21.3) 654/a, 733 (87.6) 702/a, 882 (14.2) 845/a, 891 (0.1) 853/a, 970 (7.3) 928/a, 1000(4.8)957/a, 1015 (0.1) 972/a, 1022 (0.4) 979/a, 1033 (0.3) 989/a, 1049 (0.6) 1004/a, 1056 (3.0) 1011/a, 1066 (144.7) 1021/a, 1182 (0.8) 1132/a, 1201 (3.7) 1150/a, 1202 (0.4) 1151/a, 1331 (8.0) 1275/a, 1383 (0.0) 1324/a, 1499 (22.9) 1435/a, 1500 (32.6) 1437/a, 1535(2.9)1469/a, 1602 (110.1)1534/a, 1614(0.4) 1546/a, 1635 (14.9) 1565/a, 2137 (3139) 2046/a, 3165 (0.2) 3030/a, 3180 (0.0) 3045/a, 3181(0.1) 3046/a, 3189 (0.2) 3054/a, 3196 (0.1) 3060/a, 3203 (0.1) 3067/a, 3677 (133.3) 3521/a, 3762 (258.9) 3602/a.

BW-1, 1 isomer-b $(bzH\text{-}H_2O)^+$ DFT

State: $^1A(C_1)$ Total Energy = -309.0878769 ΔE = +0.0

B.E.[a] = E (complex)-E (H_2O+bzH^+) = 11.4 D.E[b] (H_2O) = 11.4

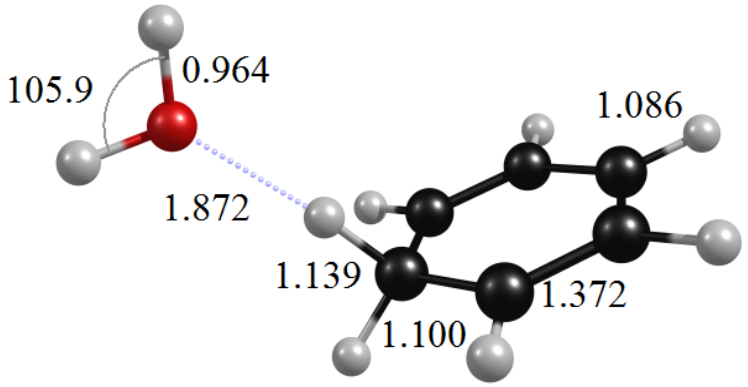

Unscaled Frequency (Intensity) Scaled Frequency /Symmetry of vibration

41 (3.5) 40/a, 46 (1.4) 44/a, 83(0.1)79/a, 166(35.5)159/a, 235 (271.4) 225/a, 281 (29.0) 269/a, 342 (0.6) 328/a, 366(37.0) 351/a, 490 (16.3) 469/a, 595 (4.0) 570/a, 600 (2.7) 574/a, 665 (62.9) 637/a, 820 (0.3) 785/a, 839 (21.2) 804/a, 922(13.0)883/a, 1001 (18.4) 958/a, 1006 (0.3) 964/a, 1012 (1.9) 969/a, 1020 (0.3) 976/a, 1040 (0.8) 996/a, 1061 (2.5) 1016/a, 1135 (5.1) 1087/a, 1166 (0.8) 1116/a, 1205(13.2) 1154/a, 1209 (31.3) 1158/a, 1277 (172.2)1223/a, 1369 (12.8)1311/a, 1425 (11.5)1364/a, 1479 (150.9) 1416/a, 1482 (24.5)1419/a, 1575(0.0)1508/a, 1632 (30.6) 1563/a, 1639(86.6) 1569/a, 2565 (1146.7) 2456/a, 3018(22.6) 2889/a, 3181 (0.0) 3046/a, 3191 (1.0) 3055/a, 3192 (2.8) 3057/a, 3208 (2.7) 3072/a, 3211 (0.6) 3074/a, 3800 (55.8) 3639/a, 3895 (119.6) 3730/a.

BW-1, 1 isomer-a $(bz\text{-}H_3O)^+$ MP2

State: $^1A(C_1)$ Total MP2 Energy = -308.1764399 $\Delta E = 0.0$

B.E.[a] = E (complex)-E (H_3O^++bz) = 28.7 D.E[b] (H_3O^+, bz) = 28.7

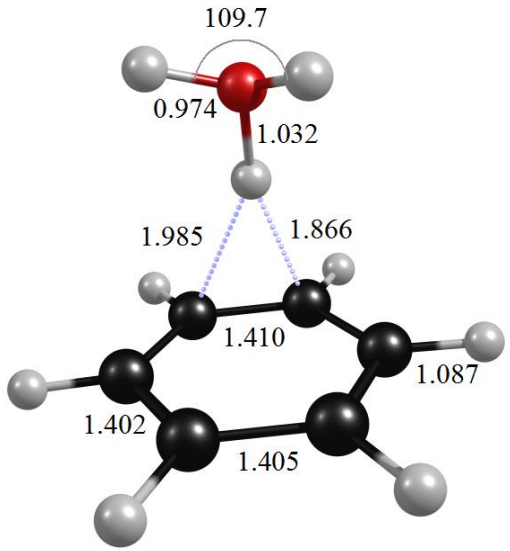

Unscaled Frequency (Intensity) Scaled Frequency /Symmetry of vibration

45(8.8) 43/a, 82 (20.8) 78/a, 96 (57.0) 92/a, 191 (0.1)182/a, 259 (68.5) 246/a, 375 (0.8) 358/a, 388(0.1) 369/a, 437(29.1) 416/a, 463 (167.5) 440/a, 604(0.3)575/a, 605(0.0)576/a, 722 (84.7) 688/a, 876(0.4) 834/a,886(1.3) 844/a,942(0.4)897/a, 948(0.1) 903/a, 966(1.9) 920/a, 998(1.1) 951/a, 1006 (0.1) 958/a, 1052 (2.6) 1002/a, 1056 (2.9)1006/a, 1099 (190.7) 1047/a, 1183 (0.2) 1126/a, 1203 (0.3) 1146/a, 1204 (0.6) 1147/a, 1371(0.0)1306/a, 1440 (1.1) 1371/a, 1497(22.6) 1426/a, 1498 (16.0)1427/a, 1571(7.6)1496/a, 1618(3.8)1541/a, 1627(1.8)1549/a, 1649 (53.8) 1571/a, 2660 (2143.1) 2533/a,3208 (0.0)3055/a, 3217(0.1)3064/a, 3218(0.2)3065/a,3 2280.8) 3074/a, 3231(0.3) 3077/a, 3238 (0.3) 3083/a, 3711(149.5)3534/a, 3798 (259.5) 3617/a.

BW-1, 1 (bz-H_3O)$^+$ transition state MP2

State: $^1A(C_1)$ Total MP2 Energy = -308.1764186 $\Delta E = 0.0$

B.E.[a] = E (complex)-E (H_3O^++bz) = 28.7 D.E[b] (H_3O^+, bz) = 28.7

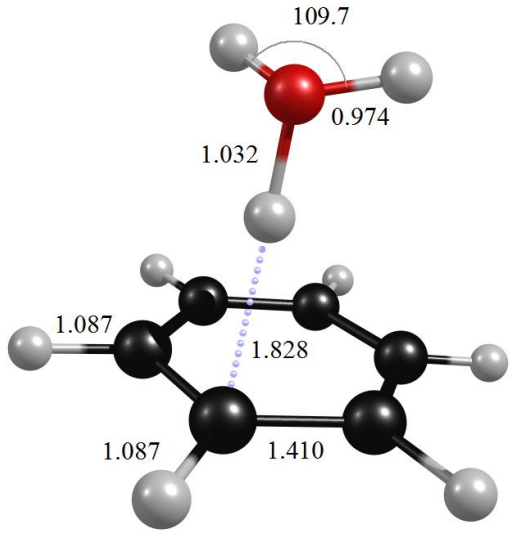

Unscaled Frequency (Intensity) Scaled Frequency /Symmetry of vibration

---

-47 (3.0) -45/a, 82 (76.4) 78/a, 88 (9.5) 84/a, 186 (0.7) 177/a, 258 (65.7) 246/a, 378 (0.0) 360/a, 389 (1.1) 370/a, 445 (102.9) 424/a, 472 (100.8) 450/a, 604(0.0) 575/a, 605 (0.2) 576/a, 723 (84.7) 688/a, 877 (0.2) 835/a, 886 (1.3) 843/a, 947 (0.6) 901/a, 950(0.0)905/a, 963 (2.6) 918/a, 998 (1.2) 951/a, 1007 (0.2) 959/a, 1052(1.4)1002/a, 1056(2.7)1006/a, 1105(186.4)1052/a, 1183(0.1)1126/a,1204(1.1) 1146/a,1204 (0.0) 114/a, 1371(0.0) 1306/a,1439(2.0)1370/a, 1497(24.1)1426/a,1498 (15.3)1427/a, 1567(5.1)1492/a, 1622(1.2)1544/a, 1623 (5.9) 1545/a, 1651 (52.3) 1572/a, 2665 (2145.8) 2537/a, 3208 (0.1) 3055/a, 3217 (0.1) 3064/a, 3218(0.2) 3065/a, 3228 (0.9) 3074/a, 3231 (0.3) 3077/a, 3238 (0.3) 3083/a, 3711 (150.3) 3534/a, 3798 (257.6) 3617/a.

BW-1, 1 isomer-b $(bzH\text{-}H_2O)^+$ MP2

State: $^1A(C_1)$ Total MP 2 Energy = -308.1666288 ΔE = +6.2

B.E.[a] = E (complex)-E (H_2O+bzH^+) =13.6 D.E[b] (H_2O) = 13.6

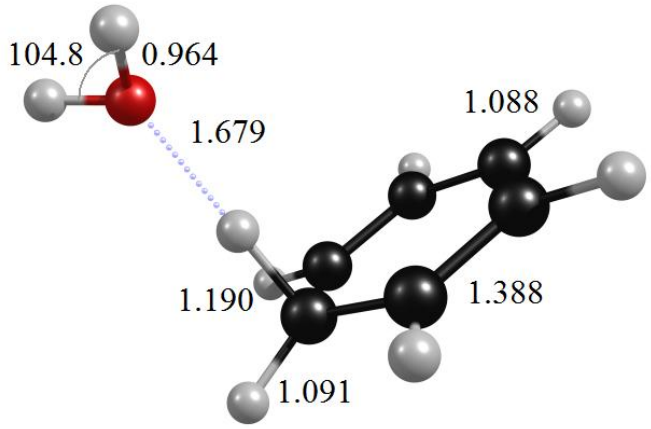

Unscaled Frequency (Intensity) Scaled Frequency /Symmetry of vibration

30 (8.1) 28/a, 61 (7.4) 58/a, 89 (4.2) 85/a, 131 (105.7) 125/a, 299 (229.9) 284/a, 345 (23.9) 328/a, 357 (10.4) 340/a, 378 (25.9) 360/a,
573 (33.8) 546/a, 591 (3.7) 563/a, 597 (1.2) 569/a, 656 (33.8) 624/a, 800 (44.0) 762/a, 821 (24.4) 782/a, 931 (47.8) 886/a,
964 (18.9) 918/a, 1009 (0.6) 961/a, 1016 (6.4) 967/a, 1020 (2.8) 972/a, 1040 (1.8) 991/a, 1050 (0.4) 999/a, 1062 (0.0) 1011/a,
1185 (0.1) 1128/a, 1209 (8.3) 1151/a, 1212 (2.1) 1154/a, 1273 (60.7) 1212/a, 1379 (2.2) 1313/a, 1463 (0.2) 1393/a,
1489 (15.0) 1418/a, 1524 (91.2) 1452/a, 1616 (12.0) 1539/a, 1625 (72.7) 1547/a, 1651 (40.5) 1573/a, 2078 (2056.8) 1979/a,
3181 (8.9) 3029/a, 3219 (0.0) 3065/a, 3226 (1.8) 3073/a, 3228 (3.9) 3074/a, 3247 (4.0) 3093/a, 3250 (1.4) 3095/a,
3833 (73.2) 3650/a, 3943 (134.2) 3755/a.

BW-1, 1-Ar isomer-a $(bz\text{-}H_3O\text{-}Ar)^+$ DFT

State: $^1A(C_1)$ Total Energy = -836.639238 ΔE = +1.9

B.E.[a] = E (complex)-E (H_3O^++bz+Ar) = 27.0 D.E[b] (Ar) = 1.9

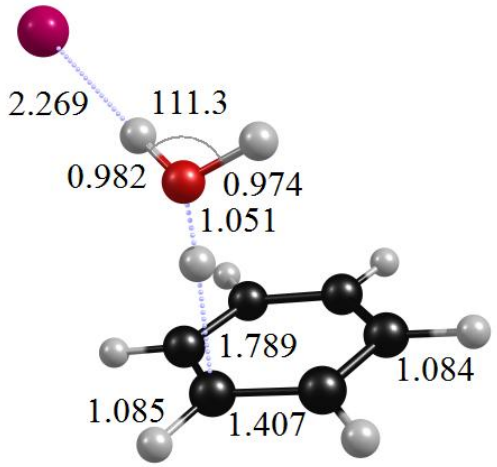

Unscaled Frequency (Intensity) Scaled Frequency /Symmetry of vibration

---

14 (4.0) 13/a, 26 (3.2) 25/a, 55 (0.8) 53/a, 62 (6.3) 60/a, 110 (21.5) 105/a, 240 (63.1) 230/a, 252 (86.4) 241/a, 319 (4.8) 306/a, 407 (0.1) 390/a, 409 (7.7) 391/a, 517 (194.3) 495/a, 617 (0.1) 591/a, 618 (0.8) 591/a, 686 (12.4) 656/a, 733 (90.3) 702/a, 888 (10.3) 850/a, 891 (1.3) 853/a, 971 (19.4) 930/a, 1000 (5.0) 958/a, 1013 (0.8) 970/a, 1022 (2.5) 979/a, 1032 (3.3) 988/a, 1041 (69.2) 997/a, 1054 (36.2) 1009/a, 1057 (17.8) 1012/a, 1182 (0.5) 1132/a, 1201 (1.2) 1150/a, 1202 (0.9) 1151/a, 1332 (4.5) 1276/a, 1383 (0.0) 1324/a, 1502 (17.5) 1438/a, 1503 (23.5) 1439/a, 1555 (8.9) 1489/a, 1614 (32.5) 1546/a, 1616 (2.1) 1548/a, 1644 (23.2) 1574/a, 2346 (3015.8) 2247/a, 3166 (0.1) 3032/a, 3180 (0.1) 3045/a, 3181 (0.0) 3046/a, 3189 (0.4) 3054/a, 3196 (0.2) 3060/a, 3202 (0.1) 3066/a, 3550 (635.8) 3399/a, 3733 (250.3) 3575/a.

BW-1,1-Ar isomer-b (bzH-H_2O-Ar)$^+$ DFT

State: $^1A(C_1)$ Total Energy = -836.6422875 $\Delta E = 0.0$

B.E.[a] = E (complex)-E (H_2O+bzH^++Ar) =11.8 D.E[b] (Ar) = 0.3

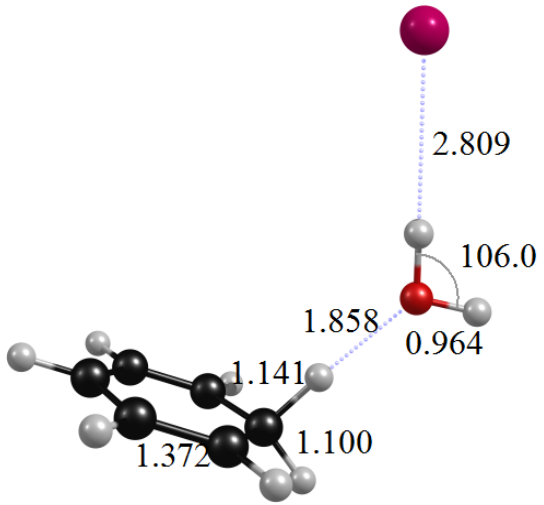

Unscaled Frequency (Intensity) Scaled Frequency /Symmetry of vibration

10 (1.3) 10/a, 17 (0.2) 16/a, 44 (6.7) 42/a, 48 (3.3) 46/a, 52 (0.9) 50/a, 131 (6.2) 125/a, 173 (38.2) 165/a, 251 (246.9) 240/a, 293 (27.8) 280/a, 342 (0.9) 328/a, 374 (37.2) 358/a, 498 (18.3) 477/a, 596 (3.9) 570/a, 600 (2.6) 575/a, 666 (64.6) 637/a, 820 (0.4) 785/a, 839 (21.1) 804/a, 924 (12.7) 885/a, 1001 (18.0) 958/a, 1007 (0.3) 964/a, 1012 (2.5) 969/a, 1020 (0.3) 976/a, 1040 (0.9) 996/a, 1062 (2.5) 1017/a, 1133 (5.4)1085/a, 1167 (0.9) 1117/a, 1206 (12.8) 1155/a, 1209 (29.0) 1158/a, 1280 (164.2) 1226/a, 1369 (12.1) 1311/a, 1424 (12.0) 1364/a, 1479 (147.5) 1416/a, 1482 (24.3) 1419/a, 1575 (0.0) 1508/a, 1632 (33.0) 1562/a, 1639 (78.0) 1570/a, 2541 (1227.1) 2433/a, 3022 (21.7) 2894/a, 3181 (0.0) 3046/a, 3191 (1.0) 3055/a, 3192 (2.7) 3056/a, 3208 (2.6) 3072/a, 3210 (0.6) 3074/a, 3798 (82.2) 3636/a, 3892 (161.0) 3727/a.

BW-1, 1-Ar isomer-a (bz-H_3O-Ar)$^+$ MP2

State: $^1A(C_1)$ Total MP2 Energy = -835.1367415 ΔE = 0.0

B.E.[a] = E (complex)-E (H_3O^++bz+Ar) = 32.3 D.E[b] (Ar) = 3.5

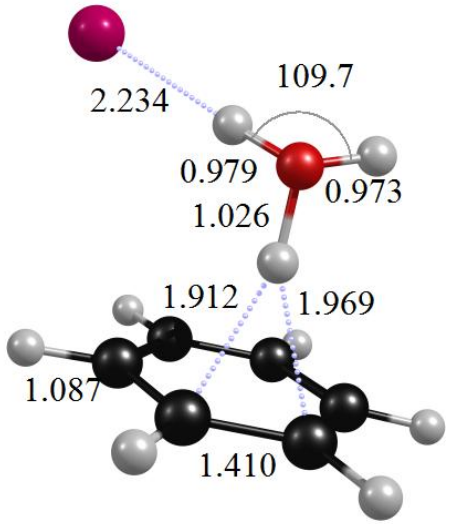

Unscaled Frequency (Intensity) Scaled Frequency /Symmetry of vibration

---

11 (3.9) 10/a, 38 (3.0) 36/a, 75 (5.3) 71/a, 92 (6.7) 87/a, 117 (23.5) 111/a, 236 (62.9) 225/a, 251 (56.9) 239/a, 255 (26.4) 243/a, 375 (1.6) 357/a, 388 (0.1) 370/a, 450 (0.4) 429/a, 484 (146.4) 461/a, 605 (0.1) 576/a, 606 (0.0) 577/a, 721 (86.4) 687/a, 875 (0.3) 833/a, 885 (0.8) 843/a, 947 (0.1) 902/a, 949 (0.0) 904/a, 968 (0.6) 922/a, 999 (1.3) 951/a, 1008 (0.0) 960/a, 1053 (1.8) 1003/a, 1056 (3.0) 1006/a, 1109 (200.5)1056/a, 1183 (0.2) 1126/a, 1203 (0.0) 1146/a, 1204 (0.7) 1147/a, 1371 (0.0) 1305/a, 1441 (0.8) 1373/a, 1498 (19.7) 1427/a, 1499 (16.3) 1427/a, 1582 (2.4) 1507/a, 1618 (1.5) 1541/a, 1629 (1.1) 1551/a, 1671 (43.0) 1591/a, 2767 (1978.3) 2635/a, 3208 (0.0) 3055/a, 3217 (0.1) 3064/a, 3218 (0.1) 3064/a, 3228 (0.7) 3074/a, 3230 (0.2) 3076/a, 3237 (0.5) 3083/a, 3622 (488.9) 3449/a, 3773 (286.1) 3593/a.

BW-1, 1-Ar isomer-b (bzH-H_2O-Ar)$^+$ MP2

State: $^1A(C_1)$ Total MP2 Energy =-835.124332 ΔE = +7.8

B.E[a] = E (complex)-E (H_2O+bzH^++Ar) = 15.5 D.E[b] (Ar) = 1.9

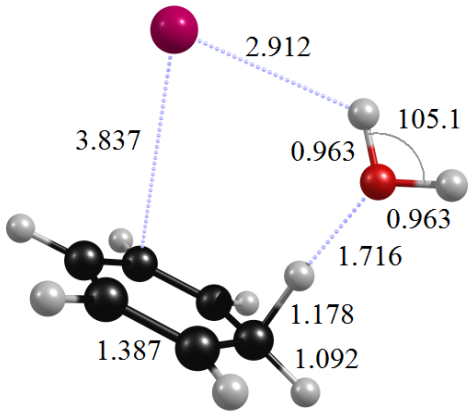

Unscaled Frequency (Intensity) Scaled Frequency /Symmetry of vibration

14 (0.7) 13/a, 29 (2.9) 27/a, 47 (3.1) 45/a, 58 (9.9) 55/a, 68 (4.5) 65/a, 108 (27.7) 103/a, 147 (70.1) 140/a, 226 (222.3) 215/a, 323 (41.2) 308/a, 350 (0.9) 333/a, 378 (28.0) 360/a, 583 (15.8) 555/a, 590 (3.3) 562/a, 605 (8.9) 576/a, 657 (55.1) 625/a, 762 (27.3) 726/a, 820 (30.0) 781/a, 912 (29.0) 869/a, 961 (17.3) 916/a, 1010 (0.6) 961/a, 1012 (4.6) 963/a, 1020 (2.5) 971/a, 1036 (2.0) 987/a, 1044 (0.1) 994/a, 1062 (0.0) 1012/a, 1182 (0.2) 1125/a, 1209 (10.0) 1152/a, 1213 (2.7) 1155/a, 1287 (94.5) 1225/a, 1377 (2.7) 1311/a, 1462 (0.0) 1393/a, 1490 (11.8) 1418/a, 1526 (103.7) 1453/a, 1615 (13.9) 1538/a, 1627 (43.5) 1549/a, 1650 (52.3) 1571/a, 2204 (1825.2) 2099/a, 3166 (10.4) 3015/a, 3216 (0.0) 3063/a, 3228 (2.1) 3074/a, 3229 (4.2) 3075/a, 3248 (4.8) 3093/a, 3250 (0.9) 3095/a, 3840 (58.5) 3657/a, 3952 (146.2) 3764/a.

BW-1, 2 isomer-a $(bz\text{-}H_5O_2)^+$ DFT

State: $^1A(C_1)$ Total Energy = -385.5831972 $\Delta E = 0.0$

B.E.[a] = E (complex)-E (H_3O^++H_2O+bz) = 51.7 D.E[b] (H_2O, bz) = (26.7, 15.0)

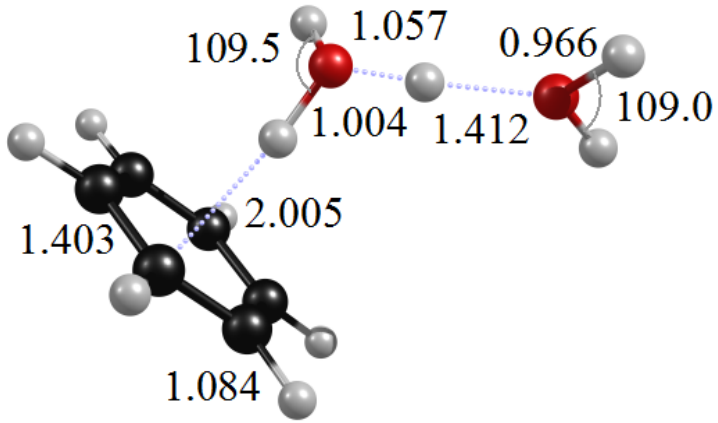

Unscaled Frequency (Intensity) Scaled Frequency /Symmetry of vibration

---

10 (2.0) 9/a, 35 (4.7) 34/a, 47 (11.7) 45/a, 56 (4.9) 54/a, 92 (94.7) 88/a, 165 (139.8) 158/a, 189 (82.5) 181/a, 324 (132.6) 310/a, 390 (137.8) 373/a, 408 (0.5) 391/a, 412 (1.2) 395/a, 430 (26.4) 412/a, 489 (8.8) 469/a, 619 (0.3) 592/a, 619 (0.1) 593/a, 695 (24.9) 665/a, 710 (82.5) 680/a, 740 (65.0) 709/a, 889 (0.5) 852/a, 900 (4.2) 862/a, 1002 (4.5) 959/a, 1003 (0.8) 960/a, 1009 (0.1) 967/a, 1019 (0.1) 976/a, 1031 (0.1) 987/a, 1054 (5.0) 1009/a, 1056 (4.6) 1011/a, 1180 (0.1) 1130/a, 1200 (0.2) 1149/a, 1201 (0.1) 1150/a, 1242 (249.6) 1189/a, 1331 (0.8) 1275/a, 1383 (0.0) 1324/a, 1505 (13.0) 1441/a, 1506 (13.1) 1442/a, 1594 (5.4) 1526/a, 1619 (0.3) 1550/a, 1623 (3.8) 1554/a, 1649(36.3)1579/a, 1660(47.1)1590/a, 2294 (3235.4) 2197/a, 3106 (1391.1) 2974/a, 3169 (0.2) 3034/a, 3178 (0.0) 3043/a, 3179 (0.2) 3044/a, 3190 (4.9) 3054/a, 3193 (2.7) 3057/a, 3200 (2.1) 3064/a, 3774 (156.5) 3614/a, 3794 (80.4) 3633/a, 3887 (205.4) 3722/a.

BW-1, 2 isomer-b $(bzH\text{-}H_2O_4)^+$ DFT

State: $^1A(C_1)$ Total Energy = -385.5612877 ΔE = +13.7

B.E.[a] = E (complex)-E (bzH^++2*H_2O) = 20.8 D.E[b] (H_2O) = 9.4

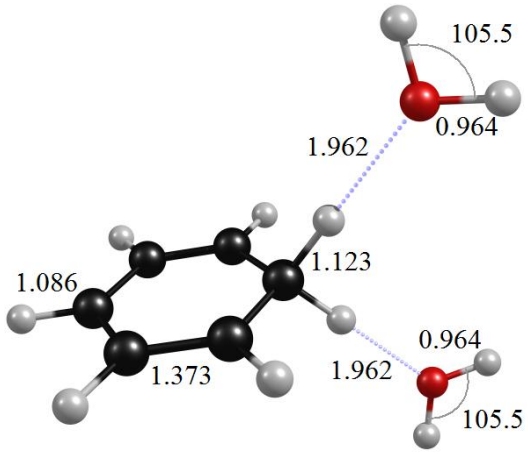

Unscaled Frequency (Intensity) Scaled Frequency /Symmetry of vibration

---

33 (0.2) 32/a, 36 (2.1) 35/a, 37 (0.5) 35/a, 42 (2.9) 40/a, 71 (0.2) 68/a, 78 (0.3) 75/a, 141 (14.7) 135/a, 161 (5.1) 154/a,
228 (28.7) 218/a, 242 (389.4) 232/a, 255 (141.0) 244/a, 313 (68.5) 300/a, 343 (0.9) 328/a, 372 (43.1) 357/a, 506 (32.4) 485/a,
598 (3.8) 573/a, 602 (7.8) 576/a, 675 (76.8) 646/a, 827 (0.0) 792/a, 844 (12.4) 808/a, 926 (13.4) 887/a, 1004 (0.6) 962/a,
1011 (0.0) 968/a, 1013 (18.8) 970/a, 1022 (0.5) 978/a, 1038 (0.3) 994/a, 1060 (2.3) 1015/a, 1154 (1.8) 1105/a,
1172 (0.8) 1122/a, 1204 (13.8) 1153/a, 1207 (49.7) 1155/a, 1267 (221.4) 1213/a, 1371 (17.5) 1312/a, 1431 (21.6) 1370/a,
1474 (132.0) 1412/a, 1484 (27.8) 1421/a, 1578 (0.2) 1511/a, 1635 (65.6) 1566/a, 1636 (8.8) 1567/a, 1640 (97.8) 1570/a,
2720 (555.8) 2605/a, 2768 (899.4) 2650/a, 3180 (0.1) 3045/a, 3189 (0.4) 3054/a, 3191 (1.5) 3055/a, 3207 (0.8) 3070/a,
3209 (0.1) 3073/a, 3805 (45.0) 3643/a, 3805 (40.0) 3643/a, 3900 (104.5) 3734/a, 3900 (108.1) 3734/a.

BW-1, 2 isomer-a $(bz\text{-}H_5O_2)^+$ MP2

State: $^1A(C_1)$ Total MP2 Energy = -384.4948164 $\Delta E = 0.0$

B.E.[a] = E (complex)-E (H_3O^++H_2O+bz) = 56.5 D.E[b] (bz) = 18.7

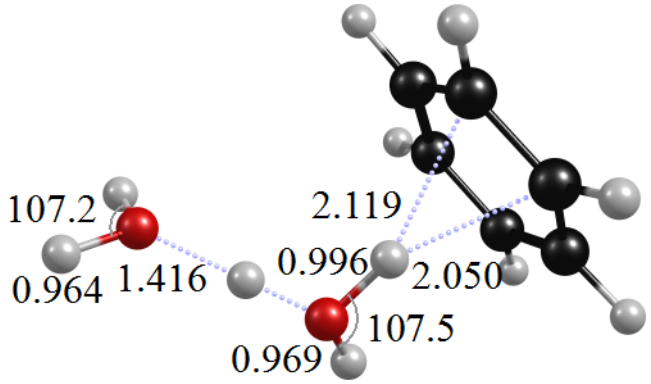

Unscaled Frequency (Intensity) Scaled Frequency /Symmetry of vibration

8 (1.9) 7/a, 37 (4.0) 35/a, 78 (13.9) 74/a, 89 (1.0) 85/a, 130 (24.0) 123/a, 194 (32.8) 185/a, 253 (204.7) 241/a, 299 (145.3) 285/a, 380 (0.6) 362/a, 390 (0.5) 372/a, 393 (115.7) 374/a, 439 (40.1) 418/a, 483 (3.3) 460/a, 505 (3.7) 480/a, 606 (0.0) 577/a, 607 (0.1) 578/a, 708 (120.4) 674/a, 773 (43.3) 736/a, 873 (0.7) 831/a, 883 (2.4) 841/a, 947 (0.0) 901/a, 958 (0.1) 912/a, 965 (0.4) 919/a, 1000 (2.2) 952/a, 1008 (0.0) 960/a, 1055 (3.4) 1005/a, 1057 (3.8) 1006/a, 1181 (0.0) 1124/a, 1202 (0.1) 1145/a, 1203 (0.0) 1145/a, 1333 (276.4) 1270/a, 1370 (0.0) 1305/a, 1441 (0.8) 1372/a, 1500 (13.4) 1428/a, 1501 (12.8) 1429/a, 1613 (27.5) 1536/a, 1622 (2.0) 1544/a, 1624 (1.3) 1547/a, 1657 (26.2) 1578/a, 1724 (40.1) 1641/a, 2408 (2803.9) 2293/a, 3207 (0.0) 3054/a, 3215 (0.1)3062/a, 3216 (0.3) 3062/a, 3228 (1.4) 3074/a, 3229 (0.7) 3075/a, 3235 (7.0) 3081/a, 3269 (1069.2) 3113/a, 3816 (146.6) 3634/a, 3837 (88.2) 3654/a, 3944 (196.7) 3756/a.

BW-1, 2 isomer-b $(bzH\text{-}H_2O_4)^+$ MP2

State: $^1A(C_1)$ Total MP2 Energy = -384.4560766 ΔE = +24.3

B.E.[a] = E (complex)-E (bzH^++2*H_2O) = 23.2 D.E[b] (Ar) = 9.6

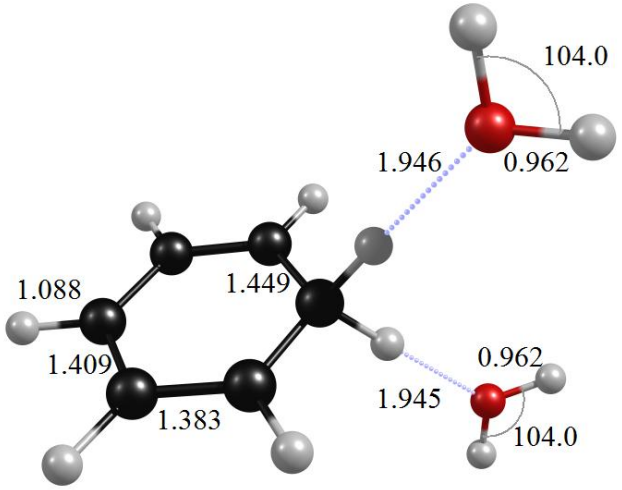

Unscaled Frequency (Intensity) Scaled Frequency /Symmetry of vibration

-32 (3.4) -30/a, 25 (4.2) 24/a, 27 (0.0) 26/a, 36 (0.9) 34/a, 61 (0.8) 58/a, 82 (0.0) 78/a, 138 (16.7) 131/a, 159 (2.6) 151/a,
210 (40.2) 200/a, 215 (466.4) 205/a, 238 (46.5) 226/a, 307 (57.9) 292/a, 323 (4.9) 308/a, 344 (14.1) 328/a, 418 (66.4) 398/a,
589 (4.5) 561/a, 594 (5.6) 66/a, 647 (70.3) 616/a, 804 (21.8) 766/a, 817 (0.0) 778/a, 936 (43.3) 892/a, 977 (2.0) 930/a,
978 (0.0) 931/a, 985 (1.1) 938/a, 1018 (23.2) 969/a, 1023 (1.7) 974/a, 1033 (2.6) 983/a, 1134 (1.5) 1080/a,
1148 (6.7) 1094/a, 1193 (222.8) 1136/a, 1212 (5.4) 1154/a, 1221 (89.1) 1163/a, 1363 (11.6) 1298/a, 1463 (11.3) 1393/a,
1490 (19.7) 1419/a, 1530 (140.8) 1457/a, 1610 (17.6) 1533/a, 1648 (13.6) 1570/a, 1651 (65.2) 1572/a, 1654 (74.0) 1575/a,
2772 (530.1) 2640/a, 2803 (977.0) 2670/a, 3213 (0.0) 3060/a, 3225 (0.8) 3071/a, 3225 (3.1) 3072/a, 3250 (2.4) 3095/a,
3251 (0.6) 3096/a, 3855 (42.9) 3671/a, 3855 (39.8) 3671/a, 3966 (116.7) 3777/a, 3966 (103.2) 3777/a.

BW-1, 2-Ar isomer-a (bz-H_5O_2-Ar)$^+$ DFT (Argon is "cis" to benzene)

State: $^1A(C_1)$ Total Energy = -913.1387812 $\Delta E = 0.0$

B.E.[a] = E (complex)-E (H_3O^++H_2O+bz+Ar) = 52.8 D.E[b] (Ar) = 1.1

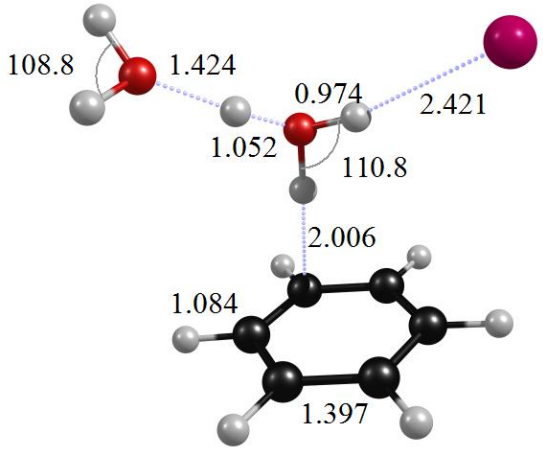

Unscaled Frequency (Intensity) Scaled Frequency /Symmetry of vibration

---

20 (2.2) 19/a, 24 (1.3) 23/a, 32 (1.7) 30/a, 36 (5.1) 34/a, 57 (1.9) 55/a, 63 (5.5) 60/a, 86 (3.4) 82/a, 118 (80.4) 113/a, 166 (149.3) 159/a, 189 (107.9) 181/a, 375 (138.6) 359/a, 388 (110.9) 371/a, 411 (3.0) 393/a, 412 (0.1) 395/a, 429 (24.6) 411/a, 515 (7.2) 493/a, 619 (0.2) 593/a, 620 (0.1) 593/a, 698 (17.2) 668/a, 710 (110.3) 680/a, 747 (46.1) 715/a, 888 (0.4) 850/a, 900 (4.3) 862/a, 1000 (1.8) 958/a, 1003 (3.1) 960/a, 1009(0.2) 967/a, 1019 (0.1) 976/a, 1031 (0.0) 987/a, 1055 (4.9) 1010/a, 1057 (4.6) 1012/a, 1180 (0.1) 1130/a, 1200 (2.6) 1149/a, 1201 (0.1) 1150/a, 1219 (211.6) 1168/a, 1333 (0.5) 1276/a, 1384 (0.0) 1325/a, 1506 (12.8) 1442/a, 1507 (11.9) 1443/a, 1588 (9.0) 1521/a, 1621 (0.6) 1552/a, 1624 (3.1) 1555/a, 1650 (28.9) 1580/a, 1659 (54.8) 1589/a, 2361 (3011.7) 2261/a, 3112 (1523.4) 2979/a, 3168 (0.4) 3033/a, 3178 (0.2) 3043/a, 3179 (0.1) 3044/a, 3190 (7.2) 3054/a, 3193 (3.5) 3057/a, 3201 (2.7) 3065/a, 3695 (439.9) 3538/a, 3796 (85.1) 3635/a, 3889 (198.5) 3724/a.

BW-1, 2-Ar isomer-b (bz-H_5O_2-Ar)$^+$ DFT (Argon is "trans" to benzene)

State: $^1A(C_1)$ Total Energy = -913.1383365 ΔE = +0.3

B.E.[a] = E (complex)-E (H_3O^++H_2O+bz+Ar) = 52.5 D.E[b] (Ar) = 0.8

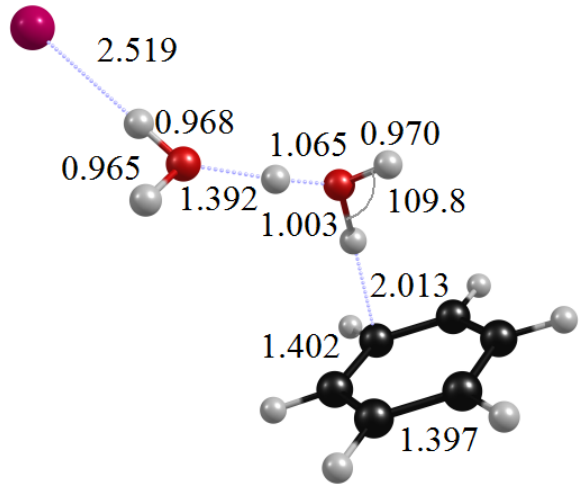

Unscaled Frequency (Intensity) Scaled Frequency /Symmetry of vibration

11 (3.0) 11/a, 14 (3.2) 14/a, 25 (1.8) 24/a, 29 (2.9) 28/a, 53 (1.4) 51/a, 58 (4.4) 55/a, 79 (15.2) 75/a, 124 (136.3) 118/a,
184 (53.1) 176/a, 261 (76.6) 250/a, 333 (165.3) 319/a, 403 (147.0) 386/a, 408 (0.2) 391/a, 412 (6.9) 395/a,
457 (27.7) 437/a, 495 (9.9) 474/a, 619 (0.2) 592/a, 619 (0.0) 593/a, 697 (15.6) 667/a, 710 (100.9) 680/a, 747 (60.3) 715/a,
888 (0.4) 850/a, 900 (5.7) 862/a, 1000 (2.6) 958/a, 1002 (2.9) 960/a, 1008 (0.3) 966/a, 1019 (0.1) 976/a,
1030 (0.1) 986/a, 1054 (5.3) 1009/a, 1056 (4.6) 1012/a, 1180 (0.1) 1130/a, 1200 (0.1) 1149/a, 1201 (0.1) 1150/a,
1265 (233.6) 1211/a, 1332 (0.5) 1275/a, 1383 (0.0) 1324/a, 1505 (13.4) 1441/a, 1507 (11.3) 1442/a, 1574 (54.8) 1507/a,
1619 (0.8) 1551/a, 1623 (3.0) 1554/a, 1650 (44.5) 1579/a, 1655 (33.0) 1585/a, 2194 (3332.0) 2101/a, 3121 (1451.4) 2988/a,
3168 (0.3) 3033/a, 3178 (0.1) 3043/a, 3179 (0.1) 3044/a, 3190 (7.7) 3054/a, 3192 (3.2) 3057/a, 3200 (2.8) 3064/a,
3764 (266.2) 3604/a, 3781 (132.2) 3620/a, 3871 (262.7) 3706/a.

BW-1, 2-Ar isomer-a (bz-H_5O_2-Ar)$^+$ MP2 (Argon is "cis" to benzene)

State: $^1A(C_1)$ Total MP2 Energy = -911.45386 $\Delta E = 0.0$

B.E.[a] = E (complex)-E (H_3O^++H_2O+bz+Ar) = 59.2 D.E[b] (Ar) = 2.7

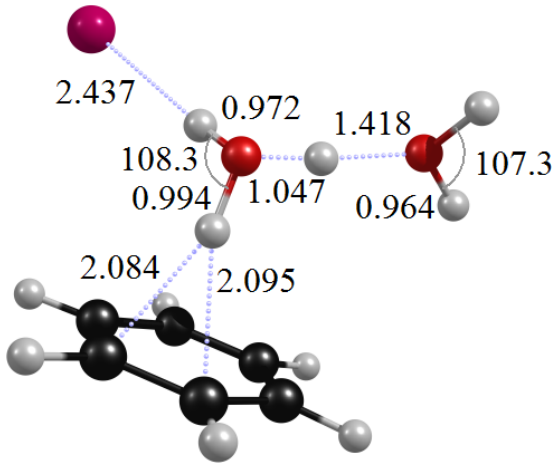

Unscaled Frequency (Intensity) Scaled Frequency /Symmetry of vibration

10(0.9) 10/a, 22(5.1) 21/a, 30(4.2)28/a, 35(4.9)33/a, 70 (5.6) 66/a, 87 (4.7) 83/a, 98 (14.5) 93/a, 111 (12.9) 106/a, 186 (27.2) 177/a, 217 (205.2) 207/a, 342 (108.9) 326/a, 380 (1.7) 362/a, 389 (8.8) 371/a, 396 (122.6) 377/a, 427 (30.5) 407/a, 502 (2.7) 478/a, 535 (31.9) 509/a, 606 (0.0) 577/a, 607 (0.1) 578/a, 706 (116.4) 673/a, 790 (51.4) 752/a, 872 (0.6) 831/a, 883 (4.1) 841/a, 948 (0.1) 902/a, 959 (0.1) 913/a, 964 (0.3) 918/a, 1000 (2.1) 953/a, 1009 (0.0) 961/a, 1056 (3.8) 1006/a, 1057 (3.2) 1006/a, 1181 (0.1) 1124/a, 1202 (0.1) 1144/a, 1203 (0.0) 1146/a, 1302 (243.2) 1240/a, 1371 (0.0) 1305/a, 1442 (0.3) 1373/a, 1500 (13.8) 1429/a, 1501 (12.0) 1429/a, 1612 (8.3) 1535/a, 1622 (0.3) 1545/a, 1626 (2.9) 1549/a, 1667 (51.0) 1587/a, 1734 (38.8) 1651/a, 2426 (2544.5) 2310/a, 3205 (0.1) 3052/a, 3214 (0.1) 3060/a, 3215 (0.3) 3062/a, 3226 (1.2) 3072/a, 3228 (0.7) 3074/a, 3235 (1.5) 3080/a, 3302 (1069.7) 3145/a, 3767 (383.3) 3587/a, 3844 (79.5) 3661/a, 3952 (194.8) 3763/a.

BW-1, 2-Ar isomer-b (bz-H_5O_2-Ar)$^+$ MP2 (Argon is "trans" to benzene)

State: $^1A(C_1)$ Total Energy = - -911.4514554 ΔE = +1.5

B.E.[a] = E (complex)-E (H_3O^++H_2O+bz+Ar) = 57.7 D.E[b] (Ar) = 1.2

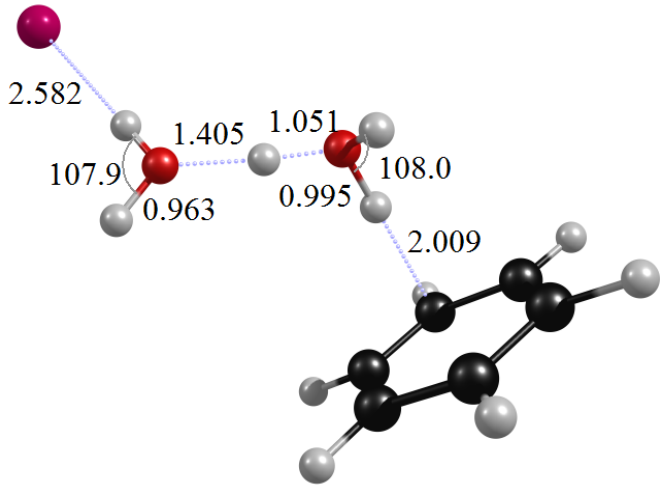

Unscaled Frequency (Intensity) Scaled Frequency /Symmetry of vibration

12 (4.1) 11/a, 17 (4.7) 16/a, 21 (1.5) 20/a, 31 (6.6) 30/a, 56 (115.1) 53/a, 69 (15.7) 66/a, 89 (46.0) 84/a, 92 (28.8) 87/a, 197 (43.4) 188/a, 262 (21.8) 249/a, 331 (154.3) 315/a, 383 (0.4) 364/a, 390 (3.5) 372/a, 401 (128.9) 382/a, 456 (36.3) 434/a, 482 (0.5) 459/a, 496 (9.4) 472/a, 606 (0.0) 577/a, 607 (0.2) 578/a, 710 (118.7) 676/a, 754 (50.7) 718/a, 873 (0.6) 832/a, 887 (1.9) 845/a, 949 (0.1) 904/a, 958 (0.1) 913/a, 966 (0.2) 920/a, 997 (2.4) 949/a, 1007 (0.0) 959/a, 1053 (3.7) 1003/a, 1056 (3.5) 1006/a, 1181 (0.0) 1125/a, 1201 (0.1) 1143/a, 1204 (0.0) 1146/a, 1326 (264.5) 1263/a, 1371 (0.0) 1306/a, 1435 (0.3) 1367/a, 1499 (12.5) 1428/a, 1500 (13.1) 1428/a, 1605 (10.2) 1528/a, 1619 (0.5) 1542/a, 1621 (0.2) 1544/a, 1671 (45.9) 1592/a, 1698 (41.5) 1617/a, 2369 (3085.0) 2256/a, 3195 (0.1) 3043/a, 3200 (0.1) 3048/a, 3211 (0.2) 3058/a, 3216 (0.4) 3063/a, 3225 (1.2) 3071/a, 3229 (1.7) 3075/a, 3290 (1124.8) 3133/a, 3802 (166.9) 3621/a, 3821 (157.3) 3639/a, 3934 (261.5) 3746/a.

BW-1, 3 isomer-a $(bz\text{-}H_7O_3)^+$ DFT

State: $^1A(C_1)$ Total Energy = -462.0750758 $\Delta E = 0.0$

B.E.[a] = E (complex)-E (H_3O^++2*H_2O+bz) = 72.7 D.E[b](H_2O,bz) = (21,11.4)

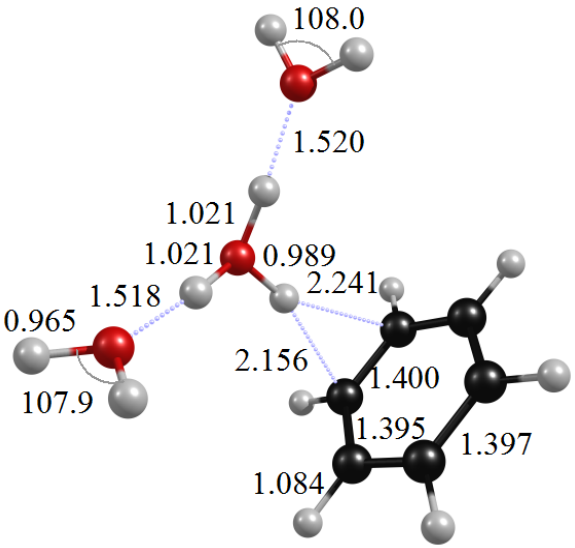

Unscaled Frequency (Intensity) Scaled Frequency /Symmetry of vibration

---

19 (0.2) 18/a, 21 (0.1) 21/a, 37 (5.0) 35/a, 54 (2.2) 51/a, 64 (0.4) 62/a, 83 (5.8) 80/a, 88 (14.0) 84/a, 131 (19.0) 126/a, 158 (11.6) 151/a,
161 (79.5) 154/a, 207 (464.1) 198/a, 317 (91.1) 304/a, 337 (96.9) 323/a, 368 (2.6) 352/a, 400 (60.5) 383/a, 411 (0.3) 393/a,
413 (0.1) 396/a, 596 (2.6) 571/a, 620 (0.1) 594/a, 621 (0.0) 595/a, 659 (89.5) 631/a, 704 (0.1) 674/a, 724 (81.5) 693/a,
884 (0.1) 847/a, 893 (1.5) 855/a, 987 (41.8) 945/a, 1004 (2.8) 962/a, 1005 (8.5) 962/a, 1007 (6.7) 964/a, 1017 (0.0) 974/a,
1030 (0.2) 986/a, 1056 (4.2) 1011/a, 1057 (5.5) 1012/a, 1167 (265.6) 1117/a, 1179 (0.2) 1129/a, 1200 (0.5) 1149/a,
1200 (0.3) 1149/a, 1333 (0.3) 1276/a, 1383 (0.0) 1324/a, 1507 (11.4) 1443/a, 1508 (11.2) 1444/a, 1611 (8.5) 1542/a,
1623 (1.0) 1554/a, 1627 (9.4) 1558/a, 1639 (24.6) 1569/a, 1661 (71.5) 1590/a, 1685 (37.6) 1613/a, 2768 (2718.1) 2650/a,
2864 (1441.5) 2743/a, 3167 (0.0) 3032/a, 3176 (0.0) 3041/a, 3176 (0.1) 3041/a, 3188 (4.8) 3052/a, 3190 (7.7) 3055/a,
3198 (1.6) 3062/a, 3365 (1168.3) 3222/a, 3805 (98.8) 3643/a, 3806 (33.2) 3645/a, 3899 (57.2) 3733/a, 3900 (277.1) 3734/a.

BW-1, 3 isomer-b $(bzH\text{-}H_6O_3)^+$ DFT

State: $^1A(C_1)$ Total Energy = -462.0417494 ΔE = +21.0

B.E.[a] = E (complex)-E (bzH^++3*H_2O) = 34.6 D.E[b] = -

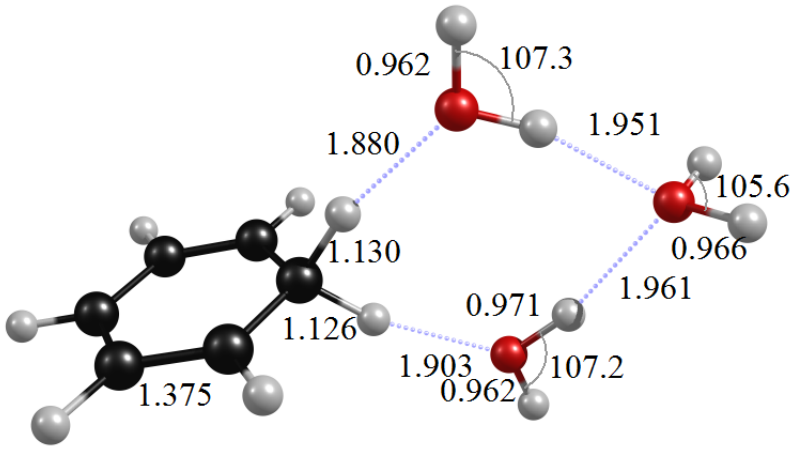

Unscaled Frequency (Intensity) Scaled Frequency /Symmetry of vibration

28 (0.4) 26/a, 30 (2.1) 28/a, 31 (3.7) 30/a, 44 (17.3) 42/a, 75 (1.3) 72/a, 142 (48.0) 136/a, 146 (0.3) 140/a, 155 (43.7) 148/a, 161 (135.0) 154/a, 180 (11.8) 172/a, 203 (1.0) 194/a, 227 (95.5) 218/a, 261 (0.3) 250/a, 340 (1.5) 326/a, 348 (0.0) 333/a, 401 (0.1) 384/a, 476 (13.0) 456/a, 480 (311.1) 459/a, 580 (53.8) 555/a, 601 (4.2) 575/a, 605 (26.1) 579/a, 608 (0.2) 582/a, 672 (241.3) 643/a, 680 (89.2) 651/a, 834 (0.1) 798/a, 843 (13.8) 807/a, 938 (17.3) 898/a, 1005 (3.3) 962/a, 1011 (0.8) 968/a, 1017 (18.0) 974/a, 1024 (1.7) 981/a, 1035 (0.1) 991/a, 1059 (2.1) 1014/a, 1152 (2.5) 1103/a, 1165 (0.7) 1115/a, 1187 (484.0) 1137/a, 1203 (11.9) 1152/a, 1219 (137.7) 1167/a, 1370 (17.7) 1311/a, 1431 (37.4) 1370/a, 1476 (99.1) 1413/a, 1487 (34.2) 1424/a, 1581 (0.5) 1513/a, 1621 (19.3) 1552/a, 1627 (124.0) 1558/a, 1638 (51.3) 1568/a, 1659 (0.0) 1589/a, 2613 (531.3) 2502/a, 2728 (1345.0) 2612/a, 3180 (0.2) 3045/a, 3190 (0.2) 3054/a, 3191 (1.0) 3056/a, 3206 (0.2) 3070/a, 3209 (0.0) 3073/a, 3670 (188.6) 3514/a, 3694 (618.7) 3537/a, 3788 (18.3) 3627/a, 3877 (126.1) 3712/a, 3880 (237.1) 3715/a, 3883 (27.2) 3718/a.

BW-1, 4 isomer-a $(bz\text{-}H_9O_4)^+$ DFT

State: $^1A(C_1)$ Total Energy = -538.5595123 $\Delta E = 0.0$

B.E.[a] = E (complex)-E (H_3O^++3*H_2O+bz) = 89.0 D.E[b](H_2O, bz) = (16.3, 7.0)

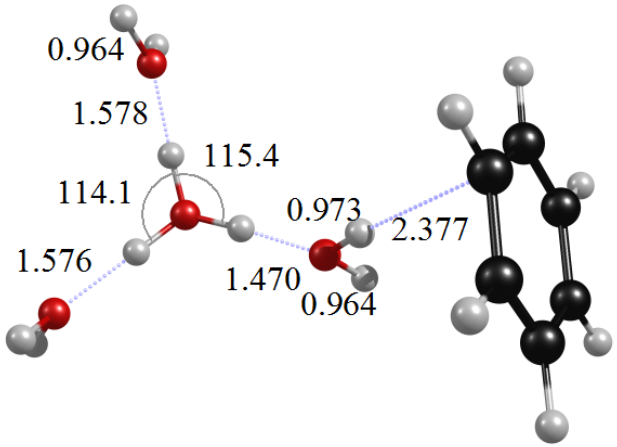

Unscaled Frequency (Intensity) Scaled Frequency /Symmetry of vibration

---

8 (0.1) 7/a, 11 (0.2) 11/a, 24 (0.8) 23/a, 33 (0.2) 32/a, 41 (5.0) 40/a, 64 (0.9) 61/a, 69 (2.4) 66/a, 84 (4.0) 80/a, 102 (8.9) 98/a, 110 (17.7) 105/a, 122 (5.5) 116/a, 158 (5.6)151/a, 197 (152.1) 189/a, 232 (354.1) 223/a, 268 (63.1) 256/a, 319 (76.4) 305/a, 351 (52.4) 337/a, 359 (74.4) 343/a, 377 (68.4) 361/a, 390 (192.8) 373/a, 411 (0.7) 394/a, 412 (1.2) 395/a, 457 (60.9) 438/a, 621 (0.0) 594/a, 621 (0.0) 595/a, 706 (37.2) 676/a, 710 (86.0) 680/a, 720 (0.8) 689/a, 879 (0.3) 842/a, 882 (0.6) 845/a, 953 (60.0) 912/a, 998 (0.2) 956/a, 1001 (0.1) 958/a, 1006 (4.0) 963/a, 1014 (130.1) 970/a, 1016 (0.2) 973/a, 1027 (0.0) 984/a, 1056 (5.5) 1011/a, 1058 (5.5) 1013/a, 1177 (1.6) 1127/a, 1179 (261.3) 1129/a, 1199 (0.0) 1148/a, 1200 (0.3) 1149/a, 1332 (0.2) 1275/a, 1382 (0.0) 1324/a, 1507 (10.0) 1443/a, 1508 (11.0) 1444/a, 1625 (0.2) 1556/a, 1627 (1.4) 1558/a, 1633 (81.0) 1564/a, 1634 (63.8) 1565/a, 1645 (10.1) 1575/a, 1687 (13.6) 1616/a, 1701 (15.9) 1629/a, 2600 (3708.7) 2490/a, 3029 (2555.3) 2900/a, 3090 (703.5) 2958/a, 3164 (0.5) 3030/a, 3173 (0.3) 3038/a, 3176 (0.3) 3041/a, 3187 (11.6) 3051/a, 3190 (12.0) 3055/a, 3198 (0.3) 3062/a, 3669 (412.3) 3513/a, 3808 (77.4) 3646/a, 3809 (28.2) 3647/a, 3856 (79.2) 3692/a, 3902 (61.1) 3736/a, 3902 (257.9) 3736/a.

BW-1, 4 isomer-b $(bzH\text{-}H_8O_4)^+$ DFT

State: $^1A(C_1)$ Total Energy = -538.5197066 ΔE = +25.0

B.E.[a] = E (complex)-E (bzH^++4*H_2O) =46.9 D.E[b] (H_2O) = 12.2

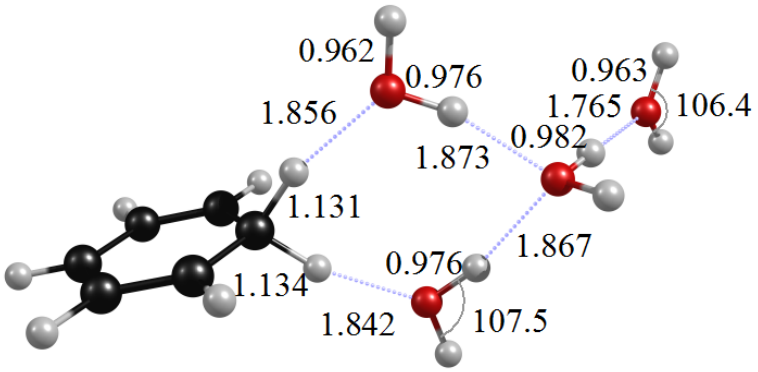

Unscaled Frequency (Intensity) Scaled Frequency /Symmetry of vibration

17 (0.8) 16/a, 20 (5.7) 19/a, 29 (1.1) 28/a, 42 (2.8) 40/a, 44 (0.1) 43/a, 52 (11.1) 50/a, 79 (3.4) 76/a, 91 (0.4) 87/a, 156 (83.2) 149/a, 159 (17.1) 152/a, 160 (45.7) 153/a, 174 (17.5) 166/a, 194 (72.8) 186/a, 200 (102.4) 192/a, 204 (304.5) 196/a, 280 (12.5) 268/a, 296 (45.9) 284/a, 351 (0.0) 336/a, 356 (2.9) 341/a, 384 (17.0) 367/a, 400 (7.6) 383/a, 459 (93.2) 439/a, 513 (11.6) 491/a, 602 (3.6) 577/a, 604 (20.5) 578/a, 607 (34.7) 582/a, 662 (64.5) 634/a, 689 (107.7) 660/a, 757 (204.7) 725/a, 836 (0.1) 801/a, 844 (13.2) 808/a, 882 (127.2) 845/a, 943 (18.0) 903/a, 1005 (4.8) 963/a, 1010 (0.3) 967/a, 1020 (19.9) 976/a, 1025 (2.3) 982/a, 1033 (0.3) 989/a, 1056 (2.0) 1011/a, 1152 (4.0) 1103/a, 1163 (44.1) 1113/a, 1179 (587.1) 1129/a, 1203 (11.0) 1152/a, 1215 (84.8) 1163/a, 1370 (18.6) 1311/a, 1429 (42.1) 1368/a, 1477 (85.4) 1414/a, 1488 (35.9) 1425/a, 1582 (0.7) 1515/a, 1622 (14.8) 1553/a, 1637 (77.7) 1567/a, 1638 (75.4) 1568/a, 1642 (53.2) 1572/a, 1675 (14.5) 1604/a, 2543 (582.5) 2435/a, 2676 (1705.4) 2562/a, 3179 (0.2) 3044/a, 3190 (0.1) 3054/a, 3191 (0.6) 3056/a, 3206 (0.0) 3070/a, 3209 (0.0) 3072/a, 3491 (1277.0) 3342/a, 3573 (318.9) 3421/a, 3622 (546.5) 3468/a, 3816 (34.4) 3653/a, 3853 (93.0) 3689/a, 3881 (180.8) 3716/a, 3884 (37.6) 3719/a, 3912 (124.5) 3746/a.

BW-2, 1 isomer-a $(bz_2\text{-}H_3O)^+$ DFT

State: $^1A(C_1)$ Total Energy = -541.4190482 $\Delta E = 0.0$

B.E.[a] = E (complex)-E (H_3O^++2*bz) = 41.1 D.E[b] (bz) = 16.0

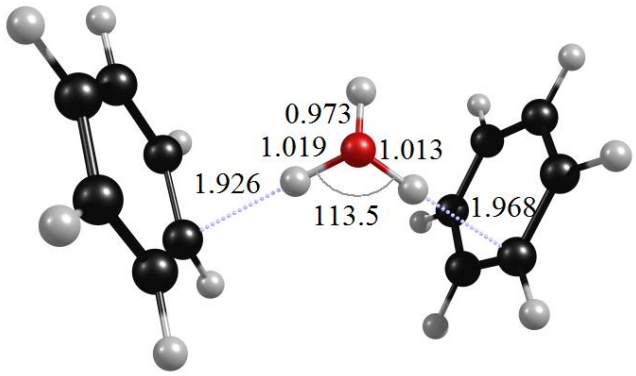

Unscaled Frequency (Intensity) Scaled Frequency /Symmetry of vibration

---

13 (1.7) 12/a, 16 (1.0) 15/a, 30 (2.6) 29/a, 39 (2.4) 38/a, 49 (1.0) 47/a, 51 (0.5) 49/a, 64 (1.1) 61/a, 178 (4.9) 170/a, 233 (126.0) 223/a,
265 (36.4) 254/a, 356 (24.4) 340/a, 408 (0.8) 391/a, 410 (0.1) 393/a, 412 (4.5) 394/a, 413 (2.0) 395/a, 571 (43.9) 547/a,
618 (0.3) 592/a, 619 (0.3) 593/a, 619 (0.3) 593/a, 620 (0.3) 593/a, 696 (10.2) 666/a, 700 (20.0) 671/a, 723 (213.8) 693/a,
730 (44.8) 699/a, 884 (3.5) 847/a, 889 (2.5) 851/a, 892 (13.2) 854/a, 902 (1.4) 864/a, 977 (45.6) 936/a, 1000 (4.1) 957/a,
1001 (14.2) 959/a, 1003 (0.9) 960/a, 1006 (13.1) 963/a, 1011 (0.2) 968/a, 1018 (39.0) 974/a, 1020 (0.2) 977/a, 1024 (2.3) 980/a,
1031 (1.4) 987/a, 1033 (2.0) 989/a, 1053 (5.6) 1009/a, 1054 (9.1) 1009/a, 1057 (3.7) 1012/a, 1058 (14.7) 1013/a, 1180 (0.0) 1130/a,
1181 (0.1) 1131/a, 1200 (0.1) 1149/a, 1201 (0.2) 1150/a, 1201 (0.2) 1150/a, 1201 (0.9) 1150/a, 1332 (0.9) 1275/a, 1336 (1.5) 1279/a,
1383 (0.0) 1324/a, 1383 (0.0) 1324/a, 1504 (6.8) 1440/a, 1505(10.1) 1441/a, 1506 (18.4) 1442/a, 1507 (20.8) 1443/a,
1595 (8.4) 1527/a, 1616 (2.5) 1547/a, 1621 (1.0) 1552/a, 1621 (2.0) 1552/a, 1626 (5.2) 1557/a, 1640 (45.1) 1570/a,
2819 (4224.4) 2700/a, 2977 (725.9) 2851/a, 3164 (0.6) 3029/a, 3169 (0.1) 3034/a, 3178 (0.9) 3043/a, 3179 (0.0) 3044/a,
3181 (0.2) 3046/a, 3181 (0.1) 3046/a, 3189 (3.1) 3053/a, 3190 (2.0) 3055/a, 3194 (1.6) 3058/a, 3195 (1.8) 3059/a,
3201 (0.7) 3065/a, 3203 (0.3) 3067/a, 3744 (114.8) 3585/a.

BW-2, 1 isomer-b $(bz_2H\text{-}H_2O)^+$ DFT

State: $^1A(C_1)$ Total Energy = -541.4084667 ΔE = +6.6

B.E.[a] = E (complex)-E (bzH^++H_2O+bz) = 17.3 D.E[b] (bz) = 5.8

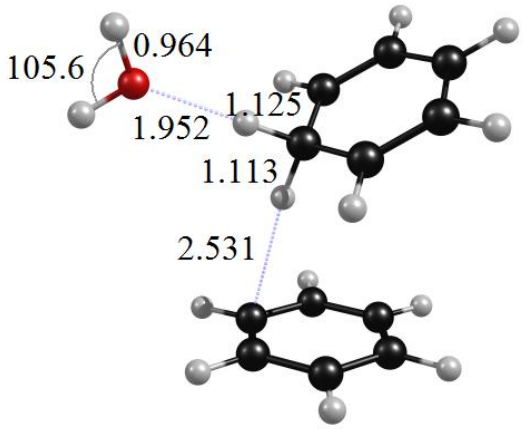

Unscaled Frequency (Intensity) Scaled Frequency /Symmetry of vibration

---

10 (0.0) 9/a, 23 (0.5) 22/a, 34 (4.0) 33/a, 37 (1.5) 36/a, 43 (3.5) 41/a, 58 (0.3) 56/a, 65(0.6) 62/a, 82 (0.4) 79/a, 90 (5.8) 86/a,
157 (19.5) 150/a, 234 (245.6) 224/a, 261 (24.6) 250/a, 344 (1.3) 329/a, 351 (47.5) 336/a, 409 (0.6) 392/a, 411 (0.0) 393/a,
476 (24.1) 456/a, 597 (4.0) 571/a, 599 (5.7) 574/a, 619 (0.0) 593/a, 620 (0.8) 593/a, 669 (60.6) 641/a, 707 (53.9) 677/a,
709 (83.6) 679/a, 818 (1.8) 783/a, 842 (10.6) 806/a, 878 (0.2) 840/a, 882 (0.6) 845/a, 920 (9.3) 881/a, 1000 (1.0) 958/a,
1002 (1.6) 960/a, 1004 (7.4) 962/a, 1005 (1.6) 962/a, 1006 (5.1) 963/a, 1008 (4.4) 966/a, 1016 (0.0) 972/a, 1021 (0.1) 977/a,
1029 (0.0) 986/a, 1035 (1.8) 991/a, 1055 (3.1) 1010/a, 1058 (1.7) 1013/a, 1059 (4.7) 1014/a, 1150 (1.5) 1101/a,
1163 (4.5) 1113/a, 1178 (0.0) 1128/a, 1198 (0.7) 1147/a, 1199 (4.2) 1148/a, 1203 (14.0) 1152/a, 1207 (30.6) 1156/a,
1270 (122.7) 1216/a, 1337 (0.3) 1280/a, 1369 (13.0) 1310/a, 1383 (0.0) 1324/a, 1425 (22.2) 1365/a, 1471 (130.7) 1409/a,
1482 (28.8) 1419/a, 1507 (11.6) 1443/a, 1510 (9.7) 1446/a, 1575 (0.5) 1508/a, 1622 (0.3) 1553/a, 1626 (11.3) 1557/a,
1634 (24.8) 1565/a, 1638 (101.1) 1568/a, 2712 (761.9) 2597/a, 2862 (471.0) 2741/a, 3164 (0.0) 3029/a, 3172 (0.1) 3037/a,
3173 (0.0) 3038/a, 3180 (0.2) 3045/a, 3186 (10.2) 3050/a, 3187 (10.7) 3052/a, 3190 (0.7) 3055/a, 3195 (0.8) 3059/a,
3200 (0.6) 3064/a, 3208 (0.8) 3072/a, 3212 (0.4) 3076/a, 3805 (44.3) 3643/a, 3900 (101.4) 3734/a.

BW-2, 1-Ar isomer-a (bz_2-H_3O-Ar)$^+$ DFT

State: $^1A(C_1)$ Total Energy = -1068.9744595 $\Delta E = 0.0$

B.E.[a] = E (complex)-E (H_3O^++2*bz+Ar) = 42.0 D.E[b] (Ar) = 1.0

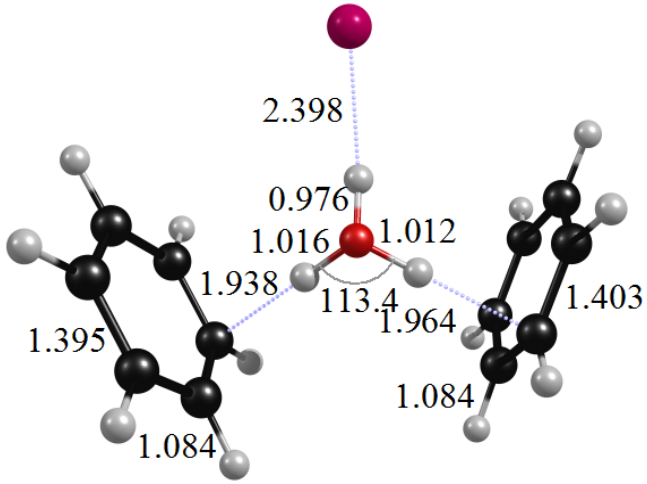

Unscaled Frequency (Intensity) Scaled Frequency /Symmetry of vibration

---

12 (0.0) 12/a, 16 (0.1) 15/a, 19 (0.5) 19/a, 22 (0.3) 21/a, 29 (1.9) 28/a, 40 (0.2) 38/a, 43 (1.0) 41/a, 49 (0.5) 47/a, 63 (6.0) 60/a, 93 (5.0) 89/a, 179 (13.7) 171/a, 224 (110.9) 215/a, 332 (15.5) 318/a, 380 (46.5) 364/a, 409 (2.4) 392/a, 410 (2.3) 393/a, 411 (0.1) 394/a, 412 (2.5) 395/a, 603 (43.2) 577/a, 618 (0.2) 592/a, 619 (0.1) 593/a, 620 (0.3) 593/a, 620 (3.8) 594/a, 697 (14.7) 667/a, 701 (15.7) 671/a, 721 (211.4) 690/a, 729 (48.4) 698/a, 883 (8.3) 845/a, 886 (2.9) 848/a, 888 (4.9) 850/a, 902 (2.7) 864/a, 966 (42.0) 925/a, 1000 (0.7) 957/a, 1002 (13.2) 959/a, 1003 (0.3) 961/a, 1008 (7.2) 965/a, 1010 (0.4) 967/a, 1017 (41.8) 974/a, 1021 (1.0) 977/a, 1023 (4.0) 980/a, 1031 (0.9) 987/a, 1033 (3.2) 989/a, 1054 (5.1) 1009/a, 1054 (12.8) 1010/a, 1057 (5.1) 1012/a, 1058 (7.9) 1013/a, 1180 (0.1) 1129/a, 1180 (0.2) 1130/a, 1200 (0.2) 1149/a, 1200 (0.4) 1149/a, 1201 (0.5) 1150/a, 1201 (0.3) 1150/a, 1332 (1.4) 1276/a, 1335 (1.3) 1279/a, 1383 (0.0) 1324/a, 1383 (0.0) 1324/a, 1504 (11.1) 1441/a, 1505 (3.3) 1441/a, 1506 (24.1) 1442/a, 1507 (14.7) 1443/a, 1583 (4.7) 1515/a, 1615 (1.7) 1546/a, 1621 (2.0) 1552/a, 1622 (2.1) 1553/a, 1624 (3.4) 1555/a, 1634 (13.4) 1565/a, 2862 (4105.0) 2740/a, 2994 (731.7) 2867/a, 3164 (0.4) 3030/a, 3167 (0.1) 3033/a, 3178 (0.6) 3043/a, 3179 (0.1) 3044/a, 3180 (0.6) 3045/a, 3180 (0.2) 3045/a, 3188 (4.4) 3053/a, 3190 (2.5) 3054/a, 3194 (2.4) 3058/a, 3195 (2.6) 3059/a, 3201 (0.8) 3065/a, 3202 (0.4) 3066/a, 3654 (409.4) 3499/a.

BW-3, 1 isomer-a (bz_3-H_3O)$^+$ DFT

State: $^1A(C_1)$ Total Energy =-773.7472826 $\Delta E = 0.0$

B.E.[a] = E (complex)-E (H_3O^++3*bz) = 51.7 D.E[b] (bz) = 10.6

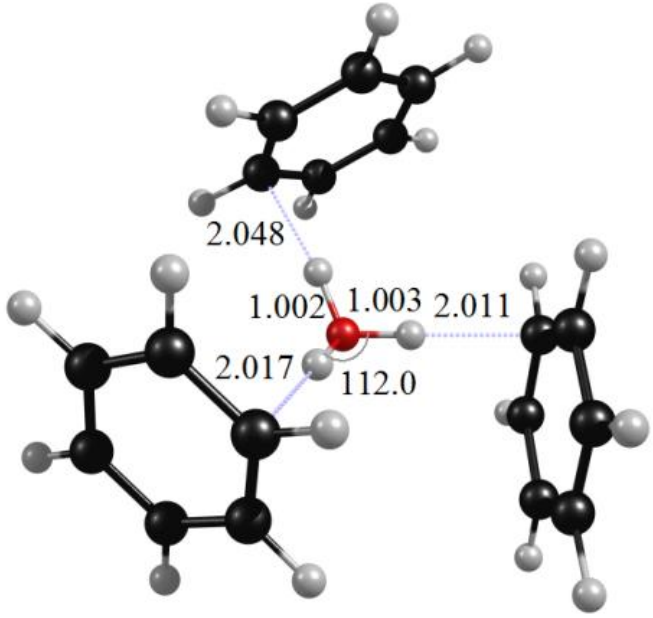

Unscaled Frequency (Intensity) Scaled Frequency /Symmetry of vibration

8 (0.1) 7/a, 11 (0.0) 11/a, 15 (0.1) 14/a, 22 (0.2) 21/a, 27 (0.1) 26/a, 31 (0.3) 30/a, 33 (0.7) 31/a, 41 (0.5) 39/a, 43 (0.3) 41/a,
46 (0.4) 44/a, 54 (0.6) 52/a, 64 (1.2) 62/a, 136 (1.1) 130/a, 198 (53.1) 189/a, 202 (60.8) 193/a, 400 (20.2) 383/a, 408 (0.5) 391/a,
410 (0.2) 392/a, 411 (1.0) 393/a, 412 (3.8) 394/a, 414 (2.4) 397/a, 425 (19.2) 407/a, 481(38.9) 460/a, 548 (15.4) 525/a,
619 (0.3) 593/a, 619 (0.0) 593/a, 620 (0.2) 593/a, 620 (0.1) 593/a, 620 (0.2) 594/a, 621 (0.1) 594/a, 701 (39.1) 671/a,
702 (29.9) 672/a, 703 (9.9) 673/a, 716 (187.8) 686/a, 718 (180.7) 687/a, 722 (19.5) 692/a, 865 (24.0) 828/a, 880 (1.0) 843/a,
881 (0.2) 844/a, 888 (7.5) 850/a, 893 (11.1) 855/a, 896 (0.9) 858/a, 917 (30.3) 878/a, 996 (9.4) 954/a, 997 (6.9) 955/a,
1003 (7.4) 961/a, 1004 (3.3) 961/a, 1004 (3.4) 961/a, 1005 (0.7) 963/a, 1007 (0.7) 964/a, 1007 (1.0) 965/a, 1009 (2.6) 966/a,
1020 (0.0) 976/a, 1021 (0.1) 978/a, 1022 (0.1) 978/a, 1030 (0.3) 986/a, 1031 (0.1) 987/a, 1032 (0.3) 988/a, 1054 (6.0) 1009/a,

1054 (7.1) 1010/a, 1055 (6.1) 1011/a, 1057 (3.6) 1012/a, 1058 (0.7) 1013/a, 1059 (10.1) 1014/a, 1178 (0.4) 1128/a, 1179 (0.1) 1129/a, 1180 (0.1) 1129/a, 1199 (0.4) 1148/a, 1200 (0.4) 1149/a, 1200 (0.4) 1149/a, 1201 (0.6) 1150/a, 1201 (0.1) 1150/a, 1201 (0.3) 1150/a, 1334 (1.6) 1277/a, 1335 (0.3) 1278/a, 1336 (1.1) 1279/a, 1382 (0.0) 1323/a, 1383 (0.0) 1324/a, 1383 (0.0) 1325/a, 1506 (10.7) 1442/a, 1506 (10.9) 1442/a, 1507 (3.8) 1443/a, 1508 (7.7) 1444/a, 1509 (2.7) 1445/a, 1509 (27.2) 1445/a, 1615 (6.7) 1547/a, 1622 (0.2) 1553/a, 1622 (0.8) 1553/a, 1624 (3.1) 1555/a, 1626 (4.3) 1557/a, 1627 (1.3) 1557/a, 1632 (4.1) 1562/a, 1659 (9.2) 1588/a, 3075 (2728.9) 2944/a, 3101 (2626.6) 2969/a, 3163 (5.5) 3029/a, 3164 (4.2) 3030/a, 3165 (2.9) 3031/a, 3172 (154.1) 3037/a, 3176 (0.3) 3041/a, 3176 (4.9) 3041/a, 3177 (1.3) 3042/a, 3179 (7.8) 3044/a, 3179 (1.1) 3044/a, 3180 (0.4) 3044/a, 3188 (12.8) 3053/a, 3188 (16.8) 3053/a, 3189 (10.6) 3054/a, 3193 (4.1) 3057/a, 3193 (6.1) 3057/a, 3193 (7.1) 3058/a, 3200 (8.3) 3064/a, 3200 (3.1) 3064/a, 3201 (1.6) 3065/a.

BW-3, 1 isomer-b $(bz_3H\text{-}H_2O)^+$ DFT

State: $^1A(C_1)$ Total Energy = -773.7272378 ΔE = +12.6

B.E.[a] = E (complex)-E (bzH^++H_2O+2*bz) = 22.0 D.E[b] (bz) = 4.7

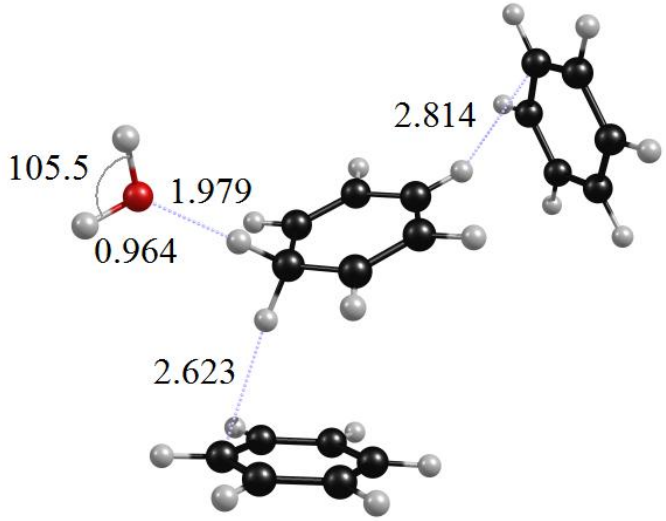

Unscaled Frequency (Intensity) Scaled Frequency /Symmetry of vibration

---

9 (0.6) 9/a, 12 (0.5) 12/a, 14 (0.8) 14/a, 20 (0.3) 19/a, 22 (0.2) 21/a, 34 (3.9) 32/a, 38 (0.9) 36/a, 43 (0.4) 41/a, 52 (5.0) 49/a,
58 (0.2) 56/a, 60 (1.2) 58/a, 64 (0.2) 61/a, 65 (2.5) 62/a, 81 (0.2) 78/a, 90 (9.6) 86/a, 153 (19.8) 147/a, 231 (243.3) 221/a,
256 (23.2) 246/a, 342 (44.7) 328/a, 344 (0.6) 330/a, 409 (0.2) 392/a, 411 (0.0) 393/a, 412 (0.1) 394/a, 413 (0.0) 395/a,
468 (21.1) 448/a, 597 (3.1) 571/a, 598 (0.9) 573/a, 620 (0.7) 594/a, 620 (0.0) 594/a, 620 (0.1) 594/a, 621 (0.3) 595/a, 665 (45.9) 637/a,
704 (198.5) 674/a, 706 (92.1) 676/a, 709 (3.1) 679/a, 712 (0.0) 682/a, 815 (1.3) 780/a, 846 (7.2) 810/a, 877 (0.2) 840/a,
877 (0.1) 840/a, 878 (0.1) 840/a, 880 (0.5) 843/a, 917 (17.1) 878/a, 999 (0.1) 957/a, 1000 (1.2) 957/a, 1001 (0.0) 958/a,
1001 (1.1) 958/a, 1004 (4.2) 961/a, 1005 (7.8) 962/a, 1007 (3.6) 964/a, 1007 (2.3) 964/a, 1010 (2.3) 967/a, 1016 (0.0) 973/a,
1017 (0.0) 974/a, 1019 (1.6) 976/a, 1028 (0.0) 984/a, 1029 (0.0) 985/a, 1035 (0.4) 991/a, 1055 (7.5) 1010/a, 1056 (3.6) 1011/a,
1057 (4.1) 1012/a, 1058 (0.9) 1013/a, 1059 (4.1) 1014/a, 1151 (1.5) 1102/a, 1167 (3.7) 1117/a, 1177 (0.0) 1127/a, 1178 (0.1) 1128/a,
1198 (1.3) 1147/a, 1198 (3.3) 1147/a, 1198 (1.2) 1147/a, 1198 (2.5) 1147/a, 1199 (0.2) 1148/a, 1205 (30.7) 1154/a,
1280 (160.1) 1225/a, 1334 (0.0) 1278/a, 1336 (0.2) 1279/a, 1368 (10.9) 1310/a, 1382 (0.0) 1323/a, 1383 (0.0) 1324/a,

1427 (8.6) 1366/a, 1477 (136.2) 1414/a, 1479 (42.9) 1416/a, 1508 (10.5) 1444/a, 1508 (10.0) 1444/a, 1509 (9.2) 1445/a,
1510 (9.2) 1446/a, 1572 (0.6) 1505/a, 1624 (6.3) 1555/a, 1626 (8.7) 1557/a, 1627 (1.4) 1558/a, 1627 (0.8) 1558/a, 1635 (43.8) 1565/a,
1638 (157.9) 1568/a, 2749 (692.2) 2632/a, 2887 (434.6) 2765/a, 3163 (0.1) 3028/a, 3163 (0.0) 3029/a, 3171 (0.0) 3036/a,
3171 (0.1) 3037/a, 3173 (0.0) 3038/a, 3173 (0.0) 3038/a, 3185 (12.0) 3050/a, 3185 (13.3) 3050/a, 3187 (13.5) 3051/a,
3187 (6.7) 3051/a, 3187 (8.4) 3052/a, 3192 (21.7) 3057/a, 3195 (0.5) 3059/a, 3195 (0.7) 3060/a, 3200 (9.6) 3064/a,
3208 (2.3) 3072/a, 3212 (3.2) 3076/a, 3806 (41.8) 3644/a, 3902 (97.1) 3736/a.

BW-2, 2 isomer-a $(bz_2\text{-}H_5O_2)^+$ (benzenes are in "cis" position) DFT

State: $^1A(C_1)$ Total Energy = -617.9115719 $\Delta E = 0.0$

B.E.[a] = E (complex)-E (H_3O^++H_2O+2*bz) = 62.4 D.E[b] (bz) = 10.7

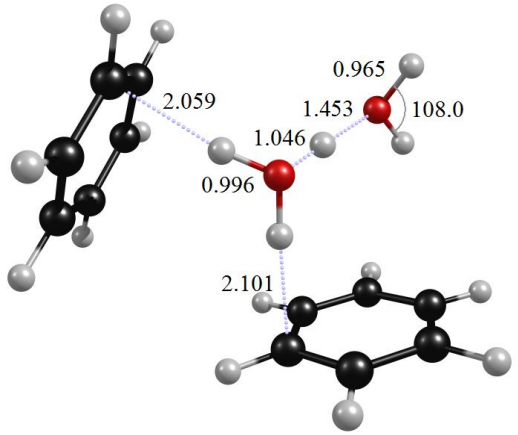

Unscaled Frequency (Intensity) Scaled Frequency /Symmetry of vibration

---

8 (0.8) 7/a, 21 (3.1) 20/a, 26 (5.6) 25/a, 27 (0.9) 26/a, 35 (1.8) 33/a, 45 (0.0) 43/a, 49 (0.7) 47/a, 58 (1.4) 56/a, 65 (0.0) 63/a,
141 (5.2) 135/a, 142 (29.2) 136/a, 184 (41.5) 176/a, 322 (145.1) 309/a, 380 (172.9) 364/a, 410 (0.4) 393/a, 411 (0.5) 393/a,
412 (0.5) 395/a, 415 (3.1) 397/a, 421 (16.5) 403/a, 477 (75.5) 456/a, 607 (55.4) 581/a, 619 (0.1) 593/a, 620 (0.3) 594/a,
620 (0.1) 594/a, 621 (8.3) 595/a, 700 (16.9) 670/a, 702 (11.3) 672/a, 715 (66.7) 684/a, 718 (183.2) 688/a, 748 (20.3) 716/a,
883 (0.4) 846/a, 884 (0.6) 847/a, 892 (6.2) 854/a, 895 (0.7) 857/a, 997 (3.4) 955/a, 999 (3.7) 957/a, 1004 (2.1) 961/a,
1004 (2.2) 962/a, 1007 (0.2) 964/a, 1007 (0.1) 965/a, 1017 (0.0) 974/a, 1019 (0.0) 976/a, 1030 (0.1) 986/a, 1031 (0.3) 987/a,
1054 (5.7) 1009/a, 1055 (4.3) 1010/a, 1057 (2.8) 1012/a, 1058 (3.8) 1013/a, 1154 (125.5) 1105/a, 1178 (0.6) 1128/a,
1179 (0.1) 1129/a, 1198 (0.0) 1147/a, 1200 (0.1) 1149/a, 1201 (0.9) 1150/a, 1201 (0.4) 1150/a, 1332 (0.6) 1276/a, 1334 (0.6) 1277/a,
1383 (0.0) 1324/a, 1383 (0.0) 1324/a, 1506 (7.1) 1442/a, 1507 (11.2) 1442/a, 1507 (8.9) 1443/a, 1508 (18.3) 1444/a,
1607 (10.0) 1539/a, 1620 (13.5) 1551/a, 1622 (14.0) 1553/a, 1624 (22.4) 1555/a, 1626 (0.6) 1557/a, 1630 (7.9) 1560/a,
1749 (69.7) 1675/a, 2432 (2004.3) 2329/a, 3164 (0.4) 3030/a, 3164 (0.5) 3030/a, 3170 (0.2) 3035/a, 3175 (0.1) 3040/a,
3178 (0.1) 3043/a, 3179 (0.6) 3044/a, 3186 (4.2) 3050/a, 3187 (9.7) 3052/a, 3192 (4.8) 3056/a, 3193 (2.4) 3057/a, 3199 (16.3) 3063/a,
3199 (1.1) 3063/a, 3245 (1893.2) 3107/a, 3326 (921.1) 3185/a, 3781 (47.8) 3620/a, 3873 (211.8) 3709/a.

BW-2, 2 isomer-b $(bz_2\text{-}H_5O_2)^+$ (benzenes are in "trans" position) DFT

State: $^1A(C_1)$ Total Energy = -617.9092657 ΔE = +1.4

B.E.[a] = E (complex)-E (H_3O^++H_2O+2*bz) = 61.0 D.E[b] (bz) = 9.3

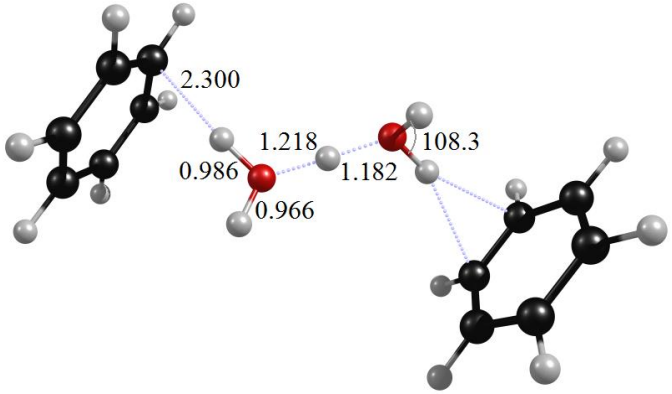

Unscaled Frequency (Intensity) Scaled Frequency /Symmetry of vibration

1 (2.8) 1/a, 9 (3.7) 9/a, 19 (0.8) 18/a, 22 (2.0) 21/a, 27 (0.6) 26/a, 40 (5.9) 38/a, 46 (4.3) 44/a, 57 (4.7) 55/a, 61 (12.8) 59/a,
121 (275.4) 116/a, 149 (2.3) 142/a, 197 (73.6) 188/a, 294 (42.7) 281/a, 401 (135.6) 384/a, 410 (0.6) 393/a, 411 (3.0) 394/a,
413 (0.4) 396/a, 420 (54.5) 402/a, 524 (87.8) 502/a, 565 (169.3) 541/a, 611 (52.7) 585/a, 619 (0.3) 593/a, 620 (0.1) 593/a,
620 (0.5) 593/a, 621 (0.0) 594/a, 657 (51.7) 629/a, 703 (4.4) 673/a, 705 (0.3) 675/a, 720 (368.3) 689/a, 721 (34.3) 690/a,
882 (400.8) 844/a, 885 (24.1) 847/a, 889 (142.9) 851/a, 892 (0.7) 854/a, 941 (2701.2) 901/a, 1000 (1.8) 958/a, 1003 (0.3) 960/a,
1003 (1.8) 961/a, 1005 (39.7) 962/a, 1006 (0.4) 964/a, 1008 (125.2) 965/a, 1017 (2.1) 974/a, 1020 (1.4) 976/a, 1029 (0.4) 986/a,
1030 (0.4) 986/a, 1054 (3.5) 1009/a, 1055 (12.7) 1010/a, 1056 (10.4) 1011/a, 1057 (4.3) 1012/a, 1179 (0.3) 1129/a, 1179 (0.2) 1129/a,
1199 (0.1) 1148/a, 1200 (0.2) 1149/a, 1200 (0.5) 1149/a, 1201 (0.2) 1150/a, 1329 (0.7) 1273/a, 1330 (2.6) 1273/a, 1383 (0.0) 1324/a,
1383 (0.0) 1324/a, 1429 (97.4) 1368/a, 1505 (12.9) 1441/a, 1506 (10.8) 1442/a, 1507 (16.5) 1443/a, 1507 (16.7) 1443/a,
1575 (570.2) 508/a, 1619 (0.2) 1551/a, 1620 (0.4) 1552/a, 1624 (3.7) 1555/a, 1624 (1.4) 1555/a, 1671 (17.9) 1600/a,
1729 (931.5) 1655/a, 3161 (0.0)3026/a, 3165 (0.0) 3031/a, 3170 (0.6) 3035/a, 3174 (0.9) 3039/a, 3174 (0.1) 3040/a, 3175 (0.2) 3040/a,
3184 (4.7) 3049/a, 3185 (6.0) 3050/a, 3186 (4.8) 3051/a, 3189 (4.9) 3053/a, 3196 (1.9) 3061/a, 3196 (0.8) 3061/a,
3371 (1490.8) 3228/a, 3421 (757.8) 3276/a, 3804 (118.6) 3642/a, 3834 (122.7) 3671/a.

BW-2, 2-Ar isomer-a (bz_2-H_5O_2Ar)$^+$ (benzenes are in "cis" position, Argon on the other OH) DFT

State: $^1A(C_1)$ Total Energy = -1145.466415 ΔE = +0.0

B.E.[a] = E (complex)-E (H_3O^++H_2O+2*bz+Ar) = 63.0 D.E[b] (Ar) = 0.6

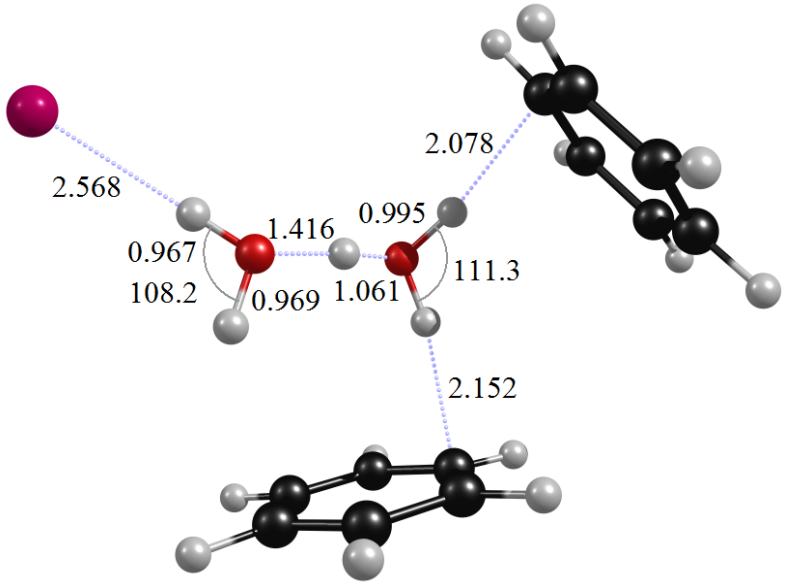

Unscaled Frequency (Intensity) Scaled Frequency /Symmetry of vibration

-12 (0.1) -12/a, 13 (0.3) 12/a, 19 (0.3) 18/a, 24 (2.5) 23/a, 27 (0.4) 25/a, 29 (0.5) 28/a, 34 (0.8) 32/a, 48 (0.5) 46/a, 50 (0.4) 48/a, 58 (2.1) 56/a, 72 (0.6) 69/a, 84 (13.0) 80/a, 132 (8.8) 126/a, 175 (41.5) 167/a, 240 (32.7) 230/a, 366 (90.3) 351/a, 410 (3.7) 392/a, 410 (2.6) 393/a, 412 (0.2) 395/a, 415 (1.2) 398/a, 426 (205.9) 408/a, 439 (15.5) 420/a, 478 (78.3) 457/a, 616 (15.5) 590/a, 619 (0.1) 593/a, 620 (0.0) 593/a, 620 (0.0) 594/a, 628 (47.4) 602/a, 700 (11.4) 670/a, 702 (6.7) 672/a, 717 (70.3) 686/a, 718 (192.3) 687/a, 748 (25.2) 716/a, 884 (0.2) 846/a, 885 (0.4) 847/a, 892 (4.5) 855/a, 894 (1.3) 856/a, 999 (3.9) 956/a, 1000 (4.3) 958/a, 1004 (0.9) 961/a, 1005 (2.3) 962/a, 1007 (0.1) 964/a, 1008 (0.1) 965/a, 1015 (0.1) 972/a, 1018 (0.0) 975/a, 1030 (0.1) 986/a, 1031 (0.1) 987/a, 1054 (4.9) 1009/a, 1055 (4.9) 1010/a, 1057 (3.3) 1012/a, 1057 (3.8) 1012/a, 1178 (7.3) 1128/a, 1179 (2.8) 1129/a, 1184 (109.6) 1133/a, 1197 (0.6) 1146/a, 1200 (0.4) 1149/a, 1201 (3.0) 1150/a, 1201 (1.7) 1150/a,

1332 (0.7) 1275/a, 1333 (0.4) 1277/a, 1382 (0.0) 1324/a, 1383 (0.0) 1324/a, 1506 (8.1) 1442/a, 1506 (9.3) 1442/a, 1507 (9.4) 1443/a, 1508 (20.0) 1444/a, 1588 (39.1) 1521/a, 1619 (13.2) 1550/a, 1622 (4.1) 1553/a, 1623 (9.3) 1554/a, 1626 (1.0) 1557/a, 1628 (6.5) 1559/a, 1765 (108.6) 1690/a, 2220 (2194.0) 2125/a, 3162 (1.1) 3028/a, 3164 (0.3) 3030/a, 3166 (0.4) 3032/a, 3175 (0.0) 3040/a, 3179 (0.1) 3044/a, 3180 (0.1) 3045/a, 3185 (3.8) 3050/a, 3187 (6.1) 3052/a, 3192 (4.7) 3056/a, 3194 (3.0) 3058/a, 3198 (0.5) 3062/a, 3199 (5.1) 3063/a, 3271 (1597.1) 3132/a, 3412 (918.0) 3267/a, 3741 (72.6) 3582/a, 3829 (461.6) 3666/a.

BW-2, 2-Ar (bz_2-H_5O_2Ar)$^+$ (benzenes are in "trans" position, Argon on the other OH) DFT

State: $^1A(C_1)$ Total Energy = -1145.4649879 ΔE = +0.9

B.E.[a] = E (complex)-E (H_3O^++H_2O+2*bz+Ar) = 62.1 D.E[b] (Ar) = 1.2

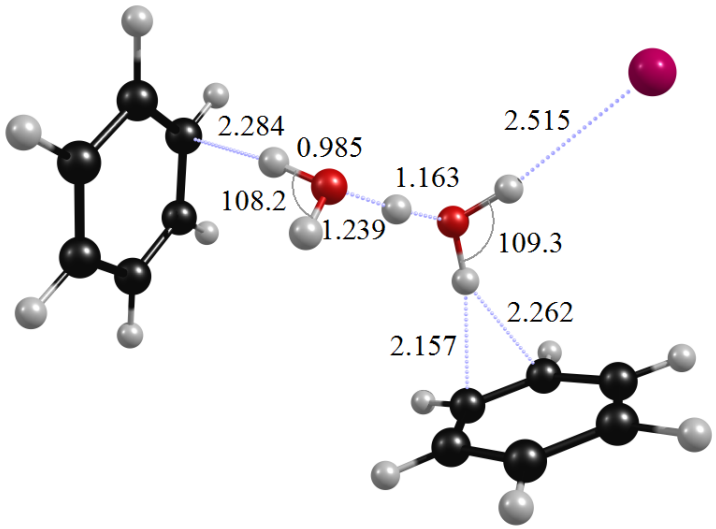

Unscaled Frequency (Intensity) Scaled Frequency /Symmetry of vibration

---

10 (0.3) 10/a, 11 (0.5) 10/a, 14 (1.4) 14/a, 19 (1.5) 18/a, 20 (0.4) 19/a, 26 (0.2) 25/a, 28 (3.4) 26/a, 46 (0.4) 44/a, 48 (4.0) 46/a,
62 (2.4) 59/a, 64 (7.4) 61/a, 78 (6.3) 74/a, 136 (109.9) 130/a, 153 (27.6) 146/a, 260 (71.5) 249/a, 340 (75.8) 326/a,
410 (2.3) 393/a, 411 (1.0) 393/a, 413 (1.0) 395/a, 413 (0.2) 395/a, 491 (124.3) 470/a, 521 (63.4) 499/a, 562 (149.4) 538/a,
611 (91.5) 585/a, 620 (0.1) 593/a, 620 (0.1) 594/a, 620 (0.2) 594/a, 622 (9.8) 595/a, 672 (41.0) 644/a, 703 (0.1) 673/a,
703 (4.9) 673/a, 717 (244.9) 687/a, 723 (107.5) 692/a, 884 (25.3) 846/a, 885 (1.3) 847/a, 888 (87.0) 850/a, 892 (3.2) 854/a,
995 (450.9) 953/a, 1001 (59.8) 959/a, 1003 (3.6) 960/a, 1004 (1.5) 962/a, 1005 (6.8) 962/a, 1006 (0.9) 963/a, 1017 (2.2) 974/a,
1018 (2.0) 975/a, 1029 (0.3) 985/a, 1030 (24.3) 986/a, 1040 (1775.9) 995/a, 1056 (6.0) 1011/a, 1057 (1.0) 1012/a,
1057 (5.8) 1012/a, 1061 (584.6) 1015/a, 1179 (0.2) 1129/a, 1179 (0.1) 1129/a, 1199 (0.6) 1148/a, 1200 (1.3) 1149/a,
1200 (0.1) 1149/a, 1201 (0.5) 1150/a, 1332 (1.4) 1275/a, 1332 (0.3) 1276/a, 1383 (0.0) 1324/a, 1383 (0.0) 1324/a,
1423 (334.5) 1362/a, 1507 (13.1) 1443/a, 1507 (10.0) 1443/a, 1507 (15.9) 1443/a, 1508 (14.1) 1444/a, 1571 (97.6) 1504/a,
1623 (0.4) 1554/a, 1623 (0.5) 1554/a, 1625 (1.8)1556/a, 1626 (0.8) 1557/a, 1684 (10.2) 1613/a, 1731 (879.3) 1658/a,

3166 (0.0) 3032/a, 3167 (0.0) 3033/a, 3176 (0.3) 3041/a, 3176 (0.1) 3041/a, 3177 (0.2) 3042/a, 3177 (0.1) 3042/a, 3188 (3.9) 3053/a, 3189 (5.3) 3053/a, 3190 (6.4) 3054/a, 3191 (6.8) 3055/a, 3198 (0.8) 3062/a, 3199 (1.1) 3063/a, 3379 (1204.6) 3235/a, 3447 (861.4) 3300/a, 3756 (363.1) 3596/a, 3830 (104.7) 3667/a.

BW-3, 2 $(bz_3\text{-}H_5O_2)^+$ DFT

State: $^1A(C_1)$ Total Energy = -850.2350923 $\Delta E = 0.0$

B.E.[a] = E (complex)-E (H_3O^++H_2O+3*bz) = 70.1 D.E[b] (bz) = 7.7

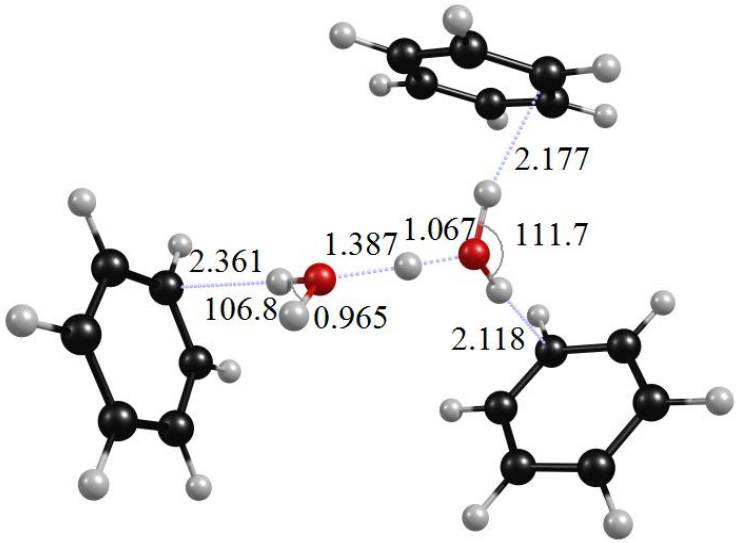

Unscaled Frequency (Intensity) Scaled Frequency /Symmetry of vibration

10 (0.2) 10/a, 13 (0.3) 12/a, 14 (0.2) 14/a, 17 (0.1) 17/a, 18 (0.1) 18/a, 24 (1.0) 23/a, 29 (0.6) 27/a, 31 (0.2) 30/a, 37 (0.8) 36/a, 42 (0.3) 40/a, 44 (1.0) 42/a, 52 (2.5) 50/a, 61 (0.5) 58/a, 90 (4.1) 86/a, 105 (10.3) 100/a, 135 (18.9) 129/a, 178 (37.3) 170/a, 202 (34.2) 194/a, 366 (90.8) 350/a, 409 (0.9) 392/a, 410 (0.2) 393/a, 412 (11.1) 394/a, 412 (1.7) 394/a, 412 (0.7) 395/a, 412 (0.6) 395/a, 422 (114.0) 404/a, 461 (62.0) 441/a, 505 (20.9) 483/a, 593 (34.5) 568/a, 620 (0.1) 594/a, 620 (0.2) 594/a, 620 (0.0) 594/a, 621 (0.1) 594/a, 621 (0.2) 594/a, 621 (0.1) 595/a, 694 (106.8) 665/a, 704 (4.2) 674/a, 705 (6.9) 675/a, 707 (25.8) 677/a, 711 (137.5) 681/a, 718 (52.5) 688/a, 729 (135.6) 698/a, 879 (0.2) 842/a, 881 (0.6) 844/a, 882 (0.1) 844/a, 884 (1.2) 847/a, 890 (8.2) 852/a, 892 (5.0) 854/a, 996 (1.7) 954/a, 1000 (0.5) 958/a, 1000 (1.6) 958/a, 1003 (0.1) 960/a, 1004 (0.1) 961/a, 1005 (4.5) 962/a, 1005 (0.3) 962/a, 1005 (4.8) 962/a, 1006 (0.1) 963/a, 1016 (0.0) 973/a, 1018 (0.0) 975/a,

1020 (0.0) 976/a, 1028 (0.0) 985/a, 1029 (0.1) 985/a, 1029 (0.0) 986/a, 1056 (5.5) 1011/a, 1056 (1.2) 1011/a, 1056 (8.7) 1011/a, 1057 (2.7) 1013/a, 1058 (3.8) 1013/a, 1058 (8.1) 1013/a, 1178 (0.1) 1127/a, 1178 (0.1) 1128/a, 1179 (0.2) 1129/a, 1198 (0.4) 1148/a, 1199 (0.1) 1148/a, 1200 (0.0) 1149/a, 1200 (0.1) 1149/a, 1200 (0.1) 1149/a, 1201 (0.0) 1150/a, 1268 (103.3) 1214/a, 1332 (0.1) 275/a, 1333 (0.9) 1277/a, 1334 (0.5) 1278/a, 1382 (0.0) 1324/a, 1383 (0.0) 1324/a, 1383 (0.0) 1324/a, 1506 (8.1) 1442/a, 1507 (4.1) 1443/a, 1507 (9.9) 1443/a, 1508 (13.9) 1444/a, 1508 (1.6) 1444/a, 1509 (15.1) 1445/a, 1561 (146.0) 1495/a, 1620 (51.9) 1551/a, 1624 (1.2) 1555/a, 1624 (0.3) 1555/a, 1625 (0.3) 1556/a, 1626 (1.8) 1557/a, 1628 (0.6) 1558/a, 1634 (58.8) 1564/a, 1679 (27.1) 1608/a, 2140 (3384.2) 2049/a, 3164 (0.2) 3030/a, 3165 (0.2) 3031/a, 3166 (0.0) 3032/a, 3174 (0.1) 3039/a, 3176 (0.6) 3041/a, 3176 (0.4) 3041/a, 3176 (0.1) 3041/a, 3177 (0.1) 3042/a, 3178 (0.8) 3043/a, 3187 (7.9) 3052/a, 3188 (7.5) 3052/a, 3188 (3.6) 3052/a, 3190 (8.3) 3055/a, 3191 (7.0) 3055/a, 3192 (10.3) 3056/a, 3198 (0.1) 3062/a, 3199 (2.3) 3063/a, 3200 (2.0) 3064/a, 3356 (1432.4) 3214/a, 3367 (1168.7) 3224/a, 3645 (471.2) 3490/a, 3845 (74.6)3 682/a.

BW-4, 2 isomer-a $(bz_4\text{-}H_5O_2)^+$ DFT

State: $^1A(C_1)$ Total Energy = -1082.5554622 $\Delta E = 0.0$

B.E.[a] = E (complex)-E (H_3O^++H_2O+4*bz) = 75.8 D.E[b] (bz) = 5.7

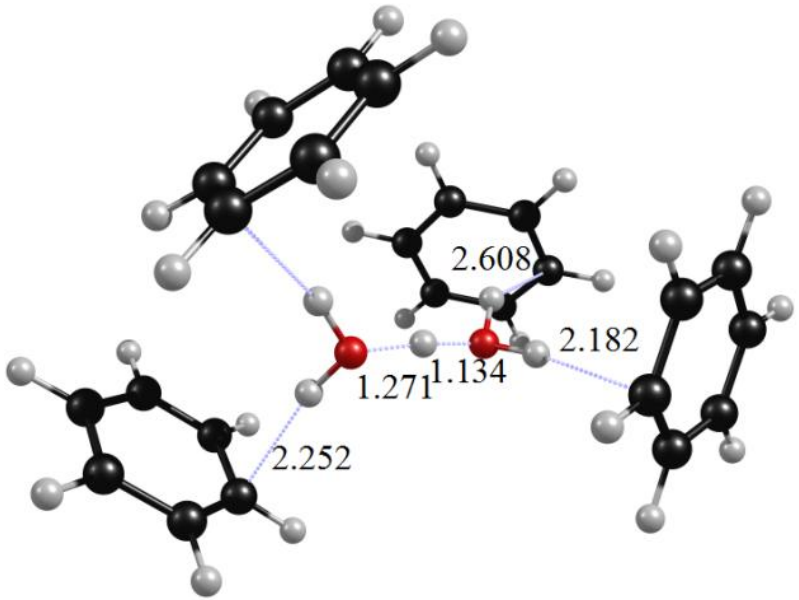

Unscaled Frequency (Intensity) Scaled Frequency /Symmetry of vibration

---

-8 (0.5) -7/a, -3 (0.0) -3/a, 11 (0.2) 11/a, 18 (0.2) 17/a, 19 (0.0) 18/a, 20 (0.2) 19/a, 22 (0.3) 21/a, 25 (0.9) 24/a, 28 (1.2) 27/a,
31 (0.5) 30/a, 32 (0.1) 30/a, 32 (0.4) 31/a, 34 (0.1) 32/a, 36 (0.1) 35/a, 39 (0.1) 37/a, 43 (3.3) 41/a, 47 (0.2) 45/a, 53 (5.8) 51/a,
59 (0.4) 57/a, 98 (25.0) 94/a, 114 (45.1) 109/a, 149 (13.5) 143/a, 164 (26.5) 157/a, 385 (24.9) 369/a, 409 (3.4) 392/a, 410 (1.6) 392/a,
410 (0.2) 393/a, 411 (6.3) 394/a, 412 (9.6) 395/a, 412 (1.4) 395/a, 414 (10.1) 396/a, 414 (1.3) 397/a, 425 (100.8) 407/a,
446 (110.6) 427/a, 516 (250.6) 495/a, 583 (79.6) 558/a, 607 (7.7) 581/a, 620 (0.3) 594/a, 621 (0.0) 594/a, 621 (0.2) 595/a,

621 (0.1) 595/a, 622 (0.2) 595/a, 622 (0.2) 595/a, 622 (0.4) 595/a, 622 (0.1) 596/a, 647 (24.7) 620/a, 704 (112.1) 674/a,
704 (107.9) 674/a, 705 (122.3) 675/a, 707 (18.8) 677/a, 710 (96.0) 680/a, 711 (83.7) 680/a, 711 (74.8) 681/a, 715 (14.0) 685/a,
875 (0.4) 838/a, 875 (0.7) 838/a, 877 (3.1) 840/a, 879 (0.1) 842/a, 882 (11.7) 845/a, 882 (6.0) 845/a, 885 (5.1) 848/a, 886 (6.9) 848/a,
995 (6.3) 952/a, 996 (13.9) 954/a, 996 (3.7) 954/a, 998 (5.3) 955/a, 1001 (1.4) 958/a, 1001 (0.1) 959/a, 1002 (0.7) 959/a,
1003 (0.3) 960/a, 1005 (37.6) 962/a, 1006 (2.4) 963/a, 1006 (2.6) 963/a, 1007 (0.1) 964/a, 1017 (0.2) 974/a, 1018 (0.0) 974/a,
1018 (0.0) 975/a, 1019 (0.1) 975/a, 1027 (0.2) 984/a, 1028 (0.2) 984/a, 1028 (0.1) 984/a, 1029 (0.1) 985/a, 1056 (36.4) 1011/a,
1056 (5.2) 1012/a, 1057 (2.4) 1012/a, 1057 (4.3) 1012/a, 1058 (4.6) 1013/a, 1058 (2.0) 1013/a, 1058 (5.2) 1013/a, 1059 (6.4) 1014/a,
1168 (2836.6) 1118/a, 1177 (8.7) 1127/a, 1177 (0.5) 1127/a, 1177 (0.2) 1127/a, 1178 (25.9) 1128/a, 1198 (4.8) 1147/a,
1198 (8.9) 1147/a, 1199 (0.5) 1148/a, 1199 (2.6) 1148/a, 1199 (3.5) 1148/a, 1199 (6.7) 1149/a, 1200 (2.1) 1149/a, 1200 (14.0) 1149/a,
1334 (1.6) 1277/a, 1334 (0.9) 1278/a, 1335 (1.8) 1278/a, 1335 (2.4) 1278/a, 1382 (0.0) 1323/a, 1382 (0.0) 1323/a, 1382 (0.0) 1323/a,
1382 (0.0) 1324/a, 1415 (157.7) 1355/a, 1508 (8.2) 1444/a, 1508 (5.5) 1444/a, 1508 (14.6) 1444/a, 1508 (6.1) 1444/a,
1509 (13.8) 1445/a, 1509 (13.9) 1445/a, 1509 (10.7) 1445/a, 1510 (10.6) 1446/a, 1587 (158.1) 1519/a, 1625 (0.2) 1556/a,
1626 (0.3) 1556/a, 1626 (0.1) 1557/a, 1627 (0.1) 1558/a, 1627 (1.6) 1558/a, 1628 (0.4) 1559/a, 1629 (1.6) 1560/a,
1629 (0.6) 1560/a, 1675 (6.9) 1604/a, 1761 (910.6) 1686/a, 3161 (0.5) 3027/a, 3161 (0.5) 3027/a, 3162 (0.1) 3028/a,
3164 (0.2) 3030/a, 3171 (0.2) 3037/a, 3172 (0.4) 3037/a, 3173 (0.3) 3038/a, 3175 (0.4) 3040/a, 3175 (0.5) 3040/a,
3175 (0.5) 3040/a, 3176 (0.4) 3041/a, 3177 (0.8) 3042/a, 3185 (13.3) 3050/a, 3185 (7.1) 3050/a, 3186 (7.2) 3050/a,
3188 (7.8) 3052/a, 3188 (10.1) 3053/a, 3189 (11.3) 3054/a, 3190 (8.3) 3055/a, 3191 (12.2) 3055/a, 3197 (1.3) 3061/a,
3197 (0.5) 3061/a, 3198 (1.0) 3062/a, 3199 (1.1) 3063/a, 3457 (550.0) 3310/a, 3483 (1525.9) 3335/a, 3565 (330.0) 3414/a,
3610 (1169.8) 3457/a.

Table S1: Computed binding energies and relative energies (with respect to the most stable isomer) of $(benzene)_mH^+(H_2O)_nAr_x$ complexes in kcal/mol. Calculations are done with MP2 and/or B3LYP levels of theory with 6-311+G (d, p) basis set. Energies are not ZPVE or BSSE corrected.

	DFT		MP2	
Complex	B.E.	ΔE	B.E.	ΔE
BW-1, 1 isomer-a $(bz\text{-}H_3O)^+$	25.0	+3.5	28.7	0.0
BW-1, 1 isomer-b $(bzH\text{-}H_2O)^+$	11.4	0.0	13.6	+6.2
BW-1, 1-Ar isomer-a $(bz\text{-}H_3O\text{-}Ar)^+$	27.0	+1.9	32.3	0.0
BW-1, 1-Ar isomer-b $(bzH\text{-}H_2O\text{-}Ar)^+$	11.8	0.0	15.5	+7.8
BW-1, 2 isomer-a $(bz\text{-}H_5O_2)^+$	51.7	0.0	56.5	0.0
BW-1, 2 isomer-b $(bzH\text{-}H_2O_4)^+$	20.8	+13.7	23.2	+24.3
BW-1, 2-Ar isomer-a $(bz\text{-}H_5O_2\text{-}Ar)^+$ (Argon is "cis" to benzene)	52.8	0.0	59.2	0.0
BW-1, 2-Ar isomer-b $(bz\text{-}H_5O_2\text{-}Ar)^+$ (Argon is "trans" to benzene)	52.5	+0.3	57.7	+1.5
BW-1, 3 isomer-a $(bz\text{-}H_7O_3)^+$	72.7	0.0	--	--
BW-1, 3 isomer-b $(bzH\text{-}H_6O_3)^+$	34.6	+21.0	--	--
BW-1, 4 isomer-a $(bz\text{-}H_9O_4)^+$	89.0	0.0	--	--
BW-1, 4 isomer-b $(bzH\text{-}H_8O_4)^+$	46.9	+25.0	--	--
BW-2, 1 isomer-a $(bz_2\text{-}H_3O)^+$	41.1	0.0	--	--
BW-2, 1 isomer-b $(bz_2H\text{-}H_2O)^+$	17.3	+6.6	--	--
BW-2, 2 isomer-a $(bz_2\text{-}H_5O_2)^+$ bz-cis	62.4	0.0	--	--
BW-2, 2 isomer-a $(bz_2\text{-}H_5O_2)^+$ bz-trans	61.0	+1.4	--	--
BW-3, 1 isomer-a $(bz_3\text{-}H_3O)^+$	51.7	0.0	--	--
BW-3, 1 isomer-b $(bz_3H\text{-}H_2O)^+$	22.0	+12.6	--	--

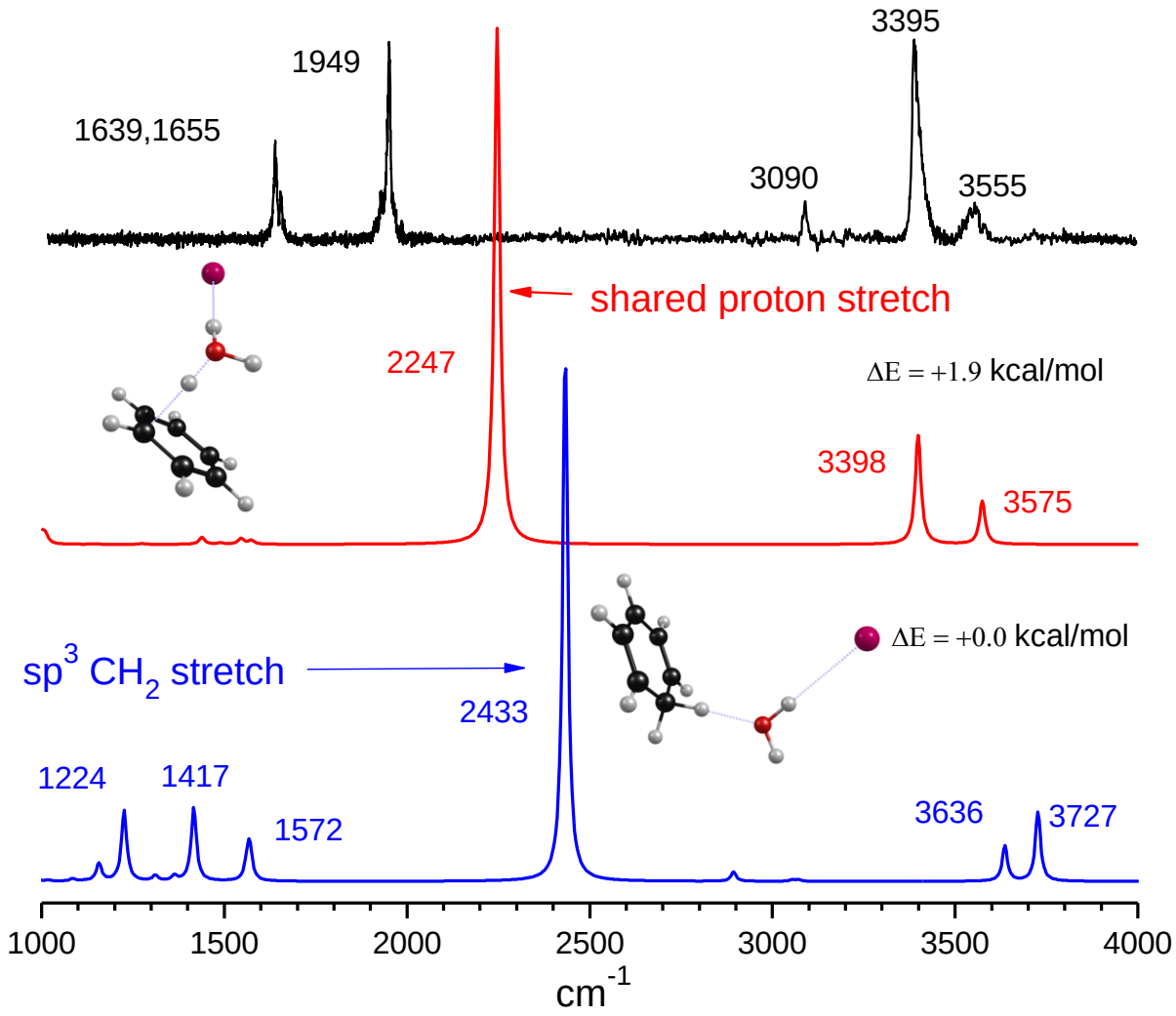

Figure S1. B3LYP/6-311+G (d, p) predicted spectra for two isomers of $(bz)H^{+}(H_2O)Ar$. Top trace shows the experimental infrared spectrum.

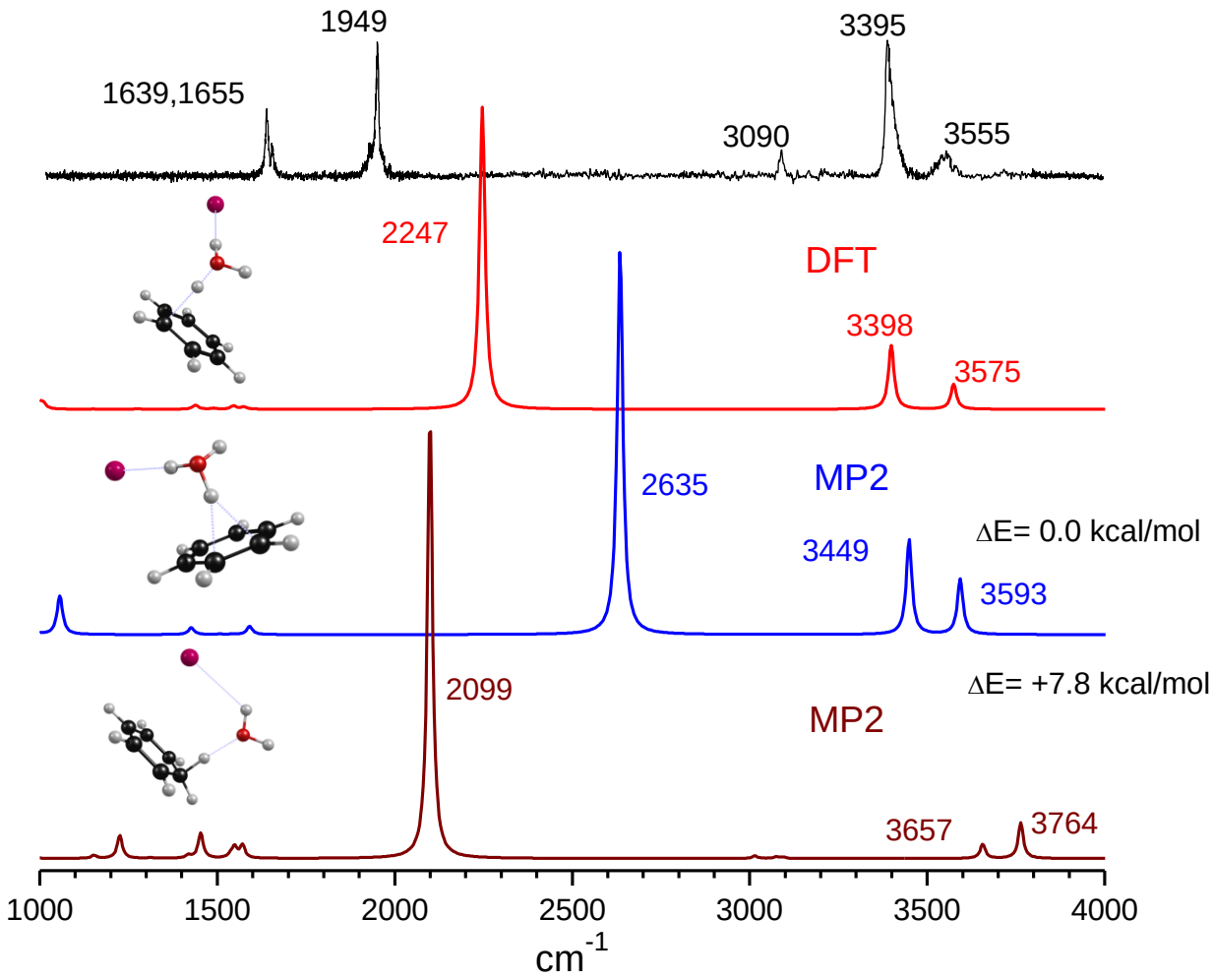

Figure S2. DFT-B3LYP and MP2/6-311+G (d,p) predicted spectra corresponding to various isomers of $(bz)H^{+}(H_2O)Ar$. Upper trace shows the experimental infrared spectrum.

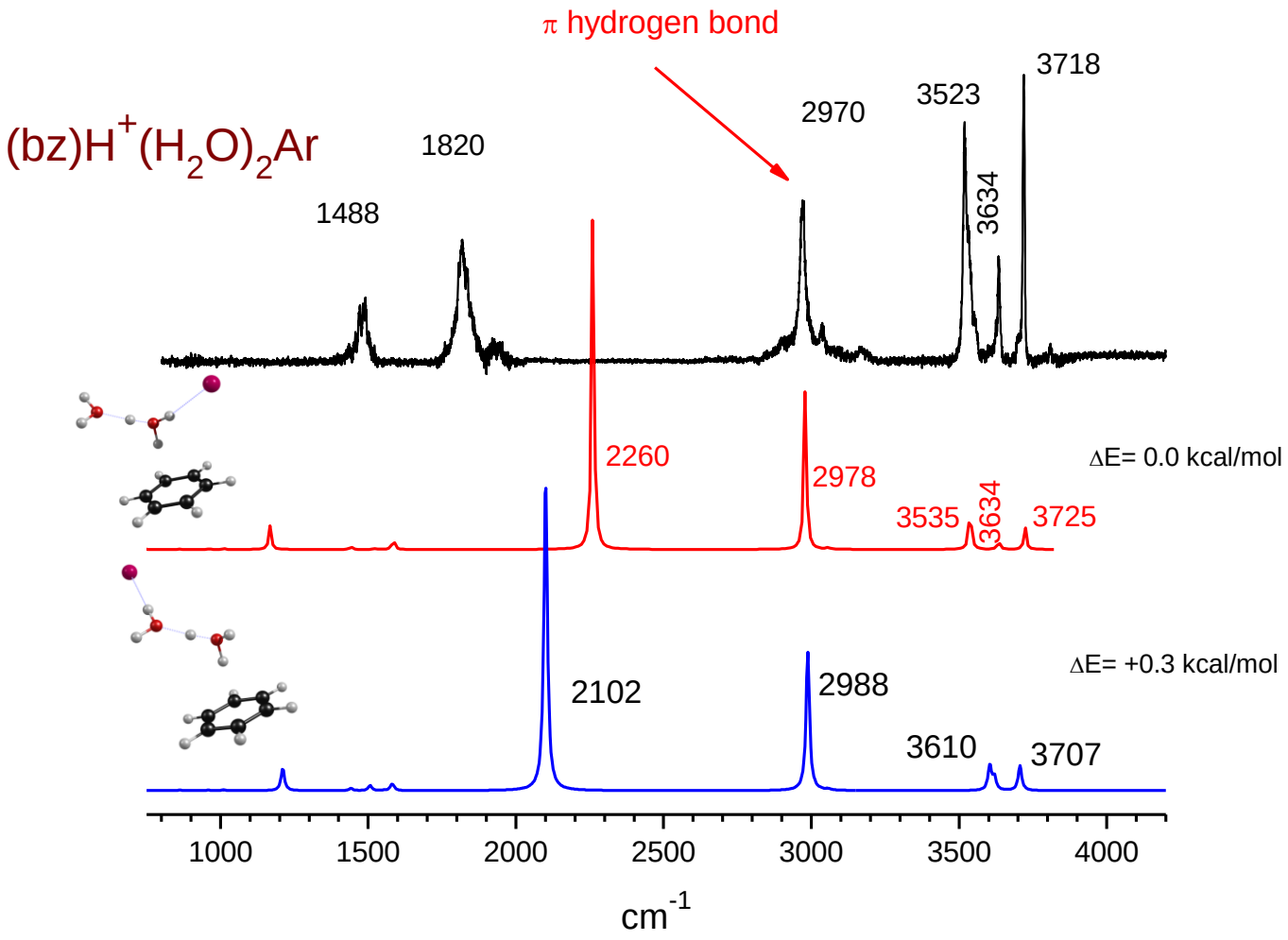

Figure S3. Comparison of predicted spectra of two different isomers of $bzH^+(H_2O)_2Ar$ calculated in DFT with the observed experimental spectrum.

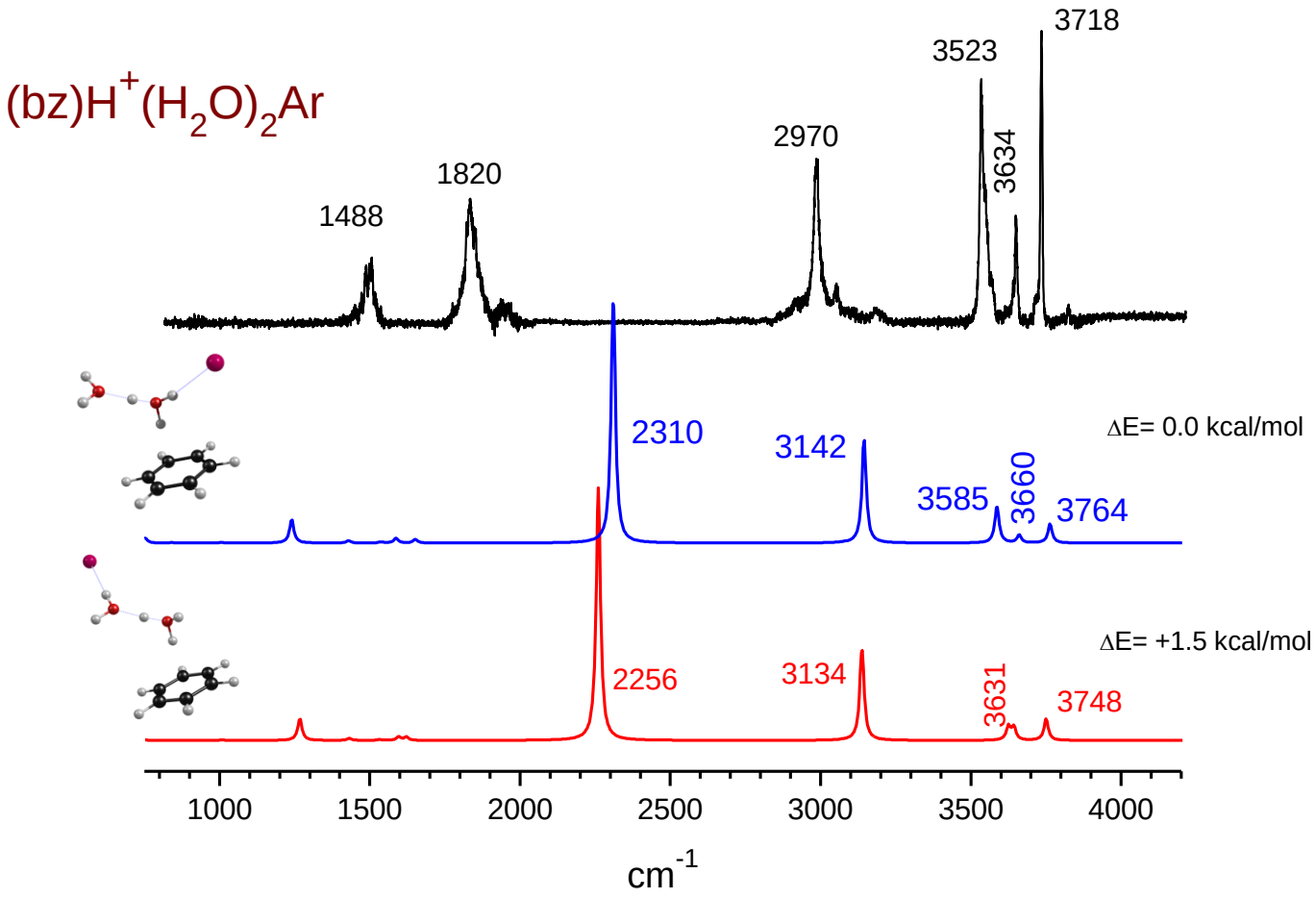

Figure S4. Comparison of predicted spectra of two different isomers of $bzH^+(H_2O)_2Ar$ calculated in MP2 level of theory. Upper trace shows the observed experimental spectrum.

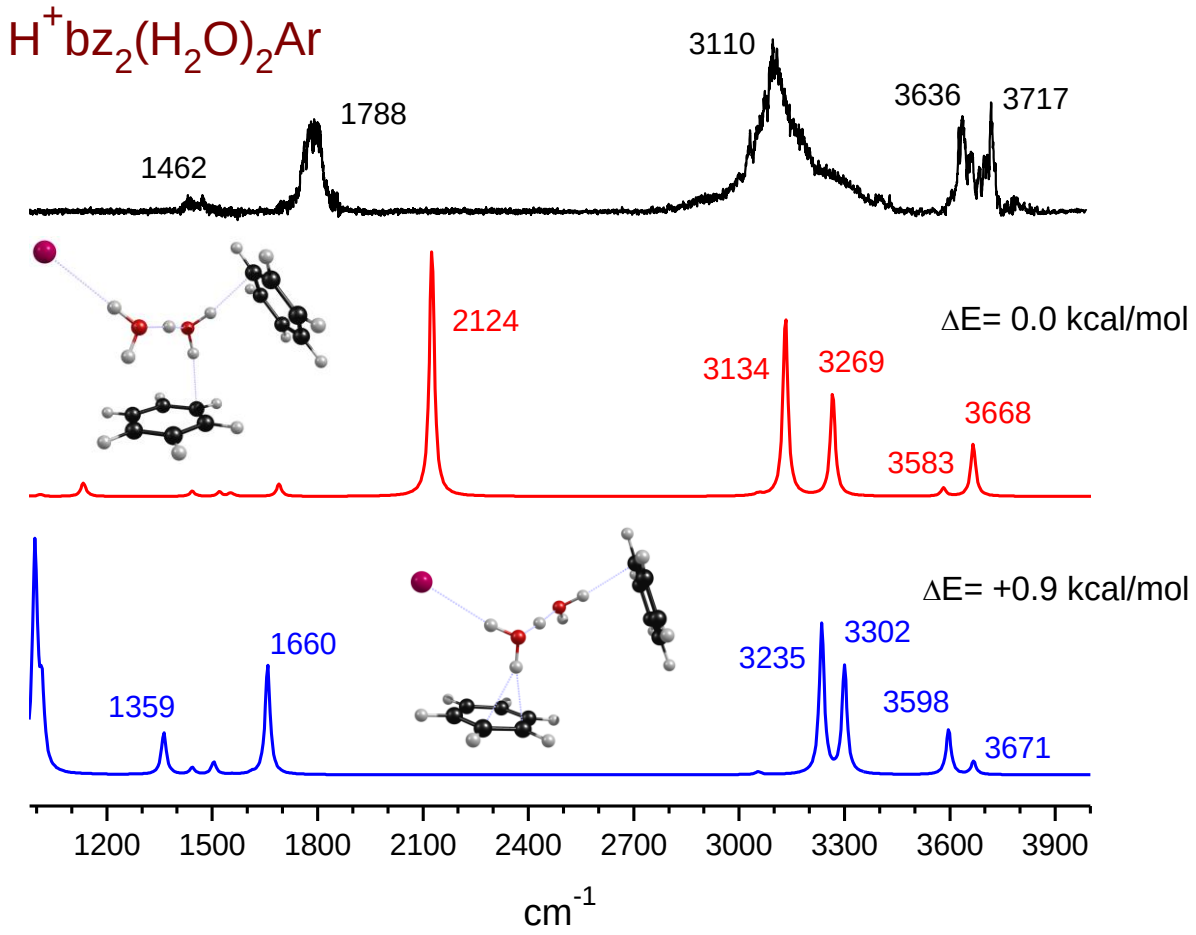

Figure S5. Comparison of predicted spectra of two different isomers of $bz_2H^+(H_2O)_2Ar$ calculated in DFT-B3LYP level of theory. Upper trace shows the observed experimental spectrum.

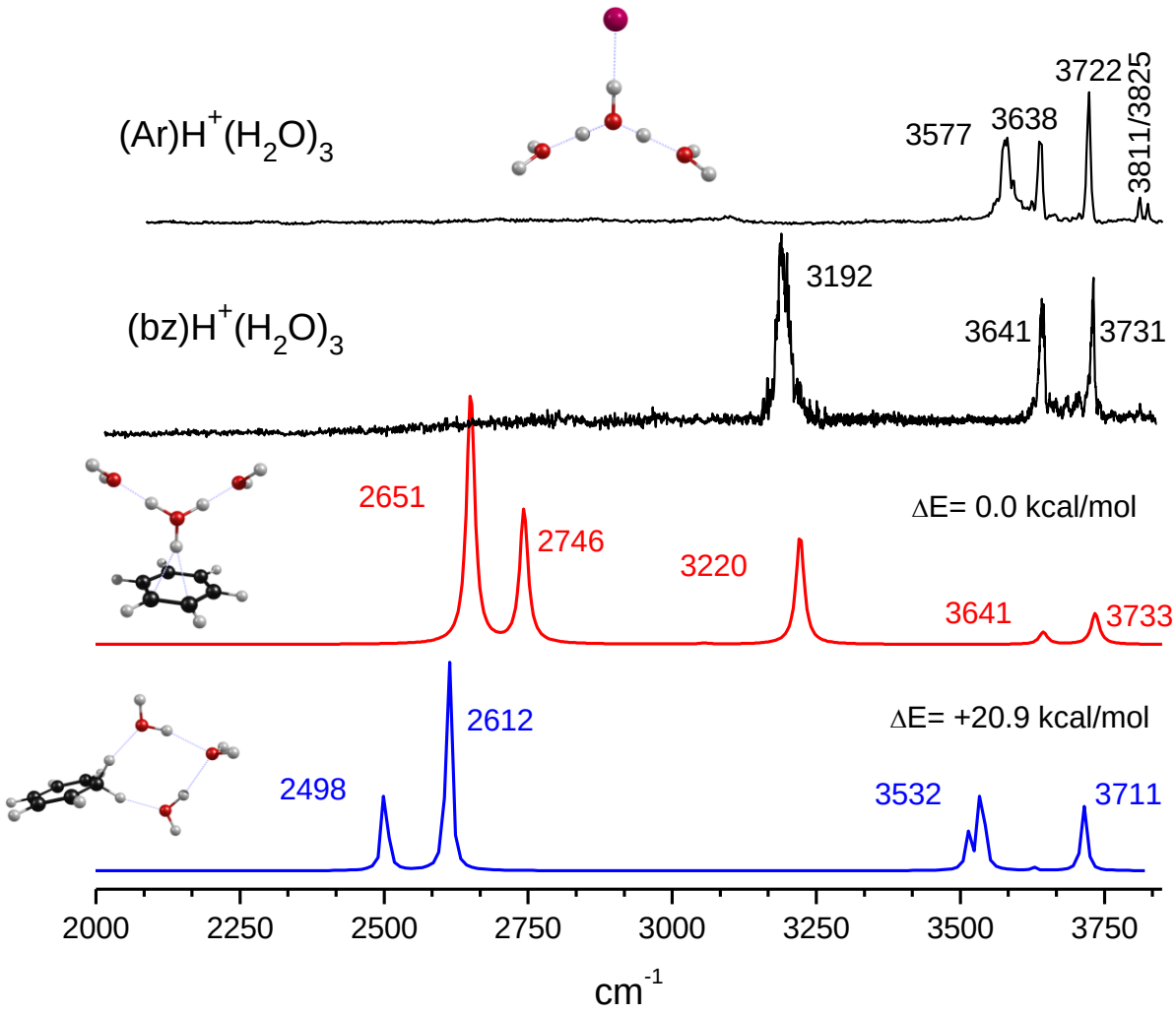

Figure S6. Comparison of observed and predicted spectra for the $(bz)H^+(H_2O)_3$ complex. Bottom two traces show DFT predicted spectra for two isomers of $(bz)H^+(H_2O)_3$ comparing the observed infrared spectrum (second trace from the top). Upper trace shows the infrared spectrum of $H^+(H_2O)_3Ar$ complex to compare with the spectrum of $(bz)H^+(H_2O)_3$ complex.

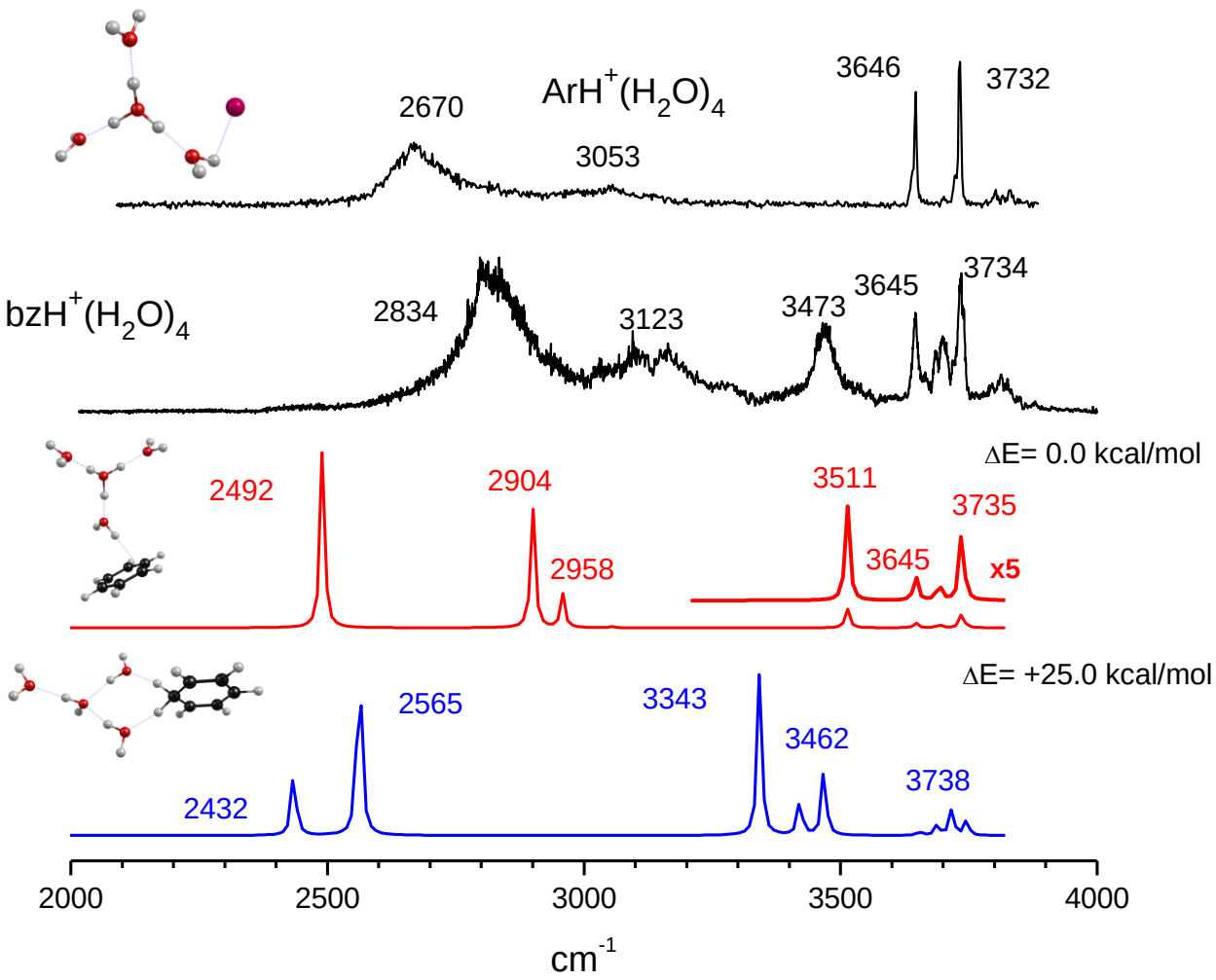

Figure S7. Comparison of observed and predicted spectra for the $(bz)H^+(H_2O)_4$ complex. Bottom two traces show DFT predicted spectra for two isomers of $(bz)H^+(H_2O)_4$ comparing the observed infrared spectrum (second trace from the top). Upper trace shows the infrared spectrum of $H^+(H_2O)_4Ar$ complex to compare with the spectrum of $(bz)H^+(H_2O)_4$ complex .

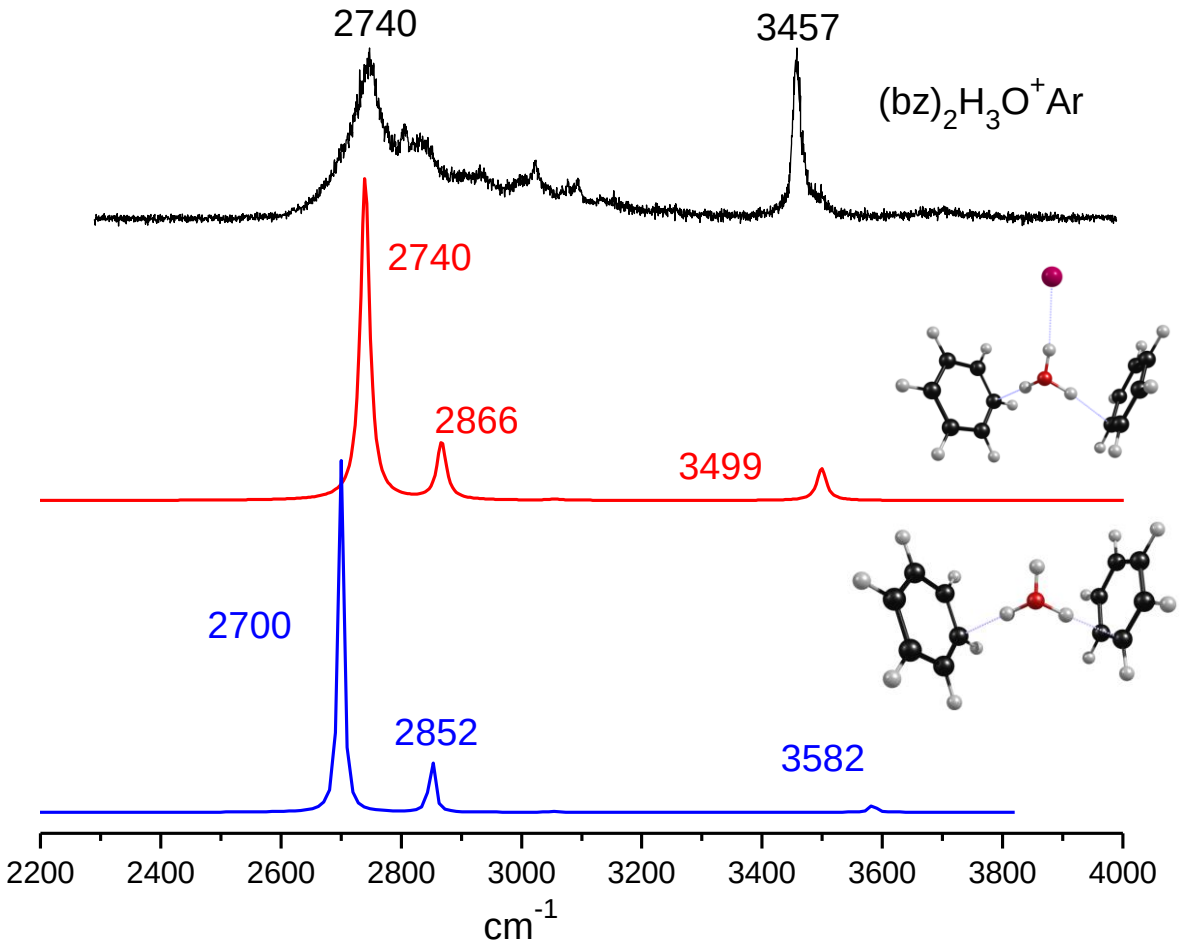

Figure S8. Comparison of observed and predicted spectra for the $(bz)_2(H_3O)^+$ Ar complex with and without the argon atom. Bottom trace shows predicted spectrum without the argon and middle one shows the spectra for the structure with the argon.

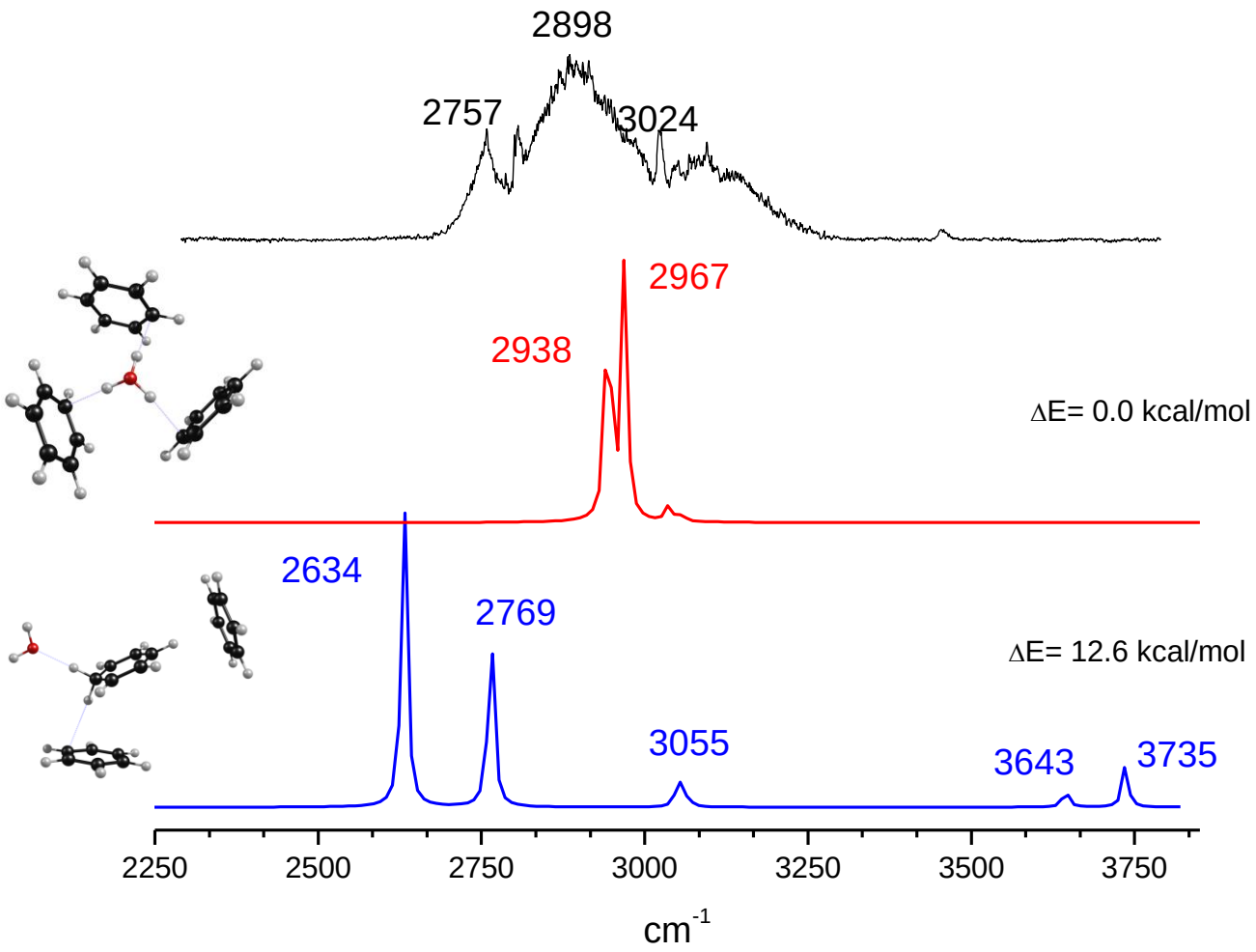

Figure S9. Comparison of observed and predicted spectra for the $(bz)_3(H_3O)^+$complex.

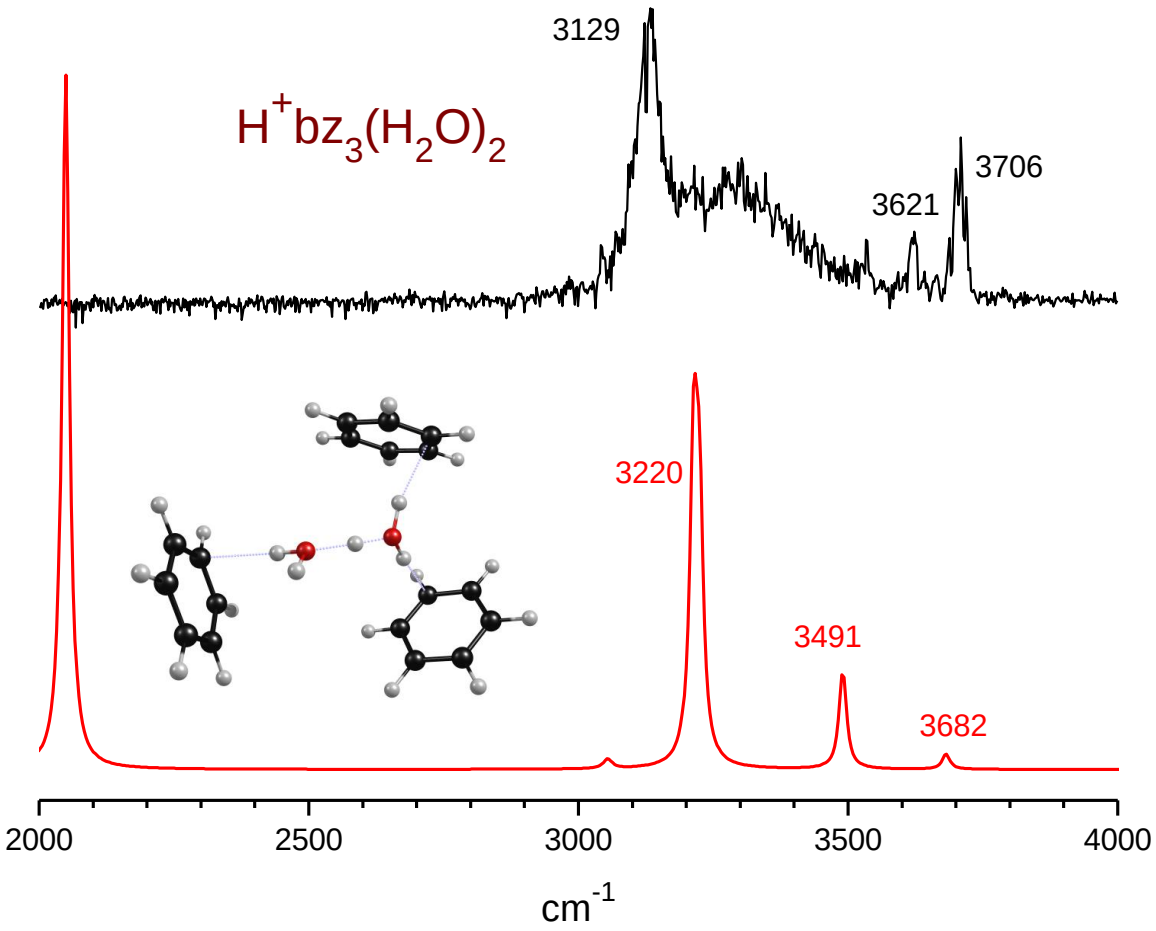

Figure S9. Comparison of observed and predicted spectra for the $(bz)_3(H_2O)_2^+$complex.